Adaptive motivational signals in the anterior cingulate cortex and ventral tegmental area.

Thomas Ward Elston

A thesis submitted for the degree of

Doctor of Philosophy

at the University of Otago

in Dunedin, New Zealand

August 2017

Where is it, this present? It has melted in our grasp, fled ere we could touch it, gone in the instant of becoming.

- William James, *Principles of Psychology* (1890)

My formula for greatness in a human being is *amor fati*: that one wants nothing to be different, not forward, not backward, not in all eternity. Not merely bear what is necessary, still less conceal it—all idealism is mendacity in the face of what is necessary—but *love* it.

- Frederick Nietzsche, *Ecce Homo* (1908)

When I let go of what I am, I become what I might be.

- Lao Tzu, *Tao Te Ching* (~400 BCE)

Abstract

This thesis focused on the role of the anterior cingulate cortex's (ACC) interactions with the dopaminergic neurons in the ventral tegmental area (VTA) during adaptive behaviour. The overall question guiding this work was: how does information gained during goal pursuit modify and motivate subsequent behaviour? This larger question was operationalized as two projects: (i) to determine whether cortical influence over the dopaminergic midbrain is a mechanism by which ACC signals are implemented as VTA motivation signals; and (ii) to determine the interplay between the ACC and VTA during the initiation and maintenance of behavioural change. In the first project, we monitored and modelled ACC and VTA local field potentials of rats running laps of varying physical difficulty for fixed rewards. The effortful condition required rats to climb over a 30-cm barrier, whereas no barrier was present under the non-effortful condition. The key finding was that ACC→VTA 4-12 Hz signalling increased in trials when the lap was easier than expected. Importantly, this increase was significantly correlated with, but not confounded by, changes in motivation, as measured by running speed. The findings of this first project indicated that the ACC-VTA circuit is a plausible mechanism by which behaviour is modified. This led us to ask whether changes in the ACC-VTA circuit are related to the initiation and persistence of behavioural change.

To assess the interplay between the ACC and VTA during the initiation and persistence of behavioural change, we monitored ACC single units and LFPs as well as LFPs in VTA of rats performing a cost-benefit foraging task with changing contingencies. Through a combination of behavioural, electrophysiological, and modelling analyses, we found that the initiation of exploratory behaviour and the persistence of behavioural change were associated with ACC → VTA signalling. Additionally, we characterized the content of ACC neuronal task models, and showed that ensembles of ACC neurons encode simple actions and values. This was important because, despite the longstanding assumption that the ACC encodes neuronal models of the task at hand, the content of those internal representations remained unclear. Furthermore, we demonstrated that value-coding elements of ACC neuronal task models are particularly influenced by the VTA. This is important because it suggests that mesocortical dopaminergic signalling is a means by which ACC models of the task at hand could be both initiated and modified.

The thesis concludes by presenting a novel incentive-salience, task-model onset theory of ACC function.

Acknowledgements and reflections

I will hand in this dissertation soon and, in reflection, the greatest achievement of my PhD is the sense that I now have the 'know how' and 'can do' necessary to be a successful, independent scientist. For this, I am immensely grateful to my supervisor, David Bilkey. David, thank you for encouraging me to think differently and allowing me to take risks. I don't think I would've had such a positive PhD experience in another lab. Thank you.

Thanks is also in order for the members of the Bilkey lab from 2014-2017; although we all worked hard, the lab has been a fun place to be. I've enjoyed spending all day and all night here and appreciate the sense of 'home' the lab and its members provided. In particular, I want to thank Blake Porter, who sat next to me in the lab and who also hails from the USA. Blake, thank you for the lab beers, the late night discussions on science, life, and philosophy, and for always being eager to help. You set a positive example that I can only aim to aspire towards. Thank you.

A highlight during my time in Dunedin has been a 'paper round' club where neuroscience PhD students and postdocs from around the University meet on Thursday afternoons in a craft beer pub (Ombrello's) to discuss the papers we've each read during the week. In addition to the regular feedback on my communication skills, I've come to appreciate so many subfields of neuroscience through these casual conversations. Through experiences like paper round, I've learned that, for me, the neuroscientific community are 'my people.' So, thank you Maddy, Owen, Megan, Jodi, and Blake for making each Thursday something to look forward to.

Thanks is also in order for the technicians of the Otago Psychology department. I'd like to specifically thank Jeremy Anderson, Meric Hoffman, Lindsey Roberts, and Russel Phillips for always being eager and happy to help with just about anything I wanted to try. There's no way the maze or the new microdrive would have gotten off the ground without your help. Thank you.

Thank you to my family and friends back in America – my parents, sister, and grandparents; Stephen Codara, Richard Kan, and Cole Short. I know it must have been hard for you all that I left the USA for New Zealand but I appreciate your support more than you know. In many ways, I've felt adrift in the last years – not feeling particularly 'in place,' realizing that I will always be the 'other' while living abroad. Then again, I've always felt this way – I have always been different. Your spontaneous Facebook and WhatsApp messages

and Skype calls have meant so much to me because I know that I am not alone – that no matter where I am and what I am doing, you all are there for me. Thank you.

Through this PhD experience, I've learned that, for me, being a neuroscientist is more than a job – it's an avenue to fully express an aspect of myself which is otherwise inaccessible. I am well aware of the great privilege pursuing a PhD has been and I am 'ambiently grateful.'

Table of Contents

List of Figures

List of tables

List of Abbreviations

[DA] – dopamine concentration

ACC – anterior cingulate cortex

aVTA – anterior VTA

BDA – biotinylated dextran amine

BNST – bed nucleus of the stria terminalis

BOLD – blood-oxygen-level-dependent

Caud – caudate nucleus

CC – corpus callosum

ChR2 – channel rhodopsin

DA – dopamine

DRN – dorsal Raphe nucleus

EEG – electroencephalogram

eYFP – yellow fluorescent protein

fMRI – functional magnetic resonance imaging

FSCV – fast-scan cyclic voltammetry

GABA – gamma-amino-butric-acid

HCHR – high cost, high reward

HPC – hippocampus

ICSS – intracranial self-stimulation

iFR – instantaneous firing rate

IP – intraperitoneal

ISTMO – incentive-salience, task-model onset

LCLR – low cost, low reward

LDTg – laterodorsal tegmentum nucleus

LEDs – light emitting diodes

LFP – local field potential

LHb – lateral habenula

LHT – lateral hypothalamus

MG – medial geniculate nucleus

ML – medial lemniscus

mPFC – medial prefrontal cortex

MSN – medium spiny neuron

MT – mammilothalamic tract

nAcc – nucleus accumbens

PAG – periaqueductal grey

PDC – partial directed coherence

PPTg – pedunculopontine tegmentum

PV – parvalbumin

pVTA – posterior VTA

RMTg – rostromedial mesoopontine tegmental nucleus; also known as the pVTA

SC – superior colliculus

TH – tyrosine hydroxylase

VP – ventral pallidum

VTA – ventral tegmental a

Chapter 1 General Introduction

1.1 Overview of anterior cingulate cortex

The anterior cingulate cortex (ACC) is a prefrontal cortical structure which is heavily interconnected with motor and subcortical areas. Recent theories of ACC function (e.g. Kolling, Behrens, Wittmann, & Rushworth, 2016) suggest that the ACC monitors internal models of environments and motivates goal-directed behaviour by modulating cognitive, affective, and motor processes related to drive, based on those internal models (Holroyd & Yeung, 2012). The ACC is also implicated in monitoring and updating those internal models when behaviours do not lead to the predicted outcome, which can then adapt future behaviour (Bryden, Johnson, Tobias, Kashtelyan, & Roesch, 2011; Kennerley, Walton, Behrens, Buckley, & Rushworth, 2006). This chapter aims to provide an overview of the anatomy and physiology which undergirds these core functions.

1.1.1 *ACC anatomy*

1.1.1.1 Definition of the ACC

The rat cingulate cortex is a large structure comprised of three subdivisions, the anterior cingulate cortex, the mid-cingulate cortex, and the retrosplenial cortex (see Figure 2A). The anterior cingulate cortex (ACC) is a major subdivision of the prefrontal cortex and is considered conserved across rodents, humans, and non-human primates (Vogt & Paxinos, 2014; Zilles & Wree, 1995; see Figure 1). Definitions of the structure vary widely; for instance, Zilles and Wree (1995) divide this region into Cg1 (cingulate gyrus 1), Cg2, and Cg3 whereas Paxinos & Watson (1997) divide the ACC into Cg1 and Cg2 and treat Cg3 as part of the infralimbic (IL) cortex. However, recent work by Vogt & Paxinos (2014) indicates that Cg1, Cg2, and Cg3/IL are all continuous portions of the ACC. This thesis will treat the ACC according to Vogt & Paxinos (2014)'s most recent definition (see Figure 1A). Areas 24b and 32 in Figure 2A and C correspond to the specific subregions of the ACC examined in this thesis.

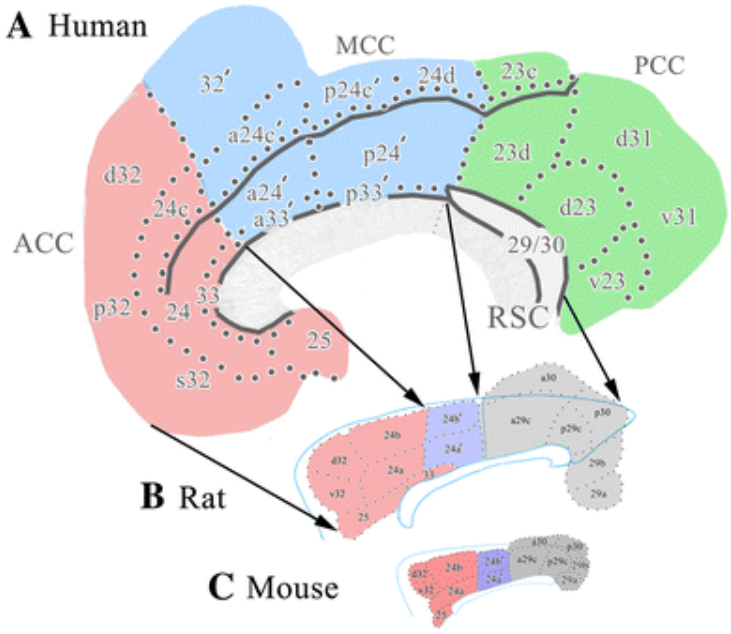

Figure 1. Homology of cingulate cortex areas from humans to rats to mice. From figure 6 in Paxinos and Vogt (2014).

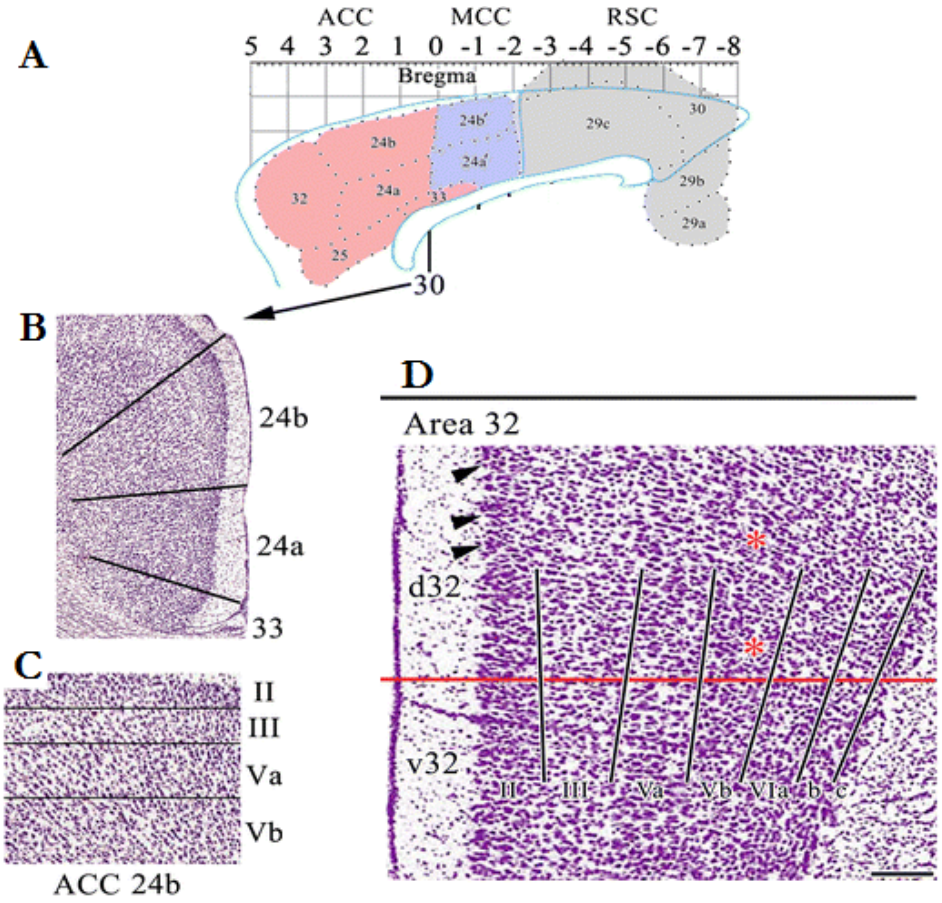

Figure 2. Location and cytoarchitecture of the rat ACC. **A.** Localisation of major cingulate cortex divisions in the rat. The salmon coloured areas 24b and 32 are the portions of the ACC studied in this thesis. **B.** Macrograph of Nissl-stained sections of areas 24a, 24b, and area 33. **C.** Micrograph of laminae in area 24b. **D.** Cytoarchitecture and lamellae of area 32. Images are from Paxinos and Vogt (2014) figures 1 and 2.

1.1.1.2 Primary cell types of ACC areas 24b and 32.

Areas 24b and 32 contain a multitude of cell types, many of which, are unique to these divisions of the ACC. Here I will address inverted pyramidal neurons, several classes of multipolar neurons, bipolar, and bi-tufted neurons. This section will aim to highlight the intracortical and extracortical nature of these cell types with a view to the next section, which will review the major inputs and outputs of ACC areas 24b and 32.

Areas 24b and 32, uniquely, contain large numbers of inverted pyramidal neurons (Vogt & Peters, 1981; see Figure 3a and 3b). These cells share many of the characteristics of typical pyramidal cells (e.g. the somas occur in layers II-VI, especially layers IV and V, branch at least three times, and have apical tufts in white matter), except that their orientating apical dendrite is towards the medial white matter, the cingulum bundle, rather than the pia mater, which is more typical of pyramidal neurons in other cingulate areas. The axons of inverted pyramidal neurons typically project into the cingulum bundle; thus, these neurons are the primary extra-ACC input-output neurons of ACC areas 24b and 32.

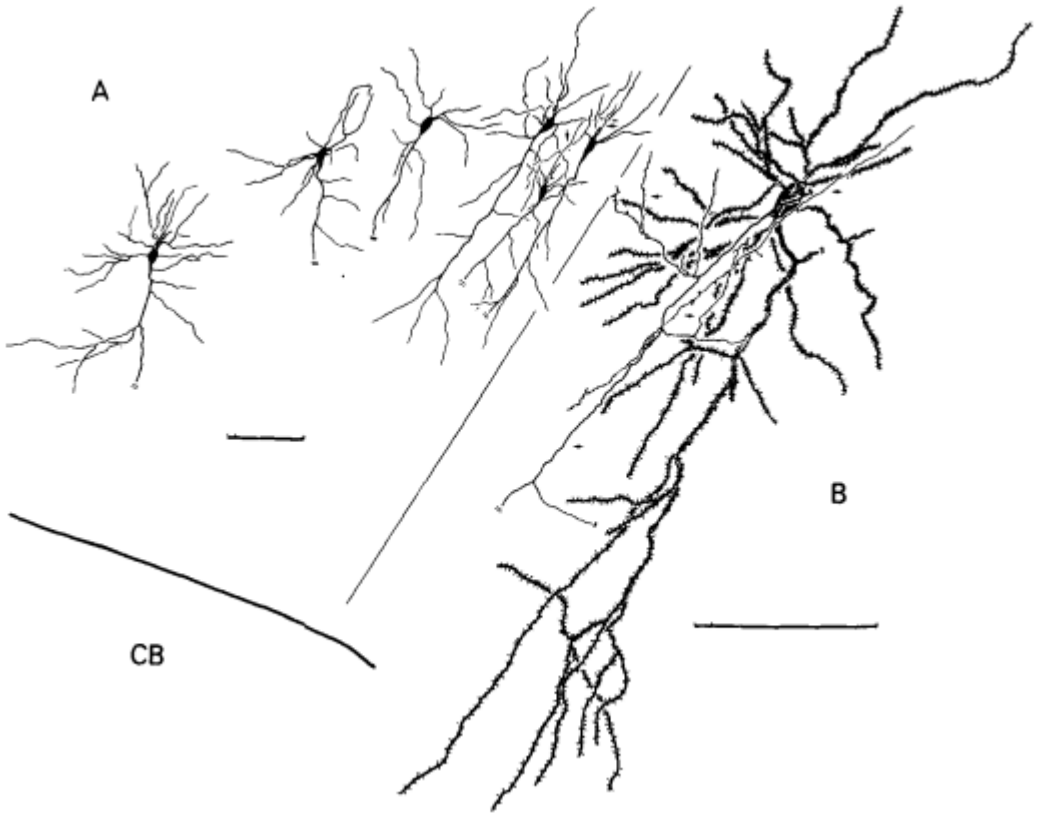

Figure 3. Inverted pyramidal cells of area 24b, immediately rostral from the corpus callosum. **A.** Six inverted pyramidal cells. **B.** Magnified inverted pyramidal cell. From figure 6 in Vogt & Peters (1981).

Multipolar neurons are characterized by a dendritic arbour which enshrouds the soma and an axon which terminates within the cortex (see Figure 4). Thus, multipolar neurons, generally, are the integrators and maintainers of local information in the ACC. Multipolar

neurons vary greatly in soma size, dendritic arborisation, and axonal distribution and are thus sub-classified as being either small, medium, or large.

Figure 4. Large (**A**) and medium (**B**) multipolar neurons with axonal and dendritic arbours rendered separately. Figure 12 in Vogt & Peters (1981).

Bi-tufted and bipolar neurons are the final major cell types comprising areas 24b and 32 in the ACC. These cell types are characterised by their cylindrical, fusiform somata. However, they are distinguished by the shape of their dendritic arbours and axon projections: bi-tufted neuron arbours have an hourglass shape and contain many vertical and horizontal axon collaterals whereas bipolar arbours and axon collaterals tend to be more vertically oriented (see Figure 5). Neither of these cell types tend to collateralise in the cingulum

bundle, and both tend to span multiple layers of the cortex, suggesting that these cells traffic information between cortical layers.

Figure 5. Bi-tufted and bipolar neurons from ACC areas 24b and 32. **A.** Bi-tufted neuron from layer III of area 32. **B.** Bi-tufted neuron from layer III of area 32. **C.** Bipolar neuron from layer III of area 24b. **D.** Bipolar neuron from layer III of area 24b. **E.** Bipolar neuron from layer V in area 24b. Figure 15 in Vogt & Peters (1981).

To summarize, inverted pyramidal, varieties of multipolar, bi-tufted, and bipolar neurons comprise the majority of cell types in areas 24b and 32 in the ACC. Inverted pyramidal neurons are the primary cells which handle extra-cortical inputs and outputs whereas multipolar neurons are more likely to process, and perhaps maintain, information within the cortical layer in which the neuron occurs. Bi-tufted and bipolar neurons span several cortical layers but do not project into the medial or lateral white matter, suggesting

that these neurons traffic information between layers within the ACC. Taken together, the constellation of cell types comprising areas 24b and 32 in the ACC suggest a cortical volume which is specialized at loading in extracortical information via inverted pyramidal dendritic arbours adjacent to the cingulum bundle which is then intracortically processed by multipolar, bi-tufted, and bipolar neurons before the output of such computations is sent out by inverted pyramidal axons projecting into the cingulum bundle.

1.1.1.3 Primary inputs and outputs of the ACC

Areas 24b and 32 of the ACC (henceforth referred to as ACC) have an extensive array of connections, which are summarized in Table 1. It is notable that the ACC is reciprocally connected to many neuromodulatory centres (e.g. the ventral tegmental area, locus coeruleus, and Raphe nuclei) and the hippocampus, suggesting that the ACC might play a role in monitoring and influencing both neuromodulatory and hippocampal states, respectively.

Table 1.

Inputs and outputs of the rat ACC

Inputs		Outputs	
Structure	Reference	Structure	Reference
Basal nucleus of Meynert	Zilles & Wree (1995)	Caudal interstitial nucleus of the medial longitudinal fasciculus	Zilles & Wree (1995)
Basolateral amygdala	Zilles & Wree (1995)	Intralaminar thalamic nuclei	Zilles & Wree (1995)
Caudal interstitial nucleus of the interstitial fasciculus	Zilles & Wree (1995)	Laternal habenular nucleus	Zilles & Wree (1995)
Dorsal raphe nucleus	Zilles & Wree (1995)	Pontine nuclei	Zilles & Wree (1995)
Median raphe nucleus	Zilles & Wree (1995)	Anterior pretectal nucleus	Zilles & Wree (1995)
Locus coeruleus	Zilles & Wree (1995)	Mediodorsal thalamalic nucleus	Zilles & Wree (1995)
Lateral hypothalamic area	Zilles & Wree (1995)	Periventricular hypothalamic nucleus	Zilles & Wree (1995)
Mediodorsal thalamic nucleus	Zilles & Wree (1995)	Median raphe nucleus	Zilles & Wree (1995)
Zona incerta	Zilles & Wree (1995)	Superior colliculus	Zilles & Wree (1995)
Parabrachial pigmented nucleus	Zilles & Wree (1995)	Agranular insular cortex	Zilles & Wree (1995)
Ventromedial thalamic nucleus	Zilles & Wree (1995)	Entorhinal cortex	Zilles & Wree (1995)
Ventral tegmental area	Zilles & Wree (1995)	Ventral tegmental area	Carr & Sesack (2000)
Centrolateral thalamic nucleus	Zilles & Wree (1995)	Presubiculum	Zilles & Wree (1995)
Laterodorsal thalamic nucleus	Zilles & Wree (1995)	Nucleus accumbens core	Brog, Salyapongse, Deutch, & Zahm (1993)
Perivertricular hypothalamic nucleus	Zilles & Wree (1995)	Nucleus accumbens shell	Brog et al., (1993)
Intrinsic (within ACC)	Zilles & Wree (1995)	Contralateral ACC	Zilles & Wree (1995)
Contralateral ACC	Zilles & Wree (1995)	dCA1 hippocampus	Rajasethupathy et al. (2015)
Agranular insula cortex	Zilles & Wree (1995)	Basolateral amygdala	Zilles & Wree (1995)
dCA1 hippocampus	Rajasethupathy et al. (2015)	Orbitofrontal cortex	Zilles & Wree (1995)
Superior colliculus	Comoli et al. (2012)		

1.1.2 *ACC function*

The ACC is strongly implicated in many key functions, such as pain (Ballantine, Cassidy, Flanagan, & Marino, 1967; Bliss, Collingridge, Kaang, & Zhuo, 2016; Foltz & White, 1962), affect (George et al., 1993; Meyer, McElhaney, Martin, & McGraw, 1973; Vogt, 2005), the subjective effects of the psychedelic drug d-lysergic acid diethylmide (LSD; Gresch, Barret, Sanders-Bush, & Smith, 2006), detections of errors of when outcomes do not match predictions (Bryden et al., 2011; Kawai, Yamada, Sato, Takada, & Matsumoto, 2015; Kennerly, Behrens, & Wallis, 2011), and the subsequent adaptation of behaviour following an error (Bryden et al., 2011; Cavanagh, Frank, Klein, & Allen, 2010; B. Y. Hayden, Heilbronner, Pearson, & Platt, 2011). Grand theories attempting to account for all of the activities of the ACC are, understandably, general. This section will review two prominent theories of ACC function, the theories of cognitive control and internal model monitoring and updating.

1.1.2.1 The cognitive control theory of ACC function

Until recently, the prevailing notion regarding ACC function was cognitive control (culminated in Shenhav, Botvinick, & Cohen, 2013), which suggests that the ACC is continuously monitoring task performance and performing a moment-by-moment cost-benefit analysis calculation, the outcome (and magnitude) of which corresponds to the magnitude of control the ACC exerts via its efferent outputs to direct behaviour. The most convincing experiments supporting this notion centre around the Stroop task, which is thought to examine cognitive control. Participants performing a classic Stroop task are timed while they name the printed colour of stimuli of three different types of stimuli (a) colour patches, (b) non-colour words, and (c) words that name a colour but are printed in a conflicting colour (Stroop, 1935; see Figure 6). Stroop (1935) found that participants were considerably slower at naming the ink colour of a word when the stimuli were colour words incongruent with the ink colour (e.g. C in Figure 6), which led Stroop (1935) to conclude that participants cannot help but to read the word and that this automatic reading process conflicts with the controlled process of naming the ink colour. Thus, reaction times and neural responses in the Stroop task are thought to represent the degree of cognitive control the participant must employ in order to resolve the conflict engendered in the task.

Figure 6. Examples of Stroop task stimuli which require escalating degrees of cognitive control to correctly name. **A.** A patch of colour. **B.** A non-colour word printed in blue. **C.** A word which names a colour but is printed in a conflicted colour.

Numerous reports implicate the ACC in facilitating Stroop-task performance (Barch et al., 2001; Sheth et al., 2012; Swick & Jovanovic, 2002). The most convincing of these recorded ACC single-units of human patients undergoing stereotactic cingulatomy for treatment-resistant obsessive-compulsive disorder as they performed a Stroop-like task (Sheth et al., 2012). Sheth et al. (2012) found positive correlations between the difficulty (e.g. the amount of cognitive control required) on a given trial and participant reaction time (Figure 7A). Strikingly, the firing rate of individual ACC neurons also corresponded to the degree of cognitive control required to complete a given trial (Figure 7B). Subsequent functional magnetic resonance imaging (fMRI) revealed that the ACC is the primary brain area active during the task (Figure 7C). Taken together, these experiments provide compelling evidence of the role of the ACC in cognitive control.

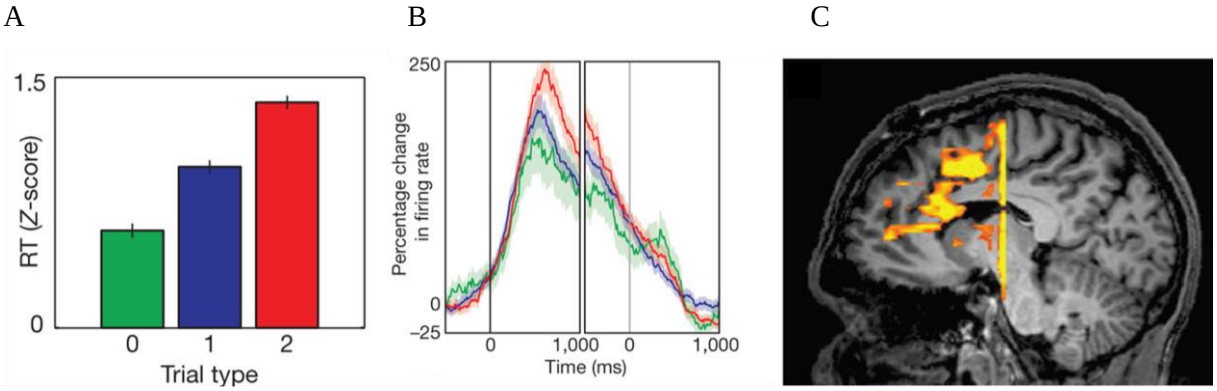

Figure 7. Data implicating the ACC in cognitive control. **A.** In a Stroop-like task, participant reaction times increase as task difficulty increases. 0 = naming a coloured block, 1 = naming a coloured, non-colou word, and 2 = naming a colour word printed in an incongruent ink colour. **B.** Firing rates of human ACC neurons responsive to the Stroop-task increase as task difficulty increases. **C.** Blood-oxygen-level-dependent (BOLD) signalling from fMRI experiments indicating that the ACC is the brain area primarily activated by the Stroop task. Adapted from Sheth et al. (2012).

Findings from rodent and non-human primate electrophysiology experiments can also be interpreted as additional evidence for ACC's role in cognitive control. Ma, Hyman, Phillips, & Seamans (2014) recorded ACC neurons of rats trained to press levers in a sequence and found that ACC neurons increased their firing rates in a step-wise manner as rats completed each element of a given sequence (Figure 8A). That ACC neurons increased their firing rates as rats progressed towards a goal suggests that ACC neurons might either track progress towards a goal or, alternatively, provide a signal indicating persistence or commitment to a goal. Blanchard, Strait, & Hayden (2015)'s recordings of non-human primate ACC neurons while subjects persisted in a commitment to a decision offer some clarity. Blanchard et al. (2015) required non-human primates to make a choice by depressing a lever and continue holding that lever for a specific amount of time until a reward was delivered. They found that ACC unit ensembles ramped up during the course of commitment

to a decision (Figure 8B and C). The ramping shape indicates that ACC unit ensemble states gradually came to resemble the goal state while persisting in a decision. Together, the findings of both Ma et al. (2014) and Blanchard et al. (2015) suggest that ACC neurons in these tasks, respectively, correspond to an organism's cognitive commitment and behavioural persistence towards a goal. Thus, these findings can be construed as instances of cognitive control if one considers that committed pursuit of one goal excludes the pursuit of other goals and that the active exclusion of alternative-goal-related-information is an example of the ACC controlling the strength and effect of internal representations.

Additional support for ACC having a role in cognitive control comes from Hillman & Bilkey (2010)'s recordings of rodent ACC neurons as the rodents completed a cost-benefit decision making T-maze task. The task required rats to turn left or right, taking into consideration the amount of reward they would receive and the physical effort required to attain that reward. For example, in the baseline configuration of their experiment, "2:6B," rats could turn left to pursue a reward of two chocolate cereal pellets with no additional physical effort (low cost, low reward; LCLR) or turn right to overcome a 30cm barrier to attain a reward of 6 chocolate cereal pellets (high cost, high reward; HCHR).

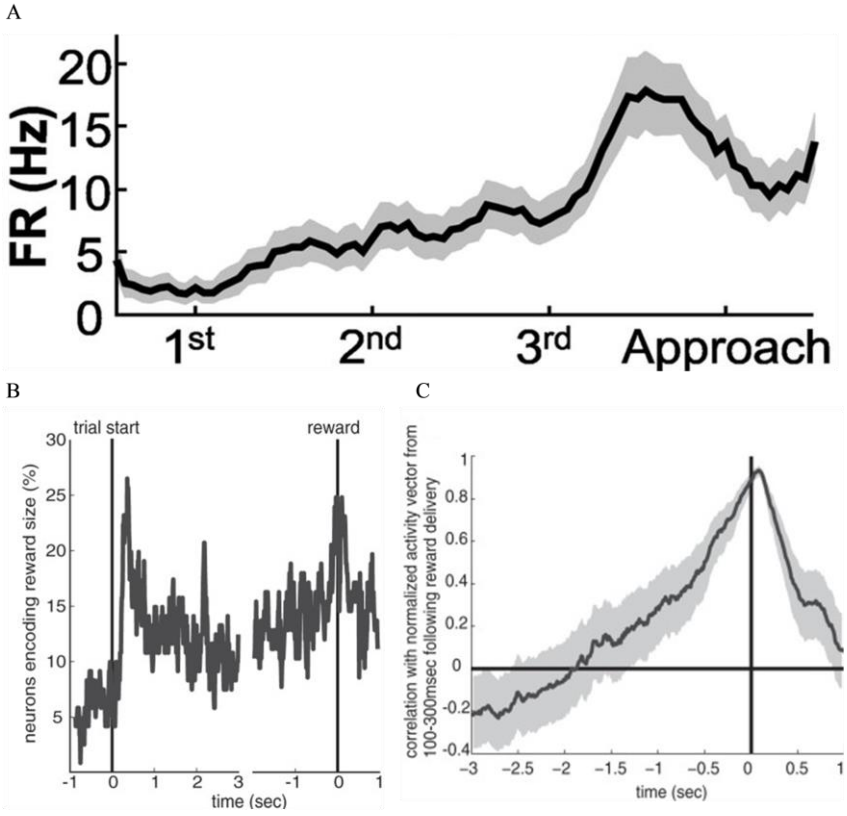

Figure 8. ACC unit activity corresponds to progress towards and, perhaps, commitment to a choice. **A.** Rat ACC unit activity increases in a stepwise manner as a rat completes each step in a sequence of lever presses. **B.** Non-human primate ACC unit activity is modulated by the initiation of a choice trial and begins to ramp up as the temporal proximity to reward increases. **C.** Correlations of non-human primate ACC unit principal component

vector states at various temporal windows with the vector state during the time of reward delivery. A is from Ma et al. (2014); B is from Blanchard et al. (2015).

Hillman & Bilkey (2010) found that the majority of their animals (7/10) preferred the HCHR option whereas three animals did not exhibit a significant preference for one choice over the other. Despite the differences in choice behaviour, ACC neurons in all 10 animals fired significantly more in HCHR-associated regions of the maze as compared to matched LCLR regions (Figure 9).

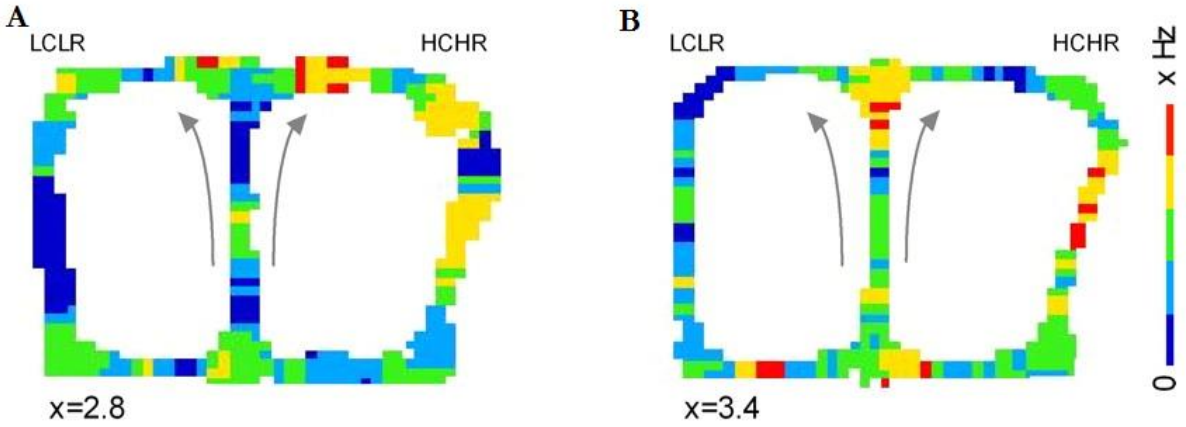

Figure 9. Example rat ACC neurons responding to HCHR trajectories more than LCLR trajectories. For each cell, firing rate data are pseudo-colour mapped onto position in the maze. Firing rate scale values are beneath each plot. **A.** Rat ACC neuron which maximally responds to the maze region immediately after the decision. **B.** Rat ACC neuron which maximally responds to the pre-reward region of the maze. Adapted from Hillman & Bilkey (2010).

Since difference were not detected between either the ACC neuron firing profiles or number of cells biased towards HCHR trajectories contained within HCHR-preferring rats and no-preference rats, Hillman & Bilkey (2012) suggested that these neurons encode the anticipation of some future feature of the rats' current path, such as physical effort. Alternatively, it may be that ACC neuron activity prospectively encodes the integrated value of anticipated benefit discounted by anticipated cost. Importantly, Hillman & Bilkey (2010) demonstrated that ACC neurons rapidly adapted to changes in the maze configuration which altered the spatial arrangement of the barriers and reward magnitudes (Figure 10 A,B). Taken together, these data suggest that the ACC dynamically integrates cost and benefit information and may bias an organism towards the most economically advantageous actions and is thus another instance of ACC's role in cognitive control.

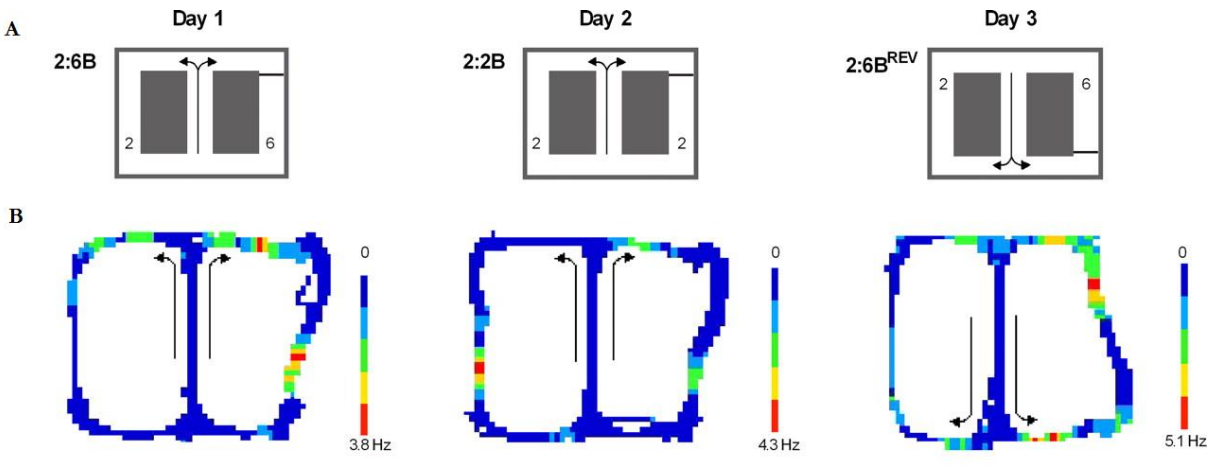

Figure 10. ACC neurons dynamically and relatively encode value. 10 ACC neurons from four rats were recorded across three maze configurations over three days. **A.** Schematic of different maze configurations across days. On day one, the standard 2:6B configuration, described earlier. On day two, the same reward, two cereal pellets, was available as a consequence of turning either left or right; however, a physical barrier was added to right turns. On day three, the standard 2:6B configuration was reinstated except that the path of the rats was reversed. **B.** Firing rate maps for an example neuron which was stably recorded across the three configurations. For all 10 cells, firing rates were significantly higher for the more economical trajectory and, in the case of the reversed trajectory, remapped to a spatially-proportional position in the maze as the non-reversed configuration. Adapted from Hillman & Bilkey (2010).

1.1.2.2 The internal state monitoring and updating theory of ACC function

An alternative recent theory of ACC function suggests that the ACC constructs and tunes internal models of the environment that are relevant for future behaviour and biases behaviour based on those models (Kolling et al., 2016; O'Reilly et al., 2013). Such a notion is supported by reports of large, transient bursts of ACC neuron activity, in both rodents and non-human primates, when an outcome is different than expected (Bryden et al., 2011; Gemba, Sasaki, & Brooks, 1986; Kawai et al., 2015; Kennerly et al., 2011). Although such prediction errors are now regularly reported in dopaminergic and other brain areas (e.g. Eshel et al., 2015), they were first detected in the ACC (Gemba et al., 1986; Figure 11) Strikingly, the magnitude of the activity increase correlates with the magnitude of the prediction error. The most important finding across these studies is that ACC activity on error trials strongly predicted a change in behavioural strategy on the next trial, a finding which has been replicated in human electroencephalographic (EEG) and single unit investigations of the adaptive role of ACC signalling (Cavanagh et al., 2010; Debener et al., 2005; Sheth et al., 2012). Collectively, these data suggest that the ACC plays a fundamental role in adaptive behaviour, perhaps by motivating extended behaviours based on dynamic internal models of environments and task requirements (Holroyd & Yeung, 2012; Kolling et al., 2016).

A human functional magnetic resonance imaging (fMRI) study by O'Reilly et al. (2013) provides compelling evidence that the ACC does indeed dynamically encode internal models of task requirements and most strongly responds when that model requires updating.

In the study, human participants were initially instructed to fixate on a point at the centre of a circle. A coloured target dot then appeared somewhere on the perimeter of the circle and participants were directed to shift their gaze such that they came to fixate on the target dot.

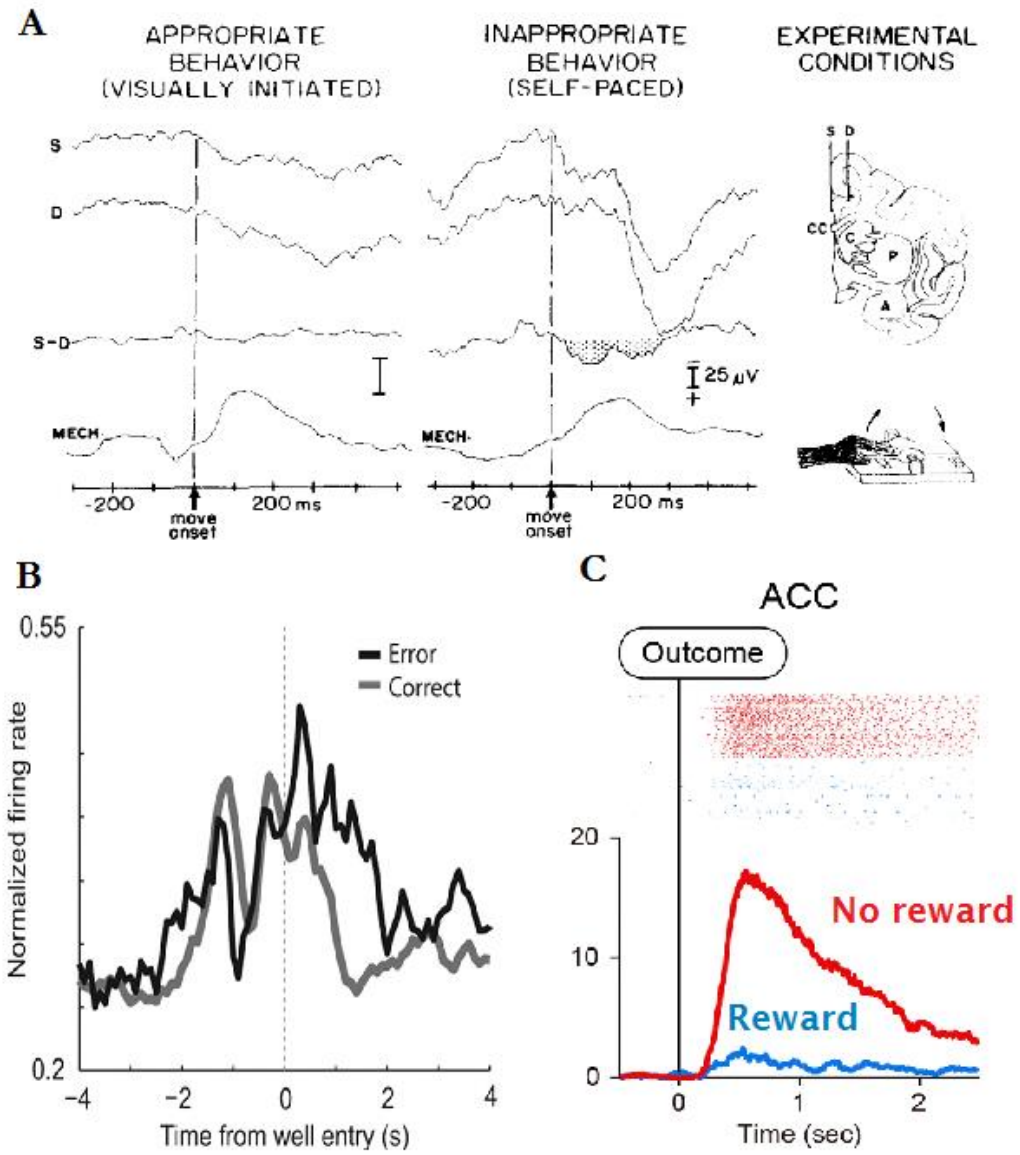

Figure 11. Examples of prediction error in the ACC of the rat and non-human primate. **A.** The first reported example of prediction error. When non-human primates committed an error, which did not yield reinforcement when it was expected, the local field potential, the aggregate electrical signal of the neurons which comprise a brain area, strongly deflected. This deflection pattern is associated with more neurons firing in a synchronized manner (Buzsaki, 2006). **B.** ACC neurons contained in rats increase their firing rate after the animal committed an error and reward was omitted when it had been expected. **C.** ACC neurons of non-human primates respond most when reward is omitted after a reward-associated action. A is adapted from Gemba et al. (1986); B is adapted from Bryden et al. (2011); C is adapted from Kawai et al. (2015).

Dots of a specific colour, red, for instance, indicated a characteristic location the dots would appear in the subsequent 10-20 trials (Figure 12A,B). After a block of trials of a given colour

and spatial distribution, a new dot colour would appear in a new location on the circle, updating the location of the next distribution of dots. Occasionally, a grey dot in a surprising location that was inconsistent with the prior spatial distribution of the coloured dots (Figure 12B). These types of trials were one-off in nature and were not predictive of future dot-location occurrences and, thus, should not induce updates in the participants' internal task models.

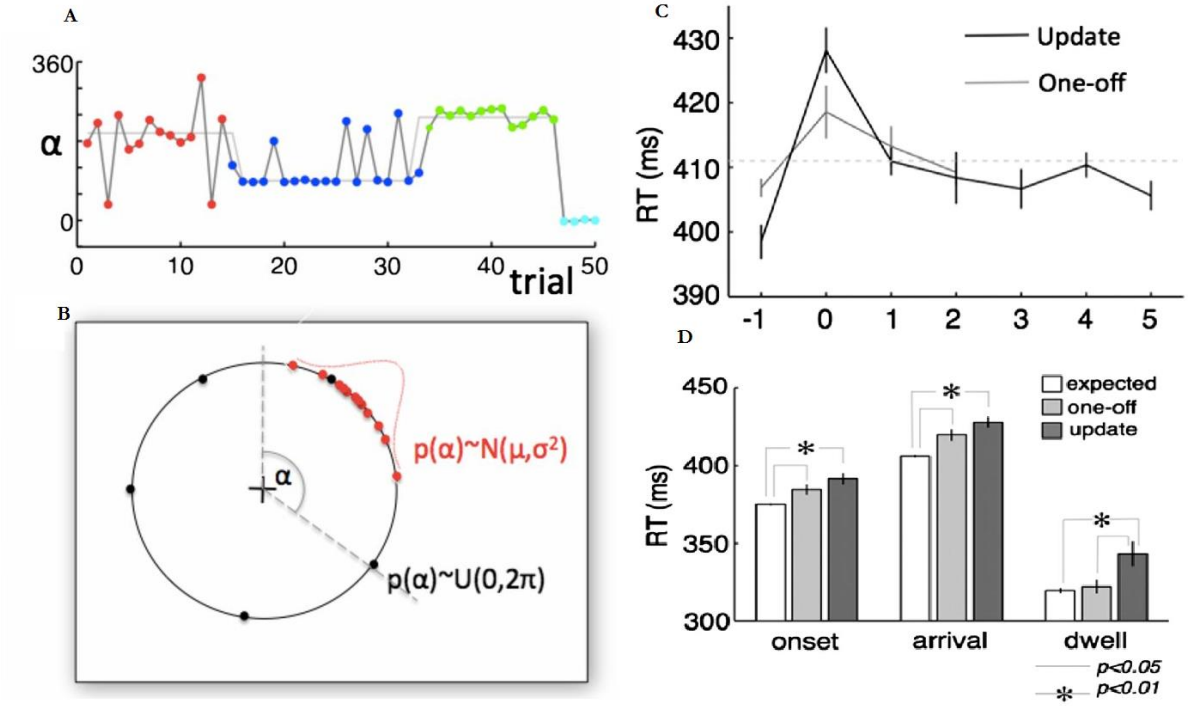

Figure 12. Task schematic and behavioural performance in a study demonstrating ACC responds to internal task-model updating. **A.** Plot of target dot locations as portrayed as angles (α) from vertical as a function of trial number. **B.** Example of dot-position distributions for red dots, which were associated with fixation changes to the upper-right quadrant of the circle. One-off dot targets are shown in grey. **C.** Reaction times for gaze to arrive at the target dot one-off and update trials, respectively. Zero indicates the instance of a one-off or update trial. The dotted line indicates the mean reaction time across all trials. **D.** Saccadic reaction times from onset of cue, how long it took for gaze to arrive at the dot target, and the duration of fixation upon the target dot as a function of trial type. Adapted from O'Reilly et al. (2013).

Participants made speeded saccades (rapid eye movements) to the expected location of a dot significantly faster than one-off, 'surprise' trials. On 'update' trials, however, participants spent more time gazing at the target dot than other trial types (Figure 12C,D). This suggests that participants formed internal models of the task-requirement by estimating the underlying spatial distribution of target dots within a given trial-block. Interestingly, blood-oxygen-level-dependent (BOLD) signalling measured in the fMRI detected the greatest ACC response to the 'update' trials as compared to both the 'expected' and 'surprise' trial types (Figure 13A,B). The lack of ACC response to one-off trials is unexpected given literature implicating ACC in prediction error. Since the ACC responded almost exclusively

to ‘update’ trials, perhaps prior studies of prediction errors detected in the ACC ought to be reinterpreted as the output of a process of updating more fundamental network processing states in the ACC. However, as the signals observed by O’Reilly et al. appeared to occur in the “middle” portion of the ACC and not its most anterior subregions, questions remain as to whether different sub-regions of the ACC do different things.

The internal-state monitoring and updating theory of ACC function accounts for the phenomenon implicating cognitive control as a core function of ACC and reconciles the literature implicating the ACC in error-minimizing adaptive behaviour. This model reconciles the previous ‘cognitive control’ theory because it is more fundamental, suggesting that cognitive control is the output of the internal model shifts. Thus, the evidence suggests that ACC likely encodes a dynamic model of the task at hand and allocates cognitive control based on that model. This theory is prescriptive in that it suggests guidelines and heuristics for both the design and interpretation of future experiments. For example, the internal-state monitoring and updating theory suggests that ACC ought to respond most when task-requirements are different than expected, which requires subsequent adaptive behaviour. It also suggests that ACC computations integrate the expected benefit of adapting behaviour as well as the relative costs of such behavioural change and is not likely to respond as much when competing action plans with different value-valences do not need to be compared, a notion explicitly validated by Shenhav, Straccia, Cohen, & Botvinick (2014).

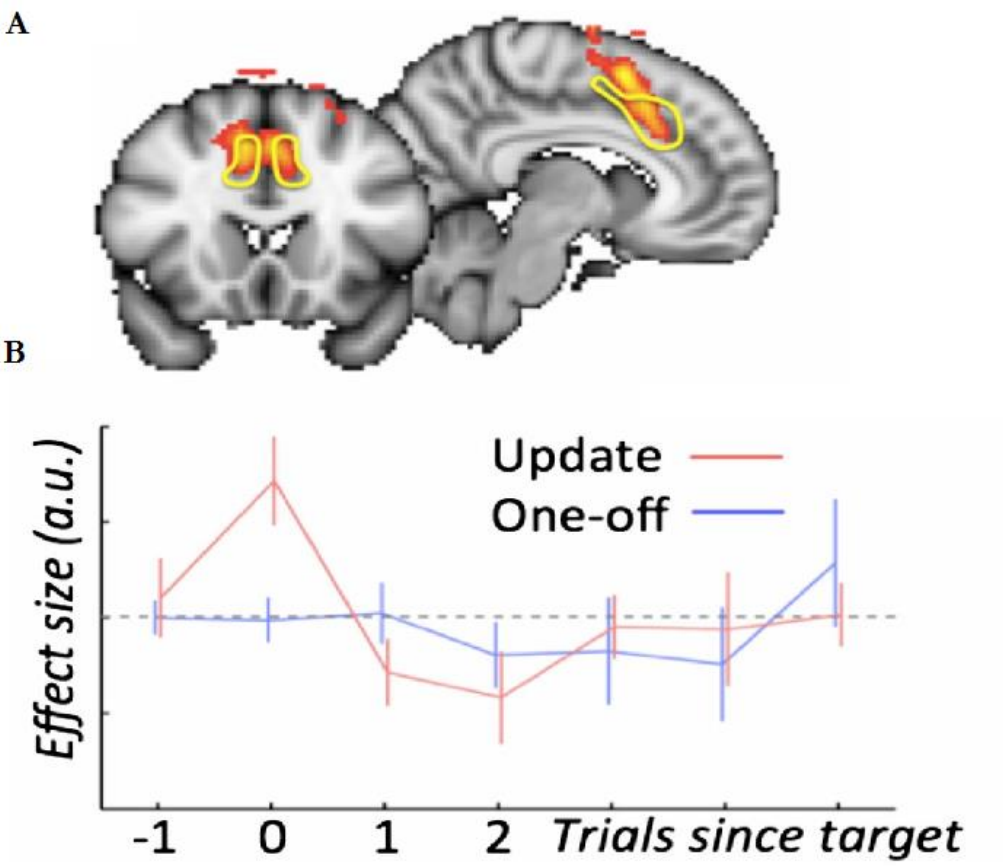

Figure 13. ACC responses to update and one-off trials. **A.** Whole-brain fMRI results showing colour-mapped responses on update trials. The yellow shape indicates the region defined as ACC in the analyses. **B.** Raw ACC activity detected across trials, where zero indicates the occurrence of either an update trial or a one-off trial. The dashed line indicates the mean across all trials.

1.1.3 *Summary of the ACC*

In summary, the ACC is a medial prefrontal cortical area which integrates intra-and-extra cortical information. Assessments of ACC activity in rodents, non-human primates, and humans suggest that the ACC is a critical for adaptive behaviour. The most convincing unifying theory of ACC function suggests that the ACC constructs and tunes internal models of the environment that are relevant for future behaviour and adapts behaviour based on those models. Nevertheless, it is mechanistically unclear how changes in ACC activity translate into behavioural change. The ACC might enact such adaptive changes in behaviour by modulating its extensive connections with motor areas and could influence motivation via its contacts with subcortical areas such as the ventral tegmental area (VTA), a dopamine-producing brain area widely implicated in adaptive behaviour and motivation (Hamid et al., 2016; Schultz, 2016; Schultz, Dayan, & Montague, 1997). The experiments contained within this thesis aim to explore such a possibility.

1.2 Overview of ventral tegmental area

The ventral tegmental area (VTA) is a midbrain structure characterized by the presence of prefrontal-and-limbic-projecting dopamine-synthesizing neurons (Oades & Halliday, 1987). The VTA is often studied for its implication in a wide variety of functions such as reinforcement learning, motivation, aversion, natural or drug-related reward, mood, decision making, and related pathologies (Berridge, 2004; Morales & Margolis, 2017). This section aims to provide an overview of the anatomy and physiology which undergirds these core functions with a specific emphasis on motivation and decision-making.

1.2.1 *VTA anatomy*

First described by Tsai (1925), the VTA consists of glutamatergic, and gamma-amino-butric-acid (GABA)-containing, and dopaminergic (DA) neurons located in the midbrain, adjacent to the substantia nigra and the red nucleus (Oades & Halliday, 1987). The VTA consists of several nuclei and is typically defined by neurons expressing the DA-producing enzyme tyrosine hydroxlase (TH) and is conserved across mammals, including rats and humans (Fu et al., 2012; Hrabovszky et al., 2013; Figure 14A-D). The defining cytoarchitectural feature of VTA DA neurons is that their axons can originate from dendrites, rather than the soma, as is typical in most other neuron formations (Lapish, Kroener, Durstewitz, Lavin, & Seamans, 2007; Figure 14E). VTA DA neurons are also known to co-produce-and-release glutamate and GABA (Morales & Margolis, 2017; Seal & Edwards, 2006; Trudeau, 2004), suggesting broad heterogeneity of VTA structure and function.

The VTA exhibits a functional anterior-posterior (AP) gradient which was initially detected because local infusion of muscimol, a $GABA_A$ agonist, into the posterior VTA (pVTA) increased rodent locomotion activity whereas muscimol infusion into the anterior VTA (aVTA) did not (Arnt & Scheel-Kruger, 1979). Similar distinctions in behavioural outcomes have been reported for many other compounds infused into and manipulations of the aVTA and pVTA, respectively (see Table 1 in Sanchez-Catalan, Kaufling, Georges, Veinante, & Barrot, 2014). Consistent with the essential DAergic characterization of the VTA, DA-synthesising cell locations display a similar gradient, with an anteriorly skewed distribution within the VTA (Fu et al., 2012; see Figure 15). One prominent account of the VTA's AP gradient is that the posterior portion of the VTA is an inhibitory DA control centre; while this theory is robustly supported, many reports conflict regarding the functional specialisation and projection patterns of other areas within the VTA (see Ikemoto, 2007 for an excellent and thorough review). Thus, although the AP gradient in the VTA is functionally

and cytoarchitectonically characterised, it is unclear how the distinct microcircuitries within the VTA are functionally inter-related.

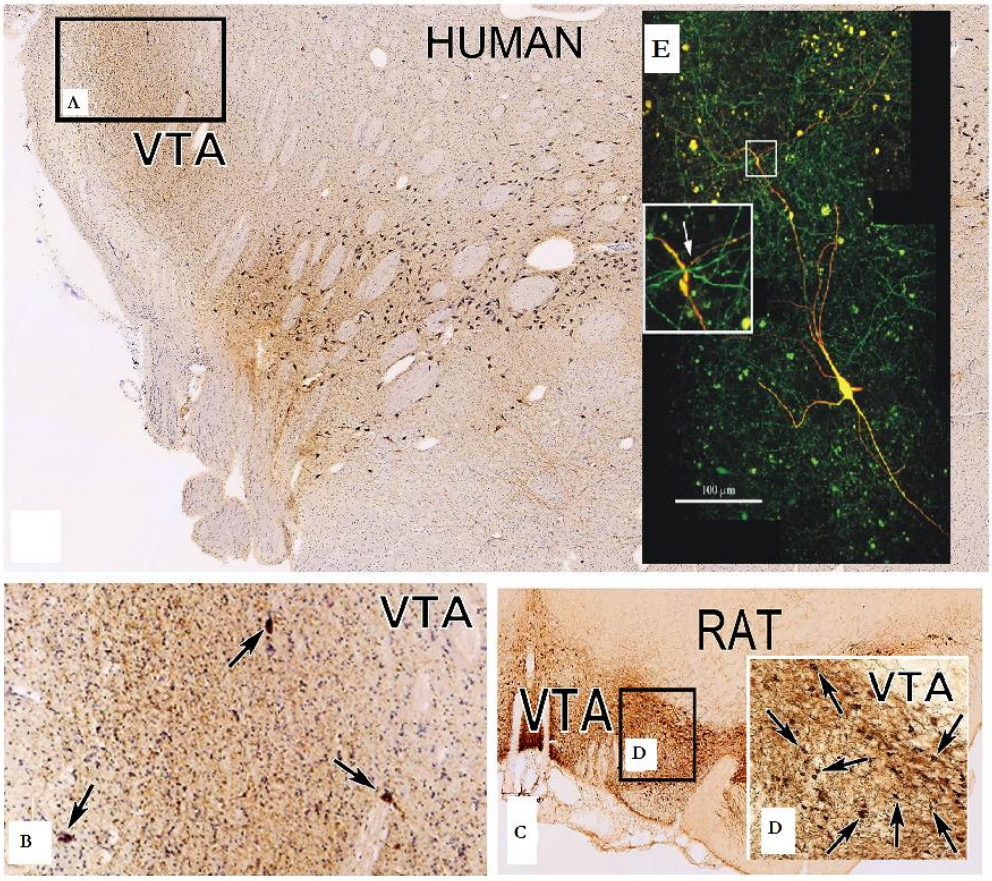

Figure 14. Tyrosine hydroxylase (TH) staining reveals dopamine neurons which define the VTA in the human and rat. **A.** Human brain section stained for TH with inset boxes showing the location of the VTA and substantia nigra. **B.** Magnified image of the box in A showing a relatively diffuse concentration of TH-positive neurons in the human VTA. **C.** Rat brain section stained for TH with inset showing the location of the VTA. **D.** Magnified image of the box in C showing that TH-positive neurons are densely arranged in the rat VTA. **E.** A mouse VTA neuron with green fluorescent protein under control of the TH promoter. This cell was injected with a red dye, resulting in a yellow colour. The insert is a magnified view of the boxed area in the main image. The arrow indicates the branching of an axon from a distally-located dendrite. A-D adapted from Hrabovszky et al. (2013); E adapted from Lapish, Kroener, Durstewitz, Lavin, & Seamans (2007).

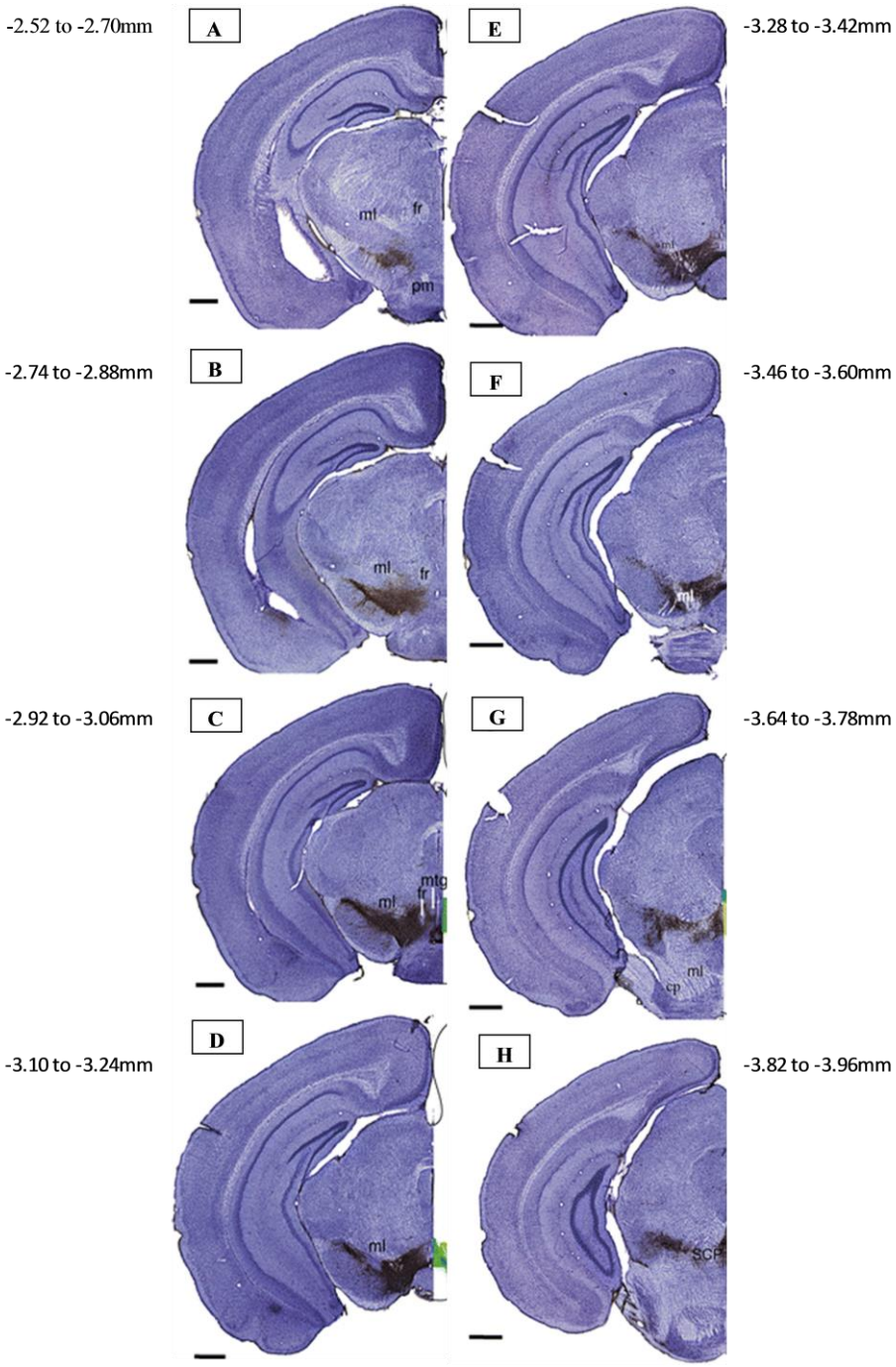

Figure 15. Anterior-posterior distribution gradient of dopamine synthesizing neurons in the mouse VTA. **A-H.** Sections of mouse brain stained for cell bodies (Nissl method; blue signal) and TH (brown signal) spanning most of the VTA; sections showing -4.00 to -4.60mm are omitted because almost no TH+ neurons in the VTA were detected. Coordinates are relative to bregma. Note maximal TH+ neurons from -2.92 to -3.42mm, panels B through E, which is slightly anterior compared to the whole length of the VTA. Adapted from Fu et al. (2012).

1.2.2 *VTA inputs and outputs*

The inputs and outputs of the VTA are, perhaps, some of the best characterised in the brain because their dysfunctions are implicated in numerous pathologies such as addiction, schizophrenia, obsessive-compulsive disorder, and depression (Dichter, Damiano, & Allen, 2012; Morales & Margolis, 2017; Narita et al., 2010; Navailles, Guillem, Vouillac-Mendoza, & Ahmed, 2015; Seeman & Seeman, 2014; Winton-Brown, Fusar-Poli, Ungless, & Howes, 2014; Yamaguchi, Wang, Li, Ng, & Morales, 2011). Morales & Margolis (2017) provide an excellent review of the inputs and outputs of the VTA (Figure 16).

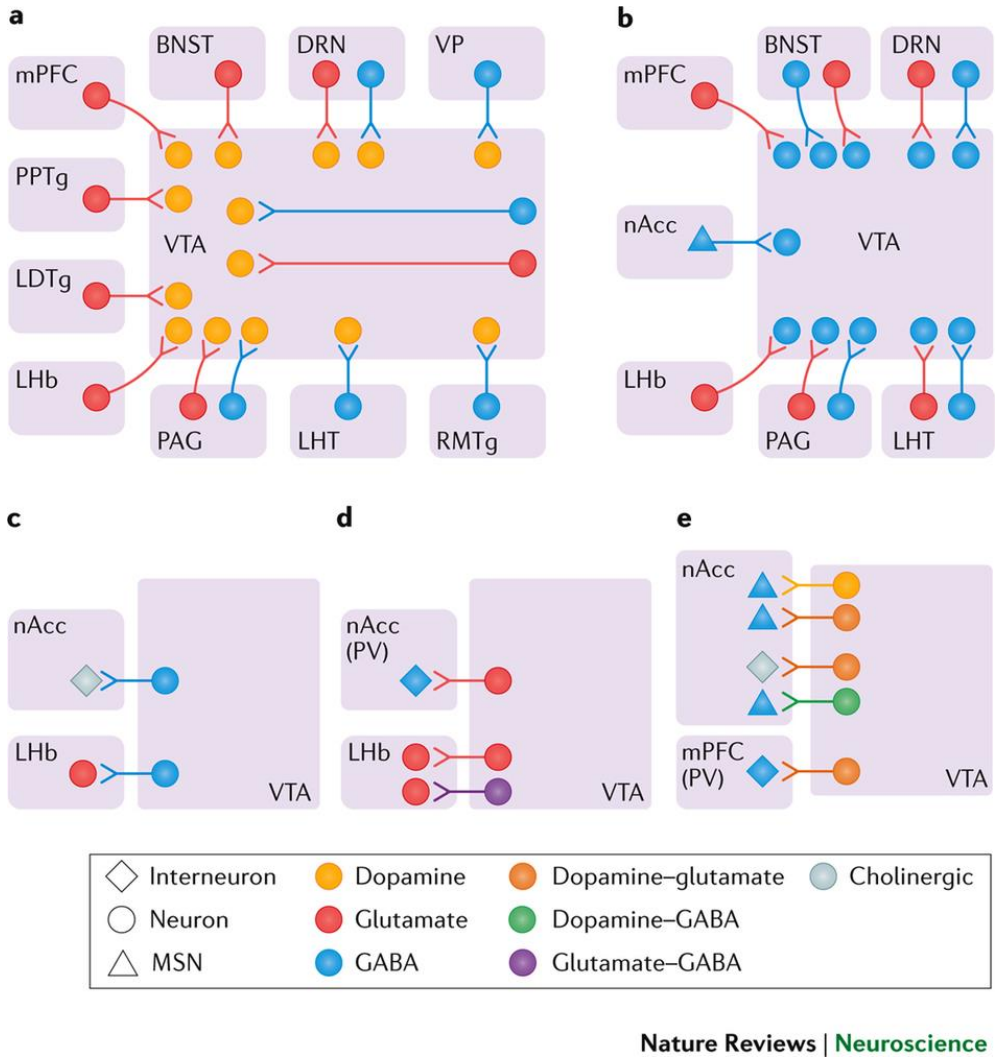

Figure 16. Confirmed inputs and outputs of the VTA. **A.** Glutamatergic inputs to VTA DA neurons include the medial prefrontal cortex (mPFC), including the ACC, pedunculopontine tegmentum (PPTg), laterodorsal tegmentum nucleus (LDTg), lateral habenula (LHb), periaqueductal grey (PAG), bed nucleus of the stria terminalis (BNST), and dorsal Raphe nucleus (DRN). GABAergic inputs to VTA DA neurons include the rostromedial mesopontine tegmental nucleus (RMTg; also known as the pVTA), PAG, DRN, lateral hypothalamus (LHT), and ventral pallidum (VP). Local intra-VTA glutamate and GABAergic circuits also exist. **B.** GABAergic VTA neurons receive glutamatergic input from LHT, PAG, LHb, mPFC, BNST, and DRN. The nucleus accumbens (nAcc) is the only documented structure with a purely GABAergic input to the VTA GABAergic neurons; LHT, PAG, BNST, and DRN projections arise from both GABAergic and glutamatergic neurons. **C-D.** Both VTA GABAergic and glutamatergic outputs project to nAcc and LHb, albeit with different targets. **E.** VTA DA neurons project to nAcc and mPFC, including the ACC. Image from (Morales & Margolis, 2017).

1.2.3 *VTA functions*

VTA neurons integrate complex inputs to encode multiple signals which influence motivation, cognition, reinforcement, and associated pathologies (Berridge, 2004; Morales & Margolis, 2017; Schultz, 2016; Schultz, 2007). This section will review key data implicating the VTA in motivation, prediction error, and task-state monitoring and will build to a position that the VTA dynamically encodes the value of engaging in or switching from a task with respect to past reinforcement history.

1.2.3.1 Motivation in the VTA

VTA neurons are strongly implicated in the motivation to obtain a reward in that they respond to reward cues and elevate their activity prior to the initiating a goal-directed behaviour (Fiorillo, Tobler, & Schultz, 2003; Ljungberg, Apicella, & Schultz, 1992; Schultz, 1998). Interestingly, VTA DA neurons transfer their response to the earliest reward-predicting stimulus over the course of learning (Figure 17). Inhibition of VTA DA neurons by optogenetic activation of pVTA GABAergic neurons during reward consumption disrupts reward consumption (van Zessen, Phillips, Budygin, & Stuber, 2012) and optogenetic activation of VTA DA neurons during reward consumption enhances generalization learning (Steinberg et al., 2013). Together, these findings suggest that neurons in the VTA are critically involved in the establishment and maintenance of goal-directed behaviour.

In a classic and seminal study, Olds & Milner, (1954) trained rats to press a lever to stimulate electrodes implanted in various locations in their brains (intracranial self-stimulation; ICSS). They found that rats would press at very high rates for a large proportion of the time animals were monitored when the electrodes were placed in the septal area, the medial geniculate nucleus, and the VTA (Figure 18A). Subsequent rodent studies (reviewed in Olds, 1958) found that VTA ICSS was so reinforcing for the animals that their lever press rates would exceed 7,000 presses per minute and that animals would elect to engage in VTA ICSS rather than eat, drink, or mate with a female rat in heat. VTA ICSS was so reinforcing that the animals frequently needed be removed from the testing apparatus to prevent their death by exhaustion. These data clearly indicate that the VTA in a critical component in the initiation and maintenance of goal-directed behaviour.

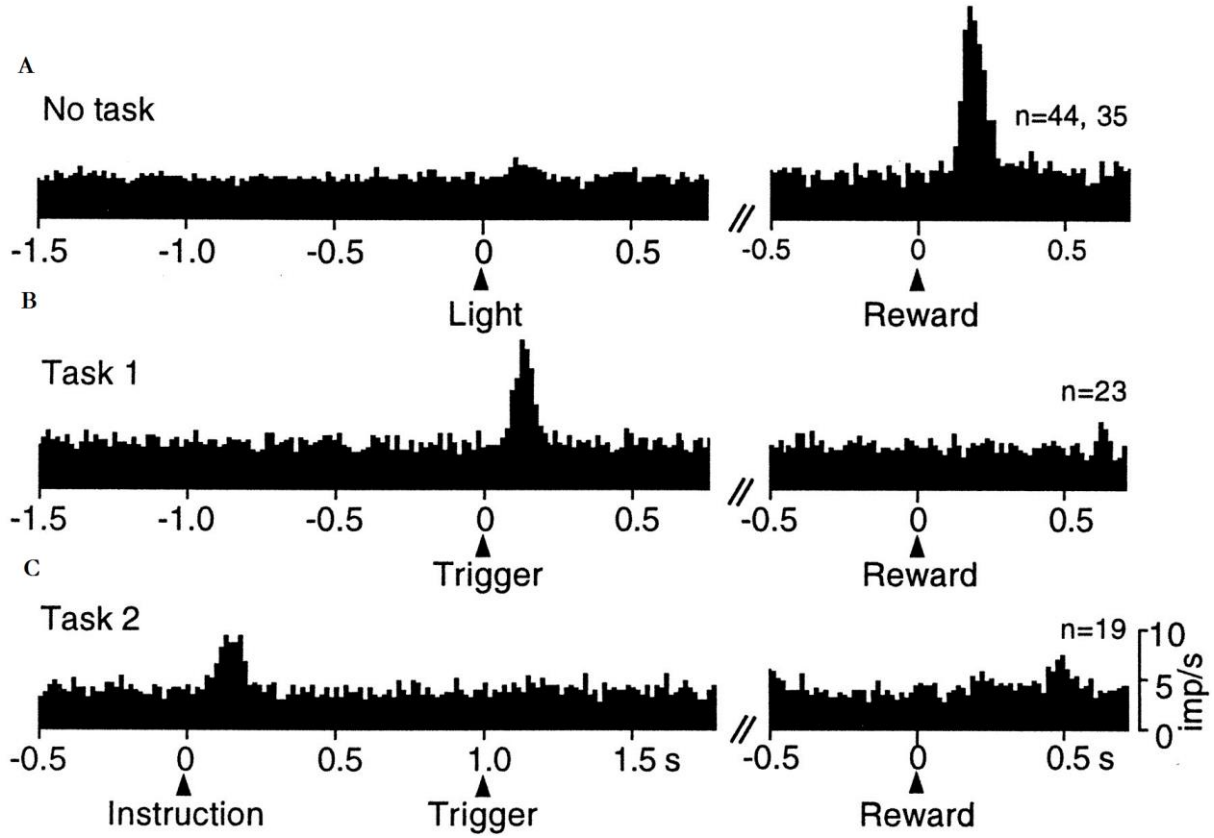

Figure 17. VTA DA neurons respond to the earliest stimulus predictive of reward. Data shown are peri-event histograms of normalized DA single-units contained within the VTA of Rhesus Macaque monkeys. **A.** VTA DA neurons respond do not respond to the illumination of a lamp when the lamp is not predictive of reward but do transiently respond to the delivery of reward. **B.** VTA DA neurons respond to a reward-triggering stimulus in a 2-choice spatial reaching task. These same cells do not respond to the reward itself. **C.** VTA DA neurons respond to an instruction cue preceding the onset of a reward-predicting trigger stimulus, as in B; VTA DA neurons respond to neither the trigger stimulus nor the reward itself. Adapted from Schultz (1998).

Studies of substance abuse and addiction also suggest that motivation is a core function of the VTA, specifically, its afferents to the nAcc and the mPFC, including the ACC (Narita et al., 2010; Nestler, 2005; Wanat, Willuhn, Clark, & Phillips, 2009; Wise, 2008). For example, DA concentrations measured in the nAcc, the output of VTA DA neurons, mediate the reinforcing effects and pursuit of psychostimulants, such as cocaine, and opiates, like heroin. Cocaine administration to VTA-ICSS trained rats dramatically increases the press rate and elevates simultaneously-recorded nAcc DA concentrations while the drug is in effect (Figure 18B,C; Phillips, Blaha, & Fibiger, 1989). Interestingly, intra-nAcc infusion of a dopaminergic antagonist causes mice trained to optogenetically self-stimulate their VTA to cease self-stimulation (Figure 19A, B). Taken together, these findings strongly suggest that the VTA and its received dopaminergic output are critically involved in reinforcement and motivation.

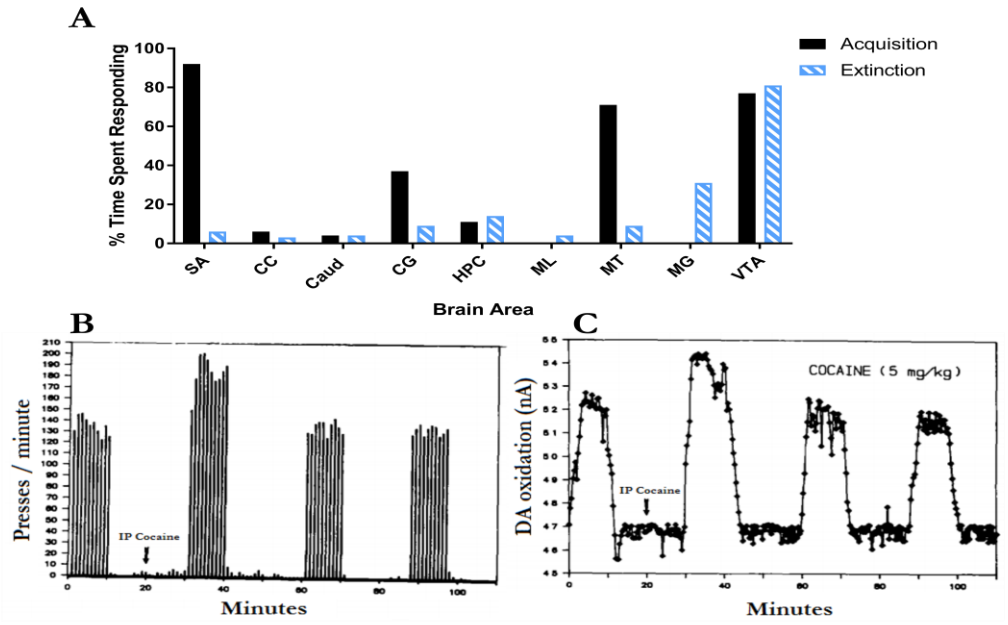

Figure 18. Intracranial self-stimulation of the VTA. **A.** Rats spent varying proportions of experimental sessions self-stimulating depending on where an implanted electrode was placed. SA, septal area; CC, corpus callosum; Caud, caudate nucleus; CG, cingulate gyrus; HPC, hippocampus; ML, medial lemniscus; MT, mammilothalamic tract; MG, medial geniculate nucleus; VTA, ventral tegmental area. **B.** Lever presses rate for VTA ICSS and **C.** simultaneously voltammetically recorded dopamine concentrations in the nucleus accumbens are elevated following cocaine administration. Arrows indicate time point of systemic cocaine administration via intraperitoneal (IP) injection. A. adapted from Olds & Milner (1954); B and C adapted from Phillips et al. (1989).

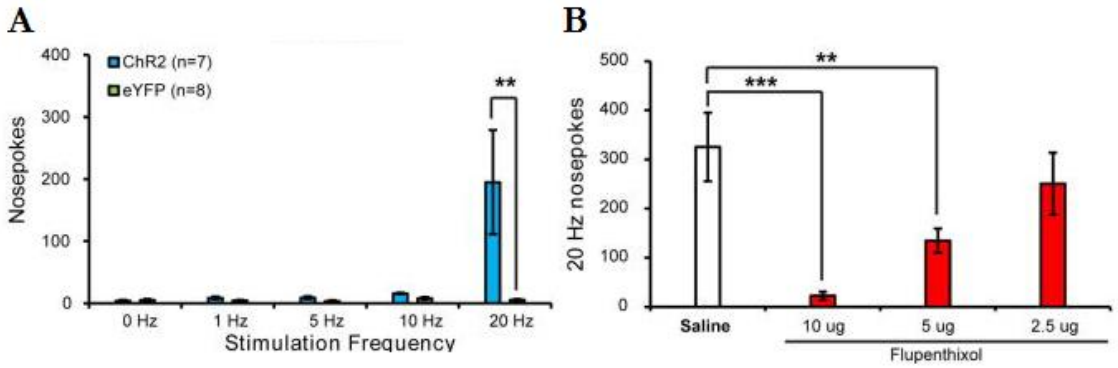

Figure 19. Mouse optogenetic self-stimulation of anterior-cortical input to the VTA is dose-dependently reduced by DA blockade in the nucleus accumbens. **A.** Mice expressing channel rhodopsin (ChR2) choose to self-stimulate excitatory inputs to the VTA at the largest available stimulation magnitude (20 Hz). **B.** Intra-accumbens infusion of flupenthixol, a general dopaminergic antagonist, dose-dependently reduces optogenetic self-stimulation of excitatory projections to the VTA.

1.2.4 *Prediction error in the VTA*

Dopamine neurons in the VTA are thought to signal predictions of future outcomes and discrepancies between such predictions and actual outcomes (Figure 20; Eshel, Tian, Bukwich, & Uchida, 2016; Schultz et al., 1997). Eshel et al. (2016) conducted a series of experiments which elegantly demonstrated the response properties of VTA DA neurons in the context of prediction error. The experimenters trained mice with electrodes implanted in their VTAs to associate different odors with different probabilities of receiving a reward (Figure 20A). After classifying which recorded cells were DA neurons, Eshel et al. (2016) found that VTA DA neurons respond most strongly to odor cues indicating a high probability of reward and that these same cells responded minimally to odor cues indicating a low probability of reward (Figure 20B). However, when an unexpected outcome occurred, such as a low-probability trial resulting in a reward, VTA DA neurons exhibited a transient burst of activity (Figure 20B). This pattern of firing activity - when the animal's prediction that it would not be rewarded on a trial was violated – is what is termed a prediction error. Interestingly, VTA DA neurons appear to scale the magnitude of the prediction error response with the magnitude of the reward which might be attained. VTA DA neurons also exhibit prediction error responses to trial outcomes which are not reward related. For example, Eshel et al. (2016) trained another set of mice to associate a given set of odors with the chances of receiving rewards; however, on some high-probability trials, instead of delivering a reward, an aversive puff of air was delivered. VTA DA neurons exhibited a similar prediction error-like response to these aversive outcomes (Figure 20D). Considering VTA DA's role in motivation, prediction errors are often interpreted as enabling an organism to learn what is rewarding and what is aversive and to pursue those rewards and avoid those aversive outcomes (Pan, Schmidt, Wickens, & Hyland, 2008; Bromberg-Martin, Matsumoto, & Hikosaka, 2010; Schultz, 2016; Wise, 2004).

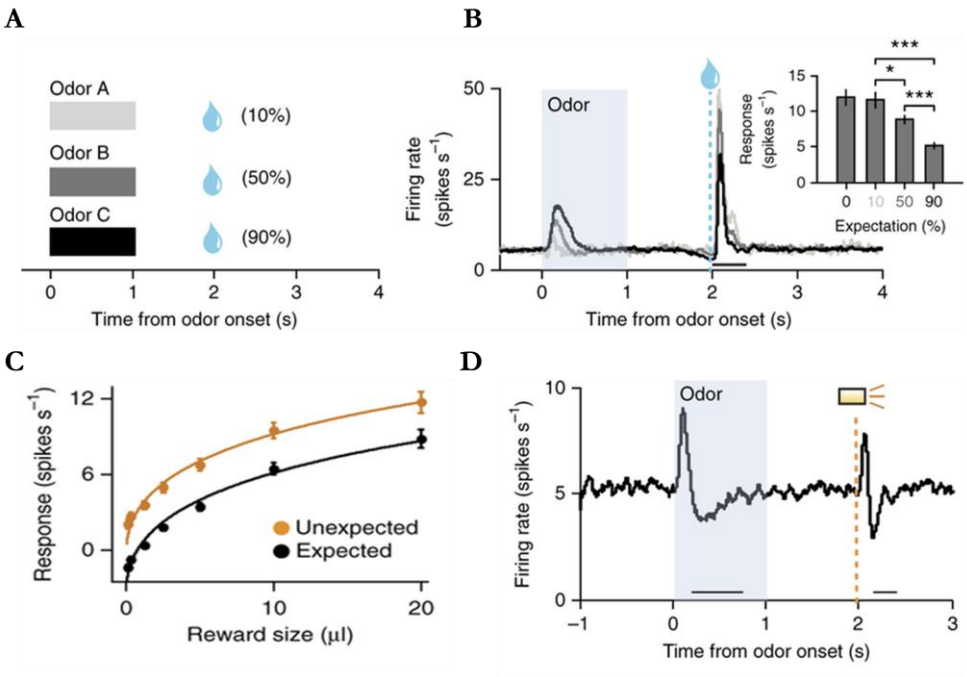

Figure 20. Examples and properties of prediction error in VTA DA neurons. **A.** Schematic of task indicating the different reward probabilities associated with each odor. This panel also indicates that trial outcomes (e.g. reward) occurred one second after the end of the one second odor presentation. **B.** VTA DA firing patterns with respect to the odor-reward probabilities and trial outcomes. **C.** Summarization of VTA DA response properties with respect to the magnitude of reward, and likelihood of receiving that reward. **D.** VTA DA neurons strongly respond to the onset of an aversive trial outcome. Adapted from Eshel et al. (2016).

1.2.5 *Ramping dopaminergic output from the VTA to the nAcc*

Several recent studies report 'ramping' patterns of DAergic output from the VTA to the nAcc as an animal approaches a goal (Howe, Tierney, Sandberg, Phillips, & Graybiel, 2013) and that this ramping is modulated by whether or not a given trial will or will not be rewarded (Hamid et al., 2016). In the first of these studies, Howe et al. (2013) recorded nAcc dopamine concentrations ([DA]; Figure 21A), the output of the VTA, via fast-scan cyclic voltammetry (FSCV) in rats trained to complete a cue-guided T-maze. When the rats reached the vertex of the maze, an auditory cue indicated whether to turn left or right. Howe et al. (2013) anticipated to detect a transient increase in [DA] concomitant with the onset of the cue; although they did detect this, more interestingly, they found that [DA] 'ramped up' as animals approached the goal and that the transient response to the cue was superimposed onto that 'ramp' (Figure 21B). The authors suggested that the ramping [DA] might indicate either spatial proximity to a goal or, perhaps, the time-elapsed since beginning the trial. Several findings suggest that this signal indicates the spatial proximity rather than time-elapsed. Firstly, the authors exploited the trial-to-trial variability in the time rats took to complete the task and compared fast, short trials to slow, long trials. They found that the peak [DA] in the goal location was generally the same, regardless of the time the animal took to complete the trial, suggesting that this signal is more indicative of spatial proximity than time-elapsed

(Figure 21B). Additional compelling evidence that these ramps are spatially modulated comes from trials where the rat stopped and groomed itself (Figure 21C). When the animal halted progress towards the goal, [DA] concentrations also plateaued; when the animal resumed its course towards the goal, [DA] similarly resumed increasing (Figure 21D). Taken together, these findings suggest that the VTA DA, as measured via its output to the nAcc, might enable an organism to track progress towards a goal. However, it was unclear from these findings whether VTA truly is the source of the [DA] ramps and whether these ramps were responsive to variable reward probabilities and outcomes, which might link this new finding to the VTA literature concerning prediction error.

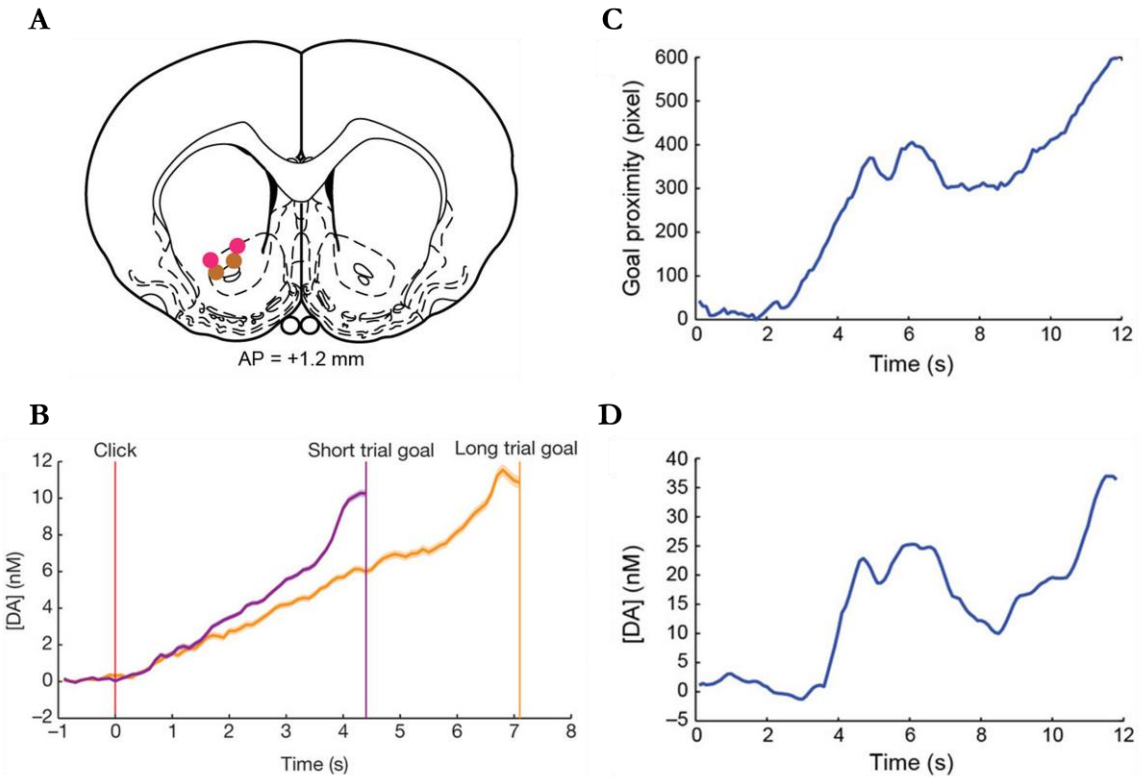

Figure 21. Ramping DA signals in the nucleus accumbens track an animal's progress towards a goal. **A.** Schematic indicating FSCV recording position in the nAcc. **B.** Dopamine concentrations in the nAcc peaked at similar levels upon goal-reaching regardless of the time rats took to reach the reward. **C.** Example of a trial where a rat stopped mid-trial; **D.** [DA] time-locked to C illustrating that when the rat paused in goal pursuit, [DA] plateaued and resumed increasing when the animal resumed goal-pursuit. Adapted from Howe et al. (2013).

Hamid et al. (2016) addressed this possibility by recording nAcc [DA] in rats trained in a two-armed bandit task. Briefly, rats were cued at the initiation of a trial by the illumination of a light; rats would then nose-poke into a central port and wait for an auditory cue which indicated the rat ought to nose-poke into the adjacent left or right port. Importantly, the cue only indicated 'go' and did not signal which port was rewarded (Figure 22A). After

making a choice, the rat had to maintain his nosepoke for 2 seconds; if the choice was rewarded, a food reward was dispensed on the other side of the chamber with an accompanying auditory click. The absence of a click indicated an unrewarded outcome to the rat. The probability of a given port being rewarded changed throughout an experimental session; thus, the animals were constantly sampling and updating their expectations about which choice was ideal.

Hamid et al. (2016) found that unexpected delivery of reward following several unrewarded trials elicited large fluxes of nAcc [DA], that the presentation of reward after increasingly fewer unrewarded trials reduced this effect in a graded manner, and that [DA] abruptly decreased when the reinforcer-associated click was omitted (Figure 22B). Such probability-modulated responses are consistent with the concept of prediction error. However, that [DA]s dropped when the reward was unexpectedly unavailable suggests that the theory of prediction error cannot fully account for these findings. The authors trained a machine-learning model on the data and concluded that this signal indicates an instantaneous value state – the value of working – which is modulated by prior outcomes.

To determine whether the changes in nAcc [DA] are changes in VTA DA neuron output, the authors optogenetically stimulated the VTA and simultaneously recorded nAcc [DA]. They found that nAcc [DA] increased as the magnitude of VTA stimulation increased (Figure 22C). This indicates that the changes in nAcc [DA] measured via FSCV are indeed a readout of VTA DA output. To verify the causal impact of VTA activity on choice preference and motivation, the authors paired either excitatory or inhibitory VTA DA neuron photostimulation with side-in, choice nosepokes. They found that excitatory photostimulation

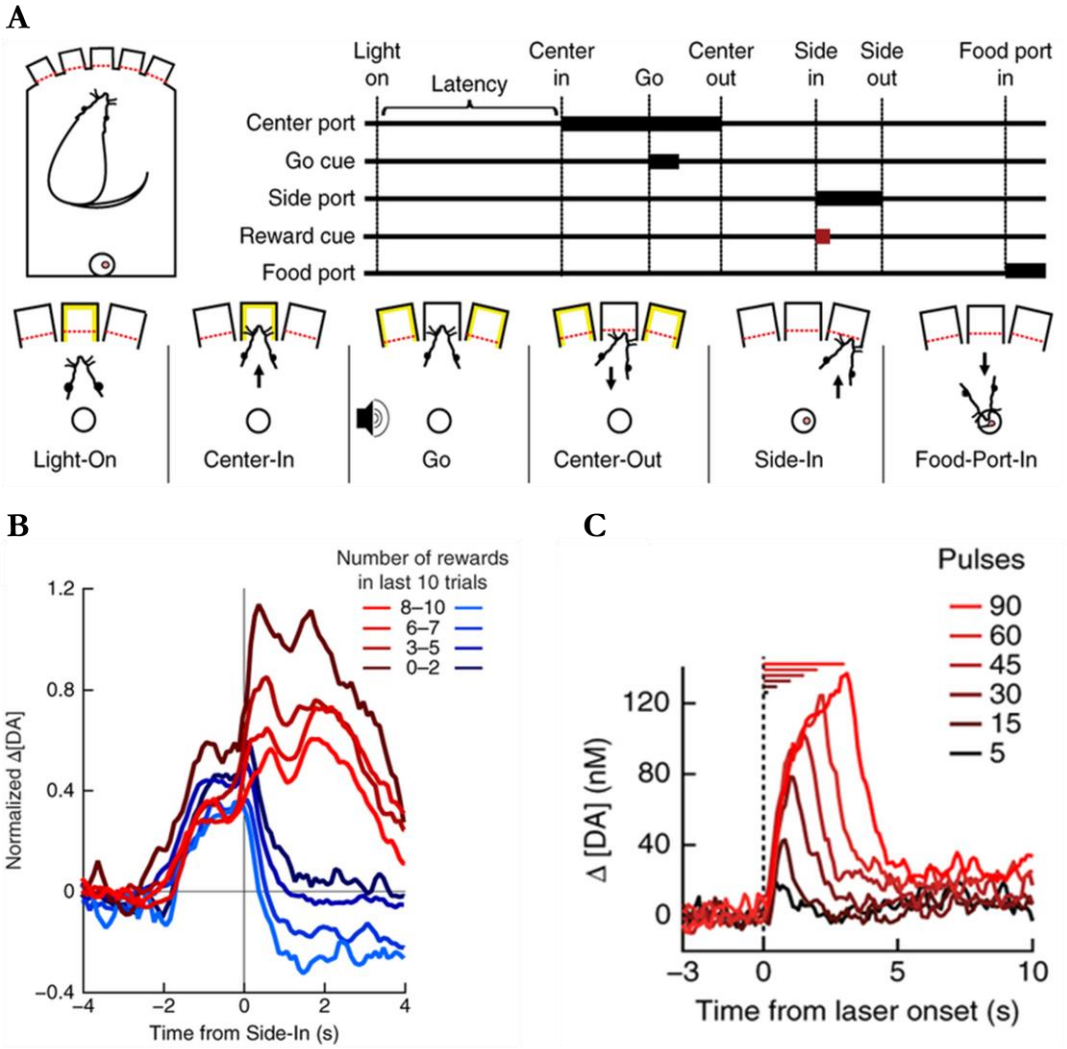

Figure 22. Nucleus accumbens DA concentrations are outputs of the VTA and modulated by trial outcomes. **A.** Schematic of task. **B.** Probability-modulated responses of nAcc recorded via FSCV. **C.** Changes in nAcc [DA] increased as number of 30 Hz optogenetic pulses of the VTA increased, indicating that the VTA is the source of DA measured in the nAcc. Adapted from Hamid et al. (2016).

of VTA DA neurons when the animal made a decision-nosepoke increased the probability that rats would repeat that same choice (Figure 23A; conversely, photoinhibition of VTA DA neurons during decision-nosepokes decreased the probability that rats would repeat that same decision (Figure 23B). Interestingly, VTA DA neuron photostimulation decreased the latency to trial initiation (Figure 23C), increasing the likelihood that rats would start a new trial sooner than trials when VTA DA neurons were not stimulated (Figure 23D), indicating that VTA DA photostimulation effects the motivation to pursue a reward. Taken together, these findings provide causal evidence that the VTA is critically involved motivation and decision-making and suggest that the representation and updating of a state thought to indicate the value of work is an essential function of the VTA. Thus, this paper agrees with prior claims that prediction errors are a mechanism by which an internal value state is updated (Bromberg-Martin, Matsumoto, & Hikosaka, 2010; Schultz, 2016; Wise, 2004) and are important because

they provide the first evidence that this putative value state is both represented and updated at the level of the midbrain.

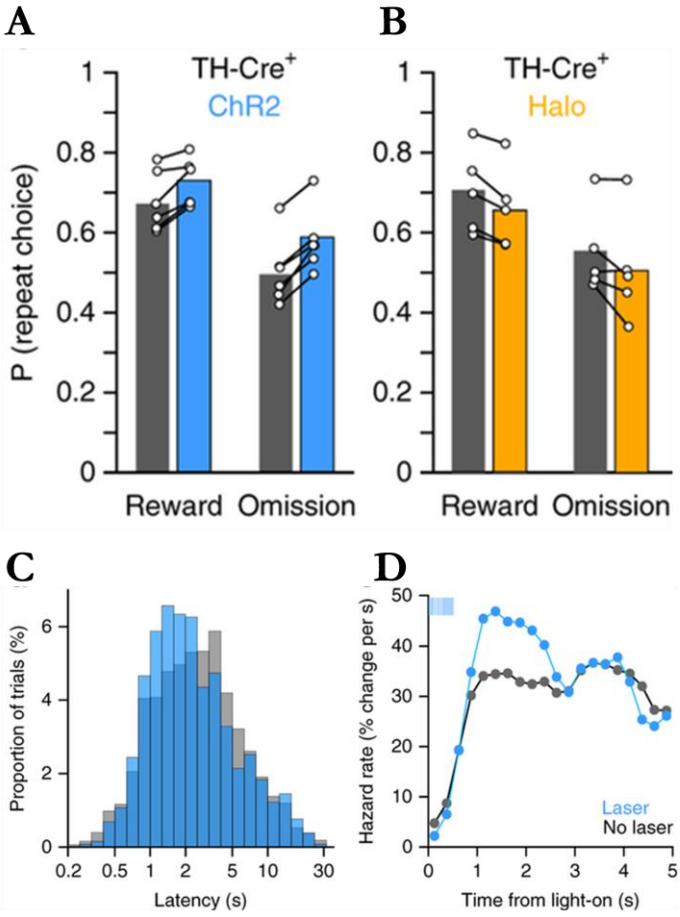

Figure 23. Effects of photostimulation and photoinhibition of VTA DA neurons on decision making and motivation. **A.** Photostimulation of VTA DA neurons increases the likelihood rats will repeat their prior decision, regardless of whether the trial was rewarded or not. **B.** Photoinhibition of VTA DA neurons decreases the probability that rats will repeat their prior choice, regardless of the trial outcome. **C.** Photostimulation of VTA DA neurons decreases the latency to begin a new trial. **D.** Photostimulation of VTA DA neurons increases the likelihood that rats will begin a new trial, sooner (same data as C). Adapted from Hamid et al. (2016).

1.2.6 *Summary of VTA*

In summary, the VTA appears to facilitate reinforcement and the motivation to pursue a reward. The VTA also appears to track the correspondence between predicted and actual outcomes of situations, perhaps enabling organisms to update its neuronal representations. Recent voltammetry studies in the rat nAcc suggest an integrative theory of VTA function: the VTA responds to behaviourally relevant cues and trial outcomes which have the potential to remodel internal representations and modulate motivation. Despite the evidence implicating the VTA in these functions, the inputs driving them and the intra-VTA microcircuitry enabling them are unclear. One question of particular interest for this thesis concerns the role of the ACC in modulating the VTA in the contexts of motivation and decision making. The next section will address this directly.

1.3 The ACC-VTA projection as a candidate signalling pathway for translating cortical signals into motivational signals

Given the functional similarities of the ACC and VTA, the question remains of their structural and physiological relationships. This section will aim to provide an overview of the anatomical and physiological relationships between the ACC and to make the case that the ACC and VTA likely interact in various behavioural contexts, especially in motivation.

1.3.1 *Anatomical and physiological evidence of connectivity between the ACC and the VTA*

Anatomical and electrophysiological evidence indicate that the ACC and VTA are reciprocally connected. Scanning electron micrographs of the VTA in rats in which the anterograde tracer biotinylated dextran amine (BDA) was injected into the mPFC, including the ACC, reveal monosynaptic projections to both DAergic (Figure 24A) and GABAergic (Figure 24B) neurons (David B. Carr & Sesack, 2000). Electrical stimulation of the ACC elicits burst firing in VTA DA neurons (Gariano & Groves, 1988; Figure 24C) and, furthermore, the temporal activation patterns of VTA DA neurons are closely related to the phase of the mPFC LFP (Gao Liu, Chang-Liang, Jin, Guo-Zhang, Bunney, Benjamin, S., Shi, Wei-Xing, 2007; Figure 24D). Together, these data strongly suggest that the ACC and the VTA are functionally connected.

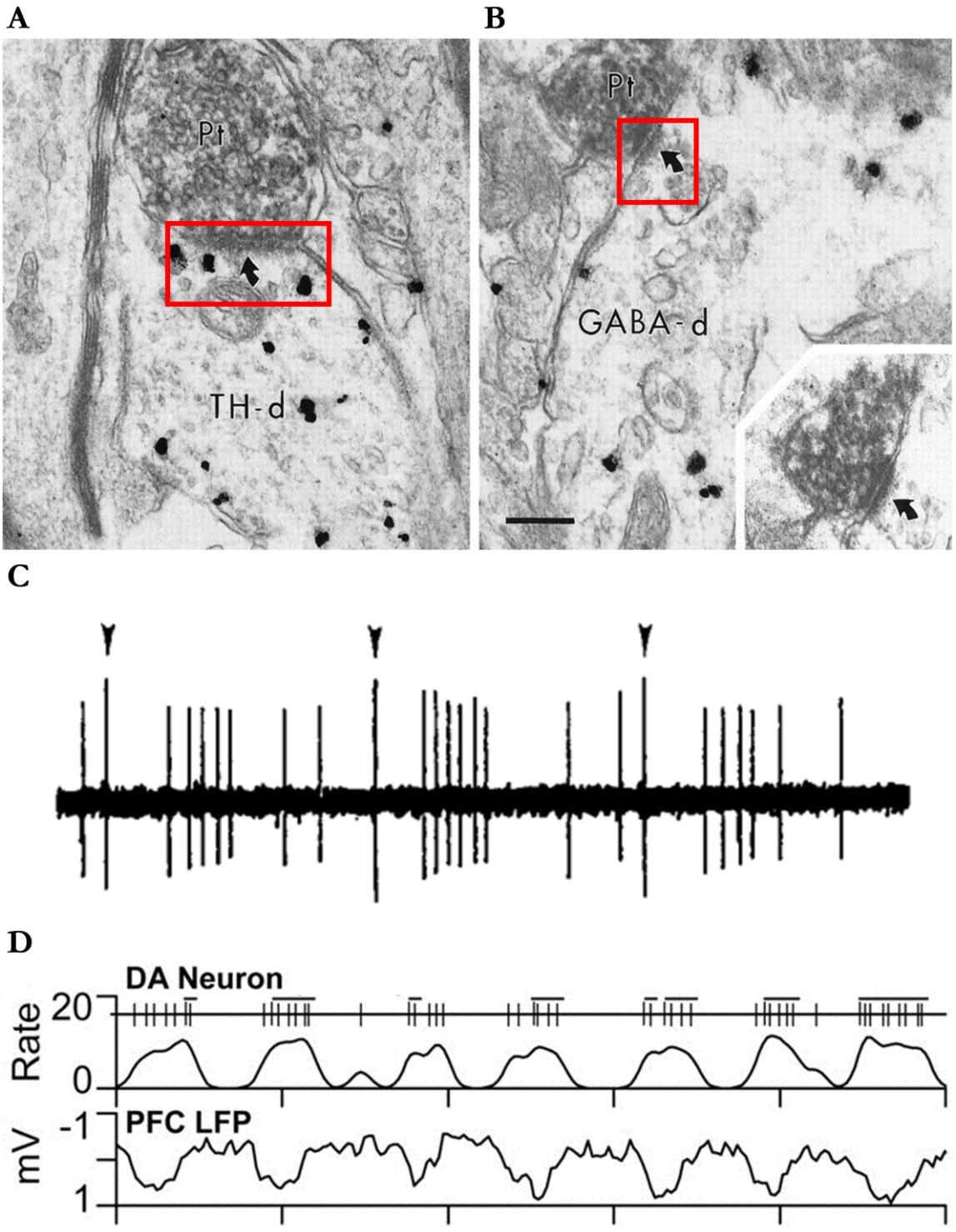

Figure 24. Anatomical and physiological evidence of ACC-VTA connectivity. **A.** Scanning electron micrograph of a VTA TH+ (i.e. dopaminergic) neuron which receives a monosynaptic input (red boxed area) from the mPFC. **B.** Scanning electron micrograph of a GABAergic neuron which receives monosynaptic input (red boxed area) from the mPFC. **C**. Recorded trace from a VTA DA neuron showing that ACC stimulation, indicated by the arrows, induces burst firing. **D.** Traces from a VTA DA neuron and the local field potential (LFP) of the mPFC of an anaesthetized rat. DA neuron firing and bursting are strongly phase-locked to the mPFC LFP. A and B are from Carr & Sesack (2000); C is from Gariano & Groves (1988); D is from Gao et al. (2007).

1.3.2 *Evidence for ACC-VTA communication during behaviour*

Despite the well-documented roles of the ACC and VTA in prediction error and task-switching (Bryden et al., 2011; Eshel et al., 2016; Nils Kolling et al., 2016; Roesch & Bryden, 2011), no study to date has jointly assessed the relationship between the ACC and VTA in freely moving organisms. However, prior experiments examining the prefrontal cortex, more broadly, suggest that the ACC and VTA do communicate in behaviourally relevant contexts. For instance, Fujisawa & Buzsaki (2011) simultaneously recorded mPFC, including ACC, and VTA LFPs and single units in rats performing a match-to-sample working memory task and found that the mPFC and VTA were highly synchronized at 4Hz during the working-memory component of the task (Figure 25A). In another interesting experiment, Ballard et al. (2011) used fMRI to monitor cortical and VTA activity of human participants as they performed a task which selectively manipulated their motivation to pursue a course of action. In Ballard et al. (2011)'s experiment, participants were signalled the opportunity to earn various amounts of money, either $0 or $4, as compensation for a fast reaction time to an upcoming target. Following a variable delay (4-4.5s), participants were presented with a target and were then to press a button as quickly as possible. Ballard et al. (2011) found that participants reacted faster, indicating greater motivation, when they worked for their own benefit. Strikingly, through the use of dynamic causal modelling, Ballard et al. (2011) detected enhanced cortical control of the VTA during high-motivation trials, concluding that cortical → VTA signalling may initiate motivated behaviour (Figure 25B).

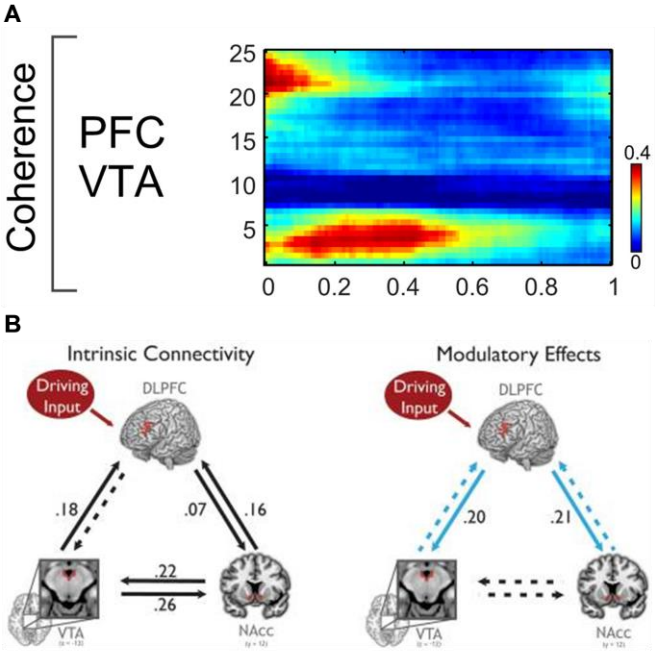

Figure 25. Examples of cortical-VTA communication during behaviour. **A.** The rat mPFC and VTA are synchronized at 4Hz during engagement of working memory in a match to sample task. **B.** The dorsolateral prefrontal cortex drives VTA activity during high motivation tasks. A adapted from Fujisawa & Buzsaki (2011); B is from Ballard et al. (2011).

1.3.1 *Summary of the ACC and VTA and thesis aim*

Robust anatomical and electrophysiological evidence indicate that the ACC and VTA are functionally linked and that top-down, ACC → VTA signalling may be involved in initiation of motivated behaviour. Despite these indications, no prior studies had jointly examined the activity of the ACC and VTA in freely moving animals. Thus, the aim of this thesis was to investigate the electrophysiological relationships between the ACC and VTA in a variety of contexts, all of which would require context-dependent changes in motivation. Specifically, the purpose of these experiments was to determine (i) whether the ACC modulates the VTA in freely moving animals, (ii) whether changes in ACC modulation of the VTA are related to changes in motivation, (iii) to directly observe ACC task models at the level of individual neurons, and (iv) to assess possible mechanisms by which ACC neuronal task models are modified. The guiding notion of this thesis was that if the ACC does encode task models and if ACC modulation of the VTA is a mechanism by which changes in those task models are behaviourally implemented, ACC modulation of the VTA should be detected in circumstances where organisms modify their behaviour.

Chapter 2 ACC modulation of the VTA in an effort task*

2.1 Summary

Information gained during goal pursuit motivates adaptive behaviour. The anterior cingulate cortex (ACC) supports adaptive behaviour, but how ACC signals are translated into motivational signals remains unclear. Rats implanted with recording electrodes in the ACC and ventral tegmental area (VTA), a dopaminergic brain area implicated in motivation, were trained to run laps around a rectangular track for a fixed reward, where each lap varied in physical effort (a 30cm climbable barrier). Partial directed coherence analysis of local field potentials revealed that ACC theta (4-12 Hz) activity increased as rats entered the barrier-containing region of the maze on trials when the barrier was absent, and predicted similar changes in VTA theta. This did not occur on effortful, barrier-present trials. These data suggest that ACC provides a top-down modulating signal to the VTA which can influence the motivation with which to pursue a reward. *****This chapter was published as:

Elston, TW., & Bilkey, DK. (2017). Anterior cingulate cortex modulation of the ventral tegmental area in an effort task. *Cell Reports*, 19(11), 2220–2230.

2.2 Introduction

Adaptation to changing circumstances is a common, critical consideration in nature (Darwin, 1865); however, the neural mechanisms enabling adaptive goal-directed behaviour have yet to be fully elucidated. The anterior cingulate cortex (ACC), a subregion of the anterior medial prefrontal cortex (AC; Vogt & Paxinos, 2014), has previously been shown to have a role in commitment to a course of action (Blanchard et al., 2015; Ma, Hyman, Phillips, et al., 2014) and encoding value associated with physical effort (Cowen, Davis, & Nitz, 2012; Friedman et al., 2015; Hillman & Bilkey, 2010; Parvizi, Rangarajan, Shirer, Desai, & Greicius, 2013; Rudebeck, Walton, Smyth, Bannerman, & Rushworth, 2009; Walton, Devlin, & Rushworth, 2003). Furthermore, ACC signals received reward, predictions of future reward, and errors in such predictions (Bryden et al., 2011; Gemba et al., 1986; Kennerly et al., 2011). These signals are thought to facilitate the integration of new information into existing internal representations which can motivate and modify future behaviour (Bryden et al., 2011; Cavanagh et al., 2010; Kolling, Behrens, Wittmann, & Rushworth, 2016b). However, it remains unclear how ACC activity is translated into an adaptive, motivational signal.

The ACC and the anterior portions of the medial prefrontal cortex are potentially able to exert direct top-down control over the ventral tegmental area (VTA) via monosynaptic

glutamatergic afferents (Beier et al., 2015; David B. Carr & Sesack, 2000; Faget et al., 2016; Ferenczi et al., 2016; Gariano & Groves, 1988; Jo, Lee, & Mizumori, 2013; Taber, Das, & Fibiger, 1995). Moreover, in anaesthetised rats, ACC stimulation elicits burst firing in VTA dopamine neurons (Gariano & Groves, 1988). The VTA is a major source of dopamine to the basal ganglia and is hypothesized to convey a motivational signal indicating progress towards and value of a future goal (Hamid et al., 2016; Howe et al., 2013; Morales & Margolis, 2017; Salamone & Correa, 2012). Large, transient bursts of single unit activity have also been reported in rodent in both ACC and VTA when an outcome is different than predicted (Bryden et al., 2011; Eshel et al., 2016). Strikingly, the magnitude of the activity increase correlates with the prediction-outcome error difference in both regions (Bryden et al., 2011; Eshel et al., 2015; Kennerly et al., 2011) suggesting that both these regions are involved in reward prediction error processes (Schultz et al., 1997). Thus, ACC top-down control over dopaminergic subcortical regions, such as the VTA, is a plausible mechanism by which ACC signals are translated into motivational signals.

Although no prior study has jointly examined the relationship between the ACC and VTA in the freely moving rat, prior investigations of anterior cortical (AC) and VTA communication suggest that these structures communicate via oscillations in the theta band (4-12 Hz). For example, firing in VTA dopamine neurons is modulated by the phase of AC theta oscillations and AC-VTA synchronization in the theta band is strongly correlated with working memory performance. However, to date, the precise relationship between the ACC and VTA and how these signals might shape future behaviour remains unknown.

To address this question directly, we monitored ACC and VTA local field potentials (LFPs) of rats trained to run laps around a rectangular track for a fixed reward, where each lap varied in physical effort (Figure 26). The effortful condition required rats to climb over a 30cm barrier while no barrier was present in the non-effortful condition. We examined task-dependent changes in theta (4-12 Hz) power and coherence and also assessed the directionality of communication between ACC and VTA via partial directed coherence (PDC), a multivariate autoregressive modelling approach which provides a frequency-resolved estimate of Granger causality (Baccalá & Sameshima, 2001; Boykin, Khargonekar, Carney, Ogle, & Talathi, 2012).

2.3 Experimental procedures

2.3.1 *Subjects and animal use statement*

All experimental procedures have been reviewed and approved by the University of Otago Animal Welfare Office. Seven male Sprague Dawley rats (Hercus-Taieri Resource Unit) between 6 and 8 months of age, weighing 450-550 g were used in the study. Rats were single housed in translucent plastic cages containing pine chips and maintained on a 12 h light/dark cycle. All training and experimentation occurred during the light phase. After 2 weeks of daily handling and weighing, animals were food deprived of standard rat chow (Specialty Feeds) to no less than 85% of their free-feeding weight to promote interest in food reward during test phases. Water was available *ad libitum* in the home cage.

2.3.2 *Preoperative training*

During the initial week of training, rats were individually habituated for 15 min/d to the experimental apparatus, a rectangular runway with a reward area which contained touchscreens, photobeams, and a retractable 30cm barrier mounted on a servo motor (Figure 26A). The apparatus was controlled by a network of four Arduino (Arduino LLC, Somerville, MA, USA) microcontrollers. Cereal pellets (Coco Pop cereal; Kellogg's) were scattered throughout the maze to encourage exploration. In the second week of training, cereal pellets were only available at the reward site and rats were trained to run the maze in a unidirectional manner, starting at the bottom of the midstem (i.e. the startbox) and received a fixed reward (3 cocopops) in a distinct reward zone. Rats were prevented from reversing course in the maze by photobeam-controlled doors. The rats were not paused between trials and set their own pace, running in a continuous, uninterrupted manner.

Once the rats were running unidirectionally around the apparatus, they were trained to press a wall-mounted touchscreen to release an adjacent starting gate and thereby initiate a new trial. This typically took two 15 minute training sessions or less. A two-second delay was then introduced between the initial press and the lowering of the start gate. Screen-press training was considered complete when rats ran >30 trials/session (2/min) across 3 consecutive training sessions. This typically took one week of training.

The final stage of training involved the introduction of a 30cm barrier (a triangular piece of Styrofoam with an affixed strip of garden trestle) into the apparatus which rats had to overcome on their route to the reward zone. The barrier was inserted into the maze by a servo motor. Rats were cued as to whether the upcoming trial was an effortful, barrier trial or a non-effortful, flat trial by images delivered on the touch screen. The screen displayed three

flashing green horizontal bars on a black background across the screen to indicate a barrier trial and a single non-flashing white bar on a magenta background to indicate a flat trial. To provide auditory camouflage for barrier insertion, the barrier was placed into the maze at the same instant the start gate was opened. Once rats were running >30 trials/session, sessions were extended such that each session required rats to run 120 laps composed of 60 trials without the barrier present (flat trials) and 60 barrier trials presented in pseudo-random order. Rats were considered fully trained when they were running 120 trials within 60 minutes (2 trials/min).

2.3.3 *Surgery*

Once animals were considered trained, five rats were anaesthetized under isoflurane and stereotaxically implanted in the ACC (AP: 2.7mm, ML: 0.4mm, DV: -1.8mm from dura) with seven 25 µm Formvar-coated nichrome wires (California Fine Wire) mounted on a 3D-printed adjustable microdrive assembly and the VTA (AP: -5.3mm, ML: 1.0mm, DV: -8.2mm from dura) with a one non-moveable 127-µm-diameter, nickel-chromium coated wire. Two rats were also implanted at the same ACC coordinate with the microdrive assembly but with a second electrode (a fixed 127-µm-diameter, nickel-chromium coated wire) located in the dorsal CA1 subregion of the hippocampus (AP: -3.6mm, ML: 2.0mm, DV: -2.8mm from dura). The electrodes were grounded by soldering a wire to a jewellers screw implanted in the cerebellum. The assembly was fasted to the skull with jeweller's screws and acrylic dental cement. Following the surgery, animals were allowed 10 days to recover during which they had *ad libitum* food and water. After 10 days, rats' food was reduced to maintain the animal at ~85% of their free-feeding weight to optimize behaviour during the experiment.

2.3.4 *Postoperative training and protocol*

After 10 days of recovery, rats were reintroduced to the maze with the head plugs connected to a tethered head stage that housed three light emitting diodes (LEDs) for tracking. Training resumed from the final preoperative stage; all 7 rats quickly recalled the task with no signs of postoperative motor impairment. Once each rat demonstrated three consecutive sessions of 120 trials in less than one hour, data acquisition began.

The data acquisition protocol consisted of a three stage, 'ABA' design where rats completed 100 trials per day (Figure 26B). During the first seven days (phase B1), the barrier was present in 50% of trials. In B1, a touchscreen press triggered a cue-presentation on the touchscreen, signalling which trial type was to commence. Phase B1 was followed by Phase 2 which lasted three days and during which the barrier was either not present (0%; n=5 animals) or always present (100%; n=2 animals, rats D and E) present for individual rats. Screen

presses in phase 2 triggered cue presentation as in B1, however, these cues were irrelevant to the upcoming trial type (i.e. cues indicating flat trials and barrier trials were presented even though the barrier was either always or never present). Phase 2 was followed by three days of phase B2, in which the barrier was present in 50% of trials (identical to phase B1). All seven rats experienced B1 and B2 identically. It should be noted that the rats probably did not attend to the touchscreen cues as we found no behavioural or electrophysiological evidence that the cues themselves elicited any specific response. Thus, in the interest of clarity, we labelled trials in B1 and B2 as either 'flat trials' or 'barrier trials,' in accordance with what occurred on a trial. Trials in phase 2 (0% or 100% barrier) are labelled as 'flat cued' or 'barrier cued' to indicate that the screen press initiating a trial did trigger a cue presentation but that cue was not predictive of the upcoming trial type.

2.3.5 *Electrophysiological recordings and data acquisition*

Local field potentials were recorded using the dacqUSB multichannel recording system (Axona Ltd.). Local field potentials were low-pass filtered at 500 Hz, and sampled at 4800 Hz. The animals' position was monitored by a ceiling-mounted video camera connected to a tracking system that monitored the LEDs mounted on the head stage. Tracking data was sampled at 50 Hz and made available to the dacqUSB system. Key events (e.g. trial initiation, the type of trial initiated, when rats got to the barrier region, and when rats reached the reward) were timestamped by inputs from a custom-built neural network of Arduino microcontrollers connected to a digital input-output port on the dacqUSB system.

2.3.6 *Power, coherence, and running speed analyses*

All analyses were done within-subject; no data was pooled across subjects. All analyses were conducted using MATLAB R2016b (The Mathworks, Boston, MA, USA). Power spectral density (PSD) and time resolved LFP power and coherence were calculated via multi-taper spectrograms and coherograms (Mitra & Bokil, 2008) which used 3 tapers, a reading window of one second, and 85% overlap amongst windows. Data was linearized by dividing the maze path into 9 bins of 3-5cm in length and the position timestamps of rats entering and exiting a given region on a given lap on a given trial type were used to collect relevant pieces of the averaged 4-12 Hz segments of spectrograms and coheragrams, which were then averaged for each maze region on each lap, separately. A similar approach was used to collect instantaneous speed data from each maze region for each lap on a given trial type.

2.3.7 *Partial directed coherence for detecting signal directionality*

Task-related causal relationships between ACC-VTA and ACC-dCA1, linearly detrended LFPs were assessed with a partial directed coherence (PDC) algorithm, a frequency-resolved measure of Granger causality which uses multivariate autoregressive modelling to exploit the predictability of information in one brain area by past activity in another (Baccalá & Sameshima, 2001; Boykin et al., 2012).

2.3.8 *Method for detecting phase-reset events*

To detect a putative phase-reset event (PRE), we first bandpass filtered the ACC and VTA LFPs between 4 and 12 Hz using the *filtfilt* function in MATLAB. We then determined the instantaneous phase and amplitude of the ACC and VTA LFPs for an entire session using the Hilbert transform. Next, we unwrapped the instantaneous phases of the ACC and VTA. Since the rate of change of the unwrapped phases will change markedly at a potential PRE (Freeman & Vitiello, 2006), we differentiated the unwrapped phase of the ACC across a one second window and marked as a trigger point a rate of change that exceeded 4 standard deviations from the mean. Since we cannot know exactly when the animal saw the barrier (*vis a vis* a peri-event histogram), we marked all the PREs which occurred in the barrier-region of the maze (regions 5-6) for each trial type, respectively.

2.3.9 *Amplitude cross-correlations for detecting signal directionality*

We adapted Adhikari et al. (2010)'s amplitude cross-correlation method in order to assess signal directionality within PRE epochs. We conducted cross-correlations across two separate windows in the waveforms: a 500ms window centered on the PRE marker and a 500ms window immediately after that.

2.3.10 *Histology and electrode site verification*

Upon completion of the study, rats were deeply anaesthetized with isoflurane and recording sites were marked with direct current (2mA for 2 s) before transcardial perfusion. Electrode tracks and microlesions marking the electrode position were identified in 32µm thick sections of formalin-fixed tissue stained for Nissl substance (see Figure 27B). Although we did not stain the VTA-containing sections with tyrosine hydroxylase (TH), a marker of dopaminergic neurons sometimes used to define the boundaries of the VTA, when comparing the tips of our electrode tracks with a photomicrograph of a TH-stained section showing the VTA (e.g. Amantea & Bowery 2004), our electrode tip location corresponds to the TH+ area, suggesting that had we stained for TH, we would have been within the TH+ area in the VTA.

2.4 Results

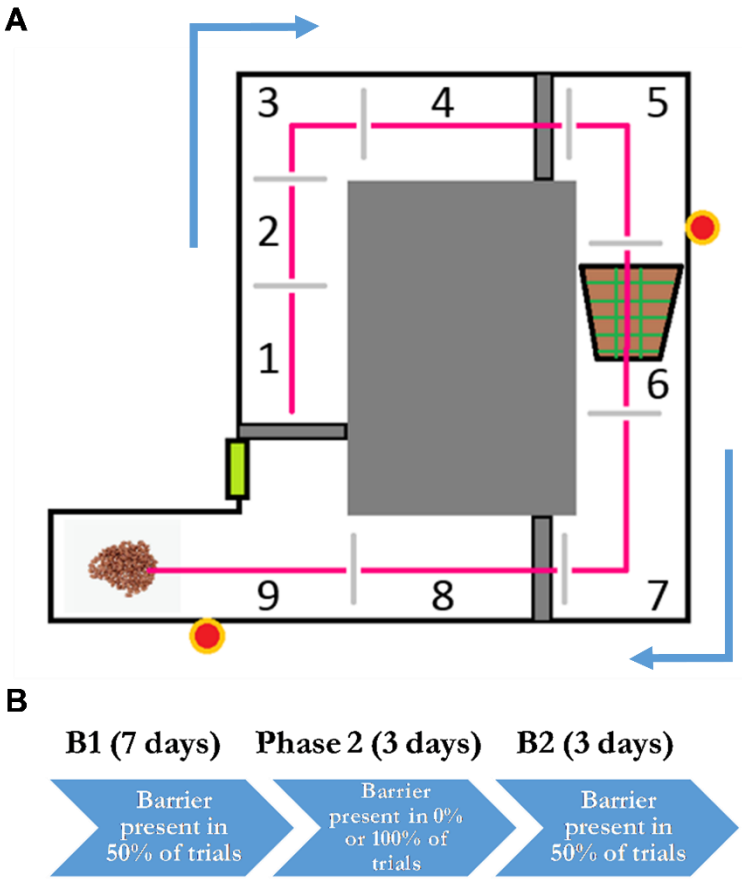

Figure 26. Schematic of maze and protocol. A. Rats initiated laps by pressing a wall-mounted touchscreen – the green rectangle just before the door at the beginning of section 1. After a 2-second delay, the startbox door opened and rats ran through regions 1-9. Arrows indicate direction of travel in the maze. The red and yellow circles indicate the position of the photobeams which controlled the doors, ensuring unidirectional travel on each trial. The mound of cereal pellets in region 9 indicates the reward zone. B. The experiment consisted of 3 phases: B1 (50% barrier), phase 2 (either 0% barrier or 100% barrier), and B2 (50% barrier, identical to B1).

2.4.1 *Task-modulated theta oscillations in the ACC and VTA*

Histology verified that electrodes were located in the regions of interest (Figure 27). LFP patterns in ACC, VTA, and dCA1 were characteristically different with PSD functions from the ACC having a primary peak at low theta frequencies (3-5 Hz), while both VTA and dCA1 exhibited prominent peaks in both the high theta band (7-9 Hz) and low theta band (3-5 Hz; Figure 28). Mapping theta power and coherence onto the maze by trial type revealed that ACC and VTA power, ACC-VTA coherence, and ACC-dCA1 coherence increased as the animal approached the barrier region of the maze on trials when the barrier was absent (Figure 29).

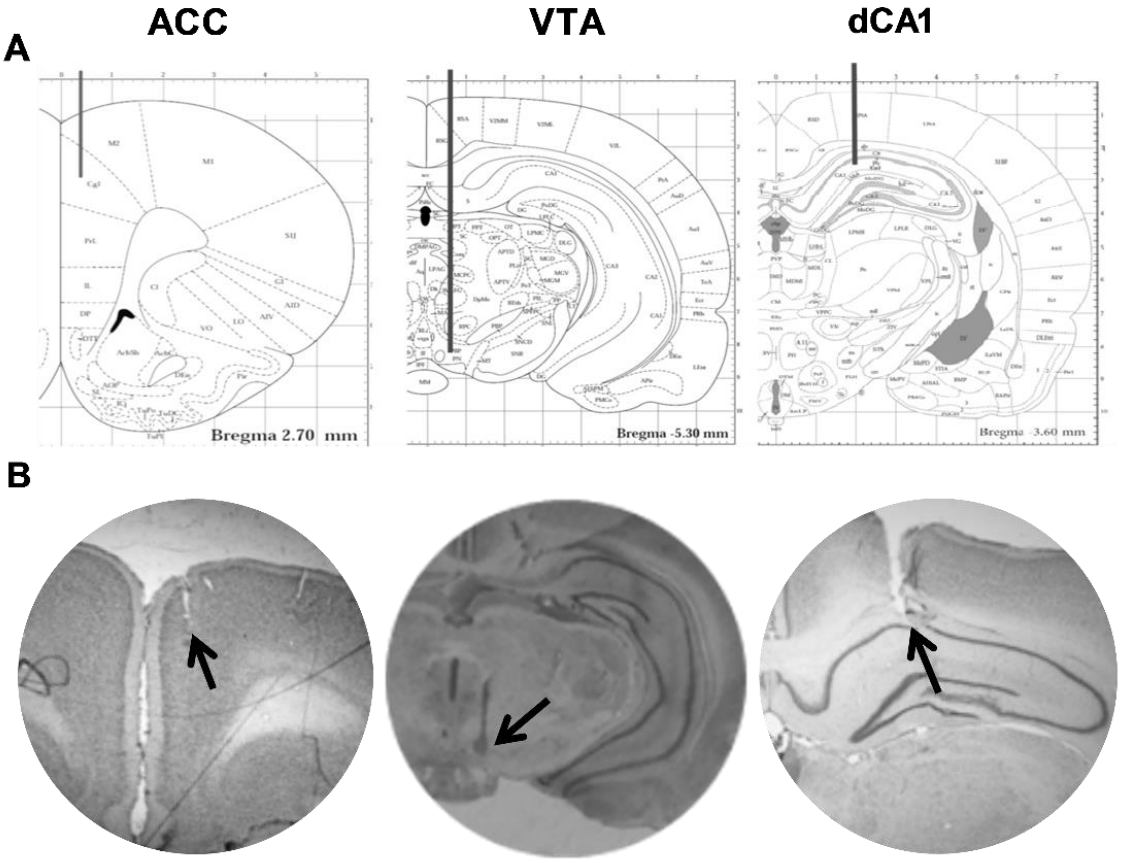

Figure 27. Electrophysiological recording sites. A. Plates from Paxinos & Watson (1997) indicating typical electrode placement in ACC (AP: 2.7mm, ML: 0.4mm, DV: -1.8mm from dura), VTA (AP: -5.3mm, ML: 1.0mm, DV: -8.2mm from dura), and dCA1 (AP: -3.6mm, ML: 2.0mm, DV: -2.8mm from dura). B. Histology indicating example electrode placement in ACC, VTA, and dCA1.

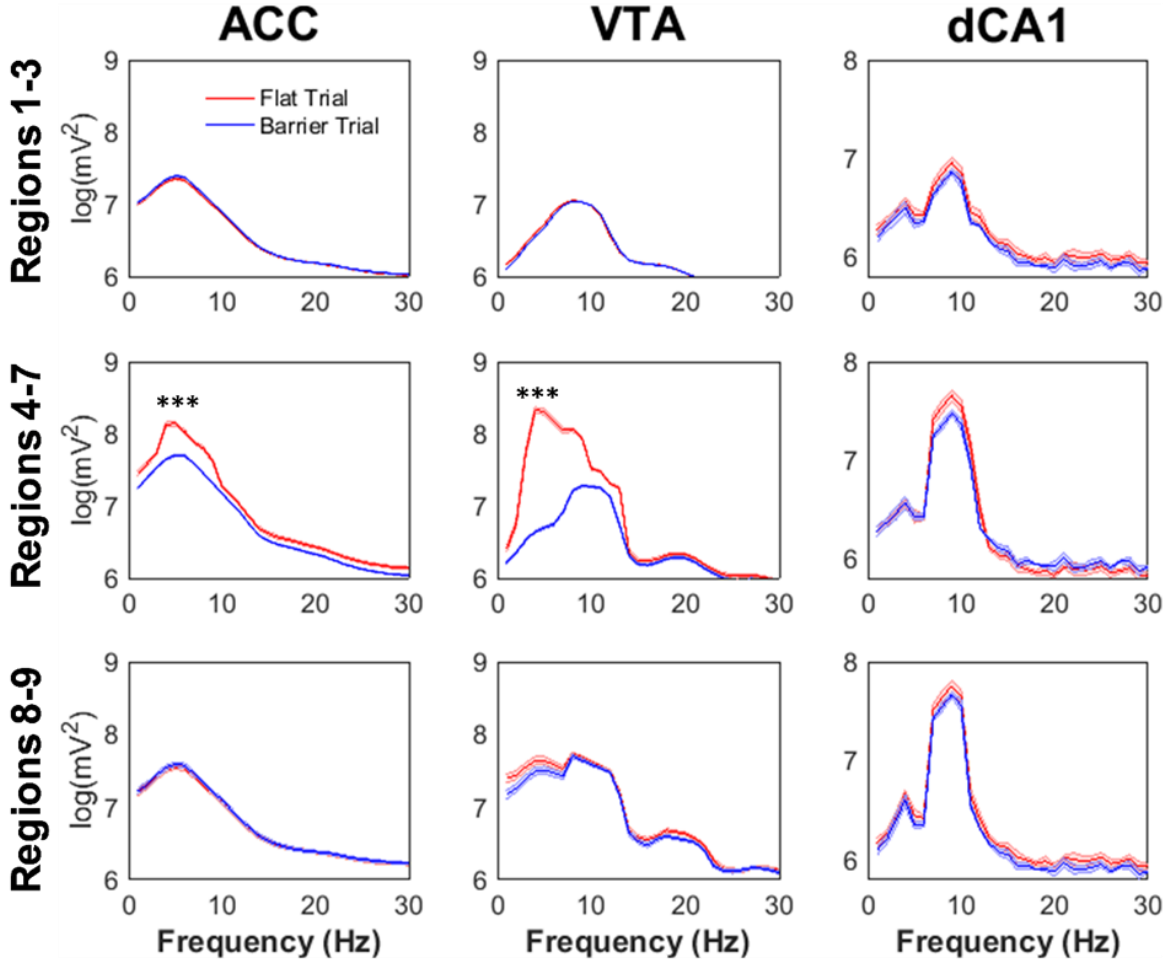

Figure 28. Power spectrum densities (PSDs) for rats A (ACC and VTA) and F (dCA1) across all sessions in B1 by maze region, brain area, and trial type. The solid line indicates the mean and the shaded areas indicate the SEM. ***p<.005, Kruskal-Wallis test.

When the LFP data were linearized and examined region-by-region, it was apparent that during phase B1 (n = 350 trials/animal), when the barrier was present 50% of the time, there was a marked difference in theta power, in both the VTA and ACC, and in the coherence between them, when the barrier-absent and barrier-present trials were compared (Figure 30). In barrier-absent trials there was a significant increase in low theta power and coherence that began once the animal approached the region of the maze immediately prior to where the barrier was usually present (region 5). Power increased through the barrier region and then was sustained above the level measured in the starting stem until the animal reached the reward zone (region 9). In barrier-present trials, however, theta power and coherence did not increase prior to or through the barrier region ($p < .005$ for regions 5-8, respectively, t-tests). Rather, levels remained suppressed from the initial turn through until the reward region, at which point ACC and VTA theta power and coherence increased suddenly to become equivalent to that observed in barrier absent trials. This was a large effect (Hedge's $g > 1$ for regions 5-8, respectively) and was observed across all animals, independently

producing significant within-subject effects for every animal (regions 5-8, $p < .0005$, t-tests; see Figure 31 for all animals). No significant difference in ACC and VTA theta power or coherence was detected in the reward zone for any animal (region 9, all $p > .05$, t-tests).

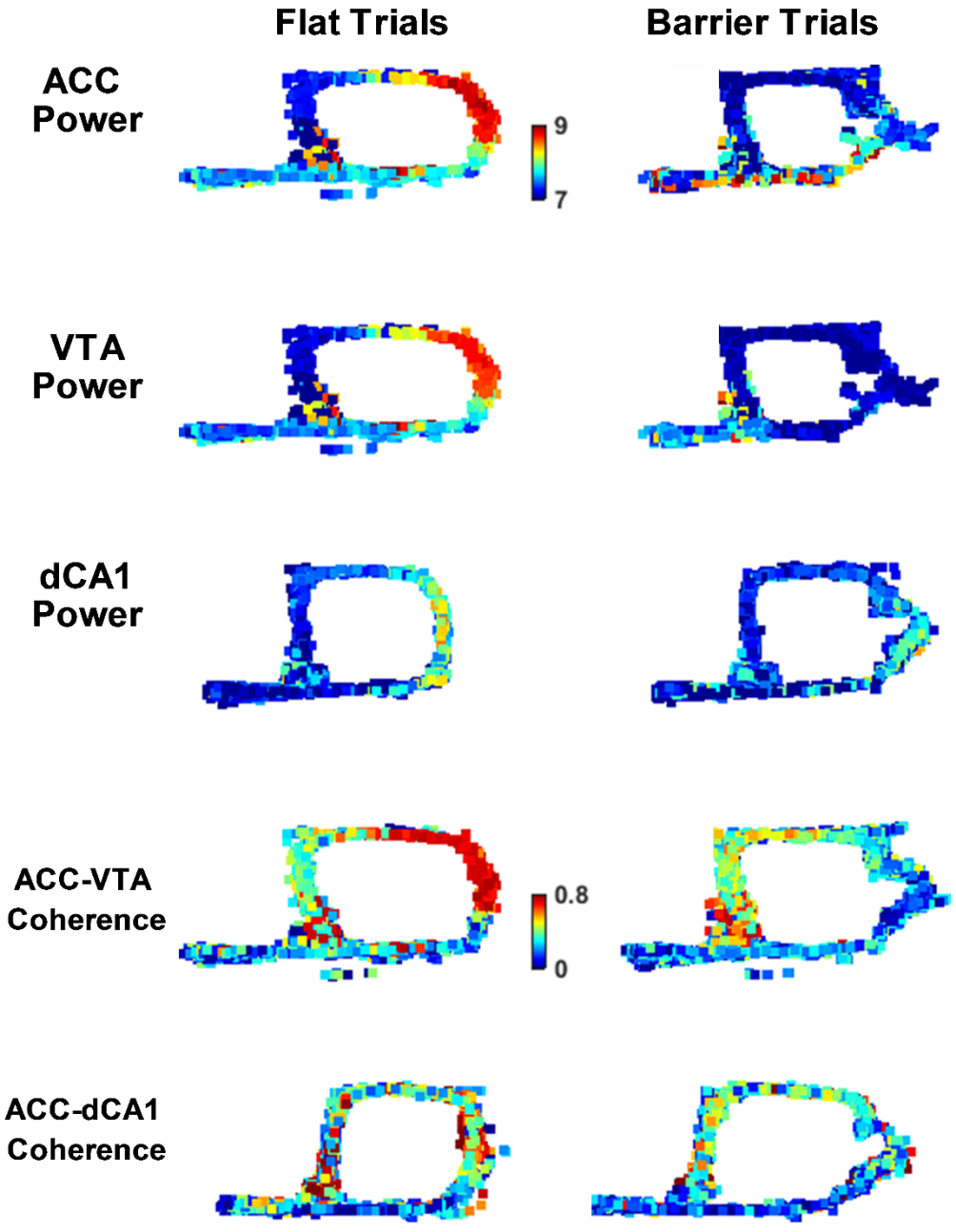

Figure 29. Theta power and coherence heat mapped onto maze positions for the ACC, VTA, dCA1 on flat and barrier trials, respectively, for one recording session during B1. The barrier was located on the right-hand side of the maze; due to the wide-field lens on our tracking camera, the animals' trajectory over the barrier on barrier trials appears as a lateral motion. ACC, VTA, and ACC-VTA coherence data are from rat A. dCA1 power and ACC-dCA1 coherence are from rat F.

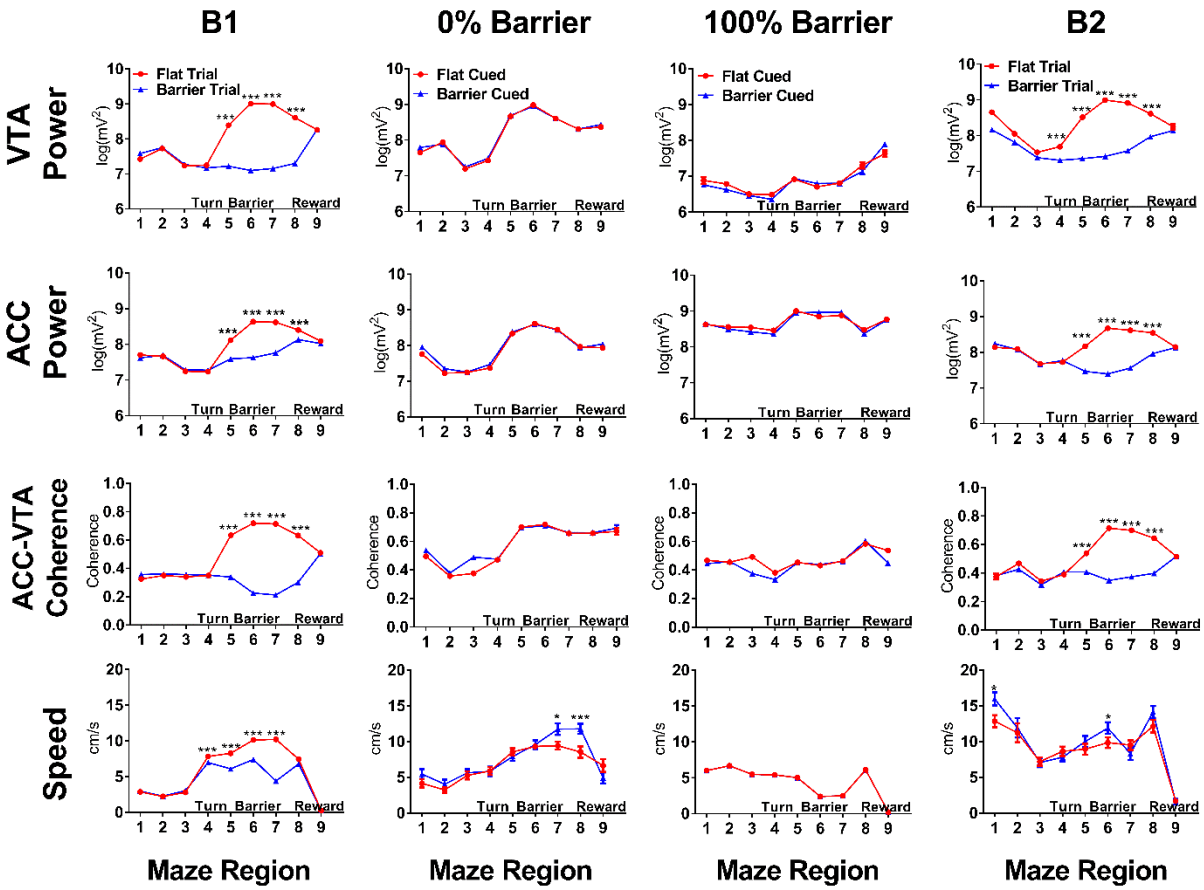

Figure 30. Enhanced theta (4-12Hz) power and coherence corresponds with the absence of the barrier. ACC and VTA time-resolved theta power, theta coherence, and running speed as a function of position for rat A (B1, 0%, and B2; mean ± SEM; n = 350 trials for B1, n = 150 trials for 0% barrier, and n = 150 trials for B2) and rat D (100% barrier; mean ± SEM; 150 trials for 100% barrier). In some cases, the SEM was smaller than the height of the symbol in the plot. In those instances, the error bars were not drawn. The average power and coherence between 4 and 12 Hz for each region on each lap was used. *p < .05, **p < .005, ***p < .0005, t-tests.

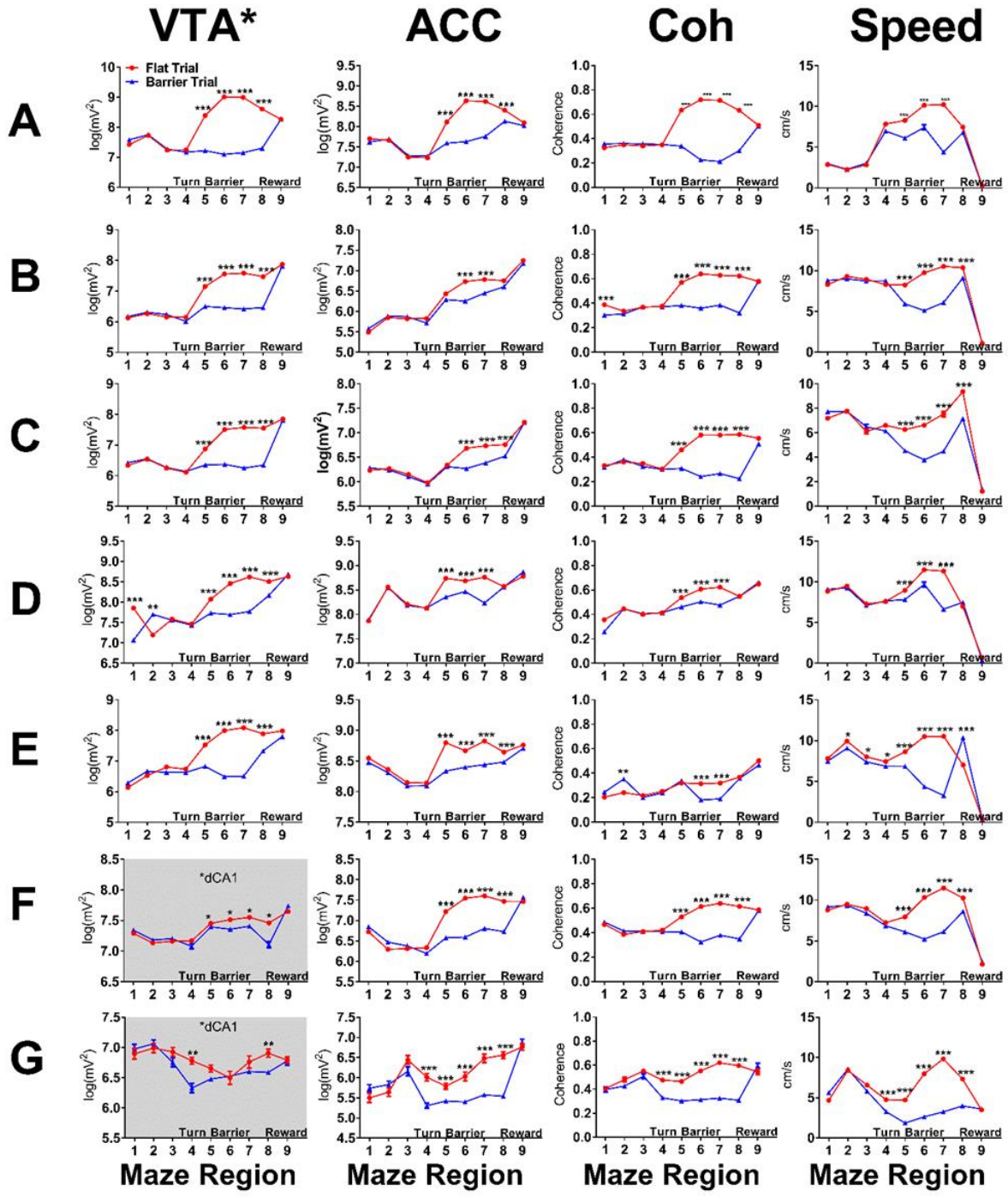

Figure 31. Enhanced theta (4-12Hz) power and coherence corresponds with the absence of the barrier in all rats. Data from all rats in phase B1. Rat name is listed on the left and brain region is listed along the top. *Data with grey background for rats F and G in the VTA column are dCA1. Data presented as mean ± SEM. In some cases, the SEM was smaller than the height of the symbol in the plot. In those instances, the error bars were not drawn. The average power and coherence between 4 and 12 Hz for each region on each lap was used. *p < .05, **p < .005, ***p < .0005, t-tests.

To assess the animals' motivation to begin a new trial following either a flat trial or a barrier trial, we calculated the inter-trial interval (ITI), defined as the time from when the rats tripped the photo-beam as they entered the reward zone until the next screen press, indicating the start of a new trial. We found that the latency to begin a trial was greater if the prior trial was a barrier trial, rather than a flat trial in phases B1 and B2 (n = 350 trials/animal for B1; n = 150 trials/animal for B2; all animals' $p < .05$, t-tests; Figures 32 and 33). No differences in latency were detected in the 0% or 100% conditions (n = 150 trials/animal). Despite this difference in behaviour, no significant difference in theta power or coherence was detected during this same period ($p > .05$ for all animals, t-tests).

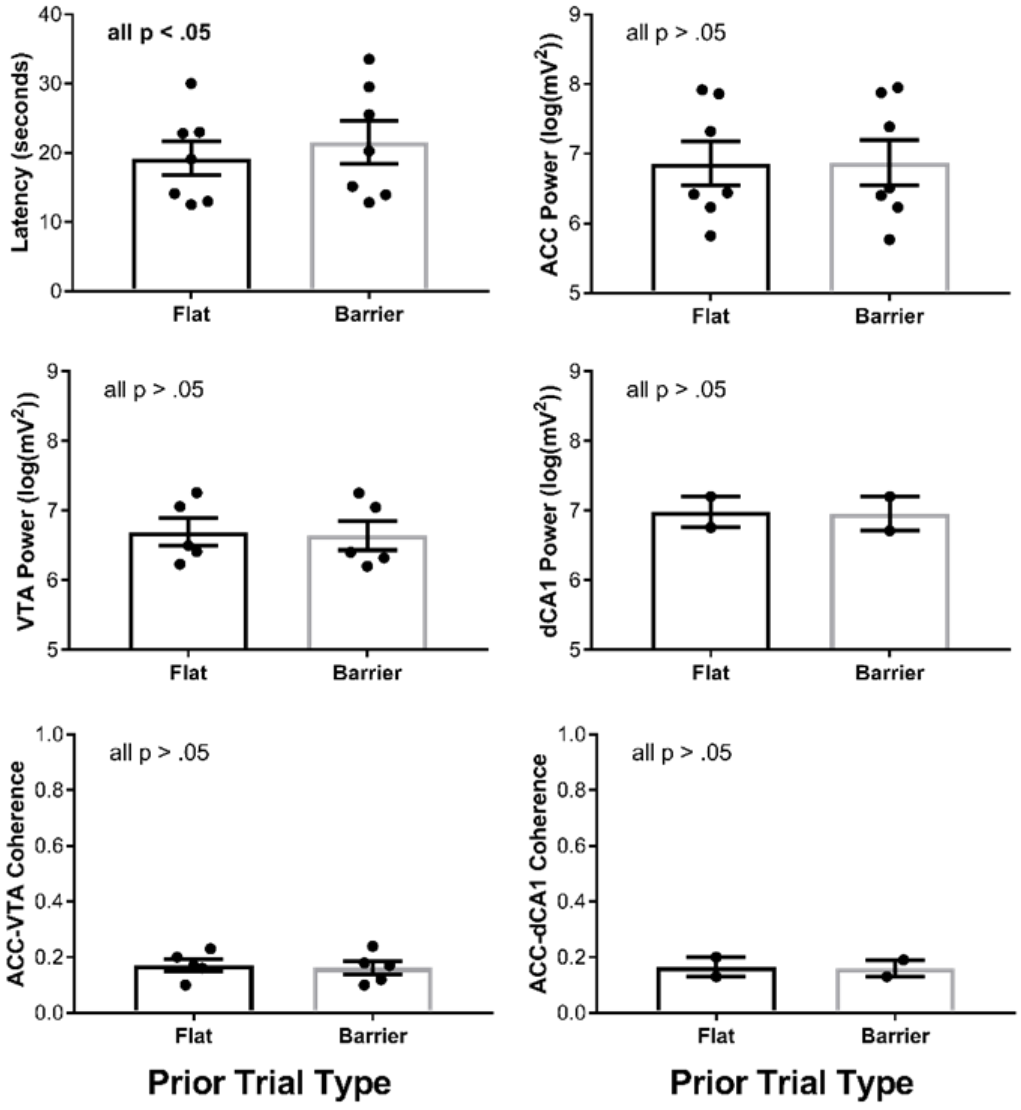

Figure 32. Behaviour and electrophysiology in the inter-trial interval. The latency to begin a new trial given a prior trial type was lower when the prior trial was a flat trial. No significant effects of prior trial type were detected in any electrophysiological measure during the inter-trial interval. Individual animal means are presented as dots and the overall mean is presented as the bar-graph bar. The standard error of measure of the overall mean across all animals is represented by the error bars. T-tests were performed within each animal (n = 350 trials per animal).

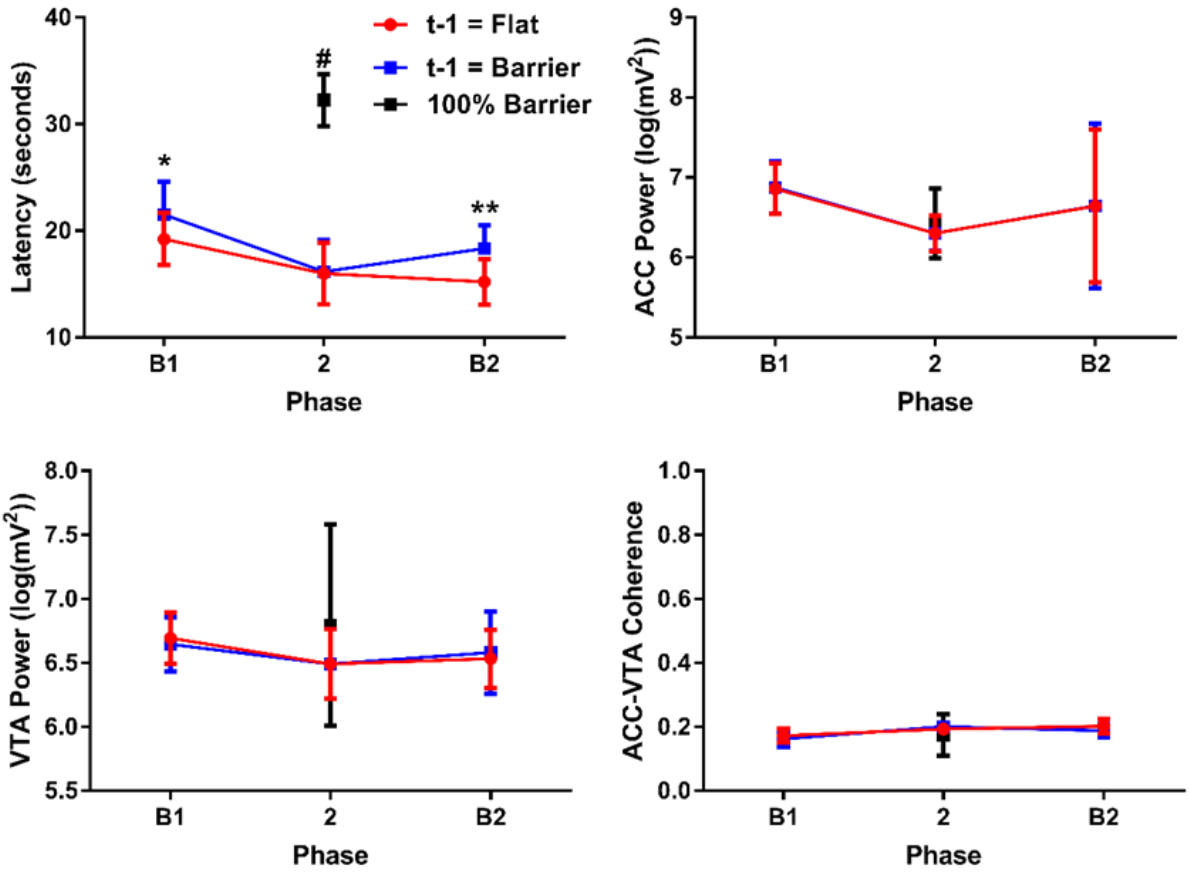

Figure 33. Behaviour and electrophysiology in the ITI across all task phases. The latency to begin a new trial given a prior trial type was lower when the prior trial was a flat trial. The latency to begin a trial was significantly greater in the 100% barrier condition than in phase B1. No significant effects of prior trial type were detected in any electrophysiological measure during the ITI. Data are presented as mean ±SEM across all animals. *p < .05 within each animal with paired t-test, **p<.005 within each animal with paired t-test, # p<.05 within each animal with unpaired t-test.

In phase 2, the barrier was either not present for all trials (n = 4 animals) or was present for all trials (n=3 animals) irrespective of the cue on the touchscreen, which continued to randomly signal the two types of trials on a 50% basis. For animals where the barrier was absent, an abrupt increase in ACC and VTA theta power, similar to that which occurred in no-barrier trials in phase B1, was detected from regions 5 through 8 in all animals regardless of the trial type cued by the touch screen (n = 150 trials/animal; Figures 30 and 31). For animals where the barrier was present on all trials, theta power remained low across these regions, replicating the effect of barrier-present trials in B1 (Figure 30). An analysis to determine whether the, now irrelevant and probably ignored cue signal altered responses during phase 2 revealed no significant differences in ACC and VTA responses in regions 5 to 8 following the two cue types (all p > .05, t-tests).

In the third phase, B2, the barrier was again present on 50% of trials (n = 150 trials/animal). In a result that replicated condition B1, an abrupt increase in running speed,

ACC and VTA theta power, and coherence was detected in regions 5-8 in all animals when the barrier was absent (Figure 30 and 34; all $p < .005$, t-tests). On barrier trials, power and coherence remained suppressed until the reward region. Again, ACC and VTA theta power and coherence in the reward zone (region 9) did not depend on the trial type ($p > .05$, t-tests). Analysis of responses across the multiple trials of each condition (n = 50 trials/animal) revealed that the significant modulation of ACC and VTA theta power and coherence by the presence or absence of the 30cm barrier in the barrier-containing region of the maze (region 6) was consistent across days and trial conditions (Figure 34).

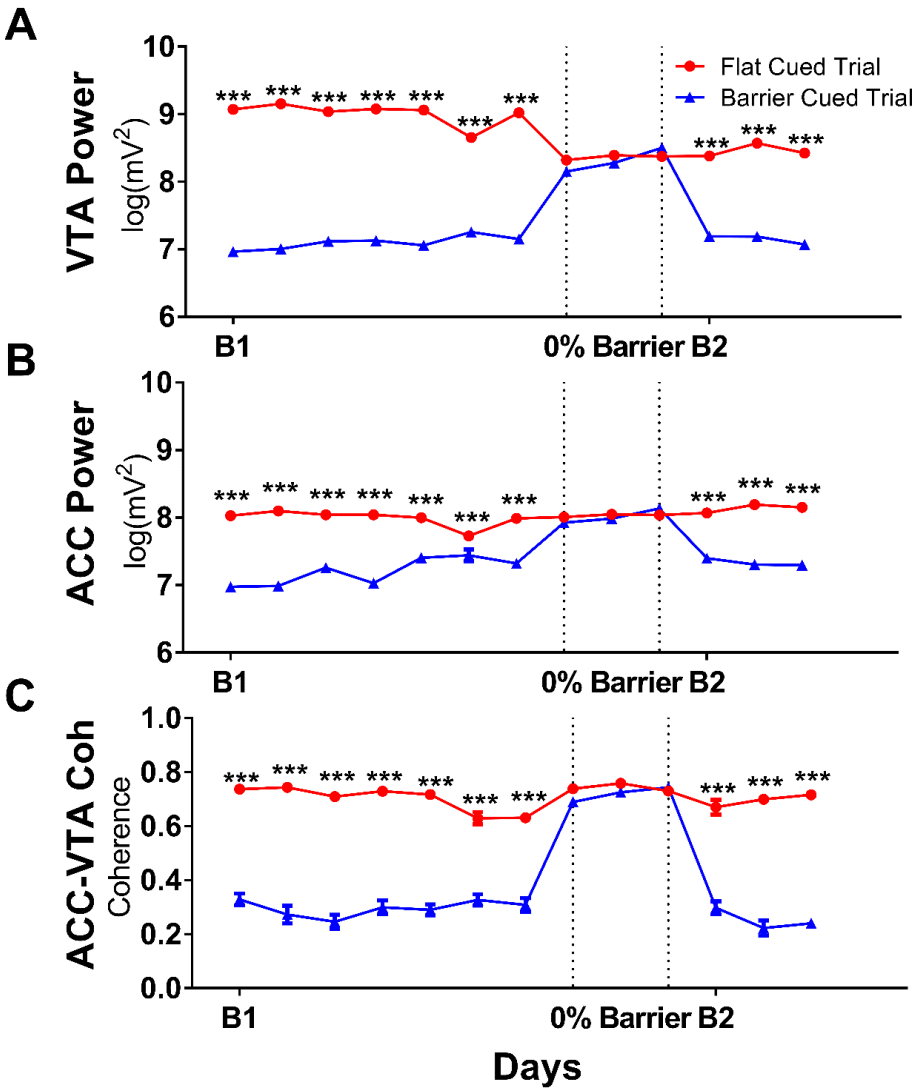

Figure 34. ACC and VTA theta and coherence responses to the presence or absence of the 30cm barrier in the barrier-containing region (region 6) of the maze were consistent across days and conditions. Data shown from rat A. VTA and ACC theta power and coherence were greater on trials when the barrier was present than when the barrier was absent across all days of B1 and B2 ($p < .0005$, t-tests). Data are presented as mean ± SEM. In some cases, the SEM was smaller than the height of the symbol in the plot. In those instances, the error bars were not drawn. n = 50 for each session. *$p < .05$, **$p < .005$, ***$p < .0005$, t-tests.

2.4.2 *Task-modulated theta oscillations in the ACC and dCA1*

To assist in determining whether we were detecting a brain-wide phenomenon or activity that might be confined to specific regions, including VTA and ACC, we implanted two rats in both dCA1 and ACC and ran these animals through the procedure. As we had shown previously, in phase B1, we detected abrupt and sustained increases in ACC theta power from region 5 to 8 on no-barrier trials compared to barrier trials ($p < .005$, t-tests) in both animals (see Figure 35). In the second phase, when the barrier was absent on all trials, a similar abrupt increase in ACC theta power was detected regardless of the, likely ignored, cue ($p > .05$, t-tests). In phase B2, a significant difference in ACC theta power was detected in regions 5 to 8 when barrier and no-barrier trials were compared (all $p < .005$, t-tests) as we had observed previously. By comparison, recordings from dCA1 showed that there was a much smaller increase in theta power in regions 5-8 in B1 no-barrier trials. The difference between barrier and no-barrier trials was statistically significant ($p < .05$, t-test; Figure 31) in one animal but not the other ($p > .05$, t-test) in phase B1. In phase B2, however, no significant barrier-related changes were detected in dCA1 theta power in either animal ($p > .05$, t-tests, Figure 31). Despite the minimal effects seen in dCA1 theta power, ACC-dCA1 theta coherence was significantly modulated by the presence or absence of the 30cm barrier. In phases B1 and B2 dCA1-ACC theta coherence abruptly increased in region 5 and remained elevated through region 8 in no barrier trials compared to barrier trials ($p < .005$, t-tests). In phase 2, when the barrier was never present, a similar abrupt and sustained elevation in theta coherence, beginning in region 5, was detected regardless of the cued condition ($p > .05$, t-tests).

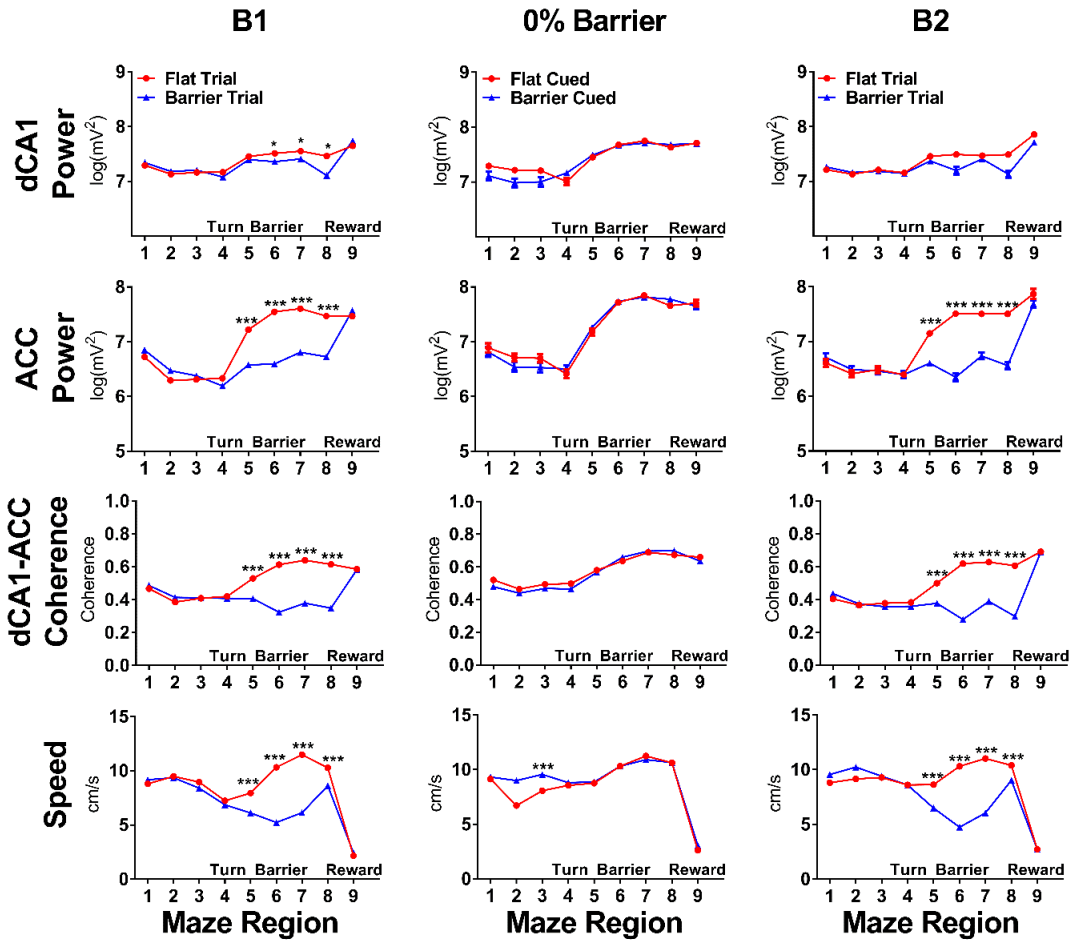

Figure 35. ACC but not dCA1 theta power was significantly modulated by the presence or absence of a 30cm barrier. Data are from Rat F. Data are presented as mean ± SEM. In some cases, the SEM was smaller than the height of the symbol in the plot. In those instances, the error bars were not drawn. n = 350 trials for B1, n = 150 trials for 0% barrier, and n = 150 trials for B2) *p < .05, **p < .005, ***p < .0005, t-tests.

2.4.3 *Relationship to running speed*

We were concerned that our results may have simply been an artefact of changes in running speed; indeed, at first glance, the patterns of power and coherence seemed to parallel changes in speed (Figure 30). However, upon closer inspection, it's clear that running speed and LFP power and coherence are not always changing together. For instance, an increase in running speed occurred in region 4 before the increase in power and coherence was observed (region 5). Furthermore, while running speed is near zero in the reward region, LFP power and coherence were elevated. To formally assess the relationship between running speed and LFP dynamics, we initially conducted correlations (Pearson's R) between the instantaneous running speed and instantaneous theta power (4-12Hz) in ACC, VTA, and dCA1, respectively, across all sessions and all regions of the maze separately for each rat, considering only instances when rats were moving (e.g. speed > 1). All correlation coefficients were near zero and none were significant (all $r < 10^{-2}$, all $p > .05$; see Table 2), suggesting that speed and LFP power were modulated independently. To further examine the

relationship between running speed and LFP power under different effort conditions, we conducted analyses of covariance (ANCOVA) with instantaneous ACC, VTA, or dCA1 theta power in the barrier region as the dependent variable, with the corresponding instantaneous running speed as a covariate, and the presence or absence of the barrier as the independent variable for all sessions of phase B1 for each animal, separately. Resultant ANCOVAs revealed a significant relationship between VTA, ACC, and dCA1 theta power in the barrier region and running speed in the barrier region (see Table 3); however, after statistically controlling for running speed as a covariate, the presence or absence of the barrier remained a highly significant factor in the ACC and VTA, but not dCA1, LFP power in all rats (all $p < .0005$; see Table 4). These results indicate that instantaneous running speed and instantaneous VTA and ACC theta power are independently modulated by the effort condition, whereas dCA1 theta power was dependent on running speed.

Table 2.
Correlations Between Running Speed and LFP Theta (4-12 Hz) Power by Brain Region and Rat.

Rat	VTA and Running Speed	ACC and Running Speed	dCA1 and Running Speed
A	$r(16693) = -1.76\text{x}10^{-5}$, $p > .05$	$r(16693) = -1.90\text{x}10^{-3}$, $p > .05$	
B	$r(96303) = -1.70\text{x}10^{-4}$, $p > .05$	$r(96303) = -6.49\text{x}10^{-4}$, $p > .05$	
C	$r(106428) = -1.53 \text{ x } 10^{-4}$, $p > .05$	$r(106428) = -6.09 \text{ x } 10^{-4}$, $p > .05$	
D	$r(145577) = 2.40 \text{ x } 10^{-3}$, $p > .05$	$r(145577) = -1.80 \text{ x } 10^{-4}$, $p > .05$	
E	$r(159581) = 4.00\text{x}10^{-3}$, $p > .05$	$r(159581) = 6.4\text{x}10^{-3}$, $p > .05$	
F		$r(78535) = 3.55\text{x}10^{-4}$, $p > .05$	$r(78535) = 2.90\text{x}10^{-4}$, $p > .05$
G		$r(123664) = 5.10\text{x}10^{-3}$, $p > .05$	$r(123664) = 5.8\text{x}10^{-3}$, $p > .05$

Table 3.
B1 ANCOVA Results for Theta (4-12 Hz) Power and Speed Relationship by Brain Region and Rat.

Rat	VTA Theta Power	ACC Theta Power	dCA1 Theta Power
A	$F_{1,116828} = 6.95\text{x}10^{3}$, $p<1.00\text{x}10^{-200}$	$F_{1,82363} = 3.52\text{x}10^{3}$, $p<1.00\text{x}10^{-200}$	
B	$F_{1,35669} = 4.59\text{x}10^{3}$, $p<1.00\text{x}10^{-200}$	$F_{1,35669} = 2.30\text{x}10^{3}$, $p<1.00\text{x}10^{-200}$	
C	$F_{1,52251} = 2.65\text{x}10^{3}$, $p<1.00\text{x}10^{-200}$	$F_{1,52251} = 6.83\text{x}10^{2}$, $p=1.25\text{x}10^{-149}$	
D	$F_{1,40881} = 3.81\text{x}10^{3}$, $p<1.00\text{x}10^{-200}$	$F_{1,40881} = 7.51\text{x}10^{3}$, $p<1.00\text{x}10^{-200}$	
E	$F_{1,73924} = 9.53\text{x}10^{3}$, $p<1.00\text{x}10^{-200}$	$F_{1,73924} = 2.91\text{x}10^{3}$, $p<1.00\text{x}10^{-200}$	
F		$F_{1,45583} = 2.01\text{x}10^{3}$, $p<1.00\text{x}10^{-200}$	$F_{1,82363} = 179.25$, $p=8.41\text{x}10^{-41}$
G		$F_{1,82363} = 104.43$, $p<1.00\text{x}10^{-200}$	$F_{1,82363} = 4.96\text{x}10^{3}$, $p<1.00\text{x}10^{-200}$

Table 4.
B1 ANCOVA Results for Barrier Presence After Controlling for Run Speed by Brain Region and Rat.

Rat	VTA Theta Power	ACC Theta Power	dCA1 Theta Power
A	$F_{1,116828}= 9.17$, $p=2.50\times10^{-3}$	$F_{1,82363}= 4.38$, $p=5.00\times10^{-3}$	
B	$F_{1,35669}= 1.77\times10^{3}$, $p<1.00\times10^{-200}$	$F_{1,35669}= 493.64$, $p=1.26\times10^{-108}$	
C	$F_{1,52251}= 2.52\times10^{3}$, $p<1.00\times10^{-200}$	$F_{1,52251}= 5.79\times10^{3}$, $p<1.00\times10^{-200}$	
D	$F_{1,40881}= 2.19\times10^{3}$, $p<1.00\times10^{-200}$	$F_{1,40881}= 507.99$, $p=8.38\times10^{-112}$	
E	$F_{1,73924}= 2.05\times10^{3}$, $p<1.00\times10^{-200}$	$F_{1,73924}= 169.73$, $p=9.35\times10^{-39}$	
F		$F_{1,45583}= 661.15$, $p=9.11\times10^{-145}$	$F_{1,82363}= 3.43$, $p>.05$
G		$F_{1,82363}= 7.23$, $p=3.26\times10^{-4}$	$F_{1,82363}= 1.37$, $p>.05$

2.4.4 *ACC influence over dCA1 and VTA is modulated by barrier presence*

We then used a partial directed coherence (Baccalá & Sameshima, 2001) procedure following Boykin, Khargonekar, Carney, Ogle, & Talathi (2012)'s method to determine if there was evidence of signal directionality in linearly detrended LFPs recorded simultaneously from ACC and VTA and ACC and dCA1 as the animal passed through the barrier-containing region (region 6) of the maze. The mean partial directed coherence (PDC) was calculated in a trial-by-trial manner for each condition for data in the theta range (4-12 Hz). An ANOVA examining the resultant PDC between ACC and VTA in B1 revealed significant main effects of directionality ($F_{1,1194} = 719.45$, $p = 2.01 \times 10^{-124}$) and barrier condition ($F_{1,1194} = 121.57$, $p = 5.46 \times 10^{-27}$) as well as a significant directionality x barrier interaction effect on ACC-VTA theta PDC responses ($F_{1,1194} = 151.02$, $p = 9.03 \times 10^{-33}$; see Figure 36A; see Table 5 for data from all rats). An ANOVA considering B2 returned nearly identical results (see Table 6). This interaction is a result of ACC → VTA PDC being higher when the barrier was absent and decreasing in barrier trials while VTA→ACC PDC remained low and unchanging across conditions. Similarly, an ANOVA examining PDC between ACC and dCA1 across all trials and conditions revealed significant main effects of directionality ($F_{1,1797} = 207.32$, $p = 5.3 \times 10^{-44}$) and barrier presence ($F_{1,1797} = 233.09$, $p = 1.43 \times 10^{-49}$) as well as a significant directionality x barrier interaction effect on ACC-dCA1 theta PDC responses ($F_{1,1797} = 35.69$, $p = 2.78 \times 10^{-9}$; see Figure 36B; Tables 4 and 5). This interaction was a result of dCA1→ACC PDC decreasing to a greater degree when the barrier was present compared to ACC→dCA1 PDC. To verify the integrity of our PDC modelling, we scrambled the recorded signals from both ACC and VTA and conducted the trial-by-trial PDC analysis again. In every case the mean of the permutated PDC distribution was significantly weaker than the non-permuted data (all permuted PDC $< 3\times10^{-5}$, all $p < 3.76\times10^{-36}$, t-tests), losing evidence for directionality.

Table 5.
Barrier Region PDC B1 ANOVA Results by Rat, Implant Type, and Effect.

Rat	Implant	Directionality	Barrier Presence	DxBP Interaction
A	ACC-VTA	$F_{1,1194}$ =362.56, p=5.57x10^{-72}	$F_{1,1194}$ =33.91, p=7.71x10^{-9}	$F_{1,1194}$ =46.82, p=1.16x10^{-11}
B	ACC-VTA	$F_{1,1194}$ =719.45, p=2.01x10^{-124}	$F_{1,1194}$ =121.57, p=5.46x10^{-27}	$F_{1,1194}$ =151.02, p=9.03x10^{-33}
C	ACC-VTA	$F_{1,1194}$ =351.65, p=4.24x10^{-74}	$F_{1,1194}$ =23.56, p=6.78x10^{-34}	$F_{1,1194}$ =54.22 p=3.96x10^{-29}
D	ACC-VTA	$F_{1,1194}$ =402.95, p=5.32x10^{-75}	$F_{1,1194}$ =14.08, p=2.00x10^{-4}	$F_{1,1194}$ =341.11, p=1.00x10^{-4}
E	ACC-VTA	$F_{1,1194}$ =352.77, p=2.78x10^{-68}	$F_{1,1194}$ =20.55, p=3.42x10^{-7}	$F_{1,1194}$ =88.45, p=4.64x10^{-22}
F	ACC-dCA1	$F_{1,1194}$ =242.50, p=1.44x10^{-50}	$F_{1,1194}$ =310.47, p=6.67x10^{-63}	$F_{1,1194}$ =30.40, p=5.02x10^{-8}
G	ACC-dCA1	$F_{1,1194}$ =528.33, p=2.15x10^{-99}	$F_{1,1194}$ =273.99, p=2.53x10^{-56}	$F_{1,1194}$ =70.1, p=1.36x10^{-16}

Table 6.
Barrier Region PDC B2 ANOVA Results by Rat, Implant Type, and Effect.

Rat	Implant	Directionality	Barrier Presence	DxBP Interaction
A	ACC-VTA	$F_{1,596}$ =118.17, p=1.10x10^{-10}	$F_{1,596}$ =12.88, p=4.00x10^{-4}	$F_{1,596}$ =12.47, p=4.00x10^{-4}
B	ACC-VTA	$F_{1,596}$ =628.74, p=2.78x10^{-95}	$F_{1,596}$ =129.12, p=3.21x10^{-27}	$F_{1,596}$ =175.93, p=2.28x10^{-35}
C	ACC-VTA	$F_{1,596}$ =482.87, p=7.69x10^{-79}	$F_{1,596}$ =125.47, p=1.46x10^{-26}	$F_{1,596}$ =92.69, p=1.74x10^{-20}
D	ACC-VTA	$F_{1,596}$ =492.48, p=1.00x10^{-82}	$F_{1,596}$ =12.69, p=4.00x10^{-4}	$F_{1,596}$ =122.42, p=1.37x10^{-25}
E	ACC-VTA	$F_{1,596}$ =416.22, p=6.88x10^{-70}	$F_{1,596}$ =50.60, p=7.80x10^{-15}	$F_{1,596}$ =8.95, p=2.90x10^{-3}
F	ACC-dCA1	$F_{1,596}$ =197.36, p=7.36x10^{-39}	$F_{1,596}$ =100.61, p=5.66x10^{-22}	$F_{1,596}$ =17.18, p=3.89x10^{-5}
G	ACC-dCA1	$F_{1,596}$ =245.74, p=1.26x10^{-46}	$F_{1,596}$ =233.99, p=8.45x10^{-45}	$F_{1,596}$ =88.32, p=1.18x10^{-19}

Table 7.
Initial Segment PDC B1 ANOVA Results by Rat, Implant Type, and Effect.

Rat	Implant	Directionality	Barrier Presence	DxBP Interaction
A	ACC-VTA	$F_{1,1194}$ =4.65, p=.032	$F_{1,1194}$ =.1117, p > .05	$F_{1,1194}$ =2.959, p > .05
B	ACC-VTA	$F_{1,1194}$ =99.43, p=9.52x10^{-22}	$F_{1,1194}$ =.4118, p > .05	$F_{1,1194}$ =1.264, p > .05
C	ACC-VTA	$F_{1,1194}$ =616.59, p=4.13x10^{-110}	$F_{1,1194}$ =1.109, p > .05	$F_{1,1194}$ =3.642, p > .05
D	ACC-VTA	$F_{1,1194}$ =292.23, p=8.75x10^{-59}	$F_{1,1194}$ =.2456, p > .05	$F_{1,1194}$ =2.595, p > .05
E	ACC-VTA	$F_{1,1194}$ =1311.0, p=7.30x10^{-194}	$F_{1,1194}$ =3.483, p > .05	$F_{1,1194}$ =2.667, p > .05
F	ACC-dCA1	$F_{1,1194}$ =306.85, p=2.48x10^{-61}	$F_{1,1194}$ =.0912, p > .05	$F_{1,1194}$ =2.823, p > .05
G	ACC-dCA1	$F_{1,1194}$ =266.10, p=4.06x10^{-54}	$F_{1,1194}$ =3.264, p > .05	$F_{1,1194}$ =3.636, p > .05

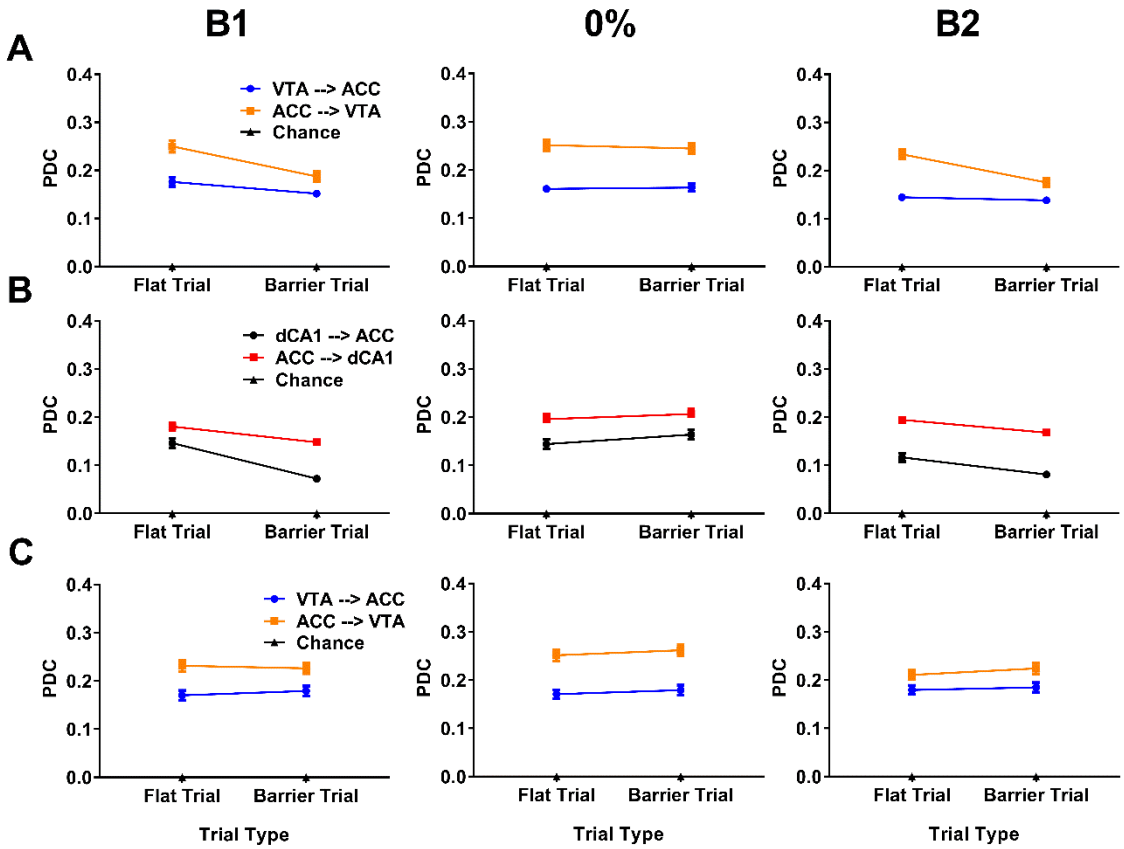

Figure 36. ACC-VTA and ACC-dCA1 PDC in the barrier region. Data indicate mean ± SEM. Some error bars were too small for display. **A.** ACC → VTA and VTA → ACC theta PDC in the barrier region across the three phases. **B.** ACC→ dCA1 and dCA1 → ACC theta PDC in the barrier region across the three phases. **C.** ACC→VTA and VTA-->ACC PDC in the initial region (region 2) across the three phases. A and C are data from rat B; B are from rat G. n = 350 trials for B1, n = 150 trials for 0% and 100% barrier, and n = 150 trials for B2. Data are represented as mean ± SEM. In some cases, the SEM was smaller than the height of the symbol in the plot. In those instances, the error bars were not drawn.

To determine if this PDC effect was specific to the barrier region, we also assessed the relationship between the ACC and VTA and ACC and dCA1 as animals passed through the initial region of the apparatus (region 2). An ANOVA examining the resultant PDC between ACC and VTA in this region revealed a significant main effect of directionality ($F_{1,1194}$ = 286.65, $p < x\ 10^{-200}$) but there was no significant effect of barrier condition ($F_{1,1194}$ = 3.46, p > .05) and no directionality x barrier interaction ($F_{1,1194}$ = 0.76, p > .05; see Figure 36C; see Table 7 for data from all rats). Similar results were obtained for the ACC-dCA1 PDC ANOVAs (see Table 7), These data indicate that in the initial portion of the apparatus, where no variation in task-demands ever occurred, ACC leads VTA and dCA1 activity, respectively, but without the large increase that occurs when the animal discovers the barrier is absent from the barrier-containing region of the apparatus.

To confirm these PDC findings, we conducted cross-correlations (Adhikari, Sigurdsson, Topiwala, & Gordon, 2010) across two separate windows in the waveforms: a

500ms window centered on the PRE marker and a 500ms window immediately after that. During the PRE-centred window on flat trials, we found that the cross-correlation of ACC and VTA LFPs peaks at 35.42 ± 2.26ms ($p < .05$, Kruskal-Wallis test), indicating that the ACC significantly leads the VTA. We also found evidence of the ACC leading the VTA by a similar amount (32.29 ± 3.19ms; $p < .0005$, Kruskal-Wallis test) in the 500ms window beginning at the end of the PRE-window. We did not detect significant lead or lag using the same procedures during barrier trials. No significant evidence of VTA leading the ACC was detected when this procedure was repeated using the VTA as the trigger for PREs. We also conducted amplitude cross-correlations triggered from entry into the barrier region (regions 5-6). The results were similar. Cross correlations conducted on the waveform itself within the same windows also showed that the ACC significantly led the VTA. Given the agreement of our PDC results with these cross-correlation findings, we conclude that our PDC implementation is likely able to adequately resolve changes in directionality occurring within very small timescales. Furthermore, the consistency between the PDC results and the amplitude cross correlation results are supportive of a lead of the ACC over the VTA rather than the converse.

2.5 Discussion

We investigated the influence of physical effort on VTA, ACC, and dCA1 theta (4-12 Hz) power, coherence, partial directed coherence (PDC), and running speed as rats ran a rectangular track requiring varying levels of effort to reach a fixed reward. PDC analysis of task-related casual relationships between brain areas revealed significant ACC → VTA and ACC → dCA1 directionality, the magnitude of which was modulated by the presence or absence of the barrier. These PDC results show that ACC activity is predictive of VTA and dCA1 responses and are consistent with prior reports showing cortical influence over VTA and dCA1. For example, Beier et al. (2015) found that the VTA dopaminergic neurons projecting to NAcc are directly regulated by anterior-cortical-VTA glutamatergic afferents and that rodents will self-stimulate those projections. Additionally, ACC control over the VTA is strongly implicated in inhibition of cocaine seeking (Navailles et al., 2015). Moreover, Rajasethupathy et al. (2015) found that ACC projections to dCA1 mediate memory retrieval and Ito et al. (2015) implicated ACC influence over dCA1 in directing goal-oriented place-cell activity. One interpretation of these findings is that ACC top-down projections to the VTA and dCA1 (Ferenczi et al., 2016; Fujisawa & Buzsaki, 2011; Taber et al., 1995) underlie a circuit via which cortical representations can update spatial and motivational brain states to guide future behaviour.

Additionally, we found that ACC and VTA, but not dCA1, theta power, ACC-VTA coherence, and, surprisingly, ACC-dCA1 coherence increased as the rat entered the barrier-containing region of the maze on trials when the barrier was absent. In contrast, theta signals did not increase to the same degree across the same region of space when the barrier was present. Once the animal reached the reward region, however, ACC and VTA theta power and coherence as well as ACC-dCA1 theta coherence were independent of the effort condition. We also found that the latency to begin a new trial, measured as the length of the inter-trial interval (ITI), was longer if the prior trial had been a barrier trial than a flat trial. The ITI start was determined by the rat tripping the photo-beam immediately prior to reward acquisition and ended with the next trial start. This longer ITI could, therefore, reflect either increased reward consumption time or increased latency to start post-consumption, raising the possibility of decreased motivation following an effortful trial. Although our assessment of theta power and coherence during this same time period found no significant differences given a prior trial type, Bryden et al. (2011) correlated elevated ACC single unit firing rates with decreased latencies to begin a trial. Thus, the fact that our principle findings were confined to the low theta band (near 4 Hz) suggests that we may have observed a long-range, integrative mechanism rather than measuring local computations (Buzsaki, 2006; Buzsaki & Watson, 2012), consistent with prior reports that cortical modulation of subcortical structures, such as the VTA and the basolateral amygdala, do occur via the low-theta frequency (Gao, Yang, Jin, Bunney, Shi, 2007; Karalis et al., 2016; Wu et al., 2013).

Rats' running speeds also increased significantly in the barrier region when the barrier was absent. This may have been due to the reduced physical demands of the task or, alternatively, may have been driven by increased motivation signals, perhaps provided in a top-down manner from the ACC. In either case, one consequence of this relationship is that changes in running speed are potentially confounded with some of the electrophysiological effects that we observed. Our analyses indicate, however, that the changes in electrophysiology we observed are over and above that which would be predicted from the changes in running speed *per se*. First, correlations between instantaneous power and instantaneous running speed when compared across all regions, were minimal and non-significant, suggesting that speed and power were independently driven by the effort condition. Second, and most importantly, after statistically controlling for speed as a covariate in an ANCOVA, the effort condition remained a highly significant factor in ACC and VTA (but not dCA1). Third, if the theta power changes were movement artefacts, it is difficult to explain why activity in the barrier region during the barrier condition, where rats would

vigorously leap atop the barrier, was generally equal to that recorded in the initial stem of the apparatus where there was never a barrier. Therefore, rather than being a secondary consequence of behavioural change, our data appear to represent fundamental differences in underlying neural activity that are responsive to the effort condition.

Our data may reflect the operation of several different mechanisms, with the possibility that more than one of these operates simultaneously. Two of these include prediction error (Pearce & Hall, 1980) and negative reinforcement (Skinner, 1938). Prediction error (PE) theory posits that, based on prior experience and outcomes, the brain predicts what will happen in a similar situation and elicits a strong signal when an outcome violates that prediction. Although prediction errors are typically studied in the context of reward (Schultz, 1998), in our study, theta power in the ACC and VTA increased markedly when the barrier was absent, suggesting an effort, rather than reward, prediction error. Framed as an effort prediction error effect, this would suggest that the baseline prediction might have been the presence of the barrier, such that the absence of the barrier was 'unexpected'. This corresponds to the notion of a positively signed prediction error (Eshel et al., 2015; Kennerly et al., 2011), but is inconsistent with other reports of unsigned, 'surprise', prediction errors (Bryden et al., 2011; Hayden, Heilbronner, Pearson, & Platt, 2011). Were these signals true prediction error signals, the presence or absence of the barrier in the B1 condition, when the barrier was present on 50% of trials, should be equally surprising with each trial type eliciting a transient response.

Negative reinforcement (NR) models suggest that the removal of an aversive stimulus, such as a barrier, is itself a reinforcer (Skinner, 1938). Typical NR studies require subjects to emit an instrumental response to remove or avoid an aversive stimulus (Qi et al., 2016) and adapt future behaviour (Oleson, Gentry, Chioma, & Cheer, 2012). Although our study was slightly different from a typical NR design in that the omission of the barrier did not require an instrumental response, the increase in theta power and coherence along with running speed is consistent with the core notion of NR: the absence of a barrier, when it could have been present, is reinforcing. Both of these interpretations would predict that, in the phase 2, barrier-absent condition, the magnitude of the power and coherence signal would decrease in the barrier region over repeated trials as the animals' predictions were modified to accept the new barrier probability (0%). The data presented in Figure 30 suggest that this was not the case, at least within the time window tested. Thus, future experiments are required to resolve whether the time course over which these neural mechanisms respond to environmental change corresponds to that observed in behavioural change, such as extinction.

Because we only tested two conditions (effort and no effort), it is possible that the rapid synchronization of the ACC and VTA was not driven by effort. Another possibility, suggested by classic studies of dopaminergic activity (Fiorillo, Philippe, Schultz, 2003; Ljungberg, Apicella, & Schultz, 1992; Schultz, 1998), is that the absence of the barrier may cause the animal to anticipate the reward well in advance of the reward zone (region 9). Although this has not been documented in the ACC, VTA neurons tend to respond to the earliest stimulus predictive of reward over the course of learning (Schultz, 1998). Through this lens, it is possible that the absence of the barrier functioned as a cue which indicated the reward was 'closer,' thus eliciting a change in theta power. Given the ACC → VTA directionality observed in our experiment, future studies are needed to determine whether ACC neurons also transfer their responses to the earliest reward-predicting stimulus over the course of learning.

A related interpretation is suggested by human fMRI experiments. These dissociated the ACC's response to surprising, presumably PE-inducing events, from its response to information indicating that the organism's underlying predictive model must be updated (N Kolling et al., 2016b; O'Reilly et al., 2013). According to this model, the responses of the ACC and the structures it influences, such as the VTA, and, ultimately, behavioural changes, are greatest when task-requirements are different than expected, such as a barrier being absent when it has previously been present. This is different from PE in that PEs are thought to signal one-off, 'surprising' events whereas Kolling et al. (2016) and O'Reilly et al. (2013) suggest these ACC signals are updating the more fundamental processing framework underlying PEs. This interpretation reconciles the key aspects of prediction error and negative reinforcement in that VTA and ACC theta power as well as running speed abruptly increased when the rat finds that the barrier is absent, when it has been present in the past. Future experiments are required to verify an assumption of this explanation which, similar to a PE account, assumes the animals' default task model includes the presence of the barrier.

It is also possible that our findings can also be explained as a neural correlate of 'relief', in that the avoidance of an aversive outcome, such as climbing a barrier, is relieving. Such a description of relief is consistent with human psychological conceptions of relief (Carver, 2009; Deutsch, Smith, Kordts-Freudinger, & Reichardt, 2015; Sweeny & Vohs, 2012). Since relief is thought to occur only when circumstances or outcomes are better than they might have been, the concept of relief synthesises the key aspects of negative reinforcement, positive prediction error, and internal task-state monitoring-and-updating without many of the caveats of other interpretations. Thus, characterisation of our findings as

a neural correlate of relief is perhaps a more parsimonious description of a process by which internal task representations are altered, specifically when an aversive task-requirement, such as climbing a barrier, is avoided.

Our data integrates and extends the evidence indicating a close link between cortical states and activity in dopaminergic brain areas (Beier et al., 2015; S Fujisawa & Buzsaki, 2011; Taber et al., 1995; Wu et al., 2013) and complements demonstrations of cortical control of other affective states, such as fear (Karalis et al., 2016; Likhtik, Stujenske, Topiwala, Harris, & Gordon, 2014), apathy (Moretti & Signori, 2016; Onoda & Yamaguchi, 2015), and pain (Navratilova & Porreca, 2014; Vogt, 2005). The idea of a continuously sampling ACC which tracks changes in task requirements complements reports of a similarly adaptive mesolimbic dopamine signal (Hamid et al., 2016; Howe et al., 2013) and provides an indication of at least some of the pathways via which this latter response could be modulated. Together, these data suggest that cortical and dopaminergic states modulate the motivation to pursue a reward in response to changing task requirements, enabling organisms to behave flexibly in order to optimize available opportunities in uncertain, changing environments (Hayden, Pearson, & Platt, 2011). Integrating the theories of prediction error, negative reinforcement, and task-requirement monitoring, we conclude that our findings may reflect a neural correlate of relief: the avoidance of a barrier, when it has been present in the past, is relieving. Future work will expand the mechanistic insight of this phenomenon by examining how changes in the ACC to VTA projection map onto changes in behavioral outcomes.

Chapter 3 Anticipation and persistence signals in the ACC and VTA

3.1 Summary

The anterior cingulate cortex (ACC) has previously been implicated in several high-level processes, including value-based decision-making and anticipation. It is, however, unclear how ACC activity in these circumstances might be transformed into motivational signals. One possibility is through the region's connections to the ventral tegmental area (VTA), a dopaminergic region implicated in motivation. We tested this hypothesis by monitoring ACC single-units and local-field-potentials (LFPs) as well as LFPs in the VTA of rats performing a spatial decision, reversal task which elicited both economic, value-based and decisions which appeared to be anticipatory. A combination of behavioural, electrophysiological, and modelling analyses revealed that transient increases in 4Hz ACC modulation of the VTA corresponded with the pre-reversal selection of a less-favoured low-cost, low reward option. The temporal pattern of this behaviour suggested that it may reflect anticipation and/or decision implementation. This interpretation was consistent with our observation that the ACC-to-VTA signal was initially high but decreased exponentially during habituation to a novel open field. Increased ACC-to-VTA signalling was also observed after the reversal as animals as the rats sustained their responses to the new optimal side. In sum, our results suggest that ACC-to-VTA signalling is important for the initiation and persistence of non-default behaviour.

3.2 Introduction

The anterior cingulate cortex (ACC) is a medial prefrontal region that has previously been implicated in a number of high-level processes, including decision making (Hillman & Bilkey, 2010; Nils Kolling et al., 2016), anticipation (Blanchard et al., 2015; Haroush & Williams, 2015; Tervo et al., 2014), and adaptation (Economides, Guitart-Masip, Kurth-Nelson, & Dolan, 2014; Sheth et al., 2012; Walton, Croxson, Behrens, Kennerley, & Rushworth, 2007). One theory which unifies such diverse functions is that the ACC dynamically encodes models of the task at hand (Nils Kolling et al., 2016; O'Reilly et al., 2013). Accordingly, this view suggests that changes in that task model underpin subsequent behavioural change. While the results of several studies illustrate how such models might neuronally manifest in the ACC (Cowen, Davis, & Nitz, 2012; Haroush & Williams, 2015; Hillman & Bilkey, 2010; Karlsson, Tervo, & Karpova, 2012; Womelsdorf, Johnston, Vinck,

& Everling, 2010), whether and how these signals influence the motivation to pursue one option or another during decision making remains unclear.

Anatomical, electrophysiological, and computational evidence suggest that the ACC can influence behaviour via the monosynaptic glutamatergic afferents that connect the ACC to the ventral tegmental area (VTA), a midbrain dopaminergic structure implicated in motivation (Ballard et al., 2011; Carr & Sesack, 2000; Elston & Bilkey, 2017; Gao et al., 2007; Gariano & Groves, 1988; Holroyd & McClure, 2015; Holroyd & Yeung, 2012; Olds, 1958). For example, in a recent study of ACC-to-VTA signalling from our lab (Elston & Bilkey, 2017), we monitored and modelled ACC and VTA local field potentials (LFPs) of rats running in a task with varying physical difficulty and found that ACC-to-VTA signalling, modulated at around 4Hz, increased during trials when the lap was easier than expected. This increase was significantly correlated with, but not confounded by, increases in motivation, as measured by running speed. Thus, ACC-to-VTA 4Hz signalling is a plausible mechanism by which ACC neural activity could influence VTA-generated motivational signals. What remains unclear, however, is whether and how the ACC and VTA interact during decision making.

To examine this circuit during decision making, we monitored ACC single units and simultaneously recorded ACC and VTA LFPs (Figure 38A-C) in rats trained to perform a spatial decision, reversal task. The task (Figure 38DE) required that rats decide whether to overcome a 30cm barrier in pursuit of a large reward (high cost, high reward; HCHR) or choose to pursue a small reward without having to overcome a barrier (low cost, low reward; LCLR). In addition to the value-guided, economic (HCHR) decisions this task highlights, we (Hillman & Bilkey, 2010) and others (Holec, Pirot, & Euston, 2014; Schweimer & Hauber, 2006; Walton, Devlin, & Rushworth, 2003) had previously found that the animals would occasionally choose the low-value (LCLR) option. Often, these experiments included a reversal component, which led us to wonder whether these LCLR choices occurred either because of some error in memory recall at the choice point or because the animals anticipated the reversal. Given that the ACC appears central for choices which involve value and effort (Kennerly, Behrens, & Wallis, 2011; Walton, Devlin, & Rushworth, 2003), its neurons firing in an anticipatory manner (Blanchard et al., 2015; Haroush & Williams, 2015), and that both decision types entail a motivational component, we were interested in whether and how the ACC's modulation of the VTA would differ between these decision types.

3.3 Experimental Procedures

3.3.1 *Subjects and animal use statement*

All experimental procedures have been reviewed and approved by the University of Otago Animal Welfare Office. Six male Sprague Dawley rats (Hercus-Taieri Resource Unit) between six and eight months of age, weighing 400-550 grams were used in this study. Rats were single housed in translucent plastic cags containing pine chips and maintained on a 12 hour light/dark cycle. All training and experimentation occurred during the light phase. After two weeks of daily handling and weighing during which rats had *ad libitum* access to food, rats were food deprived of standard rat chow (Speciality Feeds) to no less than 85% of their free-feeding weight to promote interest in reward during the experiment. Water was available *ad libitum* at all times in the home cage.

3.3.2 *Preoperative training*

During the initial week of training, rats were individually habituated for 15 minutes per day to the experimental apparatus, a figure-of-eight shaped runway which contained touchscreens, photobeams, two retractable 30cm barriers mounted on servo motors, and reward areas in which condensed milk (Highlander; Nestle) was dispensed into plastic wells by peristaltic pumps (Adafruit, New York, NY, USA; Figure 38A). The apparatus was controlled by a network of five Arduino (Arduino LLC, Somerville, MA, USA) microcontrollers. Condensed milk was freely available in plastic wells located in the reward zones in the maze. In the second week of training, rats were trained to run the maze in a unidirectional manner, starting at the bottom of the midstem, being forced to turn left or right at the vertex, and received a fixed reward (.5 ml of condensed milk) in the reward zones. Rats were prevented from reversing direction in the maze by photobeam-controlled doors. The rats were not paused between trials and completed laps in a continuous, uninterrupted manner.

Once the rats were running unidirectionally and not attempting to reverse course, they were trained to press a wall-mounted touchscreen which released an adjacent starting gate, thereby initiating a trial. The touchscreen indicated a successful press by turning from black to bright red. There was no delay between screen pressing and the lowering of the start gate. This typically took between one and four 15 minute training sessions. Screen-press training was considered complete when rats completed at least 30 trials per session for three consecutive training sessions. This typically took 6 training sessions.

The next stage of training involved the introduction of the two servo-mounted 30cm barriers into the apparatus (one in each maze arm) which rats had to overcome on their paths

to the reward zones. The servo motors both inserted and removed the barriers according to a programmed task protocol carried out by the Arduinos. These barrier-training sessions were to habituate the rats to the presence of the barrier and for them to learn how to climb over them. A fixed reward (.2 ml of condensed milk) was administered at the completion of each trial. Barrier training sessions were conducted until rats completed at least 30 trials per session for three consecutive sessions. This typically took four training sessions.

The next stage of training involved manipulations of the presence of the barrier and the magnitude of reward dispensed for different routes along the maze such that one maze arm contained a barrier and always yielded a large reward (.3 ml of condensed milk; high cost, high reward; HCHR) whereas the other maze arm would not contain a barrier and always yielded a low reward (.1 ml of condensed milk; low cost, low reward; LCLR). The HCHR arm alternated each day of this training phase. When rats completed at least 30 trials per session and were selecting the HCHR arm on at least 70% of trials, sessions were extended such that each session required rats to run 64 laps per session.

The final stage of training involved within-session manipulations of the HCHR arm. Although the initial maze configuration was counterbalanced across rats, we will, in the interest of clarity, describe the procedure where the initial HCHR maze arm was the right arm. For the rats where the initial configuration was that HCHR was the right maze arm, the first 32 trials the right maze arm was the HCHR arm and shifted such that the 33rd through 64th trials had the left maze arm as the HCHR arm. Regardless of the initial configuration (i.e. the HCHR arm being left or right), the maze configuration and outcome contingencies reversed during the inter-trial interval between trials 32 and 33 by the initial-HCHR-arm servo-mounted-barrier being removed from the maze and the opposite maze arm's servo-mounted barrier being inserted. The reward magnitudes delivered by the peristaltic pumps also automatically reversed. Within each session half, rats were sometimes forced towards the LCLR or HCHR trajectory to ensure they regularly sampled each trajectory. There were eight forced trials in each session half, four to the right, four to the left, which occurred pseudorandomly, but on average, every fourth trial. Rats were considered fully trained and ready for surgery when they completed all 64 trials in less than one hour and chose the HCHR arm in both configurations at least 70% of the time for three consecutive sessions.

3.3.3 *Surgery*

Once animals were considered trained, the nine rats were anaesthetized under isoflurane and stereotaxically implanted in the ACC (AP: 2.7 mm, ML: 0.4 mm, DV: -1.8 mm from dura) with seven 25 μm Formvar-coated nichrome wires (one tetrode and one tritrode;

California Fine Wire) mounted on a 3D-printed adjustable microdrive assembly and the VTA (AP: -5.3mm, ML: 1.0mm, DV: -8.2mm from dura) with a one non-moveable 127-µm-diameter, nickel chromium-coated wire. The electrodes were grounded by soldering a wire to a jewellers screw implanted in the cerebellum. The assembly was fasted to the skull with jeweller's screws and acrylic dental cement. Following the surgery, animals were allowed 10 days to recover, during which time they had *ad libitum* food and water. After 10 days, rats' food was reduced to maintain the animal at ~85% of their free-feeding weight to optimize behaviour during the experiment.

3.3.4 *Postoperative protocol*

After 10 days of recovery, rats were reintroduced to the maze with head plugs connected to a tethered head stage that housed three light emitting diodes (LEDs) for tracking. Training resumed from the final preoperative stage; all 9 rats quickly recalled the task with no signs of postoperative motor impairment. Once each rat demonstrated three consecutive sessions of completing all 64 trials in less than one hour and choosing the HCHR arm at least 70% of the time for each maze configuration, data acquisition began. Data acquisition occurred over the course of 10 consecutive days and was nearly identical to the postoperative training protocol except that the positions of the forced trials varied for each session, occurring, on average, every fourth trial. During the main experiment, the maze configuration discreetly changed during the inter-trial interval between the 32nd and 33rd trial such that there was no waiting period or any indication to the animal that the configuration had changed.

Following the completion of the main experiment, we recorded five of the animals as they habituated to a novel open field (a 35cm wide x 45cm long x 50cm tall cardboard box with a rubber floor) for 10 minutes per day over the course of two days. Although we only recorded the habituation of 5 of the rats, all 9 underwent this procedure and, following habituation, we recorded all 9 rats for 10 minutes per day over the course 10 days so that we could compare the electrophysiological measures obtained from the task, when the ACC and VTA were likely to be "engaged," against activities which were relatively "at rest."

3.3.5 *Electrophysiology and tracking*

Neuronal and local field potential activities were monitored and processed using the DacqUSB acquisition system (Axona, Ltd., St. Albans, UK). Neuronal signals were bandpass filtered from 360 – 7000 Hz and sampled at 48 kHz. Local field potentials (LFPs) were low-pass filtered at 500 Hz and sampled at 4800 Hz. The rats' position within the maze was monitored by a video camera mounted on the ceiling above the apparatus connected to a system which tracked the LEDs mounted on the head stage. Tracking data was sampled at 50

Hz and made available to the DacqUSB system. Key events (e.g. trial initiation, the type of trial initiated, changes in maze configuration, and breaking photo beams) were timestamped by inputs from the network of Arduino microcontrollers which controlled the maze to a digital input-output port on the DacqUSB system. Files were then read into Offline Sorter (Plexon Inc., Dallas, TX, USA) for spike sorting, based on visually dissociable clusters (principle components and peak-valley amplitudes; see Figure 37 for examples of isolated clusters). Subsequent analyses were conducted using MATLAB R2017b (The Mathworks, Boston, MA, USA) or Oriana (Kovach Computing Services, Anglesey, Wales).

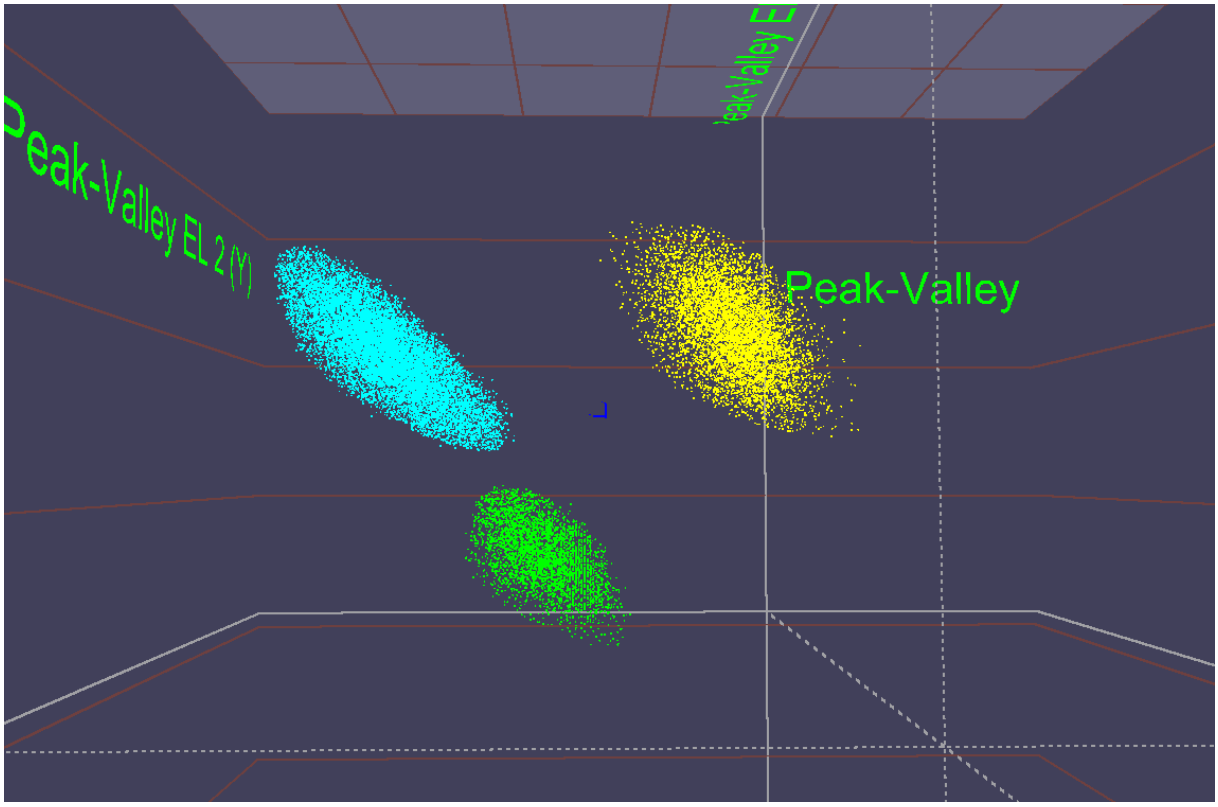

Figure 37. Example well-isolated single-unit clusters. These clusters represent three of the five neurons simultaneously recorded from rat 3 in one data collection session.

3.4 Data analysis

3.4.1 *Regression to control for between-subject variance*

We used a regression-based method, first used by Ma, Hyman, Lindsay, Phillips, & Seamans' (2014), to control for between-subject variance. This allowed us to pool/analyse via multifactorial ANOVAs the 5362 individual free choice trials across all 9 rats. No forced trials were included in our analyses. Of those 5362 free choice trials, 1540 were pre-reversal HCHR, 1142 were pre-reversal LCLR, 1654 were post-reversal HCHR, and 1026 were post-reversal LCLR.

The general approach we used was to normalize the data via the feature scaling formula (Ioffe & Szegedy, 2015), which rescaled the data between 0 and 1, and to then fit a regression model where a dependent measure of interest was regressed against a subject factor (i.e. a factor indicating which animal a particular data point was obtained from). The resulting model captured the variance in the dependent measure of interest that was explained by differences between the rats. The residuals, however, contained data that reflected to underlying variance in the parameter, independent of the effect of subject. It was these residuals which we analysed with the multifactorial ANOVAs. The benefit of this approach was that it showed much more clearly the same results as within-subject analyses and also revealed new trends. The other advantage of this approach was that it made both the interpretation and the reporting of the results more clear and concise

3.4.2 *Instantaneous neuronal firing rate estimation*

Ma, Hyman, Lindsay, Phillips, & Seamans' (2014) method was implemented to obtain a continuous, instantaneous estimate of the firing rate (iFR) of each isolated neuron. Briefly, the binary timestamps of each neuron were allocated into 200 ms bins. Exploiting the inverse relationship between frequency and period, for each bin, the iFR was calculated as the reciprocal of the inter-spike intervals, which were then convolved with a 20ms Gaussian kernel and then averaged over the bin. The iFR was computed for each neuron across the duration of the experimental session each neuron was recorded in.

3.4.3 *Selectivity analysis of individual neurons*

Cohen's d, the effect size statistic, was used to assess whether individual neurons were responsive to certain areas of the maze for the various task conditions and maze configurations. Cohen's d was computed as the mean difference in iFR between HCHR and LCLR trials divided by the pooled standard deviation of both HCHR and LCLR trials for each maze region and each maze configuration for each neuron, separately. A neuron was classified as selective in a particular maze region when Cohen's d $\geq |.5|$ and that the parameters with which Cohen's d was calculated were significantly different according to the sign rank test. Cohen's d was always calculated such that a positively signed result indicated HCHR selectivity and a negatively signed result indicated LCLR selectivity (i.e. HCHR – LCLR). The selectivity of each neuron for each maze region in each maze configuration was tested independently, which allowed a neuron to be considered selective for more than one maze region but not more than one classification (e.g. a neuron might show significant selectivity in several maze regions on HCHR trials but that neuron could not be classified as both HCHR and LCLR selective within the same session half).

3.4.4 *Phase modulation of single units to the local field potential*

Phase modulation of ACC single units was assessed by examining the distribution of unit spiking with respect to the phase angle of the simultaneously recorded ACC and VTA LFPs. Instantaneous LFP phase angles were determined by bandpass filtering the LFPs to the frequencies of interest by using a two-pole Butterworth filter with the *filtfilt* MATLAB function and then applying the standard Hilbert transform. Phase zero was defined as the positive peak of the waveform. The mean angular dispersion of spikes, henceforth referred to as the vector length, was calculated by the Pythagorean Theorem as the square root of the squared mean cosine plus the squared mean sine for all spikes for each neuron, separately. The vector length provides a measure of the concentration of firing about the unit circle. Normalized vector lengths were obtained by comparing the obtained vector lengths to vector lengths of spikes equally distributed about the unit circle for each neuron, separately. Thus, the normalized vector length indicates the extent to which spikes clustered at a specific phase angle as compared to the same number of spikes being uniformly distributed across all phase angles. The significance of angular dispersions, indicating whether the phase of firing distribution was evenly distributed or possessed a significant mean direction, was assessed using Rayleigh's test for circular uniformity (Zar, 1999).

3.4.5 *Local field potential power and coherence*

Time-resolved LFP power and coherence were calculated via multi-taper spectrograms and coherograms (Mitra & Bokil, 2008) which used three tapers, a one-second reading window, and 85% overlap amongst windows. Statistical analyses of LFP power and coherence were done across well-defined frequency bands (Buzsaki, 2006).

3.4.6 *Partial directed coherence for detecting signal directionality*

Task-related, causal relationships between the ACC and VTA LFPs were assessed with a partial directed coherence (PDC) algorithm, a frequency-resolved estimate of Granger causality, which uses multivariate autoregressive modelling to exploit the predictability of information in one brain area by past activity in another (Baccalá & Sameshima, 2001). Our implementation of PDC followed Boykin, Khargonekar, Carney, Ogle, & Talathi's (2012) method. One advantage of PDC over other measures of directionality, such as amplitude cross-correlations (e.g. Adhikari, Sigurdsson, Topiwala, & Gordon, 2010), is that PDC allows for testing the possibility of simultaneous bi-directional communication, which is particularly likely to occur between two reciprocally connected areas, such as the ACC and VTA (David B. Carr & Sesack, 2000; Narita et al., 2010).

3.4.7 *Histology and electrode placement verification*

Upon completion of the study, rats were deeply anaesthetized with isoflurane and recording sites were electrolytically lesioned with direct current (2mA for 2 seconds) before transcardial perfusion. Electrode tracks and microlesions marking the electrode position were identified in 50μm thick sections of formalin-fixed tissue stained for Nissl substance (Figure 38A and B). To verify our VTA electrodes, we used immunohistochemistry to label sections for tyrosine hydroxylase (TH; anti-TH primary antibody was AB152 from Millipore).

3.5 Results

3.5.1 *Task, apparatus, and neurophysiological recordings*

Nine rats with implants in the ACC and VTA performed a spatial decision task (see Figure 38D and E) where the optimal (most economic) choice reversed once per recording session. In this task, the rats initiated a trial by pressing a wall-mounted touchscreen and were then required to decide whether to pursue a large reward at the cost of climbing a 30cm barrier (high cost high reward; HCHR) or whether to pursue a small reward which did not require climbing a 30cm barrier (low cost, low reward; LCLR). On the basis of our prior experiments (Hillman & Bilkey, 2010) as well as those of others (Holec et al., 2014; Schweimer & Hauber, 2006; Walton et al., 2003), we expected that the rats would come to prefer the economic, HCHR option. However, in all of these prior studies, the rats never selected the HCHR arm 100% of the time, as would be optimal in terms of maximizing the amount of earned reward. We were interested in whether these choices could be construed as either exploratory or anticipatory.

In an effort to distinguish between these two possibilities (exploration vs anticipation), we included a reversal component. Two findings influenced our choice of a single-reversal in this experiment. First, Farashahi et al. (2017) reported an inverse relationship between the volatility of the environment and the value of exploring alternatives such that as volatility (e.g. the number of reversals) increased, the likelihood of subjects selecting a non-default choice decreased. Second, some of our recent work (which used 5 of the 9 rats included in this present experiment) in a "high volatility" decision context (6 reversals over the course of ~80 trials per session; data not shown) indicated that the animals rarely deviated from the optimal choice and there was no clear relationship between the non-optimal choices and reversals or any other key experimental event. This prior finding in a high-volatility environment suggested that those non-default decisions were likely errors. Thus, considering our prior findings in conjunction with Farashahi et al.'s which suggest that choices which are perhaps

anticipatory or exploratory in nature are most likely to occur in a low-volatility environment, we opted for a single-reversal (i.e. very low volatility).

The ACC and VTA have long been implicated in both anticipation and value-guided choice (Blanchard et al., 2015; Hamid et al., 2016; Howe et al., 2013; Kennerly et al., 2011; Wolfram Schultz et al., 1997); however, whether and how these structures interact during anticipatory and economic choices has remained unknown. Because our task aimed to elicit both of these choices types, we simultaneously recorded local field potentials (LFPs) in the ACC and VTA as well as single-units in the ACC. We histologically confirmed our electrode placements by staining for tyrosine hydroxylase, a marker of dopaminergic neurons (Amantea & Bowery, 2004; Carr & Sesack, 2000), in the VTA and staining for Nissl substance in the ACC.

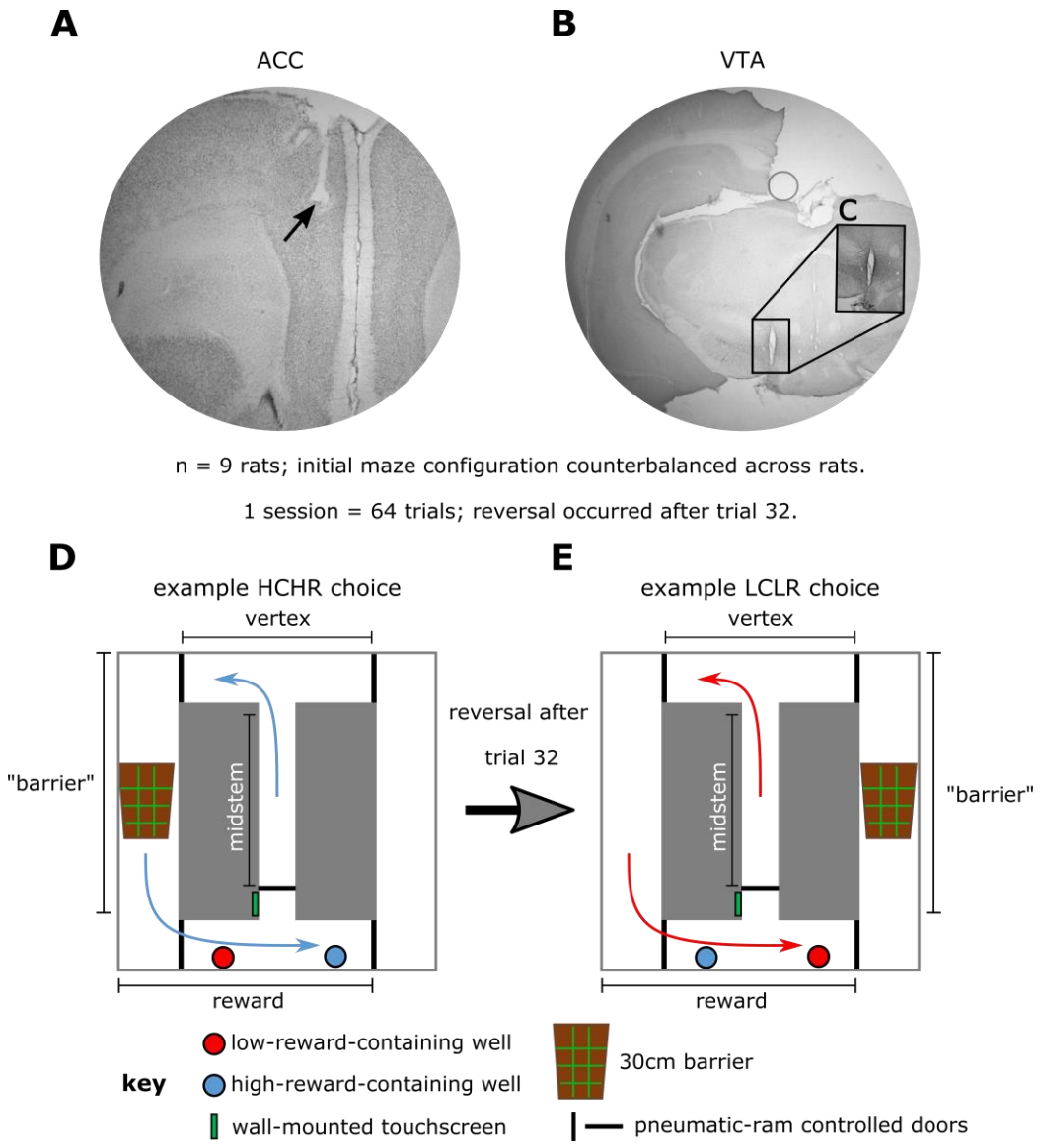

Figure 38. Histology and task diagram. (A) Nissl-stained section which shows and electrolytic lesion in the ACC, indicating electrode placement in the ACC. (B) Tyrosine-hydroxylase (TH) immunolabelled section with an electrolytric lesion in the TH+ area of the VTA, indicating electrode placement in the VTA. TH is a marker of dopaminergic neurons (Carr & Sesack, 2000; Hamid et al., 2016). (C) Enlarged portion of the boxed area in B. (D and E) task diagram and example trial trajectories.

3.5.2 *Decision patterns, running speeds, and latencies*

The first behaviour we assessed during this experiment was whether the probability of the rats making non-default, LCLR choices changed over the course of an experimental session (Fig. 39AB). We predicted that the rats would make more LCLR choices before as compared to after the reversal, which they did. We were next interested in whether these pre-reversal LCLR choices coincided with the reversal – if the number LCLR choices increased as the pre-reversal trials progressed then that would suggest that the animals had learned to anticipate the reversal and that these choices were anticipatory in nature. However, if the LCLR choices were evenly distributed across the pre-reversal trials, then that might suggest that the pre-reversal LCLR trials were exploratory. We formally assessed this by finding the

average number of LCLR choices in each session octile (i.e. the count of LCLR choices in 8 trial bins) for each session for each rat, separately. Animal grand means were then assessed via ANOVA (*anovan*, MATLAB). We found a significant main effect of octile ($F_{7,71} = 24.72$, $p < 1.0x10^{-6}$) and noticed that the number of LCLR choices was maximal during trials immediately preceding the reversal, suggesting that the animals anticipated the reversal. To be sure that it was anticipation of the reversal that explained the animals' decision behaviour, we trained 3 of the rats in a delayed reversal condition where the reversal occurred after trial 42 (rather than after trial 32). We found a significant effect of octile ($F_{7,47} = 7.45$, $p = 5.1x10^{-6}$), a significant octile x reversal interaction ($F_{7,47} = 7.22$, $p = 7.2x10^{-6}$), and that the number of LCLR choices again increased immediately prior to the reversal trial. Together, these results suggest that the pre-reversal LCLR decisions were anticipatory in nature.

Because we identified pre-reveral LCLR choices as being anticipatory, we wondered whether the overt behaviours of the animals differed throughout the maze (Fig 39C). To formally assess this, we obtained the mean running speed (see Methods) of the animals for each maze region for each lap for each animal, separately. Animal grand means were then assessed via ANOVA. Although our ANOVA did reveal significant main effects of choice ($F_{1,143} = 6.69$, $p = 0.011$), maze region ($F_{3,143} = 68.15$, $p < 1.0x10^{-6}$) and reversal ($F_{1,143} = 7.52$, $p = .0069$), it did not detect either a maze region x choice interaction ($F_{3,143} = 1.89$, $p = 0.13$), a choice x reversal interaction ($F_{1,143} = 0.13$, $p = 0.72$), or a maze region x choice x reversal interaction ($F_{3,143} = 1.74$, $p = 0.16$). These results reflect that the animals generally ran slower in the midstem and barrier region and were generally faster in the vertex (i.e. the choice point) and the reward regions and that the rats tended to run faster during HCHR trials. The lack of a either a choice x region interaction or a choice x region x reversal interaction indicates that the overt decision behaviour at the vertex associated with pre-reversal LCLR choices, as indicated by running speed, was not significantly different.

As an additional probe into the overt behaviour of the animals during decision making, we asked whether the movement trajectories of the animals different by choice type. We assessed this by plotting and overlaying the tracked positions of the animals by choice type for each session of each animal, separately, and then assessed the overlap of the trajectories with special attention to the vertex region. We found no differences here (i.e. nearly perfect overlap of the trajectories; data not shown). These findings, in conjunction with the lack of a difference in the movement speeds of the animals, indicate that although the overall pattern of decisions by the animals varied such that the likelihood of the animals to deviate from their

default HCHR choices increased as the pre-reversal trials progressed, the overt behaviours associated with the different choice types was not different.

Given how anticipation can influence motivation (Ward, Winiger, Higa, et al., 2015; Ward, Winiger, Kandel, Balsam, & Simpson, 2015), we wondered whether the outcome of one choice would influence how quickly the animals would begin a new trial. Again using animal grand means, we compared the latency to begin a new trial from the time the animals reached the reward well after having completed a trial of a given type (Fig 2D). Our ANOVA did not reveal a main effect of choice type ($F_{1,35} = 2.37$, $p = 0.13$) but it did reveal a significant main effect of reversal ($F_{1,35} = 6.29$, $p = 0.017$). No choice type x reversal effect was detected ($F_{1,35} = 0.3$, $p = 0.59$). Because our latency measure also includes the time the animals took to consume their reward, these results indicate that the animals took about the same amount of time to consume a HCHR and LCLR reward. These results also indicate that the animals took slightly longer in initiating a new trial following the reversal but that this increased latency was not associated with a given choice. Together, to the extent that a latency measure can describe the influence of a trial outcome on subsequent motivation to work again, these results suggest that our animals were not differentially motivated to begin a new trial following either a high reward or low reward outcome.

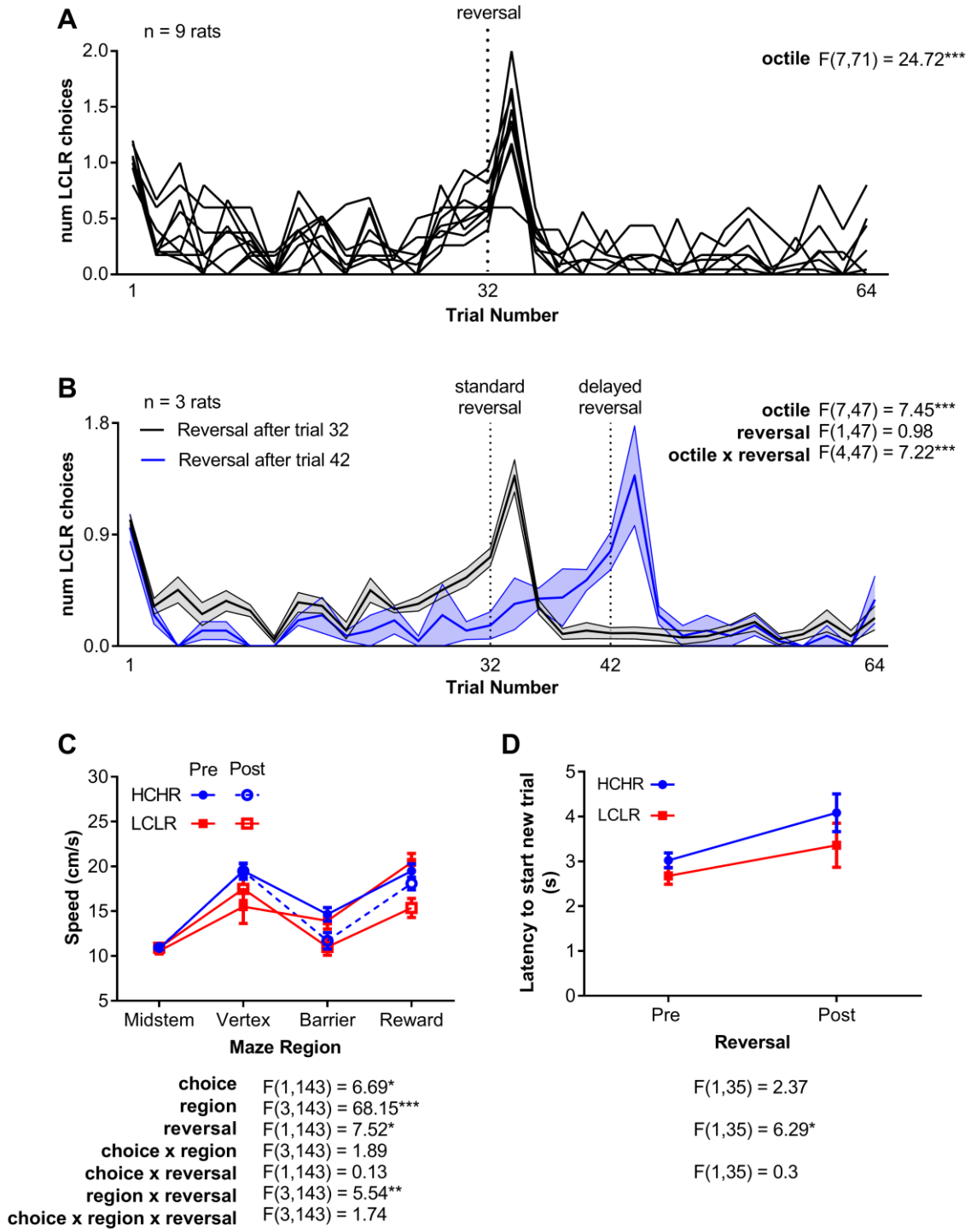

Figure 39. Rat behaviour. (A) Rats are more likely to choose the LCLR arm as the pre-reversal trials progress and are much less likely to choose the LCLR after the reversal. Data are presented as the number of LCLR trials across a two-trial bin. Each line indicates the individual grand mean for a given bin for a given rat. (B) Rats' pre-reversal LCLR choices appear linked to the reversal point, regardless of whether the reversal occurred after trial 32 or 42, suggesting that the animals anticipated the reversal. Data are presented as mean±SEM across each two-trial bin. (C) Rats' running speeds varied through the maze and, generally, were faster in the vertex during HCHR choices than LCLR choices and were slower in the reward region during post-reversal LCLR choices. Data are presented as mean±SEM. (D) Upon completion of a trial, rats were slightly longer in initiating a new trial after the reversal. Data are presented as mean±SEM. All data were assessed with ANOVAs. *p<.05, **p<.005,***p<.0005.

3.5.3 *Task-related changes in ACC and VTA LFPs*

The ACC and VTA power spectrum density (PSD) functions from 1 to 30Hz obtained from this data set were consistent with the prior reports (Elston & Bilkey, 2017; Fujisawa & Buzsaki, 2011; Parker, Chen, Kingyon, Cavanagh, & Narayanan, 2014) of the VTA and ACC exhibiting local peaks centered at about 4Hz (see Figure 40). As a comparison, we also computed the PSDs and coherences of the 9 rats roaming in a familiar open field. Specifically, for each rat, we compared the 10 task session PSDs and coherences against 10 open field recordings and found that it was only in the low frequencies, in the 2-5Hz band, that the PSDs and coherences collected from task sessions were significantly greater than the open field ($p<.005$ for each rat, t-tests). Activity within and between these structures at such frequencies has been reported several times (Elston & Bilkey, 2017; Fujisawa & Buzsaki, 2011; Gao et al., 2007; Parker et al., 2014; Parker, Chen, Kingyon, Cavanagh, & Narayanan, 2015) and has been previously described as a 4Hz oscillation. Therefore, we focused our subsequent analyses on this frequency band and, in an effort to maintain a consistent terminology, we will refer to the 2-5Hz activity we observed as 4Hz throughout the rest of this chapter.

It is unlikely that the effects we observed result from volume conduction from nearby structures because we also recorded from the ACC single units and found cells were phase-modulated at 4Hz to both local ACC and VTA LFPs, sometimes independently. Had our effects been the result of volume conduction, such 4Hz phase-modulation of ACC unit firing would not have been evident.

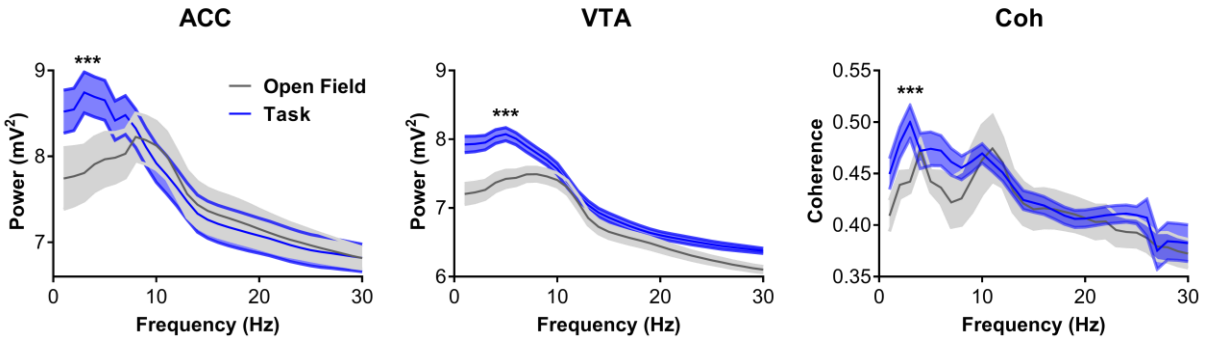

Figure 40. Our task significantly engaged the ACC and VTA at about 4Hz as compared to when the animals roamed in a familiar open field. While the comparisons of the open field and task recordings were done within each animal, separately (n = 10 paired open field and task recordings per animal), the data here are presented as the grand mean±SEM across all 5 rats used for this analysis. ***$p<.005$ via t-tests within all rats.

3.5.4 *Normalizing the spectral data and testing for normality*

Next, we asked whether and how 4Hz ACC and VTA power and coherence systematically varied as a function of choice type (HCHR or LCLR), maze region (midstem,

vertex, barrier, and reward), and the reversal. To do this, we computed multi-taper spectrograms and coherograms (Mitra & Bokil, 2008) for each session for each rat and then normalized the data via the feature-scaling formula (Ioffe & Szegedy, 2015). We then determined the mean VTA and ACC power and coherence in the 2-5Hz (hence 4Hz) band for each maze region for each trial within each session. In order to pool trials across animals, we used a regression approach, first introduced by Ma, Hyman, Phillips, & Seamans (2014), to control for between subject variance (see section 3.4.1 for method) and conducted subsequent spectral analyses on the residuals unless specifically noted. Only free choices were included in the subsequent analyses; in total 5362 single trials were analysed where 1540 were pre-reversal HCHR, 1142 were pre-reversal LCLR, 1654 were post-reversal HCHR, and 1026 were post-reversal LCLR.

Next, because we wished to analyse our data with multifactorial ANOVAs, we tested the task distributions of normalized residual VTA and ACC 4Hz power and coherence for normality. According to Lilliefors' test (*lillietest* in MATLAB), our normalized residuals were not normally distributed. However, we proceeded to use ANOVAs for two reasons: (i) because studying the interactions of factors, which is essential for our analyses, is not possible in Friedman's test, the non-parametric analogue of the ANOVA and (ii) several recent statistical studies have indicated that the ANOVA is very robust against violation of the assumption of normality such that the type 1 error rate is unaffected by violations of normality (Blanca, Alarcón, Arnau, Bono, & Bendayan, 2017; Schmider, Ziegler, Danay, Beyer, & Bühner, 2010). For these reasons, we felt confident to conduct the subsequent analyses with multifactorial ANOVAs to assess how our spectral measures changed when the ACC and VTA were engaged by our task.

3.5.5 *4Hz anticipation and persistence signals in the ACC and VTA*

The key findings from the spectral analyses were that VTA 4Hz power and ACC-VTA 4Hz coherence were significantly elevated in the vertex region as the rats made putatively anticipatory pre-reversal LCLR choices (see Figures 41 and 42; for readability, I have included the statistics in the appropriate panels of Figure 42; note that the error bars in Figure 42 denote 95% confidence intervals). After the reversal (when the HCHR and LCLR configuration reversed), however, 4Hz ACC and VTA power and coherence was significantly elevated in the vertex as rats made HCHR choices. These effects cannot be attributed to a confound of maze side because the initial maze configuration was counterbalanced across animals and, after the conclusion of this main experiment, we conducted a control experiment where the value and effort aspects of each maze arm were held equal and no significant

differences between leftward and rightward trajectories were detected (see Results subheading 3.5.7 *Our spectral and PDC findings are driven by task demands*).

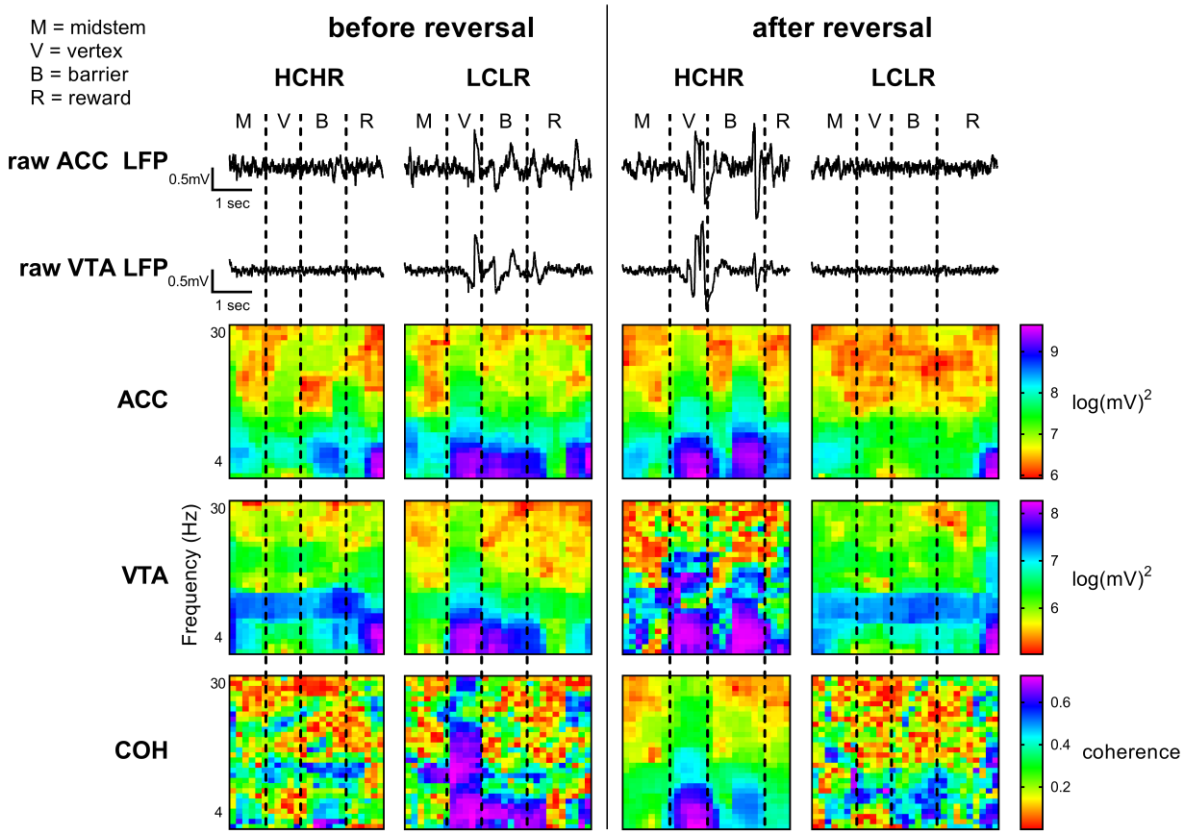

Figure 41. Representative single trial raw LFP traces and spectrograms generated from those traces for each trial type. Note increased low frequency VTA power and ACC-VTA coherence in the vertex region associated with LCLR responses in the before the reversal and elevated low frequency VTA, ACC and ACC-VTA coherence HCHR responses in the after the reversal. Example data are from one session of rat 4.

Because LFPs are thought to indicate the aggregate of inputs, rather than outputs (Buzsaki, 2006), the increases in VTA 4Hz power and the onset of higher ACC-VTA coherence that occurred during implementation of pre-reversal LCLR choices suggests that ACC signals were propagated to the VTA during this period. In contrast, after the maze configuration shifted, increases in ACC and VTA 4Hz power and coherence increased for HCHR choices, now made to the new sides. Some interpretations of these effects are (i) that one aspect of the implementation of anticipatory choices involves top-down ACC→VTA signalling and (ii) that the persistence of the behavioural shift during the second-half session required bi-directional communication between the ACC and VTA.

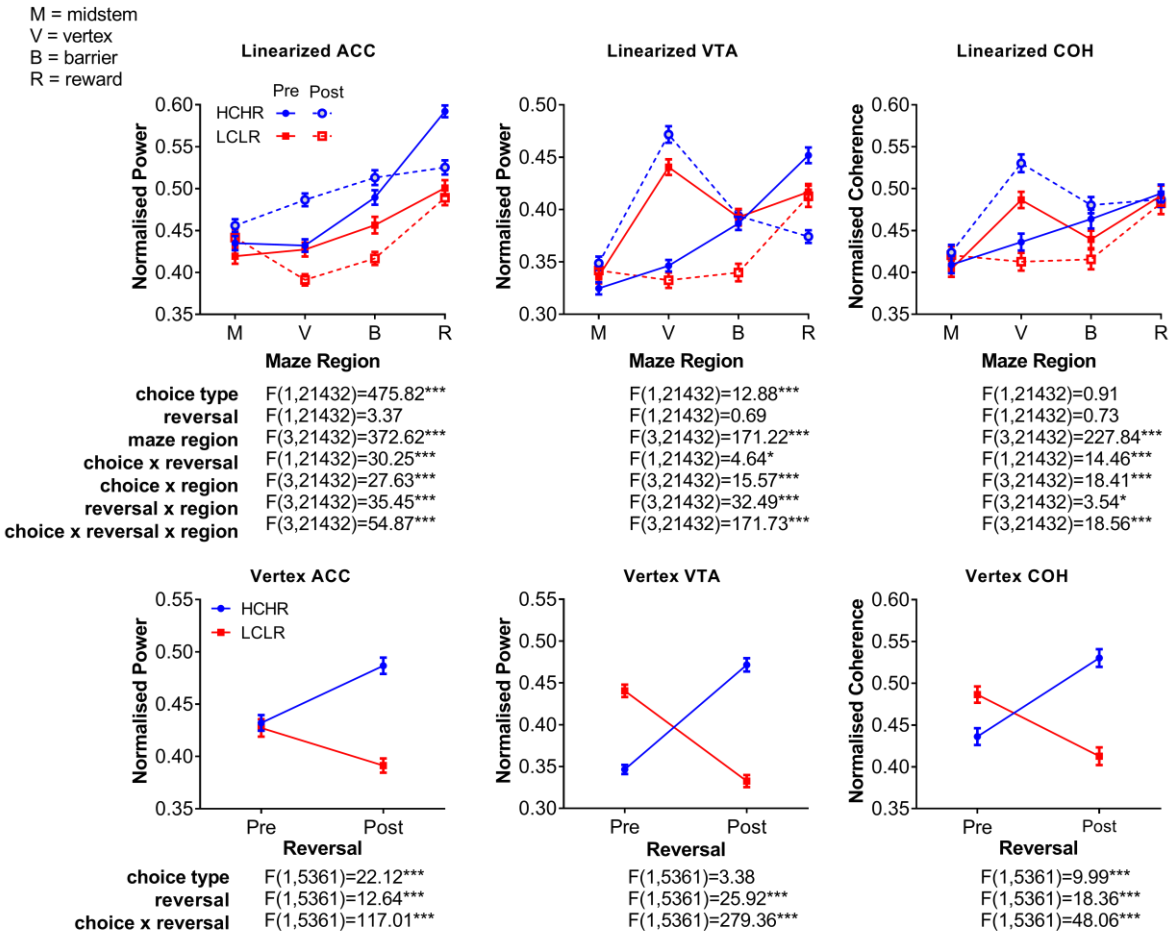

Figure 42. Changes in 4Hz ACC and VTA power and coherence by maze region and trial type. VTA 4Hz power and ACC-VTA 4Hz coherence were elevated in the vertex during pre-reversal LCLR choices. Post-reversal HCHR choices were associated with elevated 4Hz ACC and VTA power and elevated 4Hz coherence. ACC 4Hz power generally increased as the trial progressed whereas the largest changes in VTA power and ACC-VTA coherence occurred as rats made their decisions in the vertex. Significances were assessed with ANOVAs and data are presented as mean±95% confidence intervals.

3.5.6 *Directionality of ACC-VTA communication*

Our spectral results suggested 4Hz ACC-VTA communication increased in the vertex as rats made pre-reversal LCLR and post-reversal HCHR choices, respectively. While suggestive, the directionality of these communication increases were unclear. Therefore, as we have done in the past (Elston & Bilkey, 2017) we formally assessed changes in directionality via partial directed coherence (PDC) modelling (Baccalá & Sameshima, 2001; Boykin et al., 2012), which exploits the predictability of one brain area at one point in time by another brain area at a different time point in the frequency domain. The advantage of PDC modelling over other methods we have used to assess directionality, such as amplitude cross-correlations (Adhikari et al., 2010; Elston & Bilkey, 2017), is that it allows for testing the possibility of simultaneous, bi-directional communication, which is likely to occur between two reciprocally connected structures like the ACC and VTA. We fitted PDC models in the 2-5Hz (hence 4Hz) frequency band for each maze region of each trial for each animal,

separately. We then regressed off between-subject using the procedure described earlier. Because PDC is itself a normalized measure, we did not normalize the resulting PDC model magnitudes before the regression.

Our key findings here generally agreed with our spectral results: that increased 4Hz ACC→VTA signalling in the vertex was associated with anticipatory, pre-reversal LCLR choices and this signal was even larger following the reversal as animals persisted in shifting their decisions to the post-reversal HCHR side (see Figure 43; for readability, the ANOVA results are included in the relevant panels of Figure 43; note that the error bars in Figure 43 denote 95% confidence intervals). In contrast, signalling in the opposite direction (VTA→ACC) was elevated in the vertex as rats made pre-reversal HCHR choices. We also found elevated VTA→ACC signalling in the reward region (i.e. at the outcome) of post-reversal LCLR choices. Considering that the majority of post-reversal LCLR choices occurred during the trials immediately after the reversal and that the rats rapidly adapted their subsequent choice behaviour (see Figure 39AB), this finding suggests that elevated 4Hz VTA→ACC signalling may be associated with error detection and subsequent behavioural adaptation.

Next, in order to verify the integrity of our PDC models, we scrambled the recorded signals from both the ACC and VTA and conducted the trial-by-trial, region-by-region PDC analysis again. Here the comparisons were the medians of the PDC model magnitudes from the permuted and non-permuted distributions for each region by session half (e.g. permuted ACC→VTA pre-reversal vertex LCLR versus non-permuted ACC→VTA vertex pre-reversal LCLR). In every case and for both directionalities, the medians of the permuted distributions were significantly weaker than the non-permuted data (both p vals < .0005, sign rank tests). These data indicate that our PDC results were significantly different from chance.

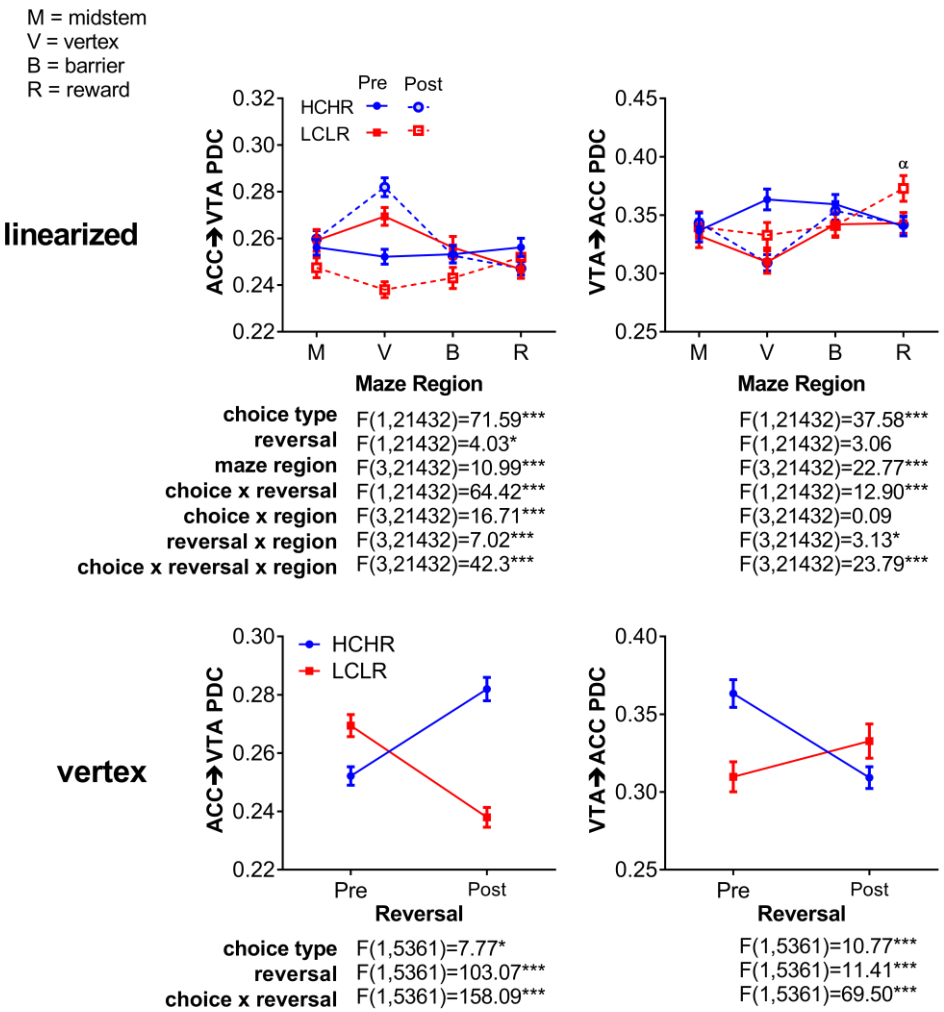

Figure 43. Changes in 4Hz ACC→VTA and VTA→ACC signal directionality by maze region and trial type. ACC→VTA 4Hz signalling was elevated in the vertex as rats made pre-reversal LCLR and post-reversal HCHR choices. VTA→ACC 4Hz signalling was elevated in the vertex as rats made pre-reversal HCHR choices and in the reward region at the outcome of post-reversal LCLR choices. Significances were assessed with ANOVAs and data are presented as mean±95% confidence intervals.

3.5.7 *Our spectral and PDC findings are driven by task demands*

Next, we wanted to ensure that our spectral and PDC results were driven by the choice-related task demands of the main experiment. We did this by conducting a control experiment (after the completion of the main experiment) where we ran 5 rats for 32 trials/day for 4 days. In this control experiment, each maze arm was equally rewarded and no barrier was ever present. Then, for each animal, we computed the session averages for each maze region of ACC and VTA 4Hz power and coherence as well as 4Hz ACC→VTA PDC and 4Hz VTA→ACC PDC. Because our main findings concerned changes as rats made their decisions in the vertex, we compared the power, coherence, and PDC models for the vertex as rats made leftward and rightward choices. This comparison was done within-subject where the four session averages for leftward and rightward trajectories were compared. We found no significant differences in the vertex between leftward and rightward trajectories in any

measure (all $p > .05$, sign rank tests, n=4 sessions per animal for each of the 5 animals). These results indicate that the changes in ACC and VTA 4Hz power and coherence and the PDC models in both directions were not systematically attributable to the rats entering any particular maze arm and, rather, indicate that they were driven by the choice-related demands of the main experiment.

3.5.8 *Our spectral and PDC measures do not exhibit ramping profile during pre-reversal trials*

Because we detected a ramping in pre-reversal LCLR choices in anticipation of the reversal (see Figure 39AB), we wondered whether our spectral and PDC measures would also exhibit such a ramping profile. We addressed this question by comparing the animal grand means for each measure for each session octile using the same approach used to measure the behavioural ramping effect in Figure 39AB. In every case, ANOVAs returned insignificant (all $F_{7,71} < 1.5$, all $p > .01$). These results indicate that 4Hz ACC and VTA power and coherence and the PDC models for both directionalities did not exhibit a ramping activation profile. Rather, these results indicate that when the responses did occur, they tended to occur at a similar magnitude at each occurrence (see Figure 44 for representative examples).

3.5.9 *Abrupt and temporary changes in power, coherence, and PDC model distributions following reversal*

To examine the dynamics of how ACC and VTA signals and communication changed following the contingency reversal, we assessed trial-by-trial changes in 4Hz VTA and ACC power and ACC-VTA coherence in the vertex region (see Figure 44). This analysis revealed that, immediately after the action-outcome contingencies reversed, LCLR-HCHR related distributions of power, coherence, and ACC→VTA PDC diverged markedly. This shift in distribution was stable for about 16 trials before becoming much more variable. We formally assessed this pattern by comparing the variance of these measures on HCHR trials in the vertex region across post-reversal trials. A comparison of the variance of trials 33-48 with trials 49-64 revealed that the variance in all these measures in immediate post-reversal trials was significantly less than variance in the later trials (sign rank tests, $p < .0005$ in all animals, n = 10 sessions per animal). This brief post-reversal bi-modal separation of the data may indicate a temporary state-change in the ACC-VTA circuit associated with shifting from rightward-HCHR choices to leftward-HCHR choices.

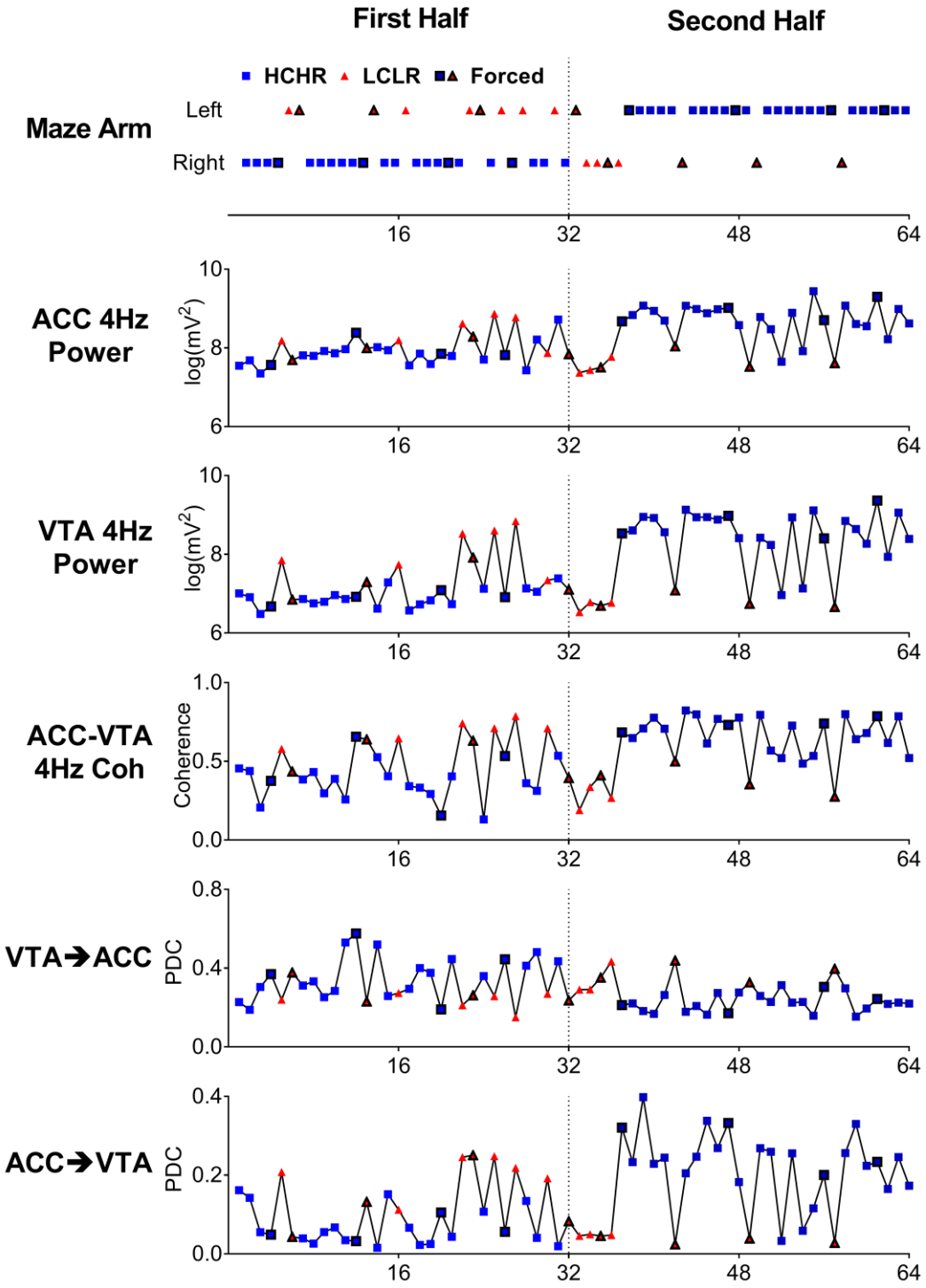

Figure 44. Trial-by-trial changes in 2-5 Hz VTA and ACC power, ACC-VTA coherence, and PDC models in the vertex region. Data are from the same session and rat as the trajectory-mapped power and coherence in Figure 42. The top panel summarizes the animals' decision behaviour and shows how, in the first half, HCHR choices were associated with the right maze arm whereas in the second half of sessions they were associated with the left maze arm. Note the bimodal distribution of ACC and VTA power and coherence in the trials immediately after the contingency reversal, indicated by the vertical dotted line.

3.5.10 *ACC-to-VTA 4Hz PDC exponentially decays during habituation*

Next, we asked whether 4Hz ACC→VTA signalling would correlate with anticipatory behaviour in a different experimental task. To assess this, we conducted a habituation

experiment where we recorded from 5 of the 9 rats used in the main experiment as they explored and habituated to a new environment (a 35x45x50cm open field) over the course of two consecutive days for 10 minutes each day. We selected this task because exploration of a novel environment appears to be driven by the anticipation that the information gained during exploration will be useful (Butz, Sigaud, & Gérard, 2003; Friston et al., 2015; Knox, Otto, Stone, & Love, 2011). Thus, the animals' exploration and habituation to a novel open field offers an alternative approach to studying whether ACC→VTA signalling is associated with anticipatory behaviours.

Prior behavioural studies indicate that exploration of a novel environment is greatest upon introduction to the new environment and then decays exponentially (Dubovický, Skultétyová, & Jezová, 1999; Terry, 1979). On this basis, we hypothesised that 4Hz ACC→VTA PDC would also be elevated as the rats explored the new environment and would then exponentially decay with habituation. To test this hypothesis, we calculated the 4Hz ACC→VTA PDC for each minute of each habituation session for each rat, separately, and then fitted them with an exponential curve. To assess the animals' behavioural habituation, we conducted an analogous analysis for the rats' minute-by-minute instantaneous movement speed. We found that 4Hz ACC→VTA PDC was maximal when the rats were first placed in the novel environment and was well-fit (day 1 R^2=.84; day 2 R^2=.33) by an exponential function across the 10 minutes of habituation (see Figure 45A). We also found that ACC→VTA 4Hz PDC just after the animals were placed in the open field was greater on the first day as compared to second day ($F_{2,96}$=33.42, p<.0005). Similarly, we found that the animals' movement speed was greatest when first exposed to the environment and then decreased across the minutes of the habituation sessions (day 1 R^2=.46; day 2 R^2=.16; see Figure 45B). Again, our analyses indicated that the exponential functions fitted to the first and second day behaviour were significantly different ($F_{2,96}$=5.33, p=.006). Interestingly the decay rates for the PDC data fit (day 1 λ = -.236; day 2 λ = -.137) were markedly greater than for the behavioural data (day 1 λ =-0.065; day 2 λ =0.033). Together, these data indicate that 4Hz ACC→VTA PDC and movement speed were greatest during the initial exposure and subsequent exploration of the novel environment and then exponentially decayed, although at different rates, as habituation ensued.

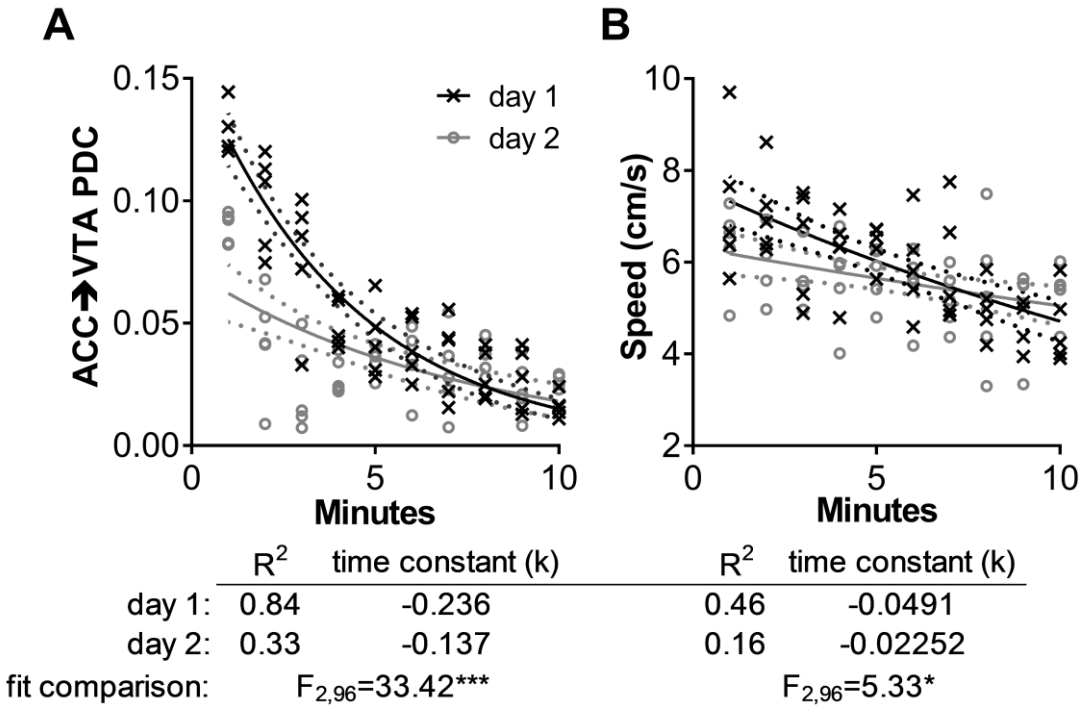

	R^2	time constant (k)	R^2	time constant (k)
day 1:	0.84	-0.236	0.46	-0.0491
day 2:	0.33	-0.137	0.16	-0.02252
fit comparison:	$F_{2,96}$=33.42***		$F_{2,96}$=5.33*	

Figure 45. ACC-to-VTA 4Hz PDC (A) and movement speed (B) exponentially decay during habituation to an open field. Each data point represents the mean of one animal for that minute. The solid lines are the fitted functions and the dotted lines are the 95% confidence intervals for each function, respectively. *p<.05, ***p<.0005.

Next, we assessed the relationship between the minute-by-minute 4Hz ACC→VTA PDC and movement speed and found that they were significantly correlated during the first day of habituation (r=.50, $p=2.03x10^{-4}$) but not during the second day (r =.21, p=.15). These data indicate that 4Hz ACC→VTA PDC and movement speed were strongly related while the animals explored the novel environment during the initial exposure to the open field but were not significantly related after the animals' initial exploration of the open field. Together, these data indicate that elevated 4Hz ACC→VTA is present during multiple types of anticipatory behaviour and that eliciting this signal does not appear to depend on our specific cost-benefit reversal task.

3.5.11 *ACC single-unit analyses*

Several prominent theories of ACC function suggest that the ACC encodes models of the task at hand (Holroyd & Yeung, 2012; Nils Kolling et al., 2016; A Shenhav et al., 2013). On the basis of prior work from our lab (Elston & Bilkey, 2017; Hillman & Bilkey, 2010, 2012) and others (Cowen et al., 2012; Wallis, Anderson, & Miller, 2001), we surmised that such models must incorporate populations of ACC neurons that encode various aspects of the task. To test this possibility, we determined the selectivity (see next section) of 167 neurons recorded from 6 rats across the 60 data collection sessions of those 6 rats. 1-6 neurons were

recorded from each rat each day with each rat contributing a somewhat similar number of cells to the analysis. All analyses were done within-cell and no data was pooled across cells unless explicitly stated. Across all cells, the mean ± SEM instantaneous firing rate (iFR; see methods) over the whole sessions was 1.13 ± 0.49 Hz, consistent with prior recordings of ACC pyramidal neurons (Fujisawa & Buzsaki, 2011; Fujisawa, Amarasingham, Harrison, & Buzsáki, 2008; Hillman & Bilkey, 2010, 2012).

3.5.12 *Orthogonal classification of ACC unit activity*

We calculated the selectivity of individual ACC neurons for the factors of value (HCHR vs LCLR), action (left vs right trajectories), and maze region. We did this by comparing the iFRs of each neuron across each maze region for each trial type, and each maze configuration within an experimental session, using Cohen's d, the effect size statistic, and the sign rank test. A positive Cohen's d indicated increased firing in the HCHR side of the maze and a negative value indicated the opposite. Neurons were deemed selective if Cohen's d > |.5| and the parameters assessed when calculating Cohen's d were significantly different ($p<.05$) via the sign rank test. To visualise whether selective neurons were consistently representing action or value across the whole recording session, we plotted the Cohen's d of the neurons deemed selective in the first session half against the Cohen's d of those same neurons in the second session half (Figure 45). An analogous procedure was conducted with neurons which were categorised as selective in the second half of the experimental sessions. Neurons with positively signed Cohen's ds in both the first and second halves of the experimental sessions mapped into quadrant 1 (Figure 46) and, if Cohen's d > .5 in both session halves, the cell was classified as HCHR selective (mean ±SEM iFR = 1.35±.10 Hz). Conversely, cells with negatively signed Cohen's d in both halves of the experiment mapped into quadrant 3 and were classified as LCLR selective (mean ±SEM iFR = 1.28±.10 Hz). Neurons with a positively signed Cohen's d in the first half and a negatively signed Cohen's d in the second half mapped into quadrant 4, and these neurons were classified as right-trajectory-selective because the cells were consistently firing according to side rather than value (mean ±SEM iFR = 1.33±.12 Hz). Conversely, left trajectory-selective cells mapped into quadrant 2 (mean ±SEM iFR = 1.29±.11 Hz). The mean iFRs of each cell of each classification were not significantly different (ANOVA; $F_{3,129}=.075$, $p>.9$). Within these groups, we classified 38 unique neurons as HCHR-selective, 36 unique neurons as LCLR-selective, 29 unique neurons as left-trajectory-selective, and 27 unique neurons as right-trajectory-selective (see Figure 47 for example neurons). It is noteworthy that more selective cells were active at any one time in the barrier region of the maze as compared to the midstem

region, suggesting that the selectivity of the task-ensembles gradually ramped up over the course of each maze run.

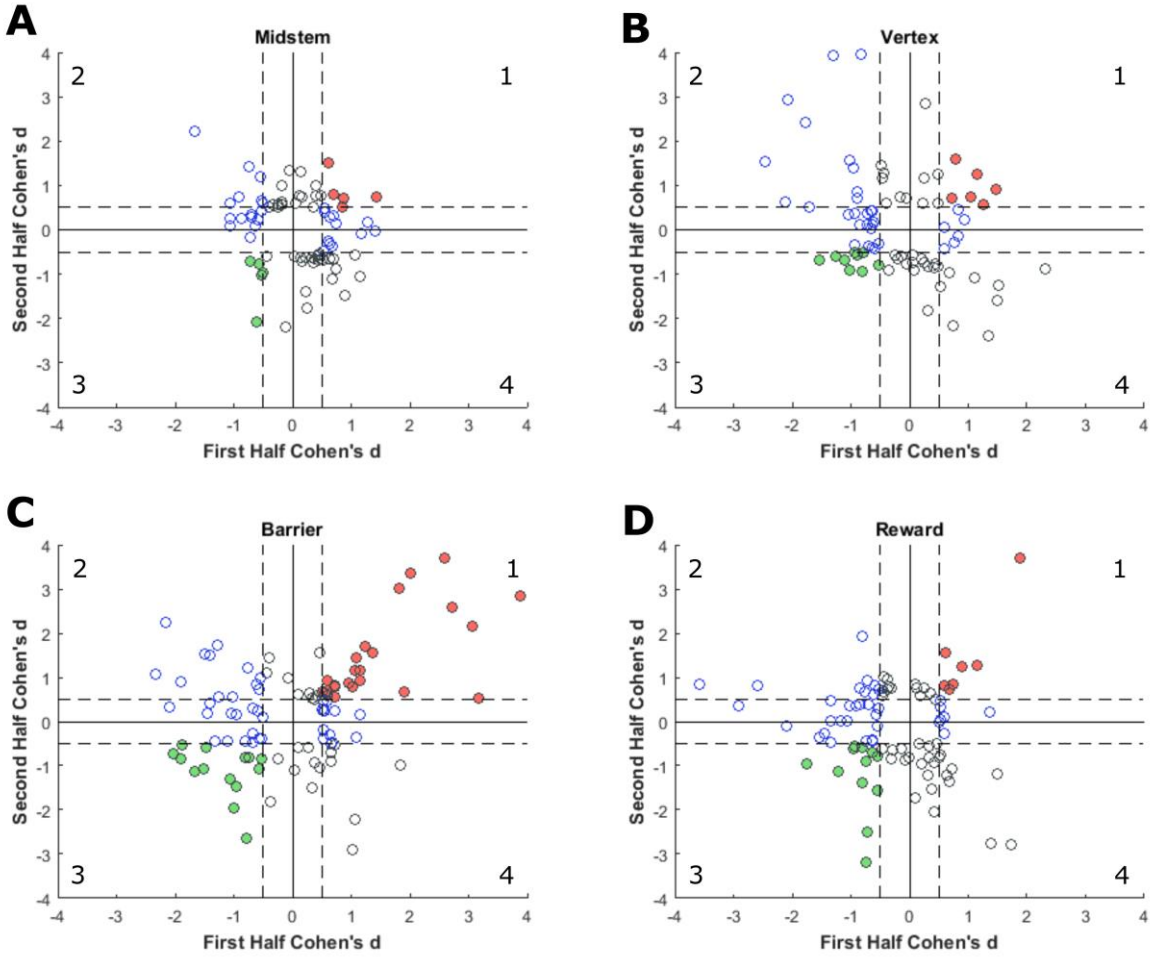

Figure 46. Characterization of trajectory and value selective ACC neurons for each maze region. HCHR-selective neurons mapped into quadrant 1 and were plotted with filled, red markers; LCLR-selective neurons mapped into quadrant 3 and were plotted with filled green markers; right-trajectory-selective neurons mapped into quadrant 4, and were plotted with empty black markers; left-trajectory-selective neurons mapped into quadrant 2 and were plotted with empty blue markers. The dashed lines indicate the positive and negative thresholds for a cell to be considered selective (Cohen's d = |.5|). (A-D) These conventions applied to cells classified as selective in the midstem – reward zones.

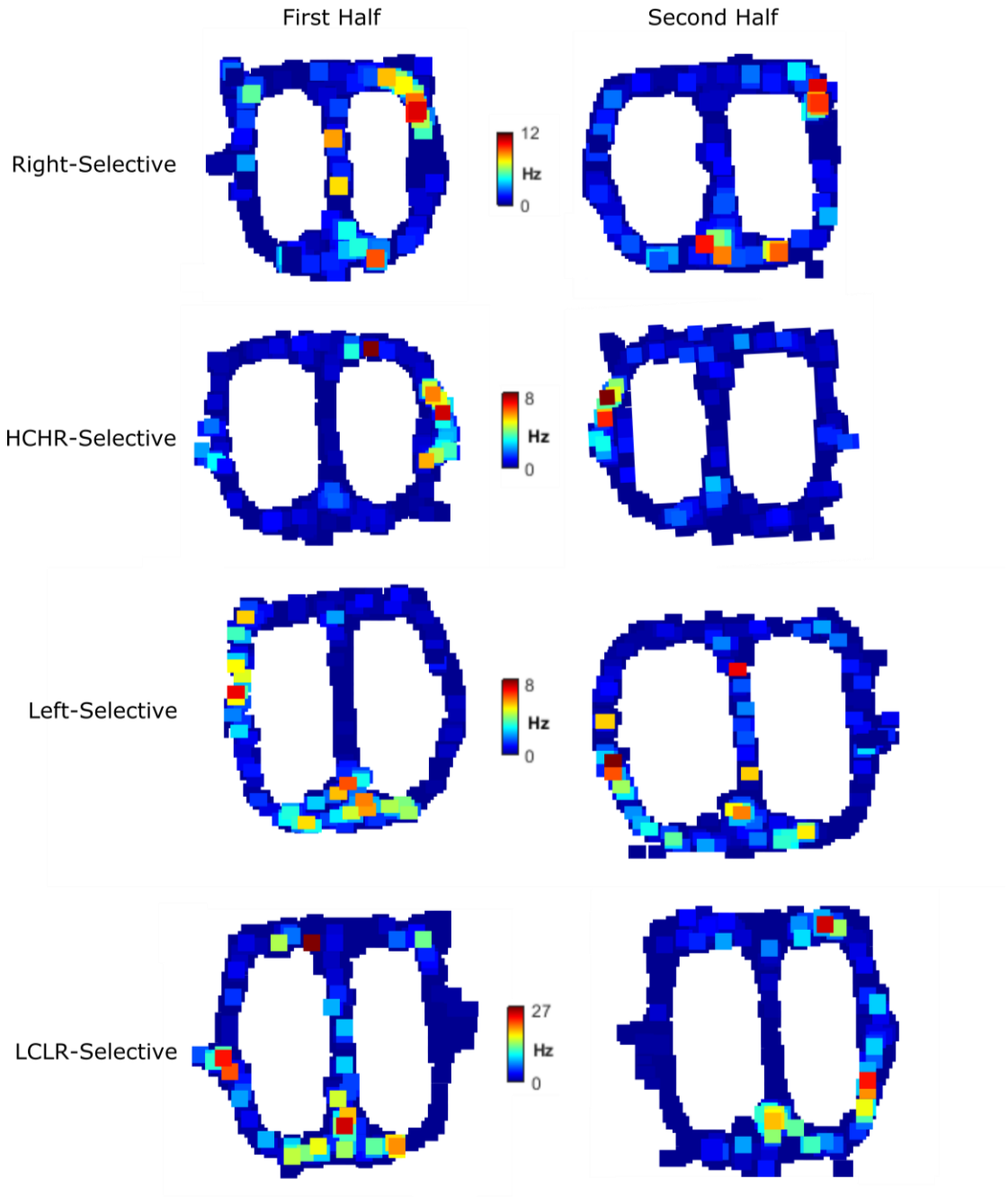

Figure 47. Example heat maps of individual action and value-selective neurons by session half. These plots were made by allocating data into 1.5cm spatial bins which were overlapped by .25cm and then averaging the iFRs for all occurrences of that spatial bin. The resulting matrices were then scatter plotted.

3.5.13 *No evidence of integrate-to-threshold firing profiles in LCLR-selective cells*

Several groups have reported that neural activity in the ACC exhibits an integrate-to-threshold firing profile in the trials preceding a shift from a default to a non-default decision strategy (B. Hayden et al., 2011; Nils Kolling, Behrens, Mars, & Rushworth, 2012; Amitai Shenhav et al., 2014). Although these studies focused on foraging, it's possible to interpret such patch-leaving decisions as being driven by the anticipation of a more fruitful future in another patch. Because our experiment elicited a ramping behavioural profile as rats made pre-reversal LCLR choices in anticipation of the reversal, we wondered whether the cells

which were maximally active during those epochs (e.g. LCLR-selective cells) would also show ramping activation.

We tested this possibility by calculating the trial-mean normalized iFR (ziFRs) of LCLR-selective cells for the three trials preceding every incidence of an LCLR choice in the first half of sessions. We then regressed those ziFRs onto a trial position factor which indicated the trial number before the LCLR choice and found a small (beta < .2) and non-significant ($p > .5$) effect. Thus, there was no indication that LCLR neurons ramped up their firing over the course of several trials to be predictive of a future LCLR choice.

To assess the effect of prior decision-type on the ziFRs of LCLR cells on trials preceding LCLR choices, we collected ziFRs as well as markers of the decision made on those trials in a manner similar to above. We then regressed the normalized iFRs onto the factor decision-type for each of the three trials preceding LCLR choices. All of the resulting beta weights for each of the three preceding trials were very small and non-significant. To rule out cell-to-cell variance as a confound, we regressed the ziFRs of each cell onto a subject factor and then conducted the above analyses again with the residuals (identical to how we handled most of the other electrophysiological measures in this paper) with similar small and non-significant effects. These data indicate that in our task, the population of cells most likely to exhibit a ramping, integrate-to-threshold firing profile did not.

3.5.14 *Entrainment of ACC unit firing to 4Hz and 8Hz oscillations*

While our single-unit analyses provide empirical support for prior theories suggesting that ensembles of ACC neurons encode models of the task at hand (Nils Kolling et al., 2016; O'Reilly et al., 2013), we did not find a single-neuron correlate which could predict the animals engaging in anticipatory decision making (LCLR-selective cells, for example, fired before and after the reversal and did not appear to significantly ramp up their firing prior to making a pre-reversal LCLR choice). This is likely because such decisions are multi-factorial and are likely carried out by the conjunction activation of several ensembles. One important question is then how the contents of such conjunctively active ensembles might be bound together.

We addressed this question by characterizing the phase-locking properties of ACC single neurons to the phase of the local ACC LFP and the distal VTA LFP oscillations. Because our spectral and PDC results detected effects around 4Hz, we initially examined we initially examined phase locking of ACC units to the ACC and VTA LFPs bandpass filtered to 2-5 Hz (henceforth referred to as 4Hz). Neurons were considered significantly phase locked

when the p value of Rayleigh's test of circular uniformity was less than 0.05. The firing of seventeen (10% of) ACC units were significantly modulated to the ACC 4Hz LFP and eight ACC units (5%) were significantly modulated to the VTA 4Hz LFP. Neither of these subpopulations fired at a consistent phase angle ($p > .1$, Rayleigh's test). We also wondered whether ACC units might be phase modulated at a higher frequency, particularly given the broad PSD peak observed from 7-11 Hz in the VTA. To test this possibility, we bandpass filtered the ACC and VTA LFPs to 7-11 Hz (henceforth referred to as 8Hz) and found 48 (29%) ACC units which were significantly modulated by the ACC 8Hz rhythm (mean angle = 35°, $p < .05$ Rayleigh's test) and 39 (23%) ACC units that were significantly modulated by the VTA 8Hz rhythm (mean angle = 118°, $p < .05$, Rayleigh's test). These results indicate that the local organization of ACC units was frequency specific, consistent with prior reports that ACC neurons have a tendency to synchronize to the 8Hz, rather than 4Hz, ACC (Womelsdorf et al., 2010) and VTA rhythms.

3.5.15 *Phase-amplitude modulation of the ACC LFP by the VTA*

Because choice-associated changes in LFP power and PDC occurred near 4 Hz and ACC unit phase modulation occurred to a greater degree at around 8Hz, we were interested in determining whether there was cross-modulation between these frequency bands. To address the relationship between the VTA and ACC LFPs, we examined the correlation between the phase angles of the VTA 4Hz oscillation and the amplitude envelopes of the ACC 8Hz LFP using linear-circular correlations. Data for each measure were obtained by bandpass filtering LFPs at the relevant frequencies as detailed above and using the Hilbert transform to generate phase profiles and amplitude envelopes. The magnitude of the ACC 8Hz amplitude envelope was significantly positively correlated with the phase of the VTA 4Hz oscillation ($p < .0005$ in all animals in all sessions, n = 10 sessions per animal, circular correlations), indicating that ACC 8 Hz LFP amplitude increased during the rising phase of the VTA 4Hz LFP. These data agree with prior examples of cross-modulation coupling exists between the 4Hz and 8Hz rhythms in these brain areas (Fujisawa & Buzsaki, 2011).

3.5.16 *Oscillatory entrainment of action and value selective ACC units*

Next, we were curious as to whether the cells which appear to comprise the task models thought to be encoded in the ACC were phase-modulated. We addressed this question by assessing the relationship between local and distal LFPs and the firing activity of the ACC neurons that appeared to be value (HCHR and LCLR) or action (left and right-trajectory) selective. Because of the relatively low numbers of cells that were significantly phase modulated to the 4Hz oscillations, we focused on the 8Hz oscillations only. We found cells of

each classification which were significantly entrained ($p < .05$ via Rayleigh's test for each cell) to the ACC and VTA 8Hz LFPs (see Table 8). When we characterised the cells as either responding to action or value, we found that more action cells synchronized to the VTA than value cells (Chi Square = 7.147, $p = .007$). These results indicate that the various task parameters encoded by ACC neuron subpopulations likely reflect the integration of local and distal information and that action encoding neurons were, generally, more likely to be synchronised to the VTA LFP than were value encoding neurons.

Table 8.
8 Hz phase-modulation of selective ACC neurons.

Classification	Total	ACC-modulated	VTA-modulated
HCHR	38	8	12
LCLR	36	10	4
Right	27	14	10
Left	29	8	14

3.5.17 *Magnitudes of selective ACC unit phase modulation*

Having established the biophysical plausibility of the phase-modulation of ACC single-units which appear to comprise the neuronal task-model by the 8Hz oscillations, we wondered whether and how the magnitude of that entrainment would vary as a function of the parameter a neuron was classified as encoding and the reversal. We addressed this question by calculating the normalized vector length as continuous measure of synchrony magnitude. The normalized vector length indicates the clustering of unit spikes around a specific phase angle of the oscillation (Dickerson, Wolff, & Bilkey, 2010; Zar, 1999). We were especially interested in assessing the normalized vectors of neurons classified as HCHR, LCLR, left turn, and right turn selective which were significantly entrained to the ACC and VTA rhythms (i.e. cells identified as significantly entrained via Rayleigh's test; see Figure 48). An ANOVA revealed a significant main effect of session half ($F_{1,27} = 4.22$, $p = .0184$) but no brain area main effect ($F_{1,27} = 2.78$, $p = .099$) and no session-half x brain area interaction ($F_{1,27} = .161$, $p = .689$). These results indicate that the firing of LCLR-selective neurons was significantly more phase-modulated during the first-half of the recording session, before the maze configuration changed, as compared to after it changed. An ANOVA considering HCHR-selective cells revealed a significant main effect of brain area ($F_{1,39} = 9.71$, $p = .00343$) but no effect of session-half and no session-half x brain area interaction. These results indicate that HCHR-coding elements of ACC neuronal task models are particularly synchronised to the VTA 8Hz LFP. ANOVAs evaluating left and right-selective cells, respectively, revealed no

significant main or interaction effects ($F < 3.9$ and $p > .05$ in all cases; see Figure 48). These results indicate that the phase-modulation of action-selective neurons was not influenced by changes in maze configuration and that the ACC and VTA's magnitude of influence on action-encoding cells could not be differentiated for these cells. These results also suggest that the discrete components of the task models might be bound together via synchronization, thus providing a partial answer to the initial question which prompted this series of phase-locking analyses.

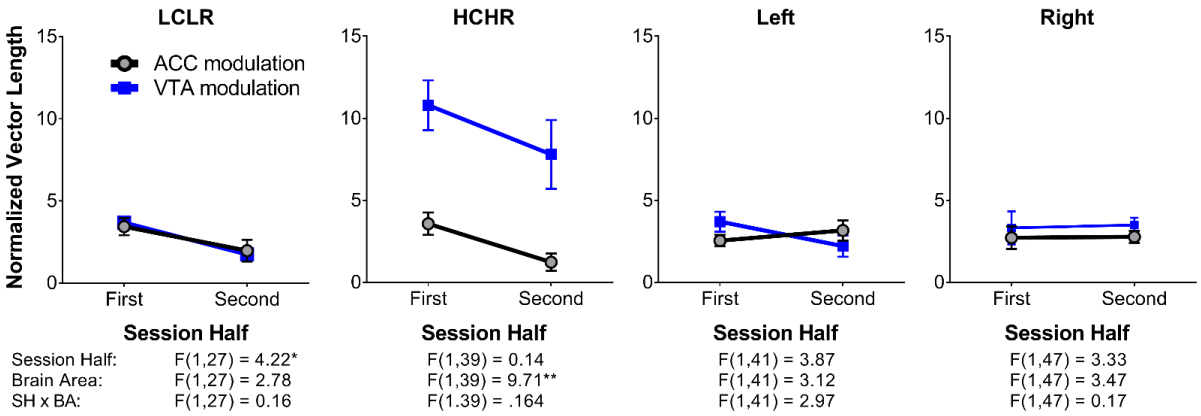

Figure 48. Magnitude of ACC and VTA 8Hz phase modulation of selective ACC units plotted against experimental session half. Data presented as mean ± SEM of unit populations with ANOVA results for each unit population below the figure. *p < .05, **p < .005.

3.6 Discussion

The present study aimed to assess activities in and communication between the ACC and VTA in a spatial-decision, reversal task. In particular, we were interested in whether and how responses differed during economic (HCHR) and putatively-anticipatory (pre-reversal LCLR) decisions. Analyses of the rats' decision behaviour indicated that the animals' likelihood of selecting the non-default, LCLR option increased as the pre-reversal trial progressed and then substantially decreased following the reversal. This decision pattern is reminiscent of the scalloped, anticipatory response pattern characteristic of animals responding on a fixed-interval schedule (Olton, 1989; Olton, Wenk, Church, & Meck, 1988), suggesting that the animals anticipated the reversal. To check whether this ramping of pre-reversal LCLR choices was linked to the reversal of the effort/value contingencies, we retrained several rats in a delayed reversal condition where the reversal occurred following trial 42 rather than trial 32. We found that the ramping of pre-reversal LCLR choices attended the delayed reversal position. Thus, because the ramping of pre-reversal LCLR choices attended the reversal, regardless of when the reversal occurred, it is plausible that the pre-reversal LCLR choices were anticipatory in nature.

In contrast, LCLR choices after the reversal tended to occur immediately after the reversal and then were much less likely to occur. This suggests that post-reversal LCLR choices reflect errors. Thus, our task appears to have elicited three distinct types of choices: value-guided HCHR choices (both before and after the reversal), anticipatory pre-reversal LCLR choices, and erroneous post-reversal LCLR choices.

Complementary analyses of task-related changes in ACC and VTA PSDs, coherence, and PDC models revealed that ACC→VTA 4Hz communication increased in the vertex of the maze when animals made pre-reversal, putatively-anticipatory decisions to the LCLR arm. ACC→VTA signalling was also significantly greater than chance during pre-reversal economic (HCHR) decisions, however, it was significantly less than that which occurred during anticipatory decisions. After the contingencies reversed, such that the previous spatial route was no longer optimal, ACC→VTA 4Hz communication during HCHR decisions increased as animals persisted in shifting their decisions to the new optimal side. These results cannot be attributed to spatial confounds given that we counterbalanced the initial maze configuration across the rats and the results of our control experiment which found no effects of maze arm when the outcomes and task demands associated with each maze arm were equal. Thus, together, these results suggest that ACC→VTA 4Hz communication may be important for carrying out anticipatory and persistent behaviour.

Because the results from our main experiment indicated a role for ACC→VTA signalling during anticipatory choice, we wondered whether this signal was present in other forms of anticipatory behaviour. To test this, we assessed how 4Hz ACC→VTA communication changed as rats explored a novel open field. Our motivation for choosing this particular behaviour is that exploration is likely driven by the anticipation that the information gained during exploration will be useful (Butz et al., 2003; Daw, O'Doherty, Dayan, Seymour, & Dolan, 2006; Friston et al., 2015; Mirza, Adams, Mathys, & Friston, 2016). Thus, the extent to which the animals explored the novel environment provided an index of the extent to which they may have anticipated gaining information. Consistent with this idea, we found that 4Hz ACC→VTA signalling was high during initial periods of exploration and reduced with habituation to the environment. Because we found that increased ACC→VTA 4Hz signalling was associated with behaviours which appear anticipatory in multiple behavioural circumstances, one possibility is that ACC→VTA 4Hz signalling reflects the operation of a general anticipation mechanism. However, this is unlikely because this interpretation cannot account for the persistence effect we detected following the reversal.

An alternative possibility, suggested by our finding that the choice-related changes in ACC→VTA signalling occurred in the vertex and not the midstem, is that our data reflect part of a process by which cortical computations are motivationally implemented (Holroyd & Yeung, 2012). For instance, had we observed changes in the midstem that were predictive of the animals' upcoming decision, it would have suggested that ACC→VTA signalling is involved in the computation underlying the decision itself (i.e. "deliberation"). This was not the case. However, because the changes in ACC→VTA signalling we observed occurred in the vertex, it may be that ACC→VTA signalling is one component of how decisions computed in the cortex are motivationally implemented.

This "implementation" interpretation suggests that ACC→VTA signalling was elevated during pre-reversal LCLR decisions because the animals needed to overcome their default, HCHR response in order to engage in a non-default, LCLR decision, where the decision itself was driven by anticipation of the reversal. Similarly, once the reversal occurred and the response towards the pre-reversal HCHR side was no longer optimal, the animals needed to shift and motivationally sustain their responses to the other side (as it had become the optimal side). This view also suggests that ACC→VTA signalling was significantly greater than zero during pre-reversal HCHR choices because the implementation of an effortful decision requires motivation and that, generally, every choice is predicated on an anticipated outcome (Skinner, 1938).

Interestingly, a recent human study has shown that ACC stimulation evokes feelings of 'persevering' and/or a drive to 'overcome adversity' (Parvizi et al., 2013). Our results suggest that this may be mediated through ACC connections to the VTA. Such an interpretation is also consistent with our prior study of the ACC→VTA signal (Elston & Bilkey, 2017) and provides empirical support for a recent computational model of ACC's role in regulating effortful behaviour (Holroyd & McClure, 2015). As a final point, numerous reports suggest that the dysfunctional cortical control over the dopaminergic midbrain (both above and below baseline) is a hallmark feature of several diseases characterised by a abnormalities of motivation, such as addiction, schizophrenia, apathy, and depression (Caravaggio et al., 2017; M. Gao et al., 2007; Le Heron, Apps., & Husain, 2017; Milner, 1963; Onoda & Yamaguchi, 2015; Wu et al., 2013). Thus, future studies are necessary to determine whether and how the ACC-VTA circuit may be a therapeutic target.

In contrast, communication in the opposite direction (VTA→ACC) increased as animals made pre-reversal economic (HCHR) choices. Additionally, VTA→ACC 4Hz signalling was elevated both as rats made post-reversal LCLR decisions in the vertex and at the outcome of those trials. One interpretation of the elevated pre-reversal HCHR signal is that VTA→ACC signalling is part of a system which biases ACC task-representations towards the most economic decisions. However, this seems unlikely because, were this the case, VTA→ACC signalling should have been elevated during both pre/post reversal HCHR choices. Another possibility is that 4Hz VTA→ACC signalling might be part of the system that biases ACC task-representations towards the well-rehearsed, default action (Ellwood et al., 2017). This, too, seems unlikely when considering the other cases of VTA→ACC signalling observed in this this data set. Another interpretation, is that the VTA→ACC signal is involved in the "selection" and modification of which components will comprise the ACC task model by altering the underlying signal-to-noise ratios in the neuronal task ensembles (Kroener, Phillips, & Seamans, 2009; Ott & Nieder, 2017). Consistent with this idea, we found that the high-value encoding (i.e. HCHR-selective) ACC cells were particularly modulated to the phase of the VTA LFP which suggests that VTA→ACC signalling might be involved in modifying, engaging, or otherwise "tuning" various aspects of the task model.

Additional support for a signal-to-noise based interpretation of the VTA→ACC signalling we observed comes from our finding that 4Hz VTA→ACC signalling was elevated in the vertex and in the reward regions during post-reversal LCLR trials. Because these decisions likely reflect errors and the rats rapidly adapted their subsequent decision patterns, it is possible that the attending mesocortical signals we observed reflects decision conflict and

feedback integration. Still, it is worth noting that rather than VTA→ACC signalling carrying out distinct functions in different circumstances, the changes we observed here that are associated with default decisions, conflict, and feedback processing can all be explained as instances of influencing the composition of neuronal task models. When considering the results of this study in conjunction with our prior study and a significant body of work by others (e.g. Ellwood et al., 2017; Holroyd & Coles, 2008; Kroener et al., 2009; Ma, Hyman, Lindsay, Phillips, & Seamans, 2014; Narayanan, Cavanagh, Frank, & Laubach, 2013; Ott & Nieder, 2017; Parker et al., 2014), it is clear that future studies which causally manipulate the VTA dopaminergic projection to the ACC while simultaneously recording whole ensembles of ACC neurons will be necessary to test the hypothesis that the general function of the mesocortical projection is to alter the composition of cortical neuronal task models.

Nearly all of the interpretations we propose for our findings assume that the ACC encodes models of the task at hand. Given the action and value encoding cells we and others (Cowen et al., 2012) have observed in the ACC, perhaps internal task models physically instantiate as sets of neurons which represent goal values and actions to attain those goals. Although our ACC single-unit recordings provided insight with regard to the contents in cortical task models, we were unable to monitor the process by which decisions were made. However, we were able to characterize the phase-locking properties of the neurons which appear to comprise the task models. This was important because synchronisation is a candidate mechanism by which the neuronal components of the task model are bound together (Buzsaki & Watson, 2012; Fries, 2015; Fujisawa et al., 2008; Womelsdorf et al., 2007; Womelsdorf et al., 2010).

Specifically, we found that ACC neurons encoding the most valuable option (HCHR) were significantly more phase-modulated at 8Hz to the VTA LFP than neurons encoding simple actions (e.g. left-trajectory) and low-value options. Although the strength of modulation of action-encoding neurons, as measured by vector length, was relatively stable across maze conditions, it was clear that these neurons were more likely to be synchronized to VTA at 8Hz compared to other subpopulations. The synchronization to the 8Hz oscillation, in particular, complements a prior report that rule-encoding ACC neurons are modulated at 8Hz (Womelsdorf et al., 2010). These findings integrate and extend the PDC findings from this present experiment and a robust literature which, together, suggests that mesocortical dopaminergic input is one mechanism by which ACC neuronal task models could be modified (i.e. alter which set of cells are currently active) and thereby influence subsequent behaviour (Ellwood et al., 2017; Jenni, Larkin, & Floresco, 2017; Kennerley, Walton, Behrens, Buckley,

& Rushworth, 2006; Ott, Jacob, & Nieder, 2014; Ott & Nieder, 2017; Schweimer & Hauber, 2006; Womelsdorf et al., 2010).

It is important to note several caveats when interpreting our data. First, it is unlikely that our VTA→ACC PDC models reflect solely DAergic signalling. While we immunohistochemically verified that our VTA electrode placements were in an area rich in DA neurons, our VTA→ACC PDC models likely reflect the aggregate of information transfer between these structures, such as co-localized glutamatergic and GABAergic neurotransmission (Carr & Sesack, 2000; David B. Carr & Sesack, 2000). This limitation could be overcome in future experiments by combining fibre-photometric measures of the DAergic mesocortical projection and high-density recording methods in the ACC. Another caveat is that, while our results suggest that ACC→VTA signalling is important for switching from a default to a non-default choice, our results reflect correlation and not causation. Future studies employing photo-stimulation/inhibition of ACC terminals in the VTA will be necessary to establish a causal role for ACC→VTA signalling in anticipatory, non-default choice. Also, given how general our effects appear to be, studying the ACC-VTA circuit in other tasks, such as responding on a fixed interval schedule, a rodent analogue of Daw et al.'s (2006) probabilistic reversal task, and/or variants of electronic competitor tasks like Tervo et al.'s (2014) will be instructional.

As a whole, our integrate and extend the evidence suggesting that the ACC and VTA are two components of a distributed and reciprocal circuit whereby cortical computations are motivationally implemented via the VTA and that feedback information broadcast from the VTA to the ACC is one way the task models underlying such computations can be updated (Ellwood et al., 2017; Elston & Bilkey, 2017; Holroyd & McClure, 2015; Holroyd & Yeung, 2012; Narayanan et al., 2013; O'Reilly et al., 2013; Parker et al., 2015). Thus, rather than reflecting a specific "anticipation signal," ACC modulation of the VTA may reflect a more general means by ACC computations are motivationally implemented. This signal is particularly evident when animals switch from default, economically-oriented behaviours, when they must persist in non-default behaviour after circumstances change, and when animals initially explore a novel environment. Furthermore, because the ACC and VTA are reciprocally connected (Carr & Sesack, 2000), it is possible that ACC modulation of the VTA could in turn lead to changes in VTA's dopaminergic output to the ACC whereby ACC task models can be modified in order to optimize future decisions (Bryden et al., 2011; Fujisawa & Buzsaki, 2011; Narita et al., 2010; O'Reilly et al., 2013; Roesch & Bryden, 2011). Future studies utilizing combined optical and recording methods are required to test this possibility.

Chapter 4 General Discussion

4.1 Experienced-derived environmental representations

The ability to exhibit adaptive behaviour depends on experience-derived internal representations of the environment and the task at hand (Karlsson et al., 2012; O'Keefe & Dostrovsky, 1971; O'Reilly et al., 2013; Tolman, 1948) such that changes in internal representations both initiate and sustain behavioural change. Considerable evidence suggests that updates to these internal task models occur on multiple timescales in response to environmental change, prompting prior representations to be discarded, with some changes occurring gradually and others in abrupt reset events (Behrens, Woolrich, Walton, & Rushworth, 2007; Elston & Bilkey, 2017; Fusi, Asaad, Miller, & Wang, 2007; Nassar, Wilson, Heasly, & Gold, 2010; O'Reilly et al., 2013; Pearce & Hall, 1980; Yu & Dayan, 2005). In each case, following an environmental change, internal representations are thought to update by resampling the environment (Hillman & Bilkey, 2010; Nassar et al., 2010; Pearce & Hall, 1980). The aim of this chapter is to review what environmental changes are thought to influence internal task models and to place the findings of this thesis into the larger context of the task-model updating literature. On the basis of data collected for this thesis, this chapter offers an incentive-salience, task-model onset (ISTMO) theory regarding the mechanisms of the onset and modification of neuronal task models. This chapter also offers a set of suggested experiments which are intended to both clarify the mechanisms underpinning the ISTMO theory and to consider the intersection of cognition, motivation, and learning in systems neuroscience.

4.2 Feedback modifies task models

From the earliest days of behavioural experimentation (Thorndike, 1898, 1928), the law of effect - of consequences and feedback - has been appreciated as the engine of behavioural change (Nassar et al., 2010). Feedback can be classified under two headings: outcome-experienced, reactive feedback and outcome-simulated, prospective feedback. In outcome-experienced models, feedback can be either explicit (rewarded or not) or relative (did it happen? To what extent? e.g. prediction error). In outcome-simulated, prospective models, feedback can be simulated as the likelihood of a particular outcome, given prior outcomes in similar circumstances, as in the case of midbrain dopamine neurons firing in response to the earliest reward-predicting stimulus (Schultz, Dayan, & Montague, 1997). In both cases, experienced-outcomes influence which dimension of a decision-prompting stimulus ought to be preferentially represented in subsequent neuronal task models and, ultimately, acted upon (Danielmeier, Eichele, Forstmann, Tittgemeyer, & Ullsperger, 2011;

Danielmeier & Ullsperger, 2011; Karlsson et al., 2012). Such outcome-dependent changes in stimulus-dimension saliency have been used to explain basic discrimination learning in a variety of species (Berridge, 2012; Bromberg-Martin et al., 2010). Feedback related changes in saliency have also been used to interpret conflict adaptation, for example, the finding that participants completing a Stroop task tend to improve over the course of the experiment (Gratton, Coles, & Donchin, 1992), akin to a Bayesian learning process. These findings suggest that a key function of task model modification is the optimization of attention in service of a goal-oriented action.

Changes in neuronal task models and behaviour incur some metabolic cost and it seems unreasonable that every outcome of every decision ought to equally influence one's neuronal worldview. For instance, surprising exceptions to a rule shouldn't cause a decision agent to entirely disregard that rule (O'Reilly et al., 2013). Furthermore, some circumstances involve great costs when outcomes are unsuccessful indicating that there are aspects of cost and risk inherent in adaptation which likely discount the value of exploring novel solutions. One prominent theory of prospective feedback suggests that the brain continuously compares the prospective costs and benefits associated with a course of action, calculating an expected value of exerting control over behaviour towards a goal (Shenhav, Botvinick, & Cohen, 2013). Although this thesis will, ultimately, diverge from the expected value of control theory (EVC), the EVC is an excellent point of departure for conceptualizing prospective instances of feedback.

One method by which decision agents might mitigate the risk of behavioural change and estimate the value of investing metabolic resources towards adaptive behaviour could be a pattern separation mechanism which provides an estimate of the 'fit' of the current task model with respect to the present context and circumstances (Bar, 2007; McCoy & Platt, 2005; McKenzie et al., 2014; Parkhurst, Law, & Niebur, 2002; Rolls, 2013; Yassa & Stark, 2011). Inputs patterns with 'good fit,' when the current task model is sufficient to solve the task would not require modification whereas input patterns with 'poor fit,' when the task model is not sufficient to solve the task at hand would require modification. In 'good fit' cases, default, well-modelled behaviours should then be rapidly executed whereas in 'poor fit' cases, response times ought to be longer and, more generally, depress the rate of behavioural output (O'Reilly et al., 2013; Perret, 1974; Stroop, 1935). Such an estimation-comparator mechanism could be achieved by activating the present task-model while integrating current contextual information, analogous to pattern-separation in the hippocampus (Yassa & Stark, 2011), and would allow creatures to devise innovative solutions to complex problems before acting,

which could then reduce the frequency of making decisions with undesirable outcomes (Bar, 2007). Although the ability to simulate multiple strategies before acting is a fortunate adaptation, experienced outcomes are more likely to influence subsequent behaviour than simulated ones (Hayden et al., 2011; Holroyd & Coles, 2008; Kool et al., 2017).

4.3 The anterior cingulate cortex dynamically encodes task models

Considerable evidence implicates the anterior cingulate cortex (ACC) in the development and modification of neuronal task models. For instance, a functional magnetic resonance imaging (fMRI) study of freestyle rappers found elevated ACC activity during the initiation and maintenance of improvised rapping (Liu et al., 2012) but not when the rappers engaged in rehearsed performance. Interestingly, this same study found that although ACC activation was high during the initiation of freestyle rapping, ACC activation dampened by the end of a 12 measure improvisation. One interpretation of these findings is that ACC activity was enhanced during the early, but not late, phases of freestyle rapping because the ACC was developing a task-model which, once established, guided future verbal sequences and no longer required the ACC.

The notion that the ACC encodes and updates task models is further supported by numerous reports of ACC single neurons in rodents, primates, and humans emitting large, transient bursts of activity when outcomes violate task model predictions (Bryden et al., 2011; Debener et al., 2005; Kennerly et al., 2011; Sheth et al., 2012). The most important finding across these studies is that increased ACC activity on these prediction-error trials strongly predicted a change in behavioural strategy on subsequent trials. One interpretation of these data is that prediction-error signals in the ACC represent an ‘update’ signal which facilitates the incorporation of new information into existing neuronal representations, thereby adapting the task model. This ‘updating’ view of ACC prediction-error signals suggests that adaptive behaviour depends on experience-derived ACC neuronal representations of the task at hand such that changes in those internal representations both initiate and sustain behavioural change.

Electrophysiological recordings of rodent ACC neurons conducted for this thesis demonstrated that single units within the ACC can represent both simple actions and value. This is important because, despite longstanding assumptions that the ACC encodes neuronal task models, the content of those internal representations remained unclear. Therefore, the finding that ACC neurons can encode simple actions, value, or complex action and value, provides a clear basis for the notion that the ACC actively maintains neuronal representations of the task at hand. Stemming from the evidence that the ACC responds to environmental

change and that those responses appear linked to behavioural change (Bryden et al., 2011; Gemba et al., 1986; Hayden et al., 2011; Karlsson et al., 2012; Kawai et al., 2015; Kolling et al., 2016; Tervo et al., 2014), a central question of this thesis has been how changes in neuronal task models are behaviourally implemented.

In conjunction with prior evidence (Ballard et al., 2011; Beier et al., 2015; Carr & Sesack, 2000; Ferenczi et al., 2016; Fujisawa & Buzsaki, 2011; Gariano & Groves, 1988; Wu et al., 2013), the findings of this thesis suggest that top-down information transfer from the ACC to the ventral tegmental area (VTA), modulated at around 4 Hz, is one mechanism by which changes in neuronal tasks models are behaviourally implemented. In Project 1, where rats implanted in the VTA, ACC, and dCA1 hippocampal sub-region ran laps of varying physical difficulty for fixed rewards, we found that ACC → VTA 4 Hz signalling increased in trials when the lap was easier than expected and that this increase was significantly correlated with, but not confounded by, changes in motivation, as measured by running speed. The findings of this first project indicated that the ACC-VTA circuit is a plausible mechanism by which behaviour is modified. This led us to ask whether changes in the ACC-VTA circuit are related to the initiation and maintenance of behavioural change.

To address that question, we monitored ACC single units as well as the local field potentials (LFPs) of the ACC and VTA in rats trained to perform effort-based cost-benefit analysis task where the cost-benefit contingencies reversed midway through experimental sessions. In the first half of experimental sessions, behaviour indicated that rats anticipated the contingency reversal but were unsure of when the reversal would occur and so would occasionally explore their non-default decision in order to determine whether the contingencies had yet reversed. After the contingencies reversed and behaviour stabilized, rats made significantly fewer exploratory choices. In regard to the accompanying brain activity, we found that ACC → VTA 4 Hz information transfer increased as animals made these exploratory decisions and that ACC → VTA signalling was supressed during typical, default behaviours. This suggests that ACC → VTA signalling is an important component in initiating behavioural modification. After the contingencies reversed, and the first-half non-default behaviour was implemented more often, we found that ACC → VTA 4 Hz information transfer increased throughout trials where animals sustained their newly modified behaviour. These results indicate that ACC → VTA 4 Hz information transfer is also important for maintaining behavioural change.

When we examined bottom up, VTA → ACC information transfer across the session halves, we found significant information transfer at 4 Hz during typical, default decisions in

the first half of sessions but no difference between decision types in the second halves. We also found that ACC neurons encoding the most valuable decision were significantly more phase-modulated to the VTA LFP than neurons encoding simple actions. These results suggest that VTA → ACC signalling may be involved in initiating ACC neuronal task models and that, when task models are of 'good fit,' subsequent modification is not necessary. These results also imply that in cases of 'poor model fit,' when task models and behaviour require modification, the ACC applies a correction signal to the VTA which then alters its signalling back to the ACC and to other areas, consistent with prior examples of cortical modification of subcortical states (Ballard et al., 2011; Likhtik et al., 2014) and vice versa (Safaai, Neves, Eschenko, Logothetis, & Panzeri, 2015; Tervo et al., 2014).

Collectively, these findings suggest that sustained behavioural change could be facilitated by ACC-driven alterations in VTA → ACC dopaminergic (DA) signalling. By altering the probability that a given neuron would be recruited to a task ensemble (Jacob, Stalter, & Nieder, 2016; Navailles et al., 2015; Puig, Rose, Schmidt, & Freund, 2014), VTA DAergic signalling could enhance the contribution of specific neuronal representations and dampen the contribution of neuronal representations which were not fruitful. Such a mechanism is consistent with the notion that the ACC accumulates evidence over time before both making a decision and stabilizing a default response (Hayden et al., 2011; Kennerley et al., 2006; Pisauro, Fouragnan, Retzler, & Philiastides, 2017; Sheth et al., 2012). Thus, post-outcome VTA → ACC signalling might act as a training signal which could remodel the ensemble of neurons representing the task at hand with the net effect of altering the probability that an individual cell recruited for the prior task-ensemble would be recruited to the next, subsequent task-ensemble in similar situations. These ideas are theoretically formalized from two different approaches in the following sections. In the first, beginning from section 4.4 titled *Content of ACC neuronal task models*, I will consider task models with respect to the cortex itself and changes in cortical neuromodulatory states. In the second, beginning from section 4.8 titled *An incentive-salience, task-model onset (ISTMO) theory of goal-oriented and adaptive behaviour*, I will address a broader view of the onset and modification of task models which aims to link task models to sensory information.

4.4 Content of ACC neuronal task models

The ability to flexibly shift between different sets of decision strategies during goal pursuit the core of executive function. The term 'set' (*vis a vis* cognitive set-shifting) is widely used to denote internal representations of a goal and the means of achieving it, analogous to the notion of an internal task model; 'set-shifting,' therefore, refers to switching

from one internal task model to another (Kolling et al., 2016; O'Reilly et al., 2013). Despite widespread use of the terms 'set' and 'set-shifting', their physical substrates have remained elusive. One possibility discussed in this thesis is that 'sets' manifest as sets of ACC neurons which represent goal values, rules which guide action selection, and actions to attain those goals. In this model, neuronal sets and their subcomponents ought to respond to contextual change, including environmental changes and goal-pursuit outcomes, such that shifts in which set of neurons are active ought to influence behavioural adaption.

Recordings of rodent and primate ACC neurons suggest that neuronal sets are comprised of distinct goal value, rule, and action components. In project 2, for instance, we recorded ACC neurons of rats performing an effort-based, cost-benefit analysis task. In this task, rats had to decide whether to climb a 30cm barrier for a large reward (high cost, high reward; HCHR) or to pursue a path with no additional effort which yielded a small reward (low cost, low reward; LCLR). We found that distinct populations of ACC neurons preferentially represented both goal values (HCHR or LCLR selective) and simple actions (turn left or right) in all portion of the maze. Similar representations of goal value and simple actions have been observed in the firing profiles of primate ACC neurons (Hayden & Platt, 2010; Kennerly, Behrens, & Wallis, 2011; Monosov, 2017) as well as human ACC activation via direct neuronal recordings and functional magnetic imaging (fMRI) studies (Nils Kolling et al., 2016; Sheth et al., 2012). Such overlapping action and value representations support the proposal that the ACC is critical for developing rule-based models which map stimuli-response policies (Thilo Womelsdorf et al., 2010). Indeed, studies of the effects of ACC damage in humans (Camille, Tsuchida, & Fellows, 2011), rodents (Walton et al., 2002), and primates (Kennerley et al., 2006) reported that ACC damage impairs subjects' ability to integrate recent outcome information to adjust and optimize rule-based approaches to goal pursuit.

Although neuronal representations of rules have not been directly studied in the ACC, numerous studies of the primate PFC, in general, indicate that single neuron representations of rules exist. In the earliest of these experiments, Wallis, Anderson, & Miller (2001) recorded PFC neurons of monkeys performing a match/non-match to sample task. In this task, monkeys were trained to grab a bar and were then presented with a sample image. Then, following a 1 second delay, monkeys were presented with a test image which was either the same or different to the sample image. Depending on the current rule (match/non-match), the monkeys released the bar if the test image was the same or different from the sample image in order to receive reinforcement. Wallis et al. observed that a significant portion of neurons

were modulated by rule – maximally responding during trials of a certain rule (e.g. ‘match’), regardless of the sample and test images. More recent studies using a similar task design have shown that primate PFC neurons also encode numerical and spatial rules (Eiselt & Nieder, 2013; Ott et al., 2014) and rule representations have also been reported in the rat PFC (Bissonette & Roesch, 2015). Importantly, across all of these studies, PFC neuronal rule representations were nearly devoid of activity attributable to purely sensory or memory-related information, indicating that the PFC encodes abstract rules for how to interact with categories of goal-related stimuli. Future studies are needed to determine the precise contribution of PFC sub-regions, such as the ACC, to such abstract rule representations.

Together, these data suggest that ACC internal task models manifest as sets of neurons representing goal value, action, and rules in service of goal pursuit. Stemming from the evidence that ACC neurons respond to environmental change and that those responses appear linked to behavioural change (Bryden, Johnson, Tobias, Kashtelyan, & Roesch, 2011; Gemba, Sasaki, & Brooks, 1986; Hayden et al., 2011; Karlsson, Tervo, & Karpova, 2012; Kawai et al., 2015; Kolling et al., 2016; Tervo et al., 2014), key questions are then: what circumstances and mechanisms alter neuronal task models and how are changes in neuronal task models behaviourally implemented?

4.5 Why and how do ‘sets’ change?

Our proposal that neural task models manifest as sets of neurons encoding values, actions, and rules predicts that environmental change ought to influence the probability that a given neuron classified as encoding an action, goal value, or rule participates in a subsequent neuronal task set. Feedback-driven changes in the probability that a neuron participates in subsequent task models would indicate that feedback influences the composition of the task model which then influences future behaviour (Figure 49).

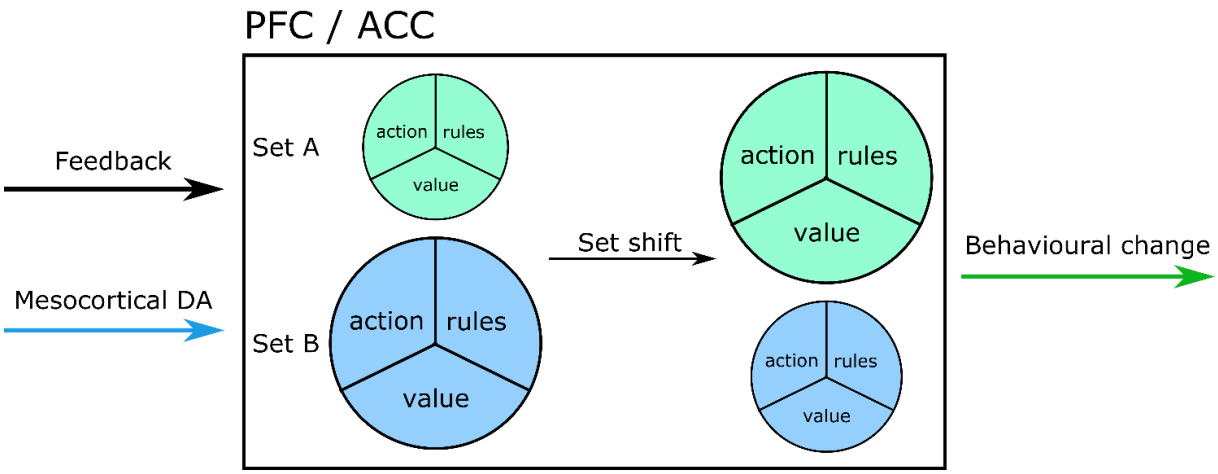

Figure 49. Diagram expressing a model of the content of neuronal sets and some of the mechanisms which may influence them.

This hypothesis could be tested in in a rule-switching task requiring subjects to turn either left or right. In such a task, it is likely that single neurons would represent those rules (turn left and right) and the goal values associated with those actions. Utilizing high-density unit recording, an experimenter could monitor whole ensembles of cells and simultaneously record neurons encoding the various aspects of the task model. If, say, right turns had been yielding reinforcement, our model predicts that the probability that a cell encoding the rule 'turn right' participated in the ensemble would be high and the probability a 'turn left' cell participated in the ensemble would be low. Should the contingencies reverse such that the optimal rule becomes 'turn left,' our model predicts that the probability of 'turn right' cells participating in the task model should decrease over several trials while the probability of 'turn left' cells participating in the task model should increase over several trials. The changes in those probabilities could then be correlated with subsequent behaviour with the prediction that the modification of the neuronal task set would correspond to behaviour modification. Thus, such probabilistic changes would be indicative of the neuronal task model updating. While this hypothesis addresses what task-model modification might look like, the precise mechanisms by which neurons comprising the task model integrate recent feedback information remain unclear.

Mesocortical dopaminergic (DA) innervation of the PFC (including the ACC) from the ventral tegmental area (VTA) is one mechanism by which feedback information could be integrated into existing neuronal representations and thereby influence future behaviour. For instance, blockade of DA D2 receptors reduced the ability of rodents to flexibly switch between rule-based response-strategies (Floresco & Magyar, 2006) and blockade of DA D1 receptors (D1Rs) impaired primates' ability to maintain a sample stimulus in working memory (Arnsten, 2011). In an elegant study, Ott et al. (2014) used a combination of

iontophoresis and single-unit recording to determine the roles of different DA receptor on the coding properties of rule-encoding PFC neurons of primates performing a numerical decision task. The task required monkeys to decide whether a test numerosity was greater or less than a sample numerosity, depending on the current rule ('>' or '<'). In addition to finding distinct populations of PFC neurons encoding each rule, Ott et al. found that D2R stimulation enhanced the specificity of rule-coding neurons by increasing their signal-to-noise (S/N) ratios whereas D2R blockade had the opposite effect. D1R stimulation/blockade increased/decreased the baseline firing rates of PFC rule-encoding neurons but did not change the coding strength of PFC neuronal rule representations. Together, these findings suggest that mesocortical DA might facilitate the integration of recent reinforcement feedback into existing neuronal representations by changing the probability that a given neuron would participate in a task model. Such changes in which set neurons comprise the task model likely have downstream effects on future behaviour (vis a vis the results of Project 1 in this thesis). Future experiments could directly explore the impact of DA and other neuromodulators (see Tervo et al., 2014) on the modification of specific components of neuronal task models and specific sub-regions of the PFC, such as the ACC. Although these data suggest that internal models of the world are influenced by feedback and that DA may play a central role in modifying neuronal task models, the question of how changes in those task models are behaviourally implemented remains.

4.6 From flexible internal models to flexible behaviour

In project 2, we aimed to characterize the ACC-VTA circuit during the initiation and persistence of behavioural change. To address that question, we monitored ACC single units as well as the local field potentials (LFPs) of the ACC and VTA in rats trained to perform effort-based cost-benefit analysis task where the cost-benefit contingencies reversed midway through experimental sessions. In the first half of experimental sessions, behaviour indicated that rats anticipated the contingency reversal but were unsure of when the reversal would occur and so would occasionally make a non-default decision in order to determine whether the contingencies had yet reversed. After the contingencies reversed and behaviour stabilized, rats made significantly fewer exploratory choices. We found that ACC → VTA 4 Hz information transfer increased as animals made anticipatory decisions and that ACC → VTA signalling was supressed during typical, default behaviours. This suggests that ACC → VTA signalling is an important component in initiating anticipatory behaviour. After the contingencies reversed and the first-half, non-default behaviour was implemented more often, we found that ACC → VTA 4 Hz information transfer increased throughout trials where

animals sustained their newly modified behaviour. These results indicated that ACC → VTA 4 Hz information transfer is also important for maintaining behavioural change.

The results of project 2 also provides additional evidence for the importance of the ACC-VTA circuit in modifying neuronal sets because we found that ACC neurons encoding the high-value goals were significantly more phase-modulated to the VTA LFP than neurons encoding simple actions. These results suggest that VTA → ACC signalling may be involved in initiating ACC neuronal task models and that, when task models are of 'good fit,' subsequent modification is not necessary. These results also imply that in cases of 'poor fit,' when task models require modification, the ACC applies a correction signal to the VTA which then alters its signalling back to the ACC and to other areas, consistent with prior examples of cortical modification of subcortical states (Ballard et al., 2011; Likhtik et al., 2014) and vice versa (Safaai et al., 2015; Tervo et al., 2014).

Collectively, these findings suggest that sustained behavioural change could be facilitated by ACC-driven alterations in VTA → ACC dopaminergic (DA) signalling. Such DAergic mesocortical signalling could influence the task ensemble by enhancing the contribution of specific neuronal representations associated with fruitful outcomes and dampen the contribution of neuronal representations which were not fruitful (Jacob et al., 2016; Navailles et al., 2015; Puig et al., 2014). Such a mechanism is consistent with the notion that the ACC accumulates evidence over time before both making a decision and stabilizing a default response (Hayden et al., 2011; Kennerley et al., 2006; Pisauro et al., 2017; Sheth et al., 2012). Thus, post-outcome VTA → ACC signalling might act as a training signal which could remodel the ensemble of neurons representing the task at hand with the net effect of altering the probability that an individual cell recruited for the prior task-ensemble would be recruited to the next, subsequent task-ensemble in similar situations (Figure 50).

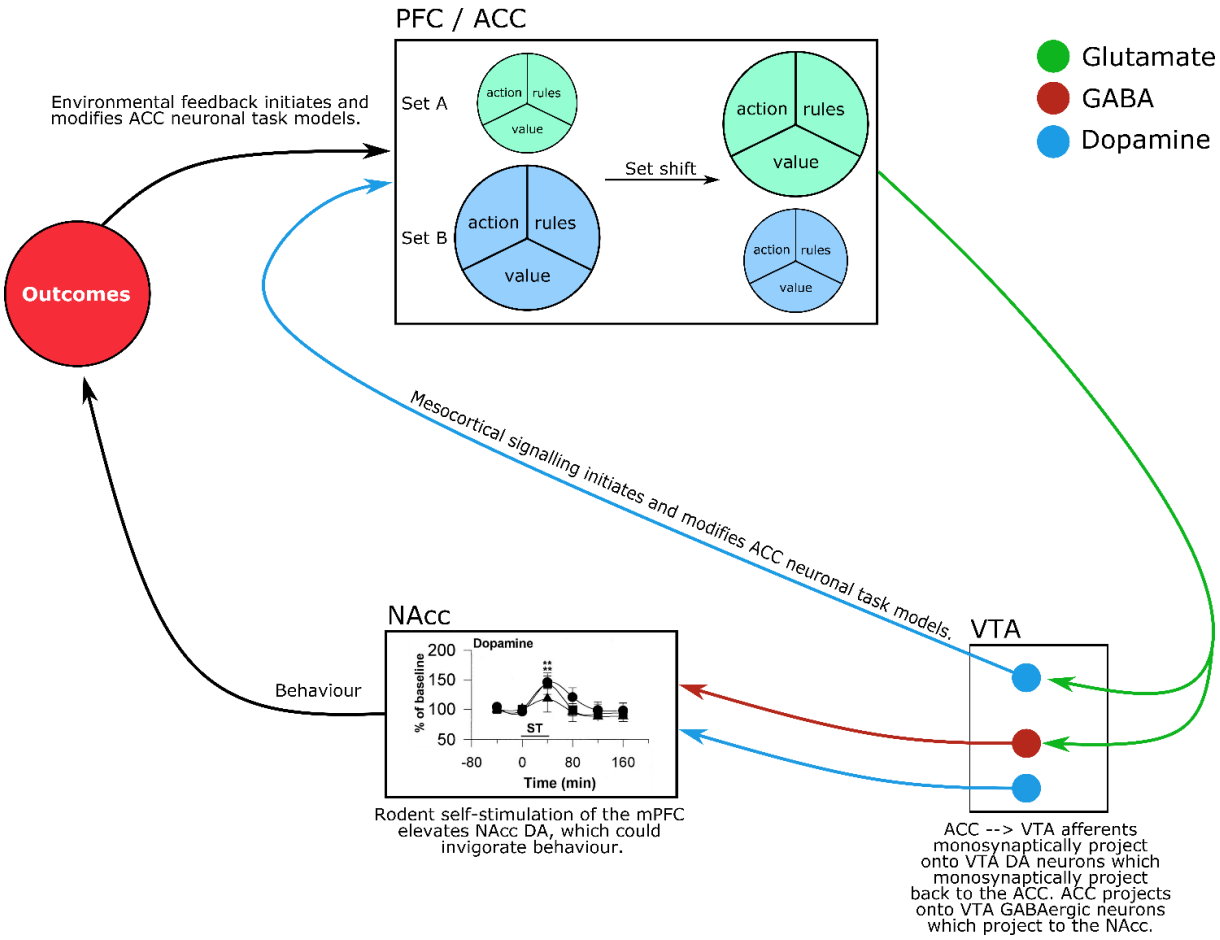

Figure 50. Potentials mechanisms by which neuronal sets are modified and implemented. Environmental feedback and mesocortical DAergic signalling alter the S/N ratios of distinct sets of neurons encoding goal values, rules, and actions such that changes in which set of neurons are most active leads to changes in behaviour. Neuronal set-shifts which occur in the cortex then motivate behavioural change via monosynaptic glutamatergic projects from the ACC/PFC to the VTA. Such cortico-basal signalling can then initiate mesolimbic signalling to the nucleus accumbens (NAcc) which can then invigorate the new behaviour. ACC-driven input to the VTA could also influence the reciprocal mesocortical pathway which could then alter the S/N ratios of the newly implemented set. Such changes could also influence default behaviour as well as response conflict *vis a vis* the rationale of Figure 49.

4.7 More specific predictions and future experiments

Our model makes specific predictions about how certain types of set-shifts would influence future behaviour. If we consider the number of neurons which comprise a set an indication of the 'magnitude' of the set, then our model predicts that in cases where decision makers change their behaviour, the prior-set magnitude would decrease and the new-set magnitude would increase (Figure 51a). In cases where a decision maker does not change their behaviour, our model predicts that both the prior-set and new-set magnitudes would not change (Figure 51b). It is also possible that, in this case, the differential magnitude between the sets could increase (e.g. the larger gets larger and the smaller gets smaller). In cases where decision makers experience conflict, or uncertainty, about what to do, our model predicts that this happens because the competing sets are now of equal magnitude (Figure 51c). In these cases, the longer response times associated with task-conflict could be interpreted as the extra

time (and cortical activation) required to resolve the difference between the competing sets (Amitai Shenhav et al., 2014).

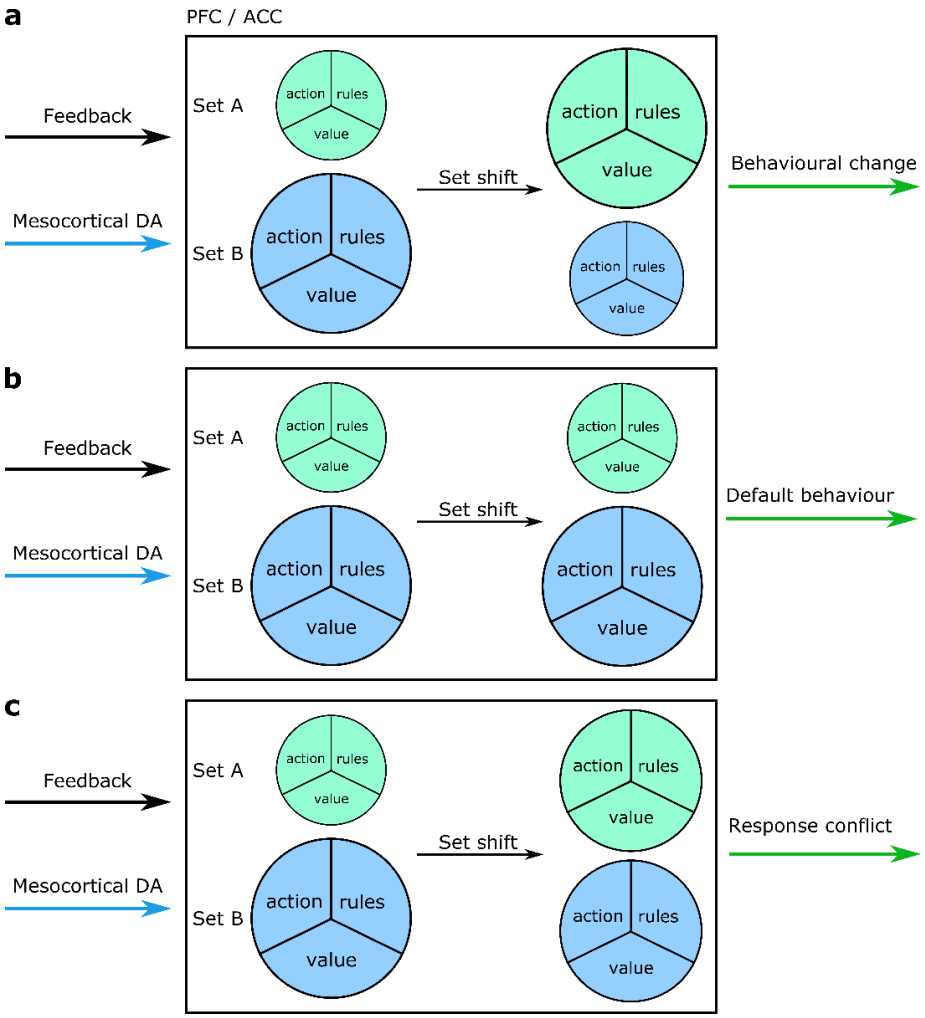

Figure 51. Various forms of neuronal set-shifts and their behavioural consequences. **(a)** Due to neuromodulatory and environmental influences, the S/N ratio of set A increases whereas the S/N ratio of set B decreases. The consequence of such shifts in neuronal set S/N ratios is behavioural change from behaviours associated with set B to behaviours associated with set A. **(b)** Neuromodulatory and environmental feedback maintain the large S/N ratio of set B, which leads to the decision-maker to continue behaving according to the information encoded in set B. **(c)** Initially, set B had a greater S/N ratio that set A, which means that the decision maker had been behaving according to the information encoded in set B. However, following neuromodulatory and environmental feedback, the S/N ratios of both sets, A and B, become very similar. Because the S/N ratios of the sets are similar, the brain must resolve which set to act upon. In these cases, response times ought to be greater, which could indicate conflict in determining which neuronal set to implement.

Our model also makes specific predictions regarding how the initial encoding of sets could influence the ease with which a decision maker flexibly switches between them. Starting from the core idea of our model that sets are fundamentally comprised of goal value, rule, and action representations, a question becomes: what happens if the same actions could be used according to different rules? Would the sets overlap? Would such overlap be constructive or destructive? Here is a simple reaction-time experiment which illustrates the question: consider a computer-based experiment which requires human participants to

flexibly switch between two rules: a digit task and a letter task. The digit task would require participants to press the ‘Z’ computer keyboard key if the digit is odd and to press the ‘M’ key if the digit is even; the letter task would require participants to press the ‘Z’ key if the presented letter was a vowel and to press the ‘M’ key is the presented letter was a consonant (Figure 52a). In this experiment, the same actions of pressing the ‘Z’ and ‘M’ keys are guided by two different rules of when to use those actions.

In such an experiment, our model predicts that the way participants train on the task should influence how task sets form and, ultimately, the reaction times of participants. If participants were split into two training-type groups, a ‘repetition’ group which learned the tasks in a repetitive, serial manner, and a ‘switch’ group which learned the tasks in an interleaved manner (Figure 52b), our model predicts differences in how those tasks are represented (Figure 52c) and subsequent behaviour (Figure 52d). Specifically, our model predicts that the ‘repetition’ group would form two distinct, non-overlapping task models whereas the ‘switch’ group would form two models which overlap in the action domain (Figure 52c) because, during training, the prior set would likely remain in working memory as the tasks switched which could lead to the same action-encoding neurons being used for both task sets. The question then becomes: would such overlap would be constructive or destructive? If task-set overlap in the action domain is constructive, then switch-trained participant reaction times (RTs) on the rule-switch trial ought to be less than the repetition-trained group (Figure 52d) because less energy would be required in order to reconfigure the dominant task set (i.e. only the prior-set rule and value, but not action components would require inhibition). If action-domain task-set overlap is destructive then switch-trained participant switch-trial RTs ought to be greater than the repetition-trained group, which would indicate that optimal task-switching requires mental representations to be distinct with minimal overlap.

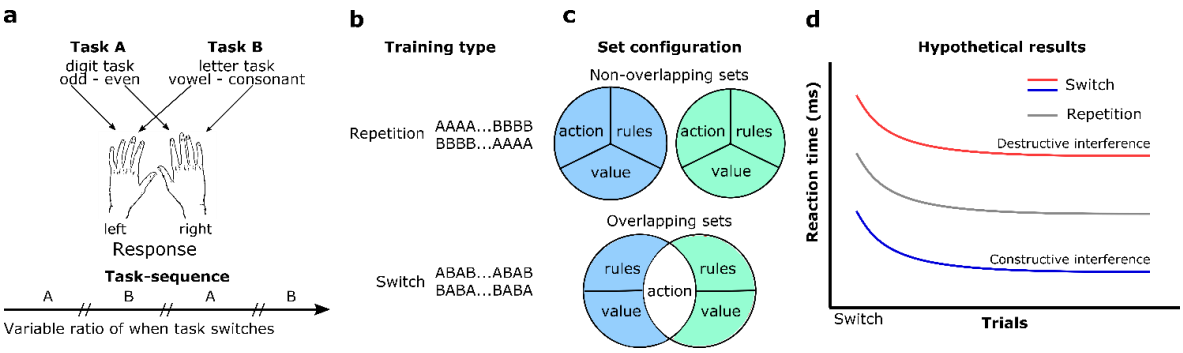

Figure 52. Experiment examining the effect of task-training type on response latencies. **(a)** Task protocol in which similar actions are used according to different rules. In this task, participants are flashed either letters or numbers on a computer screen; both tasks require participants to respond with either their left or right index fingers by pressing the 'Z' or 'M' keys on a computer keyboard, according to the rules of each task. The rules of the letter task are that left, 'Z' presses are for vowels whereas right, 'M' presses are for consonants. The rules of the digit task are that left, 'Z' presses are for odd numbers and right, 'M' presses are for even numbers. **(b)** Participants could be allocated into two training groups. One group would learn the tasks in a serial, repetitive manner (e.g. 20 digit task trials followed by 20 letter task trials) and the other would learn the tasks in an interleaved manner where the task switched every trials (e.g. one letft-hand letter task trial followed by one left-hand digit task trial, etc). **(c)** Theoretical account of the effect of training type on neuronal set-configuration. The repetition group would be expected to form two minimally overlapping sets such that the neurons which, for instance, encode left, 'Z' responses would be different for each task set. The switch group, by comparison, would be expected to form task sets which overlap in the action domain (e.g. a neuron which encodes a left, 'Z' response would be used in both task sets). **(d)** Hypothetical results of the task outlined in (a). Regarding the switch-trained group, it is possible that the task-set overlap would produce constructive interference, reducing the reaction time of participants to rule-switch trials. If this result was obtained, this could mean that overlapping task-representations are an efficient way to learn and that, more generally, because less of the prior task set requires inhibition, response times are faster. The switch-trained group might instead have greater reaction times, which would indicate that the overlap amongst distinct task sets produce destructive interference. Were this result obtained, it could mean that the entirety of a prior task set must be inhibited before the new task set can take behavioural effect.

It is also possible that the type of task-set overlap could be important. For instance, one could test rule-domain overlap in a task where the same rule could be differentially acted upon depending on the task-condition. We would predict that rule-domain task-set overlap would produce response conflict than action-domain task-set overlap. In humans, it would also be interesting to combine such tasks with functional magnetic resonance imaging or electroencephalographic analyses. Developing rodent and primate analogues of these tasks will also be important in order to further understand the neuronal basis of task-sets and how components within a set might interact.

4.8 An incentive-salience, task-model onset (ISTMO) theory of goal-oriented and adaptive behaviour

Given the action and value cells we and others (Cowen et al., 2012) have observed in the ACC and that the constellations of action and value cells can be conceptualized as neuronal representations of the task at hand, perhaps ACC neuronal task-ensembles are initiated by midbrain dopaminergic incentive-salience signalling, such that midbrain dopamine projections to ACC value-selective neurons (O'Donnell, 2003) are driven by sensory information, such as visual information relayed via the superior colliculus; such mesocortical signalling to ACC value-encoding neurons could then recruit a local network of action-encoding neurons, analogous to ACC-mediated memory retrieval in the hippocampus (David B. Carr & Sesack, 2000; Comoli et al., 2003; Dembrow & Johnston, 2014; Hansen Manahan-Vaughan, Denise, 2014; Lewis & O'Donnell, 2000; Narita et al., 2010; Puig et al., 2014; Rajasethupathy et al., 2015; Westerink, Enrico, Feimann, & De Vries, 1998). In such an incentive-salience, task-model onset (ISTMO) model (Figure 53), midbrain-dopaminergic incentive-salience signalling acts as a simple feed-forward filter (Bromberg-Martin & Hikosaka, 2009; Bromberg-Martin et al., 2010) such that a stimulus that does not excite midbrain dopamine neurons beyond some threshold (Figure 54; Ljungberg, Apicella, & Schultz, 1992; Schultz, 2016) does not activate ACC value-selective neurons. I would like to note here that the superior colliculus is likely to be but one partner of the ACC in this regard and that the inputs facilitating the initiation and modification of task models could well be polysynaptic. However, for brevity and clarity of presenting a biophysically plausible system here, I have focused discussion to visual information relayed to the midbrain via the superior colliculus.

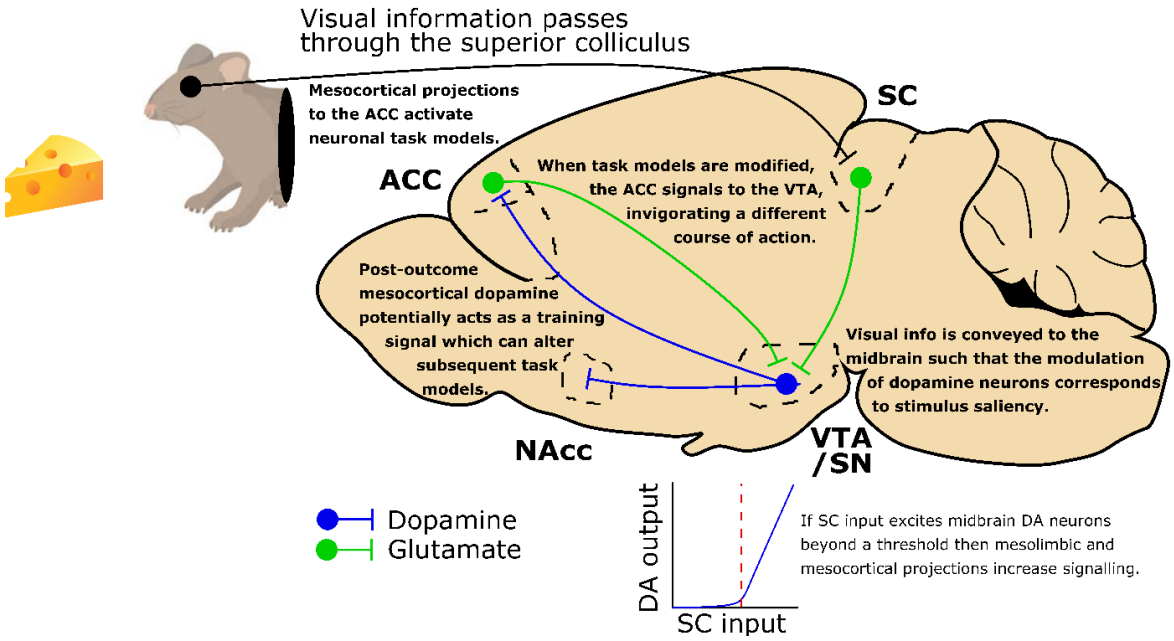

Figure 53. Schematic of circuity underpinning the ISTMO theory. Visual input via the superior colliculus (SC) modulates dopamine neurons in the ventral midbrain (ventral tegmental area (VTA) and substantia nigra (SN)). If midbrain dopamine neurons are excited beyond a certain threshold, mesolimbic and mesocortical dopaminergic output greatly increases. Elevated mesocortical dopaminergic signalling, in conjunction with sensory and other inputs, activates ACC neuronal representations of the task at hand. In cases where ACC task models are insufficient or inaccurate, the ACC exerts control over the VTA, invigorating an alternative course of action. ACC → VTA signalling could also increase VTA → ACC signalling, thereby enabling the ACC to drive modification of its task models. NAcc = nucleus accumbens.

The ISTMO view also theorizes that action-encoding cells are brought online by value-encoding cells such that a lack of incentive salience signalling in the midbrain to value-encoding cells in the ACC then precludes activation of local networks of action-encoding neurons. The behavioural summation of such a process might manifest an organism appearing uninterested towards a familiar stimulus. More concisely, the ISTMO theory suggests that when sensory-driven input via the superior colliculus (Bolton et al., 2015; Comoli et al., 2003) to midbrain does not excite dopamine neurons beyond some threshold, the mesocortical projection is not activated, precluding activation of cortical neuronal task models and, therefore, dampening subsequent behaviour towards the stimulus (David B. Carr & Sesack, 2000; Dembrow & Johnston, 2014; Lewis & O'Donnell, 2000; Puig et al., 2014; Westerink et al., 1998). The converse of this syllogism might explain the onset of cortical task models and the engagement of an organism in goal-directed behaviour.

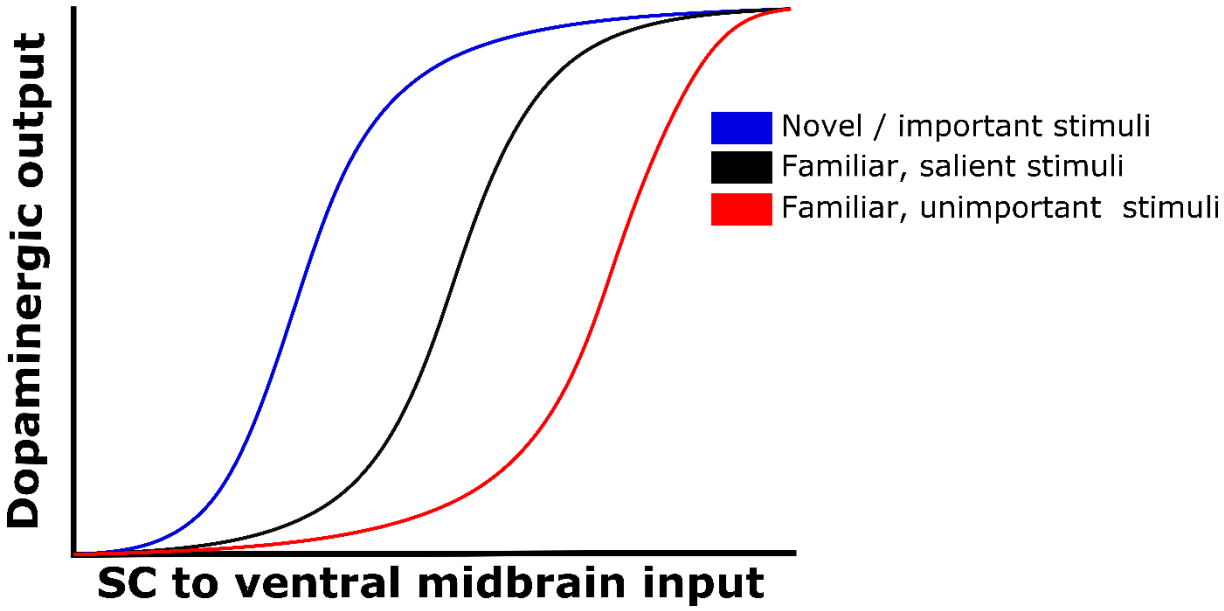

Figure 54. Stimulus-response curves showing that the sensitivity of the ventral midbrain to vision-driven input from the superior colliculus is modulated by reinforcement history. Stimuli which are novel or otherwise well differentiated from the background might require the least input to the ventral midbrain in order to evoke the mesolimbic and mesocortical pathways. Stimuli which are familiar and are predictive of reinforcement might require slightly more sustained, elevated input to the ventral midbrain in order to evoke the mesolimbic and mesocortical pathways. Familiar stimuli which are not predictive of reinforcement or punishment must strongly, persistently modulate midbrain dopamine neurons in order to evoke the mesocortical and mesolimbic projections.

Prior theories (e.g. Kool, Shenhav, & Botvinick, 2017; Shenhav, Botvinick, & Cohen, 2013) have proposed that the ACC dynamically computes the expected value of exerting control (EVC) over the rest of the brain, and thus behaviour, via ongoing cost-benefit analysis computations. In the EVC model, cost is operationalized as the expected metabolic expenditure associated with controlling the brain (and behaviour) and benefit is operationalized as the anticipated value gained by exerting control in a particular task. The results of these cost-benefit computations, the expected value of control, are suggested to dictate the response parameters to a stimulus. The rationale behind the EVC model stems from the wealth of evidence that incentivized performance is typically better than non-incentivized performance (Kool et al., 2017). In the EVC model, incentive is interpreted as the basis of the 'benefit' variable in the theorized ACC cost-benefit analyses which is weighed against the projected metabolic cost of responding such that tasks with little incentive are worth little control and that tasks with great incentive are worth great control.

Although the EVC model has been very useful (e.g. Shenhav, Straccia, Cohen, & Botvinick, 2014), its theoretical underpinnings are complex, requiring additional systems and brain areas which independently compute the cost and benefit variables which are then relayed to the ACC. In the EVC model, not only must the ACC integrate prospective cost and benefit information, it must also compute the magnitude of control to exert over the rest of the

brain. Such a multi-component cost-computing-and-relaying system has yet to be identified. Furthermore, the output of such a multi-layered, feedback-oriented system could be accomplished by a much simpler feed-forward sensory-driven incentive-salience gated mesocortical projection which either does or does not activate a cortical task model. Thus, a key distinction between these views is whether the ACC needs to be activated in order to disregard a stimulus. Specifically, the EVC model suggests that an organism appears disinterested towards a stimulus because the ACC has appraised the stimulus as not worthy of a response whereas the incentive-salience, task-model onset (ISTMO) view is that organisms appear disinterested towards a stimulus because the stimulus did not sufficiently activate the midbrain which then precludes expenditure of cortical resources appraising further reaction. It is also possible that other neuromodulatory centers, such as the locus coeruleus (Safaai et al., 2015; Tervo et al., 2014), also act to gate the onset of cortical task ensembles. The next section outlines a series of experiments intended to further clarify the mechanisms proposed to underpin the ISTMO theory.

4.9 Integrating and expanding: the work ahead

Many further experiments are necessary to confirm or refute this incentive-salience, task-model onset (ISTMO) theory of goal-oriented and adaptive behaviour. First, it is necessary to verify that in certain conditions sensory-driven input to the midbrain via the superior colliculus (Comoli et al., 2003) does indeed activate the mesocortical projection. Experimental work is also needed to determine whether changes in reinforcement history influence the probability of certain stimuli evoking the mesocortical projection. According to the ISTMO model (Figure 53), superior colliculus → midbrain DA signalling should play a critical role in the evocation of the mesocortical projection and the sensitivity of this circuit should be sensitive to reinforcement history. Specifically, the sensitivity of midbrain DA centres to superior collicular input is operationalized in the ISTMO theory as the threshold which gates the evocation of the mesocortical projection (Figure 54).

One approach to assessing whether this is the case could involve a combination of electrophysiological, iontophoretic, and electrochemical methods in anaesthetized rodents. In the first of a series of experiments, anaesthetized rats could be implanted with recording electrodes in the superior colliculus, ventral midbrain, and ACC and have a light flashed in their eyes. In circumstances where light-flash visual input would supercede the SC → midbrain DA threshold, one might expect that the firing rates of neurons all three areas would, sequentially, increase such that increases in the SC firing rates preceded midbrain DA firing rate increases which would precede ACC firing rate increases. The next experiment might

then consist of rodents implanted with a recording electrode in the SC, an iontophoretic probe to apply muscimol, a $GABA_A$ agonist, in the ventral midbrain, and a fast-scan cyclic voltammetry (FSCV) probe in the ACC. The hypothesis would be that in cases where the light was flashed in the rodent's eyes with no iontophoretic muscimol application, SC neurons would increase their firing rates and increases in dopamine concentrations would be detected via FSCV in the ACC. Conversely, in cases where muscimol was iontophoretically applied in the midbrain, one might expect to detect increases in SC neuron firing rates but not to detect stimulus-locked increases in ACC dopamine concentrations. This series of experiments could also iontophoretically apply other drugs to the midbrain, such as tetrodotoxin or baclofen, to determine ventral midbrain circuitry gating the sensory-driven evocation of the mesolimbic and mesocortical projections.

Next, large-scale neuronal recordings or fiber photometric imaging of ACC while an organism makes a rule-based decisions (e.g. Ott et al., 2014) could be used to observe the onset and reorganization dynamics of ACC neuronal task-model ensembles. In these experiments, the aim would be to test the generality of the ensemble onset mechanism identified in the hippocampus by Rajasethupathy et al. (2015). If the onset patterns of hippocampal neuronal ensembles are any indication of the onset patterns of cortical ensembles, these experiments might find that the activation of a subset of 'master' cortical neurons, perhaps value-selective cells, are necessary for activating a network of action-selective cells. Were this the case, the latency between activation of a specific value-selective ACC neuron and the activation of a specific set of action cells should be much shorter than the latency between activation of a value cell and activation of a different set of action cells. It would also be interesting to examine the activation parameters of ACC task-model ensembles with respect to cues indicating which action is appropriate for an upcoming trial.

After developing analytical tools for assessing ACC task-model ensemble dynamics, a series of experiments utilizing large scale neuronal recordings of both the ACC and VTA, as well as optogenetics, could examine the influence of mesocortical, VTA → ACC dopaminergic projections on ACC task-ensembles. If the VTA → ACC mesocortical projection is involved in the onset of ACC task-ensembles then 'master' ACC neurons ought to be significantly more phase-modulated by the VTA LFP than ACC action-encoding neurons, a prediction supported by data collected for this thesis. Furthermore, the activation of the entire task ensemble should be significantly related to the phase-modulation of the putative 'master' cells. One might also predict that selective inhibition of only the 'master' cells (*vis a vis* Rajasethupathy et al., 2015) ought to prevent the rest of the task-ensemble from

coming online which should behaviourally manifest as the organism never making the decision represented by the particular ensemble under examination.

The series of experiments proposed so far would only assess whether the onset of ACC task models is associated with incentive-salience signalling in the midbrain and do not, directly, assess how ACC task models and, presumably, behaviour are modified. On the basis of a series of experiments demonstrating that decreases in the reliability of ACC task models leads to instability of ACC ensemble activity (Karlsson et al., 2012), one framework for investigating ACC task model modification could be to examine how behavioural consequences influence the probability that a given neuron is recruited to a task ensemble. For instance, imagine an experiment where the behavioural component requires an organism to make simple choices towards the right or the left. On the basis of our findings and those of others (Cowen et al., 2012), one would expect that some single ACC units would represent simple actions, such as right or left turns, and that some units would represent value. The ISTMO theory predicts that a network of both value and action cells activate and that the relative number of right-turn selective cells versus left-turn selective cells should dictate which choice the organism makes. In cases where the organism makes an unsuccessful decision, turning right when the rewarded outcome was to turn left because more right-selective cells were active in the task-ensemble than left-selective cells, the ISTMO theory predicts that the probability of neurons encoding the unsuccessful action being recruited to the task-ensemble in subsequent trials would decrease and that the probability of cells representing an alternative action being recruited to the ensemble would increase. Conversely, the ISTMO theory predicts that in the case of successful outcomes, the probability of neurons encoding the successful action being recruited to the task ensemble would increase and that the probability of neurons encoding an alternative action being recruited to the task ensemble would decrease. One mechanism by which this theorized probability modification could occur is via neuromodulators, such as dopamine, serotonin, and norepinephrine. Indeed, an elegant series of experiments by Tervo et al. (2014) demonstrated that in circumstances where ACC task models are not useful, ACC activity is dampened by noradrenergic afferents from the locus coeruleus, which in turn leads to the onset of stochastic, rather than schematic, behaviours. Because such complex and temporally precise neuromodulation is unlikely to be carried out by a single neurochemical system and the contributions of each neuromodulatory system could be accounted for via local pharmacological infusions in the ACC or neuromodulatory centres or via optogenetic manipulation of neuromodulatory terminals in the ACC.

Although the proposed series of experiments provides a theoretical roadmap regarding the mechanisms that facilitate the onset and modification of ACC task models, they do not explicitly describe how modified ACC task models are behaviourally implemented. One possibility, suggested by our findings, is that, when a task model, and thus behavioural output, is modified, the ACC signals to the VTA which could influence the amount of dopamine projected from the VTA to the nucleus accumbens (NAcc), which could influence the vigour with which the modified task model is implemented (Hamid et al., 2016; Oleson et al., 2012; Shahidani, Reisi, Naghdi, Alaei, & Ramshini, 2012). To verify this assumption, rats implanted with a fast scan cyclic voltammetry probe in the nucleus accumbens and a fiber optic cable in the VTA could be trained to press levers on a variable-ratio 10 schedule and, at any one time, only one of the two levers yields reinforcement. One lever would remain reinforced until on average, 20 reinforcers had been acquired and then the task contingencies would discreetly reverse such that other lever is reinforced and presses to the prior lever are no longer reinforced. Behaviourally, one might expect the rats come to know that the contingencies will shift at some point and, from time to time, would sample the other lever to see if the contingency had shifted. Those sampling events could be framed as exploratory, non-default events. During those exploratory behaviours, the ISTMO theory would predict detection of elevated NAcc dopamine concentrations when rats modified their task model and explored the non-default action. Similarly, the ISTMO theory predicts that photo stimulation of ACC terminals in the VTA would directly increase NAcc dopamine concentrations, thereby causing the animal to explore the non-default option. The findings from this experiment would verify whether one step in the implementation of modified ACC task models involves changes in motivational states via VTA's dopaminergic output to the NAcc.

Chapter 5 Concluding remarks and summary

This thesis focused on the role of the ACC's interactions with the dopaminergic neurons in the VTA during adaptive behaviour. The overall question guiding this work was: how does information gained during goal pursuit modify and motivate subsequent behaviour? This larger question was operationalized as two projects: (i) to determine whether cortical influence over the dopaminergic midbrain is a mechanism by which ACC signals are implemented as VTA motivation signals; and (ii) to determine the interplay between the ACC and VTA during the initiation and maintenance of behavioural change. Central to my PhD work was the development of a unique, fully-automated 'figure of 8' maze (see Appendix) which allowed me to manipulate both the cost and benefit components of task contingencies while simultaneously recording single neurons and LFPs in the ACC and LFPs in the VTA. Also central was developing a partial directed coherence algorithm which enabled me to model task-dependent changes in ACC-VTA signal directionality.

In the first project, published in *Cell Reports*, we monitored and modelled ACC and VTA LFPs of rats running laps of varying physical difficulty for fixed rewards. The effortful condition required rats to climb over a 30-cm barrier, whereas no barrier was present under the non-effortful condition. The key finding was that ACC → VTA 4-12 Hz signalling increased in trials when the lap was easier than expected. Importantly, this increase was significantly correlated with, but not confounded by, changes in motivation, as measured by running speed. Thus, we showed for the first time that the ACC-VTA circuit is a plausible mechanism by which ACC signals are implemented as VTA motivational signals, thereby shifting behaviour from one response pattern to another.

The second projected examined the interplay between the ACC and VTA during the initiation and persistence of behavioural change. Stemming from the results of project 1, we hypothesized that the ACC → VTA circuit is a plausible mechanism by which task model signals are motivationally implemented. To test that hypothesis, we monitored ACC single units and LFPs as well as LFPs in VTA of rats performing a cost-benefit foraging task with changing contingencies. Through a combination of behavioural, electrophysiological, and modelling analyses, we found that the initiation of anticipatory behaviour and the persistence of behavioural change were associated with ACC → VTA signalling. Additionally, we characterized the content of ACC neuronal task models, and showed that ensembles of ACC neurons encode simple actions and values. This was important because, despite longstanding assumptions that the ACC encodes neuronal task models, the content of those internal representations remained unclear. Therefore, the finding that ACC neurons can encode simple

actions and values provides a clear basis for the notion that the ACC actively maintains neuronal representations of the task at hand. Furthermore, we demonstrated that value-coding elements of ACC neuronal task models are particularly influenced by the VTA. This is important because it suggests that mesocortical dopaminergic signalling is a means by which ACC models of the task at hand could be both initiated and modified. This work has been submitted for publication.

This thesis also evolved a novel incentive-salience, task-model onset (ISTMO) theory regarding ACC function. The key assertion of the ISTMO theory is midbrain-dopaminergic incentive-salience signalling acts as a simple feed-forward filter such that sensory inputs that does not excite midbrain dopamine neurons beyond some threshold does not activate the mesocortical projection. The ISTMO theory predicts that ACC task models are brought online by incentive-salience triggered mesocortical signalling to high-value-encoding ACC neurons which then bring a local network of action-encoding cells. This view is supported by our observation that high-value-encoding ACC neurons were particularly modulated by the VTA. This ISTMO perspective is worth pursuing because it offers new experimental predictions, new modelling opportunities, and new hope for the treatment of neurological and psychiatric disorders.

Chapter 6 References

Adhikari, A., Sigurdsson, T., Topiwala, M. A., & Gordon, J. A. (2010). Cross-correlation of instantaneous amplitudes of field potential oscillations: A straightforward method to estimate the directionality and lag between brain areas. *Journal of Neuroscience Methods*, *191*, 191–200. https://doi.org/10.1016/j.jneumeth.2010.06.019

Amantea, D., & Bowery, N. G. (2004). Reduced inhibitory action of a GABAB receptor agonist on [3H]-dopamine release from rat ventral tegmental area in vitro after chronic nicotine administration. *BMC Pharmacology*, *4*, 24. https://doi.org/10.1186/1471-2210-4-24

Arnsten, A. F. T. (2011). Catecholamine Influences on Dorsolateral Prefrontal Cortical Networks. *Biological Psychiatry*, *69*(12), e89–e99.

Arnt, J., & Scheel-Kruger, J. (1979). GABA in the ventral tegmental area: differential regional effects on locomotion, aggression and food intake after microinjection of GABA agonists and antagonists. *Life Sciences*, 1351–1360.

Baccalá, L., & Sameshima, K. (2001). Partial directed coherence: a new concept in neural structure determination. *Biological Cybernetics*, *84*(6), 463–474.

Ballantine, H., Cassidy, W., Flanagan, N., & Marino, R. J. (1967). Stereotaxic anterior cingulotomy for neuropsychiatric illness and intractable pain. *Journal of Neurosurgery*, *26*, 488–495.

Ballard, I. C., Murty, V. P., Carter, R. M., MacInnes, J. J., Huettel, S. A., & Adcock, R. A. (2011). Dorsolateral Prefrontal Cortex Drives Mesolimbic Dopaminergic Regions to Initiate Motivated Behavior. *Journal of Neuroscience*, *31*(28). Retrieved from http://www.jneurosci.org/content/31/28/10340

Bar, M. (2007). The proactive brain: using analogies and associations to generate predictions. *Trends in Cognitive Sciences*, *11*(7), 280–289. https://doi.org/10.1016/j.tics.2007.05.005

Barch, D. M., Braver, T. S., Akbudak, E., Conturo, T., Ollinger, J., & Snyder, A. (2001). Anterior Cingulate Cortex and Response Conflict: Effects of Response Modality and Processing Domain. *Cerebral Cortex*, *11*(9), 837–848. https://doi.org/10.1093/cercor/11.9.837

Behrens, T. E. J., Woolrich, M. W., Walton, M. E., & Rushworth, M. F. S. (2007). Learning

the value of information in an uncertain world. *Nature Neuroscience*, *10*(9), 1214–1221. https://doi.org/10.1038/nn1954

Beier, K. T., Steinberg, E. E., DeLoach, K. E., Xie, S., Miyamichi, K., Schwarz, L., … Liqun, L. (2015). Circuit architecture of VTA dopamine neurons revealed by systematic input-output mapping. *Cell*, *162*, 622–634.

Berridge, K. C. (2004). Motivation concepts in behavioral neuroscience. *Physiology and Behavior*, *81*, 179–209.

Berridge, K. C. (2012). From prediction error to incentive salience: mesolimbic computation of reward motivation. *The European Journal of Neuroscience*, *35*(7), 1124–43. https://doi.org/10.1111/j.1460-9568.2012.07990.x

Bissonette, G. B., & Roesch, M. R. (2015). Neural correlates of rules and conflict in medial prefrontal cortex during decision and feedback epochs. *Frontiers in Behavioral Neuroscience*, *9*, 266. https://doi.org/10.3389/fnbeh.2015.00266

Blanca, M. J., Alarcón, R., Arnau, J., Bono, R., & Bendayan, R. (2017). Non-normal data: Is ANOVA still a valid option? *Psicothema*, *29*(4), 552–557. https://doi.org/10.7334/psicothema2016.383

Blanchard, T. C., Strait, C. E., & Hayden, B. Y. (2015). Ramping ensemble activity in dorsal anterior cingulate neurons during persistent commitment to a decision. *Journal of Neurophysiology*, *114*(4), 2439–2449.

Bliss, T. V. P., Collingridge, G. L., Kaang, B.-K., & Zhuo, M. (2016). Synaptic plasticity in the anterior cingulate cortex in acute and chronic pain. *Nature Reviews Neuroscience*, *17*(8), 485–496. https://doi.org/10.1038/nrn.2016.68

Bolton, A., Murata, Y., Kirchner, R., Kim, S.-Y., Young, A., Dang, T., … Constantine-Paton, M. (2015). A Diencephalic Dopamine Source Provides Input to the Superior Colliculus, where D1 and D2 Receptors Segregate to Distinct Functional Zones. *Cell Reports*, *13*(5), 1003–1015. https://doi.org/10.1016/j.celrep.2015.09.046

Boykin, E. R., Khargonekar, P. P., Carney, P. R., Ogle, W. O., & Talathi, S. S. (2012). Detecting effective connectivity in networks of coupled neuronal oscillators. *Journal of Computational Neuroscience*, *32*(3), tr521-538.

Brog, J. S., Salyapongse, A., Deutch, A. Y., & Zahm, D. S. (1993). The patterns of afferent innervation of the core and shell in the ?Accumbens? part of the rat ventral striatum:

Immunohistochemical detection of retrogradely transported fluoro-gold. *The Journal of Comparative Neurology*, *338*(2), 255–278. https://doi.org/10.1002/cne.903380209

Bromberg-Martin, E. S., & Hikosaka, O. (2009). Midbrain Dopamine Neurons Signal Preference for Advance Information about Upcoming Rewards. *Neuron*, *63*(1), 119–126. https://doi.org/10.1016/j.neuron.2009.06.009

Bromberg-Martin, E. S., Matsumoto, M., & Hikosaka, O. (2010). Dopamine in Motivational Control: Rewarding, Aversive, and Alerting. *Neuron*, *68*(5), 815–834. https://doi.org/10.1016/j.neuron.2010.11.022

Bryden, D. W., Johnson, E. E., Tobias, S. C., Kashtelyan, V., & Roesch, M. (2011). Attention for learning signals in the anterior cingulate cortex. *The Journal of Neuroscience*, *31*(50), 18266–18274.

Butz, M. V., Sigaud, O., & Gérard, P. (2003). Anticipatory Behavior: Exploiting Knowledge About the Future to Improve Current Behavior. In *Anticipatory Behavior in Adaptive Learning Systems* (pp. 1–10). Berlin: Springer-Verlag. https://doi.org/10.1007/978-3-540-45002-3_1

Buzsaki, G. (2006). *Rhythms of the Brain*. New York: Oxford University Press.

Buzsaki, G., & Watson, B. O. (2012). Brain rhythms and neural syntax: implications for efficient coding of cogntive content and neuropsychiatric disease. *Dialogues in Clinical Neuroscience*, *14*, 345–367.

Camille, N., Tsuchida, A., & Fellows, L. K. (2011). Double Dissociation of Stimulus-Value and Action-Value Learning in Humans with Orbitofrontal or Anterior Cingulate Cortex Damage. *Journal of Neuroscience*, *31*(42). Retrieved from http://www.jneurosci.org/content/31/42/15048.short

Caravaggio, F., Fervaha, G., Menon, M., Remington, G., Graff-Guerrero, A., & Gerretsen, P. (2017). The neural correlates of apathy in schizophrenia: An exploratory investigation. *Neuropsychologia*. https://doi.org/10.1016/J.NEUROPSYCHOLOGIA.2017.10.027

Carr, D. B., & Sesack, S. R. (2000). GABA-containing neurons in the rat ventral tegmental area project to the prefrontal cortex. *Synapse*, *38*, 114–123.

Carr, D. B., & Sesack, S. R. (2000). Projections from the Rat Prefrontal Cortex to the Ventral Tegmental Area: Target Specificity in the Synaptic Associations with Mesoaccumbens and Mesocortical Neurons. *Journal of Neuroscience*, *20*(10).

Carver, C. S. (2009). Threat Sensitivity, Incentive Sensitivity, and the Experience of Relief. *Journal of Personality*, *77*(1), 125–138. https://doi.org/10.1111/j.1467-6494.2008.00540.x

Cavanagh, J. F., Frank, M. J., Klein, T. J., & Allen, J. J. B. (2010). Frontal Theta Links Prediction Errors to Behavioral Adaptation in Reinforcement Learning. *Neuroimage*, *49*(4). https://doi.org/10.1016/j.neuroimage.2009.11.080

Comoli, E., Coizet, V., Boyes, J., Bolam, J. P., Canteras, N. S., Quirk, R. H., … Redgrave, P. (2003). A direct projection from superior colliculus to substantia nigra for detecting salient visual events. *Nature Neuroscience*, *6*(9), 974–980. https://doi.org/10.1038/nn1113

Comoli, E., Das Neves Favaro, P., Vautrelle, N., Leriche, M., Overton, P. G., & Redgrave, P. (2012). Segregated anatomical input to sub-regions of the rodent superior colliculus associated with approach and defense. *Frontiers in Neuroanatomy*, *6*, 9. https://doi.org/10.3389/fnana.2012.00009

Cowen, S. L., Davis, G. A., & Nitz, D. A. (2012). Anterior cingulate neurons in the rat map anticipated effort and reward to their associated action sequences. *Journal of Neurophysiology*, *107*(9), 2393–2407.

Danielmeier, C., Eichele, T., Forstmann, B. U., Tittgemeyer, M., & Ullsperger, M. (2011). Posterior Medial Frontal Cortex Activity Predicts Post-Error Adaptations in Task-Related Visual and Motor Areas. *Journal of Neuroscience*, *31*(5), 1780–1789. https://doi.org/10.1523/JNEUROSCI.4299-10.2011

Danielmeier, C., & Ullsperger, M. (2011). Post-error adjustments. *Frontiers in Psychology*, *2*, 233. https://doi.org/10.3389/fpsyg.2011.00233

Darwin, C. (1865). *On the orgin of species by means of natural selection, or the preservation of favoured races in the struggle for life*. New York: D. Appleton and Company. Retrieved from http://darwin-online.org.uk/converted/pdf/1861_OriginNY_F382.pdf

Daw, N. D., O'Doherty, J. P., Dayan, P., Seymour, B., & Dolan, R. J. (2006). Cortical substrates for exploratory decisions in humans. *Nature*, *441*(7095), 876–879. https://doi.org/10.1038/nature04766

Debener, S., Ullsperger, M., Siegel, M., Fiehler, K., von Cramon, D. Y., & Engel, A. K. (2005). Trial-by-Trial Coupling of Concurrent Electroencephalogram and Functional

Magnetic Resonance Imaging Identifies the Dynamics of Performance Monitoring. *Journal of Neuroscience*, *25*(50).

Dembrow, N. C., & Johnston, D. (2014). Subcircuit-Specific Neuromodulation in the Prefrontal Cortex. *Frontiers in Neural Circuits*, *8*. https://doi.org/10.3389/fncir.2014.00054

Deutsch, R., Smith, K. J. M., Kordts-Freudinger, R., & Reichardt, R. (2015). How absent negativity relates to affect and motivation: an integrative relief model. *Frontiers in Psychology*, *6*, 152. https://doi.org/10.3389/fpsyg.2015.00152

Dichter, G. S., Damiano, C. A., & Allen, J. A. (2012). Reward circuitry dysfunction in psychiatric and neurodevelopmental disorders and genetic syndromes: animal models and clinical findings. *Journal of Neurodevelopmental Disorders*, *4*(1), 19. https://doi.org/10.1186/1866-1955-4-19

Dickerson, D. D., Wolff, A. R., & Bilkey, D. K. (2010). Abnormal Long-Range Neural Synchrony in a Maternal Immune Activation Animal Model of Schizophrenia. *Journal of Neuroscience*, *30*(37). Retrieved from http://www.jneurosci.org/content/30/37/12424.long

Dubovický, M., Skultétyová, I., & Jezová, D. (1999). Neonatal stress alters habituation of exploratory behavior in adult male but not female rats. *Pharmacology, Biochemistry, and Behavior*, *64*(4), 681–6. Retrieved from http://www.ncbi.nlm.nih.gov/pubmed/10593190

Economides, M., Guitart-Masip, M., Kurth-Nelson, Z., & Dolan, R. J. (2014). Anterior Cingulate Cortex Instigates Adaptive Switches in Choice by Integrating Immediate and Delayed Components of Value in Ventromedial Prefrontal Cortex. *Journal of Neuroscience*, *34*(9), 3340–3349. https://doi.org/10.1523/JNEUROSCI.4313-13.2014

Eiselt, A., & Nieder, A. (2013). Representation of abstract quantitative rules applied to spatial and numerical magnitudes in primate prefrontal cortex. *Journal of Neuroscience*, *33*(17), 7526–7534.

Ellwood, I. T., Patel, T., Wadia, V., Lee, A. T., Liptak, A. T., Bender, K. J., & Sohal, V. S. (2017). Tonic or phasic stimulation of dopaminergic projections to prefrontal cortex causes mice to maintain or deviate from previously learned behavioral strategies. *Journal of Neuroscience*. Retrieved from http://www.jneurosci.org/content/early/2017/07/24/JNEUROSCI.1221-17.2017

Elston, T., & Bilkey, D. (2017). Anterior cingulate cortex modulation of the ventral tegmental area in an effort task. *Cell Reports*, *19*(11), 2220–2230.

Eshel, N., Bukwich, M., Rao, V., Hemmelder, V., Tian, J., & Uchida, N. (2015). Arithmetic and local circuitry underlying dopamine prediction errors. *Nature*, *525*, 243–246.

Eshel, Tian, J., Bukwich, M., & Uchida, N. (2016). Dopamine neurons share common response function for reward prediction error. *Nature Neuroscience*, *19*(3).

Faget, L., Osakada, F., Duan, J., Ressler, R., Johnson, A. B., Proudfoot, J. A., … Hnasko, T. S. (2016). Afferent Inputs to Neurotransmitter-Defined Cell Types in the Ventral Tegmental Area. *Cell Reports*, *15*(12), 2796–2808. https://doi.org/10.1016/j.celrep.2016.05.057

Farashahi, S., Donahue, C. H., Khorsand, P., Seo, H., Lee, D., & Soltani, A. (2017). Metaplasticity as a Neural Substrate for Adaptive Learning and Choice under Uncertainty. *Neuron*, *94*(2), 401–414.e6. https://doi.org/10.1016/j.neuron.2017.03.044

Ferenczi, E., Zalocusky, K., Liston, C., Grosenick, L., Warden, M., Amatya, D., … Deisseroth, K. (2016). Prefrontal cortical regulation of brainwide circuit dynamics and reward-related behavior. *Science*, *351*(6268), aac9698-1-aac9698-12.

Fiorillo, C. D., Tobler, P. N., & Schultz, W. (2003). Discrete Coding of Reward Probability and Uncertainty by Dopamine Neurons. *Science*, *299*(5614), 1898–1902. https://doi.org/10.1126/science.1077349

Fiorillo Tobler, Philippe N., Schultz, Wolfram., C. D. (2003). Discrete coding of reward probability and uncertainty by dopamine neurons. *Science*, *299*, 1898–1902.

Floresco, S., & Magyar, O. (2006). Mesocortical dopamine modulation of executive functions: beyond working memory. *Psychopharmacology (Berlin)*, *188*, 567–585.

Foltz, E., & White, L. (1962). Pain "relief" by frontal cingulumotomy. *Journal of Neurosurgery*, *19*(89–100).

Freeman, W. J., & Vitiello, G. (2006). Nonlinear brain dynamics as macroscopic manifestation of underlying many-body field dynamics. *Physics of Life Reviews*, *3*(2), 93–118. https://doi.org/10.1016/j.plrev.2006.02.001

Friedman, A., Homma, D., Gibb, L. G., Amemori, K., Rubin, S. J., Hood, A. S., … Graybiel, A. M. (2015). A corticostriatal path targeting striosomes controls decision-making under conflict. *Cell*, *161*(6), 1320–1333.

Fries, P. (2015). Rhythms for Cognition: Communication through Coherence. *Neuron*, *88*(1), 220–35. https://doi.org/10.1016/j.neuron.2015.09.034

Friston, K., Rigoli, F., Ognibene, D., Mathys, C., Fitzgerald, T., & Pezzulo, G. (2015). Active inference and epistemic value. *Cognitive Neuroscience*, *6*(4), 187–214. https://doi.org/10.1080/17588928.2015.1020053

Fu, Y., Yuan, Y., Halliday, G., Rusznák, Z., Watson, C., & Paxinos, G. (2012). A cytoarchitectonic and chemoarchitectonic analysis of the dopamine cell groups in the substantia nigra, ventral tegmental area, and retrorubral field in the mouse. *Brain Structure and Function*, *217*(2), 591–612. https://doi.org/10.1007/s00429-011-0349-2

Fujisawa, S., Amarasingham, A., Harrison, M. T., & Buzsáki, G. (2008). Behavior-dependent short-term assembly dynamics in the medial prefrontal cortex. *Nature Neuroscience*, *11*(7), 823–833. https://doi.org/10.1038/nn.2134

Fujisawa, S., & Buzsaki, G. (2011). A 4Hz oscillation adaptively synchronizes prefrontal, VTA, and hippocampal activities. *Neuron*, *72*, 153–165.

Fusi, S., Asaad, W. F., Miller, E. K., & Wang, X.-J. (2007). A Neural Circuit Model of Flexible Sensorimotor Mapping: Learning and Forgetting on Multiple Timescales. *Neuron*, *54*(2), 319–333. https://doi.org/10.1016/j.neuron.2007.03.017

Gao, L., Chang-Liang, J., Guo-Zhang, J., Bunney, B., & S., Shi, Wei-Xing, M. (2007). Functional coupling between the prefrontal cortex and dopamine neurons in the ventral tegmental area. *The Journal of Neuroscience*, *27*(20), 5414–5421.

Gao, M., Liu, C.-L., Yang, S., Jin, G.-Z., Bunney, B. S., & Shi, W.-X. (2007). Functional Coupling between the Prefrontal Cortex and Dopamine Neurons in the Ventral Tegmental Area. *Journal of Neuroscience*, *27*(20), 5414–5421. https://doi.org/10.1523/JNEUROSCI.5347-06.2007

Gariano, R. F., & Groves, P. M. (1988). Burst firing induced in midbrain dopamine neurons by stimulation of the medial prefrontal and anterior cingulate cortices. *Brain Research*, *462*(1), 194–8. Retrieved from http://www.ncbi.nlm.nih.gov/pubmed/3179734

Gemba, H., Sasaki, K., & Brooks, V. B. (1986). “Error” potentials in limbic cortex (anterior cingulate area 24) of monkeys during motor learning. *Neuroscience Letters*, *70*(2), 223–227. https://doi.org/10.1016/0304-3940(86)90467-2

George, M. S., Ketter, T. A., Gill, D. S., Haxby, J. V, Ungerleider, L. G., Herscovitch, P., &

Post, R. M. (1993). Brain regions involved in recognizing facial emotion or identity: an oxygen-15 PET study. *The Journal of Neuropsychiatry and Clinical Neurosciences*, *5*(4), 384–394. https://doi.org/10.1176/jnp.5.4.384

Gratton, G., Coles, M. G., & Donchin, E. (1992). Optimizing the use of information: strategic control of activation of responses. *Journal of Experimental Psychology. General*, *121*(4), 480–506. Retrieved from http://www.ncbi.nlm.nih.gov/pubmed/1431740

Gresch, P. J., Barret, R. J., Sanders-Bush, E., & Smith, R. L. (2006). 5-Hydroxytryptamine (serotonin)2A receptors in rat anterior cingulate cortex mediate the discriminative stimulus properties of d-lysergic acid diethylamide. *The Journal of Pharmacology and Experimental Therapeutics*, *320*(2), 662–669.

Hamid, A., Pettibone, J., Mabrouk, O., Hetrick, V., Schmidt, R., Vander Weele, C., … Berke, J. D. (2016). Mesolimbic dopamine signals the value of work. *Nature Neuroscience*, *19*, 117–126.

Hansen Manahan-Vaughan, Denise, N. (2014). Dopamine D1/D5 receptors mediation informational saliency that promotes persistent hippocampal long-term plasticity. *Cerebral Cortex*, *4*(24), 845–858.

Haroush, K., & Williams, Z. M. (2015). Neuronal prediction of opponent's behavior during cooperative social interchange in primates. *Cell*, *160*(6), 1233–45. https://doi.org/10.1016/j.cell.2015.01.045

Hayden, B., Pearson, J., & Platt, M. (2011). Neuronal basis of sequential foraging decisions in a patchy environment. *Nature Neuroscience*, *14*(7), 933–939.

Hayden, B. Y., Heilbronner, S. R., Pearson, J. M., & Platt, M. L. (2011). Surprise signals in anterior cingulate cortex: neuronal encoding of unsigned reward prediction errors driving adjustment in behavior. *The Journal of Neuroscience : The Official Journal of the Society for Neuroscience*, *31*(11), 4178–87. https://doi.org/10.1523/JNEUROSCI.4652-10.2011

Hayden, B. Y., & Platt, M. L. (2010). Neurons in Anterior Cingulate Cortex Multiplex Information about Reward and Action. *Journal of Neuroscience*, *30*(9). Retrieved from http://www.jneurosci.org/content/30/9/3339.short

Hillman, K. L., & Bilkey, D. K. (2010). Neurons in the rat anterior cingulate cortex dynamically encode cost-benefit in a spatial decision-making task. *J Neurosci*, *30*(22),

7705–7713. https://doi.org/10.1523/JNEUROSCI.1273-10.2010

Hillman, K. L., & Bilkey, D. K. (2012). Neural encoding of competitive effort in the anterior cingulate cortex. *Nature Neuroscience*, *15*(9), 1290–1297. https://doi.org/10.1038/nn.3187

Holec, V., Pirot, H., & Euston, D. (2014). Not all effort is equal: the role of the anterior cingulate cortex in different forms of effort-reward decisions. *Frontiers in Behavioral Neuroscience*, *8*(12). https://doi.org/10.3389/fnbeh.2014.00012

Holroyd, C. B., & Coles, M. G. H. (2008). Dorsal anterior cingulate cortex integrates reinforcement history to guide voluntary behavior. *Cortex*, *44*(5), 548–559. https://doi.org/10.1016/j.cortex.2007.08.013

Holroyd, C. B., & McClure, S. M. (2015). Hierarchical control over effortful behavior by rodent medial frontal cortex: A computational model. *Psychological Review*, *122*(1), 54–83. https://doi.org/10.1037/a0038339

Holroyd, C. B., & Yeung, N. (2012). Motivation of extended behaviors by anterior cingulate cortex. *Trends in Cognitive Sciences*, *16*(2), 122–128. https://doi.org/10.1016/j.tics.2011.12.008

Howe, M., Tierney, P., Sandberg, S., Phillips, P. E. M., & Graybiel, A. M. (2013). Prolonged dopamine signalling in striatrum signals proximity and value of distant rewards. *Nature*, *500*, 575–579.

Hrabovszky, E., Molnár, C. S., Borsay, B. Á., Gergely, P., Herczeg, L., & Liposits, Z. (2013). Orexinergic Input to Dopaminergic Neurons of the Human Ventral Tegmental Area. *PLoS ONE*, *8*(12), e83029. https://doi.org/10.1371/journal.pone.0083029

Ikemoto, S. (2007). Dopamine reward circuitry: two projection systems from the ventral midbrain to the nucleus accumbens-olfactory tubercle complex. *Brain Research Reviews*, *56*(2007), 27–78.

Ioffe, S., & Szegedy, C. (2015). Batch Normalization: Accelerating Deep Network Training by Reducing Internal Covariate Shift. Retrieved from http://arxiv.org/abs/1502.03167

Ito, H. T., Zhang, S.-J., Witter, M. P., Moser, E. I., & Moser, M.-B. (2015). A prefrontal-thalamo-hippocampal circuit for goal-directed spatial navigation. *Nature*, *522*, 50–55.

Jacob, S. N., Stalter, M., & Nieder, A. (2016). Cell-type-specific modulation of targets and distractors by dopamine D1 receptors in primate prefrontal cortex. *Nature*

Communications, *7*, 13218. https://doi.org/10.1038/ncomms13218

Jenni, N. L., Larkin, J. D., & Floresco, S. B. (2017). Prefrontal dopamine D1 and D2 receptors regulate dissociable aspects of decision-making via distinct ventral striatal and amygdalar circuits. *The Journal of Neuroscience*, 30–17. https://doi.org/10.1523/JNEUROSCI.0030-17.2017

Jo, Y. S., Lee, J., & Mizumori, S. J. Y. (2013). Effects of Prefrontal Cortical Inactivation on Neural Activity in the Ventral Tegmental Area. *Journal of Neuroscience*, *33*(19).

Karalis, N., Dejean, C., Chaudun, F., Khoder, S., Rozeske, R. R., Wurtz, H., … Herry, C. (2016). 4-Hz oscillations synchronize prefrontal–amygdala circuits during fear behavior. *Nature Neuroscience*, *19*(4), 605–612. https://doi.org/10.1038/nn.4251

Karlsson, M. P., Tervo, D. G. R., & Karpova, A. Y. (2012). Network Resets in Medial Prefrontal Cortex Mark the Onset of Behavioral Uncertainty. *Science*, *338*(6103). Retrieved from http://science.sciencemag.org/content/338/6103/135

Kawai, T., Yamada, H., Sato, N., Takada, M., & Matsumoto, M. (2015). Roles of the lateral habenula and anterior cingulate cortex in negative outcome monitoring and behavioral adjustment in nonhuman primates.

Kennerley, S. W., Walton, M. E., Behrens, T. E. J., Buckley, M. J., & Rushworth, M. F. S. (2006). Optimal decision making and the anterior cingulate cortex. *Nature Neuroscience*, *9*(7), 940–947. https://doi.org/10.1038/nn1724

Kennerly, S. W., Behrens, T. E. J., & Wallis, J. D. (2011). Double dissociation of value computations in orbitofrontal and anterior cingulate neurons. *Nature Neuroscience*, *14*(12), 1581–1589.

Knox, W. B., Otto, A. R., Stone, P., & Love, B. C. (2011). The nature of belief-directed exploratory choice in human decision-making. *Frontiers in Psychology*, *2*, 398. https://doi.org/10.3389/fpsyg.2011.00398

Kolling, N., Behrens, T. E. J., Mars, R. B., & Rushworth, M. F. S. (2012). Neural mechanisms of foraging. *Science*, *336*(6077), 95–8. https://doi.org/10.1126/science.1216930

Kolling, N., Behrens, T., Wittmann, M., & Rushworth, M. (2016a). Multiple signals in anterior cingulate cortex. *Current Opinion in Neurobiology*, *37*, 36–43. https://doi.org/10.1016/j.conb.2015.12.007

Kolling, N., Behrens, T., Wittmann, M., & Rushworth, M. (2016b). Multiple signals in anterior cingulate cortex. *Current Opinion in Neurobiology*, *37*, 36–43. https://doi.org/10.1016/j.conb.2015.12.007

Kolling, N., Wittmann, M. K., Behrens, T. E. J., Boorman, E. D., Mars, R. B., & Rushworth, M. F. S. (2016). Value, search, persistence and model updating in anterior cingulate cortex. *Nat Neurosci*, *19*(10), 1280–1285. Retrieved from http://dx.doi.org/10.1038/nn.4382

Kool, W., Shenhav, A., & Botvinick, M. M. (2017). Cognitive Control as Cost-Benefit Decision Making. In *The Wiley Handbook of Cognitive Control* (pp. 167–189). Chichester, UK: John Wiley & Sons, Ltd. https://doi.org/10.1002/9781118920497.ch10

Kroener, C., Phillips, P., & Seamans, J. (2009). Dopamine modulates persistent synaptic activity and enhances the signal-to-noise ratio in the prefrontal cortex. *PLOS One*, *4*(8), e6507.

Lapish, C. C., Kroener, S., Durstewitz, D., Lavin, A., & Seamans, J. K. (2007). The ability of the mesocortical dopamine system to operate in distinct temporal modes. *Psychopharmacology*, *191*(3), 609–625. https://doi.org/10.1007/s00213-006-0527-8

Le Heron, C., Apps., M. A. J., & Husain, M. (2017). The anatomy of apathy: A neurocognitive framework for amotivated behaviour. *Neuropsychologia*. https://doi.org/10.1016/j.neuropsychologia.2017.07.003

Lewis, B., & O'Donnell, P. (2000). Ventral tegmental area afferents to the prefrontal cortex maintain membrane potential "up" states in pyramidal neurons via D(1) dopamine receptors. *Cerebral Cortex*, *10*, 1168–1175.

Likhtik, E., Stujenske, J. M., Topiwala, M. A., Harris, A. Z., & Gordon, J. A. (2014). Prefrontal entrainment of amygdala activity signals safety in learned fear and innate anxiety. *Nature Neuroscience*, *17*, 106–113.

Liu, S., Chow, H. M., Xu, Y., Erkkinen, M. G., Swett, K. E., Eagle, M. W., … Braun, A. R. (2012). Neural Correlates of Lyrical Improvisation: An fMRI Study of Freestyle Rap. *Scientific Reports*, *2*, 46–57. https://doi.org/10.1038/srep00834

Ljungberg, T., Apicella, P., & Schultz, W. (1992). Responses of monkey dopamine neurons during learning of behavioral reactions. *Journal of Neurophysiology*, *67*(1), 145–63. Retrieved from http://www.ncbi.nlm.nih.gov/pubmed/1552316

Ma, L., Hyman, J. M., Lindsay, A. J., Phillips, A. G., & Seamans, J. K. (2014). Differences in the emergent coding properties of cortical and striatal ensembles. *Nature Neuroscience*, *17*(8), 1100–1106.

Ma, L., Hyman, J. M., Phillips, A. G., & Seamans, J. K. (2014). Tracking progress toward a goal in corticostriatal ensembles. *Journal of Neuroscience*, *34*(6), 2244–2253.

McCoy, A. N., & Platt, M. L. (2005). Risk-sensitive neurons in macaque posterior cingulate cortex. *Nature Neuroscience*, *8*(9), 1220–1227. https://doi.org/10.1038/nn1523

McKenzie, S., Frank, A. J., Kinsky, N. R., Porter, B., Rivière, P. D., & Eichenbaum, H. (2014). Hippocampal Representation of Related and Opposing Memories Develop within Distinct, Hierarchically Organized Neural Schemas. *Neuron*, *83*(1), 202–215. https://doi.org/http://dx.doi.org/10.1016/j.neuron.2014.05.019

Meyer, G., McElhaney, M., Martin, W., & McGraw, C. (1973). Stereotactic cingulotomy with results of acute stimulation and serial psychological testing. In L. Laitinen & K. Livingston (Eds.), *Surgical Approaches in Psychiatry* (pp. 39–58). Lancaster (UK).

Milner, B. (1963). Effects of different brain lesions on card sorting. *Archives of Neurology*, *9*, 100–110.

Mirza, M. B., Adams, R. A., Mathys, C. D., & Friston, K. J. (2016). Scene Construction, Visual Foraging, and Active Inference. *Frontiers in Computational Neuroscience*, *10*, 56. https://doi.org/10.3389/fncom.2016.00056

Mitra, P., & Bokil, H. (2008). *Observed Brain Dynamics*. New York: Oxford University Press.

Monosov, I. E. (2017). Anterior cingulate is a source of valence-specific information about value and uncertainty. *Nature Communications*, *8*, 1–12. https://doi.org/doi:10.1038/s41467-017-00072-y

Morales, M., & Margolis, E. B. (2017). Ventral tegmental area: cellular heterogeneity, connectivity and behaviour. *Nature Reviews Neuroscience*, *18*, 73–85. https://doi.org/10.1038/nrn.2016.165

Moretti, R., & Signori, R. (2016). Neural Correlates for Apathy: Frontal-Prefrontal and Parietal Cortical- Subcortical Circuits. *Frontiers in Aging Neuroscience*, *8*, 289. https://doi.org/10.3389/fnagi.2016.00289

Narayanan, N. S., Cavanagh, J. F., Frank, M. J., & Laubach, M. (2013). Common medial

frontal mechanisms of adaptive control in humans and rodents. *Nature Neuroscience*, *16*(12), 1888–1895. https://doi.org/10.1038/nn.3549

Narita, M., Matsushima, Y., Niikura, K., Narita, M., Takagi, S., Nakahara, K., … Tsutomu, S. (2010). Implication of dopaminergic projection from the ventral tegmental area to the anterior cingulate cortex in μ-opioid-induced place preference. *Addiction Biology*, *15*(4), 434–447.

Nassar, M. R., Wilson, R. C., Heasly, B., & Gold, J. I. (2010). An Approximately Bayesian Delta-Rule Model Explains the Dynamics of Belief Updating in a Changing Environment. *Journal of Neuroscience*, *30*(37). Retrieved from http://www.jneurosci.org/content/30/37/12366

Navailles, S., Guillem, K., Vouillac-Mendoza, C., & Ahmed, S. H. (2015). Coordinated Recruitment of Cortical–Subcortical Circuits and Ascending Dopamine and Serotonin Neurons During Inhibitory Control of Cocaine Seeking in Rats. *Cerebral Cortex*, *25*(9), 3167–3181. https://doi.org/10.1093/cercor/bhu112

Navratilova, E., & Porreca, F. (2014). Reward and motivation in pain and pain relief. *Nature Neuroscience*, *17*(10), 1304–1312. https://doi.org/10.1038/nn.3811

Nestler, E. J. (2005). Is there a common molecular pathway for addiction? *Nature Neuroscience*, *8*(11), 1445–1449. https://doi.org/10.1038/nn1578

O'Donnell, P. (2003). Dopamine gating of forebrain neural ensembles. *European Journal of Neuroscience*, *17*, 429–435.

O'Keefe, J., & Dostrovsky, J. (1971). The hippocampus as a spatial map. Preliminary evidence from unit activity in the freely-moving rat. *Brain Research*, *34*(1), 171–175. https://doi.org/http://dx.doi.org/10.1016/0006-8993(71)90358-1

O'Reilly, J. X., Schuffelgen, U., Cuell, S. F., Behrens, T. E. J., Mars, R. B., & Rushworth, M. F. S. (2013). Dissociable effects of surprise and model update in parietal and anterior cingulate cortex. *Proceedings of the National Academy of Sciences*, *110*(38), E3660–E3669. https://doi.org/10.1073/pnas.1305373110

Oades, G., & Halliday, R. (1987). Ventral tegmental (A10) system: neurobiology. 1. Anatomy and connectivity. *Brain Research*, *434*(2), 117–165.

Olds, J. (1958). Self-Stimulation of the Brain: Its Use To Study Local Effects of Hunger, Sex, and Drugs. *Science*, *127*(3294), 315–324. https://doi.org/10.1126/science.127.3294.315

Olds, J., & Milner, P. (1954). Positive reinforcement produced by electrical stimulation of septal area and other regions of rat brain. *Journal of Comparative and Physiological Psychology*, *47*(6), 419–27. Retrieved from http://www.ncbi.nlm.nih.gov/pubmed/13233369

Oleson, E. B., Gentry, R. N., Chioma, V. C., & Cheer, J. F. (2012). Subsecond Dopamine Release in the Nucleus Accumbens Predicts Conditioned Punishment and Its Successful Avoidance. *Journal of Neuroscience*, *32*(42), 14804–14808. https://doi.org/10.1523/JNEUROSCI.3087-12.2012

Olton, D. S. (1989). Frontal cortex, timing and memory. *Neuropsychologia*, *27*(1), 121–30. Retrieved from http://www.ncbi.nlm.nih.gov/pubmed/2651964

Olton, D. S., Wenk, G. L., Church, R. M., & Meck, W. H. (1988). Attention and the frontal cortex as examined by simultaneous temporal processing. *Neuropsychologia*, *26*(2), 307–18. Retrieved from http://www.ncbi.nlm.nih.gov/pubmed/3399046

Onoda, K., & Yamaguchi, S. (2015). Dissociative contributions of the anterior cingulate cortex to apathy and depression: Topological evidence from resting-state functional MRI. *Neuropsychologia*, *77*, 10–18. https://doi.org/10.1016/j.neuropsychologia.2015.07.030

Ott, T., Jacob, S. N., & Nieder, A. (2014). Dopamine Receptors Differentially Enhance Rule Coding in Primate Prefrontal Cortex Neurons. *Neuron*, *84*(6), 1317–1328. https://doi.org/10.1016/j.neuron.2014.11.012

Ott, T., & Nieder, A. (2017). Dopamine D2 Receptors Enhance Population Dynamics in Primate Prefrontal Working Memory Circuits. *Cerebral Cortex*, *26*(Suppl), 180–191. https://doi.org/10.1093/cercor/bhw244

Pan, W.-X., Schmidt, R., Wickens, J. R., & Hyland, B. I. (2008). Tripartite Mechanism of Extinction Suggested by Dopamine Neuron Activity and Temporal Difference Model. *Journal of Neuroscience*, *28*(39). Retrieved from http://www.jneurosci.org/content/28/39/9619.long

Parker, K. L., Chen, K.-H., Kingyon, J. R., Cavanagh, J. F., & Narayanan, N. S. (2014). D1-dependent 4 Hz oscillations and ramping activity in rodent medial frontal cortex during interval timing. *The Journal of Neuroscience : The Official Journal of the Society for Neuroscience*, *34*(50), 16774–83. https://doi.org/10.1523/JNEUROSCI.2772-14.2014

Parker, K. L., Chen, K.-H., Kingyon, J. R., Cavanagh, J. F., & Narayanan, N. S. (2015). Medial frontal ~4-Hz activity in humans and rodents is attenuated in PD patients and in rodents with cortical dopamine depletion. *Journal of Neurophysiology*, *114*(2), 1310–20. https://doi.org/10.1152/jn.00412.2015

Parkhurst, D., Law, K., & Niebur, E. (2002). Modeling the role of salience in the allocation of overt visual attention. *Vision Research*, *42*(1), 107–123. https://doi.org/http://dx.doi.org/10.1016/S0042-6989(01)00250-4

Parvizi, J., Rangarajan, V., Shirer, W., Desai, N., & Greicius, M. D. (2013). The will to persevere induced by electrical stimulation of the human cingulate gyrus. *Neuron*, *80*(6). https://doi.org/doi:10.1016/j.neuron.2013.10.057.

Paxinos, G., & Watson, C. (1997). *The rat brain in stereotaxic coordinates 4th edition*. New York: Academic Press.

Pearce, J. M., & Hall, G. (1980). A Model for Pavlovian Learning: Variations in the Effectiveness of Conditioned But Not of Unconditioned Stimuli. *Psychological Review*, *87*(6), 532–552.

Perret, E. (1974). The left frontal lobe of man and the suppression of habitual responses in verbal categorical behaviour. *Neuropsychologia*, *12*(3), 323–330. https://doi.org/10.1016/0028-3932(74)90047-5

Phillips, A. G., Blaha, C. D., & Fibiger, H. C. (1989). Neurochemical correlates of brain-stimulation reward measured by ex vivo and in vivo analyses. *Neuroscience and Biobehavioral Reviews*, *13*(2–3), 99–104. Retrieved from http://www.ncbi.nlm.nih.gov/pubmed/2530478

Pisauro, M. A., Fouragnan, E., Retzler, C., & Philiastides, M. G. (2017). Neural correlates of evidence accumulation during value-based decisions revealed via simultaneous EEG-fMRI. *Nature Communications*, *8*, 15808. https://doi.org/10.1038/ncomms15808

Puig, M., Rose, J., Schmidt, R., & Freund, N. (2014). Dopamine modulation of learning and memory in the prefrontal cortex: insights from studies in primates, rodents, and birds. *Frontiers in Neural Circuits*, *8*, 1–15.

Qi, J., Zhang, S., Wang, H.-L., Barker, J., Miranda-Barrientos, M., & Morales, M. (2016). VTA glutamatergic inputs to nucleus accumbens drive aversion to acting on GABAeric interneurons. *Nature Neuroscience*, *79*, 725–733.

Rajasethupathy, P., Sankara, S., Marshel, J. H., Kim, C. K., Ferenczi, E., Lee, S. L., … Deisseroth, K. (2015). Projections from neocortex mediate top-down control of memory retrieval. *Nature*, *526*(653–659).

Roesch, M., & Bryden, D. (2011). Impact of Size and Delay on Neural Activity in the Rat Limbic Corticostriatal System. *Frontiers in Neuroscience, 5*(130). https://doi.org/10.3389/fnins.2011.00130

Rolls, E. T. (2013). The mechanisms for pattern completion and pattern separation in the hippocampus. *Frontiers in Systems Neuroscience*, *7*, 74. https://doi.org/10.3389/fnsys.2013.00074

Rudebeck, P. H., Walton, M. E., Smyth, A. N., Bannerman, D. M., & Rushworth, M. F. (2009). Separate neural pathways process different decision costs. *Nature Neuroscience*, *9*(9), 1161–1168.

Safaai, H., Neves, R., Eschenko, O., Logothetis, N. K., & Panzeri, S. (2015). Modeling the effect of locus coeruleus firing on cortical state dynamics and single-trial sensory processing. *Proceedings of the National Academy of Sciences of the United States of America*, *112*(41), 12834–9. https://doi.org/10.1073/pnas.1516539112

Salamone, J. D., & Correa, M. (2012). The Mysterious Motivational Functions of Mesolimbic Dopamine. *Neuron*, *76*(3), 470–485. https://doi.org/10.1016/j.neuron.2012.10.021

Sanchez-Catalan, M. J., Kaufling, J., Georges, F., Veinante, P., & Barrot, M. (2014). The antero-posterior heterogeneity of the ventral tegmental area. *Neuroscience, 282,* 198–216. https://doi.org/10.1016/j.neuroscience.2014.09.025

Schmider, E., Ziegler, M., Danay, E., Beyer, L., & Bühner, M. (2010). Is It Really Robust? *Methodology*, *6*(4), 147–151. https://doi.org/10.1027/1614-2241/a000016

Schultz, W. (1998). Predictive reward signal of dopamine neurons. *Journal of Neurophysiology*, *80*(1), 1–27. Retrieved from http://www.ncbi.nlm.nih.gov/pubmed/9658025

Schultz, W. (2007). Multiple Dopamine Functions at Different Time Courses. *Annual Review of Neuroscience, 30*(1), 259–288. https://doi.org/doi:10.1146/annurev.neuro.28.061604.135722

Schultz, W. (2016). Dopamine reward prediction-error signalling: a two-component response. *Nature Reviews Neuroscience, 17,* 183–195.

Schultz, W., Dayan, P., & Montague, P. R. (1997). A Neural Substrate of Prediction and Reward. *Science*, *275*(5306).

Schweimer, J., & Hauber, W. (2006). Dopamine D1 receptors in the anterior cingulate cortex regulate effort-based decision making. *Learning & Memory (Cold Spring Harbor, N.Y.)*, *13*(6), 777–82. https://doi.org/10.1101/lm.409306

Seal, R., & Edwards, R. (2006). Functional implications of neurotransmitter co-release: glutamate and GABA share the load. *Current Opinion in Pharmacology*, *6*(1), 114–119. https://doi.org/10.1016/j.coph.2005.12.001

Seeman, M. V, & Seeman, P. (2014). Is schizophrenia a dopamine supersensitivity psychotic reaction? *Progress in Neuro-Psychopharmacology and Biological Psychiatry*, *48*, 155–160.

Shahidani, S., Reisi, P., Naghdi, N., Alaei, H., & Ramshini, E. (2012). Lesion of medial prefrontal cortex reduces morphine-induced extracellular dopamine level in the ventral tegmental area: A microdialysis study in rats. *Pharmacology Biochemistry and Behavior*, *102*(1), 77–81. https://doi.org/http://dx.doi.org/10.1016/j.pbb.2012.03.009

Shenhav, A., Botvinick, M. M., & Cohen, J. D. (2013). The expected value of control: an integrative theory of anterior cingulate cortex function. *Neuron*, *79*(2), 217–240.

Shenhav, A., Straccia, M. A., Cohen, J. D., & Botvinick, M. M. (2014). Anterior cingulate engagement in a foraging context reflects choice difficulty, not foraging value. *Nature Neuroscience*, *17*(9), 1249–1254. https://doi.org/10.1038/nn.3771

Sheth, S. A., Mian, M. K., Patel, S. R., Asaad, W. F., Williams, Z. M., Dougherty, D. D., … Eskandar, E. N. (2012). Human dorsal anterior cingulate cortex neurons mediate ongoing behavioural adaptation. *Nature*, *488*(7410), 218–221. https://doi.org/10.1038/nature11239

Skinner, B. F. (1938). *The behavior of organisms: an experimental analysis*. New York: Appleton-Century-Crofts.

Steinberg, E. E., Keiflin, R., Boivin, J. R., Witten, I. B., Deisseroth, K., & Janak, P. H. (2013). A causal link between prediction errors, dopamine neurons and learning. *Nature Neuroscience*, *16*(7), 966–973. https://doi.org/10.1038/nn.3413

Stroop, J. R. (1935). Studies of interference in serial verbal reactions. *Journal of Experimental Psychology*, *18*, 643–662.

Sweeny, K., & Vohs, K. D. (2012). On Near Misses and Completed Tasks: The Nature of Relief. *Psychological Science*, *23*(5), 464–468. https://doi.org/10.1177/0956797611434590

Swick, D., & Jovanovic, J. (2002). Anterior cingulate cortex and the Stroop task: neuropsychological evidence for topographic specificity. *Neuropsychologia*, *40*(8), 1240–1253. https://doi.org/10.1016/S0028-3932(01)00226-3

Taber, M. T., Das, S., & Fibiger, H. C. (1995). Cortical regulation of subcortical dopamine release: mediation via the ventral tegmental area. *Journal of Neurochemistry*, *65*(3), 1407–1410.

Terry, W. S. (1979). Habituation and dishabituation of rats' exploration of a novel environment. *Animal Learning & Behavior*, *7*(4), 525–536. https://doi.org/10.3758/BF03209714

Tervo, D. G. R., Proskurin, M., Manakov, M., Kabra, M., Vollmer, A., Branson, K., & Karpova, A. Y. (2014). Behavioral Variability through Stochastic Choice and Its Gating by Anterior Cingulate Cortex. *Cell*, *159*(1), 21–32. https://doi.org/10.1016/j.cell.2014.08.037

Thorndike, E. L. (1898). *Animal intelligence*. New York: Macmillan.

Thorndike, E. L. (1928). *The measurement of intelligence*. New York: Teachers College, Columbia University.

Tolman, E. (1948). Cognitive maps in rats and men. *Psychological Review*, *55*(4), 189–208. Retrieved from http://www.ncbi.nlm.nih.gov/pubmed/18870876

Trudeau, L.-E. (2004). Glutamate co-transmission as an emerging concept in monoamine neuron function. *Journal of Psychiatry & Neuroscience : JPN*, *29*(4), 296–310. Retrieved from http://www.ncbi.nlm.nih.gov/pubmed/15309046

Tsai, C. (1925). The optic tracts and centers of the opossum, didelphis virginiana. *Journal of Computational Neurology*, 173–219.

van Zessen, R., Phillips, J. L., Budygin, E. A., & Stuber, G. D. (2012). Activation of VTA GABA neurons disrupts reward consumption. *Neuron*, *73*(6), 1184–94. https://doi.org/10.1016/j.neuron.2012.02.016

Vogt, B. A. (2005). Pain and emotion interactions in subregions of the cingulate gyrus. *Nature Reviews Neuroscience*, *6*(7), 533–544. https://doi.org/10.1038/nrn1704

Vogt, B. A., & Paxinos, G. (2014). Cytoarchitecture of mouse and rat cingulate cortex with human homologies. *Brain Structure and Function*, *219*(1), 185–192. https://doi.org/10.1007/s00429-012-0493-3

Vogt, B. A., & Peters, A. (1981). Form and distribution of neurons in rat cingulate cortex: Areas 32, 24, and 29. *The Journal of Comparative Neurology*, *195*(4), 603–625. https://doi.org/10.1002/cne.901950406

Wallis, J. D., Anderson, K. C., & Miller, E. K. (2001). Single neurons in prefrontal cortex encode abstract rules. *Nature*, *411*(6840), 953–956. https://doi.org/10.1038/35082081

Walton, M. E., Bannerman, D. M., & Rushworth, M. F. S. (2002). The role of rat medial frontal cortex in effort-based decision making. *The Journal of Neuroscience : The Official Journal of the Society for Neuroscience*, *22*(24), 10996–1003. Retrieved from http://www.ncbi.nlm.nih.gov/pubmed/12486195

Walton, M. E., Croxson, P. L., Behrens, T. E. J., Kennerley, S. W., & Rushworth, M. F. S. (2007). Adaptive decision making and value in the anterior cingulate cortex. *NeuroImage*, *36*, T142–T154. https://doi.org/10.1016/J.NEUROIMAGE.2007.03.029

Walton, M. E., Devlin, J. T., & Rushworth, M. F. (2003). Functional specialization within medial frontal cortex of the anterior cingulate for evaluating effort-related decisions. *Journal of Neuroscience*, *23*, 6475–6479.

Wanat, M., Willuhn, I., Clark, J., & Phillips, P. (2009). Phasic Dopamine Release in Appetitive Behaviors and Drug Addiction. *Current Drug Abuse Reviews*, *2*(2), 195–213. https://doi.org/10.2174/1874473710902020195

Ward, R. D., Winiger, V., Higa, K. K., Kahn, J. B., Kandel, E. R., Balsam, P. D., & Simpson, E. H. (2015). The impact of motivation on cognitive performance in an animal model of the negative and cognitive symptoms of schizophrenia. *Behavioral Neuroscience*, *129*(3), 292–9. https://doi.org/10.1037/bne0000051

Ward, R. D., Winiger, V., Kandel, E. R., Balsam, P. D., & Simpson, E. H. (2015). Orbitofrontal cortex mediates the differential impact of signaled-reward probability on discrimination accuracy. *Frontiers in Neuroscience*, *9*, 230. https://doi.org/10.3389/fnins.2015.00230

Westerink, B. H. C. ., Enrico, P. ., Feimann, J. ., & De Vries, J. B. (1998). The pharmacology of mesocortical dopamine neurons: a dual-probe microdialysis study in the ventral

tegmental area and the prefrontal cortex of the rat brain. *The Journal of Pharmacology and Experimental Therapeutics*, *285*(1), 143–154.

Winton-Brown, T. T., Fusar-Poli, P., Ungless, M. A., & Howes, O. D. (2014). Dopaminergic basis of salience dysregulation in psychosis. *Trends in Neurosciences*, *37*(2), 85–94. https://doi.org/http://dx.doi.org/10.1016/j.tins.2013.11.003

Wise, R. A. (2004). Dopamine, learning and motivation. *Nature Reviews Neuroscience*, *5*(6), 483–494. https://doi.org/10.1038/nrn1406

Wise, R. A. (2008). Dopamine and reward: The anhedonia hypothesis 30 years on. *Neurotoxicity Research*, *14*(2–3), 169–183. https://doi.org/10.1007/BF03033808

Womelsdorf, T., Johnston, K., Vinck, M., & Everling, S. (2010). Theta-activity in anterior cingulate cortex predicts task rules and their adjustments following errors. *Proceedings of the National Academy of Sciences of the United States of America*, *107*(11), 5248–53. https://doi.org/10.1073/pnas.0906194107

Womelsdorf, T., Schoffelen, J., Oostenveld, R., Singer, W., Desimone, R., Engel, A. K., & Fries, P. (2007). Modulation of Neuronal Interactions Through Neuronal Synchronization. *Science*, *316*(5831), 1609–1612.

Wu, J., Gao, M., Shen, J. X., Shi, W. X., Oster, A. M., & Gutkin, B. S. (2013). Cortical control of VTA function and influence on nicotine reward. *Biochem Pharmacol*, *86*(8), 1173–1180. https://doi.org/10.1016/j.bcp.2013.07.013

Yamaguchi, T., Wang, H.-L., Li, X., Ng, T. H., & Morales, M. (2011). Mesocorticolimbic Glutamatergic Pathway. *Journal of Neuroscience*, *31*(23).

Yassa, M. A., & Stark, C. E. L. (2011). Pattern separation in the hippocampus. *Trends in Neurosciences*, *34*(10), 515–525. https://doi.org/10.1016/j.tins.2011.06.006

Yu, A. J., & Dayan, P. (2005). Uncertainty, Neuromodulation, and Attention. *Neuron*, *46*(4), 681–692. https://doi.org/10.1016/j.neuron.2005.04.026

Zar, J. H. (1999). *Biostatistical Analysis* (4th ed.). Upper Saddle River, New Jersey: Prentice Hall.

Zilles, K., & Wree, A. (1995). *Cortex: areal and laminar structure in the rat nervous system*. (G. Paxinos, Ed.). San Diego, CA. https://doi.org/Academic Press

Chapter 7 Appendix: novel methods

7.1 Overview

In addition to the established electrophysiological and behavioural methods of the Bilkey lab, several novel methods were developed for this thesis. The new methods developed for this thesis were a fully automated continuous T-maze and a custom-designed, 3D-printed microdrive. This appendix details the development of each of these novel methods.

7.2 Fully automated continuous T-maze

7.2.1 *The T-maze and the opportunities of automation*

The T-maze is a simple maze used to study animal cognition. Shaped like the letter T (Figure A1a), most T-maze protocols involve placing a subject, often a rat, at the base of the maze and placing a reward at one or both arms of the maze. The T-maze side (goal) arms can contain discriminative stimuli (cues) that the rat must respond to in order to obtain a reward. Because the T-maze provides experimenters with a straight-forward way to assess choice behaviour (e.g. the rat turned left or right), the T-maze is a widely used apparatus in behavioural neuroscience.

There are several drawbacks to using a traditional T-maze. For instance, because most protocols require the rats to be placed at the base of the maze on each trial, the rat is regularly interrupted and physically handled during the experiment. This is particularly problematic in electrophysiology experiments because the rat can become tangled in the cable connecting its brain to the data acquisition computer. One solution to this problem is to use a 'continuous' T-maze (Figure A1b). Shaped like a 'figure of eight' turned on its side, the continuous T-maze paradigm calls for rats to start from the base of the maze midstem, turn left or right, and then re-enter the midstem to initiate a new trial. Thus, the continuous T-maze offers experimenters the benefits of the traditional T-maze while also allowing rats to complete trials in a continuous, uninterrupted manner.

Despite the advantages of the continuous T-maze, its practical operation can be cumbersome for the experimenter. For example, with a continuous T-maze, it is important that the rat completes circuits around the maze in a unidirectional manner. Prior studies from the Bilkey lab using the continuous T-maze (Hillman & Bilkey, 2010, 2012) had prevented rats from reversing course by manually inserting a barrier behind the animal. When one considers that the experimenter must both dispense reward and police the rats' trajectories, it becomes apparent that the continuous T-maze is a labour intensive apparatus.

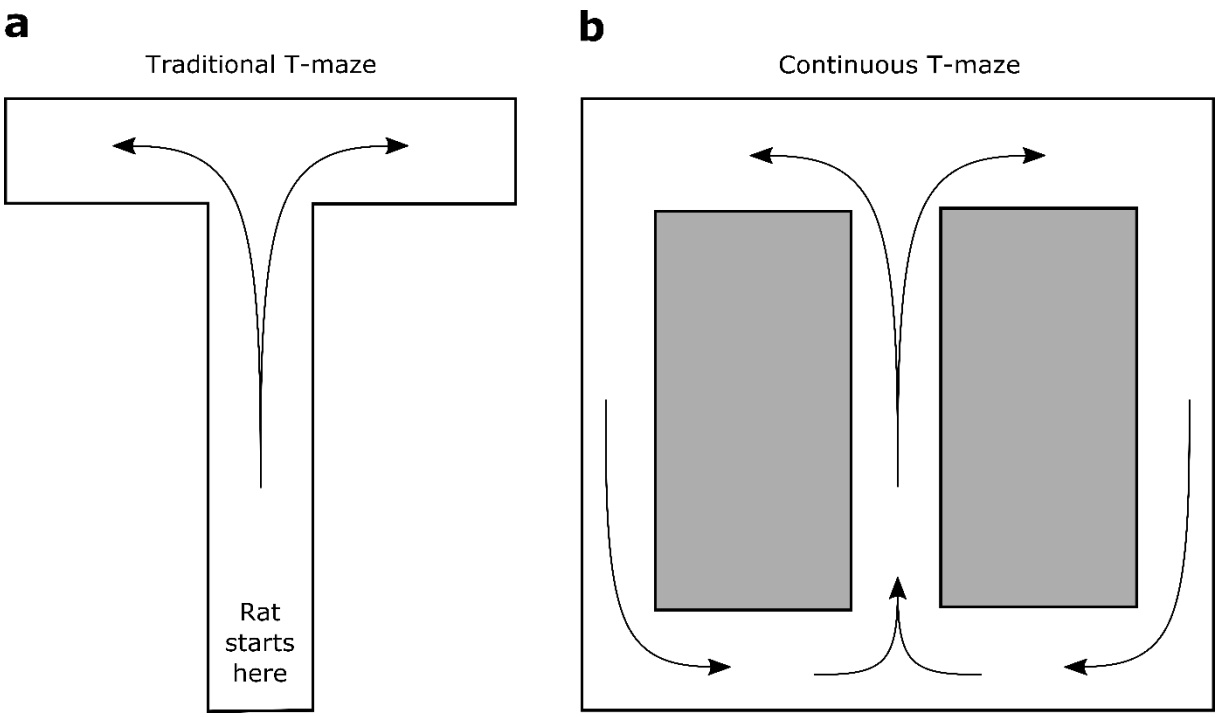

Figure A1. Examples of traditional and continuous T-mazes. **(a)** traditional T-maze; **(b)** continuous T-maze.

This additional labour can increase the rate of human error and distract the animal from the task at hand. For example, the commotion of the experimenter placing/removing the barrier insert can distract the rat, causing the rat to get off-task. Furthermore, such rapid task-switching by the experimenter can lead to reward delivery errors (e.g. giving the rat five cereal pellets when it was meant to receive only two). If trajectory policing and reward delivery could be automated, then fewer mistakes would be made and training the animals would be faster and more consistent. Therefore, I decided to automate every aspect of the continuous T-maze with the use of Arduino microcontrollers and various peripheral sensors and actuators.

7.2.2 *Implementing the automated continuous T-maze*

In total, the newly developed maze contains three touchscreens which allowed rats to initiate trials, seven photobeams which timestamped rats' locations and triggered other maze events, ten pneumatic rams which opened and closed the doors to the maze arms, two servo motors which allowed for climbable barriers to be introduced or removed from a maze arm, two custom-built peristaltic pumps which dispensed a condensed milk reward, and a network of five Arduino microcontrollers (Arduino LLC, Somersville, MA, USA) which controlled the entire apparatus and reported timestamps of key maze events to the main data acquisition computer (Figure A2). Because Arduinos have a limited number of input and output pins, it was important to distribute the computational load across several Arduinos such that computations in one microcontroller could influence computations in another (*vis a vis* a

network). As a result, the key design principle became that each region of the maze ought to sense and respond to activity and report its doings to other maze regions. When implemented, this meant that one Arduino controlled all sensors in the right maze arm whereas another controlled the left maze arm and so on. The most important microcontroller controlled the start box / reward region of the maze because that microcontroller both initiated and concluded trials. I also dedicated one Arduino entirely to controlling the pneumatic rams which opened and closed the maze doors. I used pneumatics to open/close the doors because I was concerned that electric motors would generate noise which would interfere with electrophysiological recordings. To avoid any pneumatics-related injury to the rats, I had the doors move vertically, opening by lowering and closing by raising. I used peristaltic pumps, rather than a linear motor and syringe-pump, to deliver the condensed milk reward because they do not have to be refilled between recording sessions.

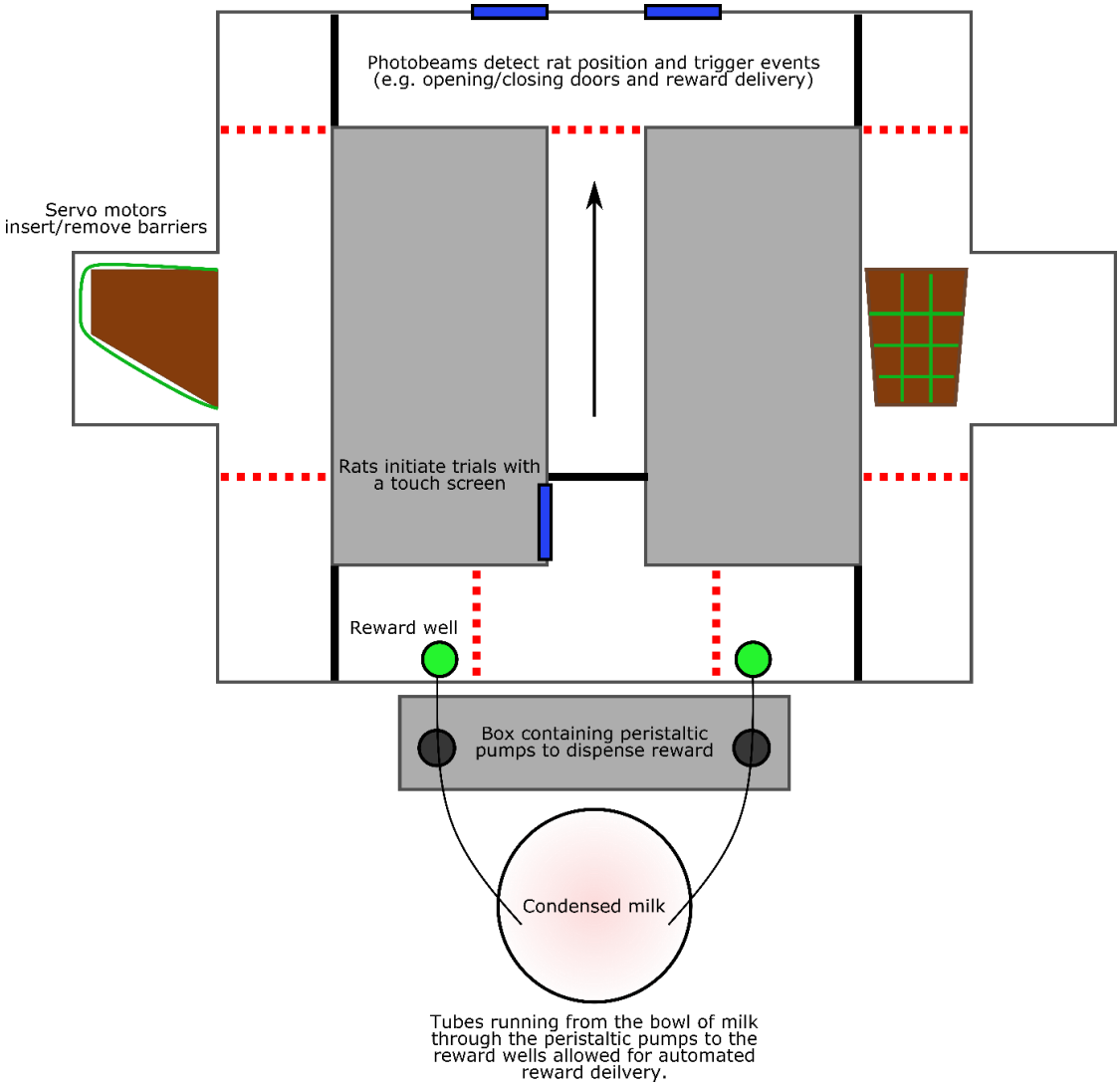

Figure A2. Schematic of the automated continuous T-maze. The blue bars indicate the locations of wall-mounted touchscreens; the dashed red lines indicate the positions of photobeams; the green circles indicate the locations of reward wells; the black circles indicate the positions of peristaltic pumps which delivered the condensed milk.

The parallel and distributed nature of the maze components, the multiple microcontrollers, and the code on each microcontroller can be best described through an example. Take, for instance, a choice-trial during the first maze configuration in Project 2: in these trials, a rat would press the touchscreen located on the wall of the start box which would then cause the start box Arduino to signal to the Arduinos controlling the left and right maze arms as well as the Arduino which controlled the pneumatic rams. The signals to the left/right Arduinos would activate the photobeams and the signal to the motor Arduino initiated the opening of the door to the midstem maze region. Once the rat made a decision, perhaps he turned right (the typical, choice in that portion of the experimental sessions), the rat would trip the photobeam just around the corner. Tripping this photobeam would cause right maze arm Arduino to send signals to the start box and motor Arduinos. The start box-bound signal would cause the startbox Arduino to signal to the Arduino which controlled the peristaltic pumps to dispense a certain amount of condensed milk as well. The startbox Arduino would also signal to the data acquisition computer to timestamp the breaking of the photobeam. The photobeam-triggered signal from the right Arduino to the motor Arduino would cause the upper-right door to close behind the rat, thus preventing the rat from reversing direction, as well as opening the lower-right door, enabling the rat to access the reward zone after climbing over the barrier. Once the rat entered the reward zone, he would trip another photobeam which caused the start box Arduino to signal to the motor Arduino to close the door behind the rat so that only by pressing the touchscreen could the rat exit the start box, thereby initiating a new trial. In this way, each Arduino sensed and responded to maze events in each maze region and regularly updated every other Arduino. See Figures A3-A4 for photos of the maze and the implemented neural network of Arduinos. See the following sections for the code for each Arduino used in project 2.

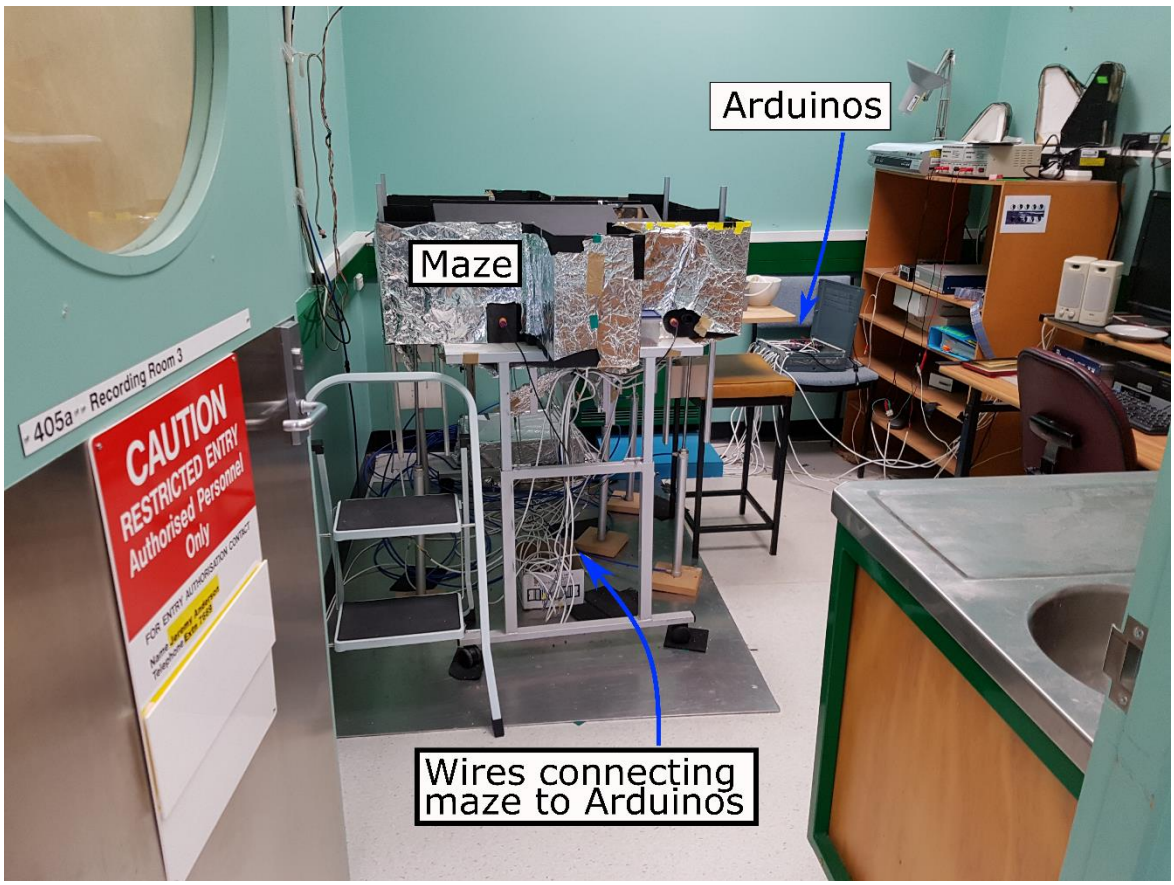

Figure A3. Wide –angle view of the maze and electronics.

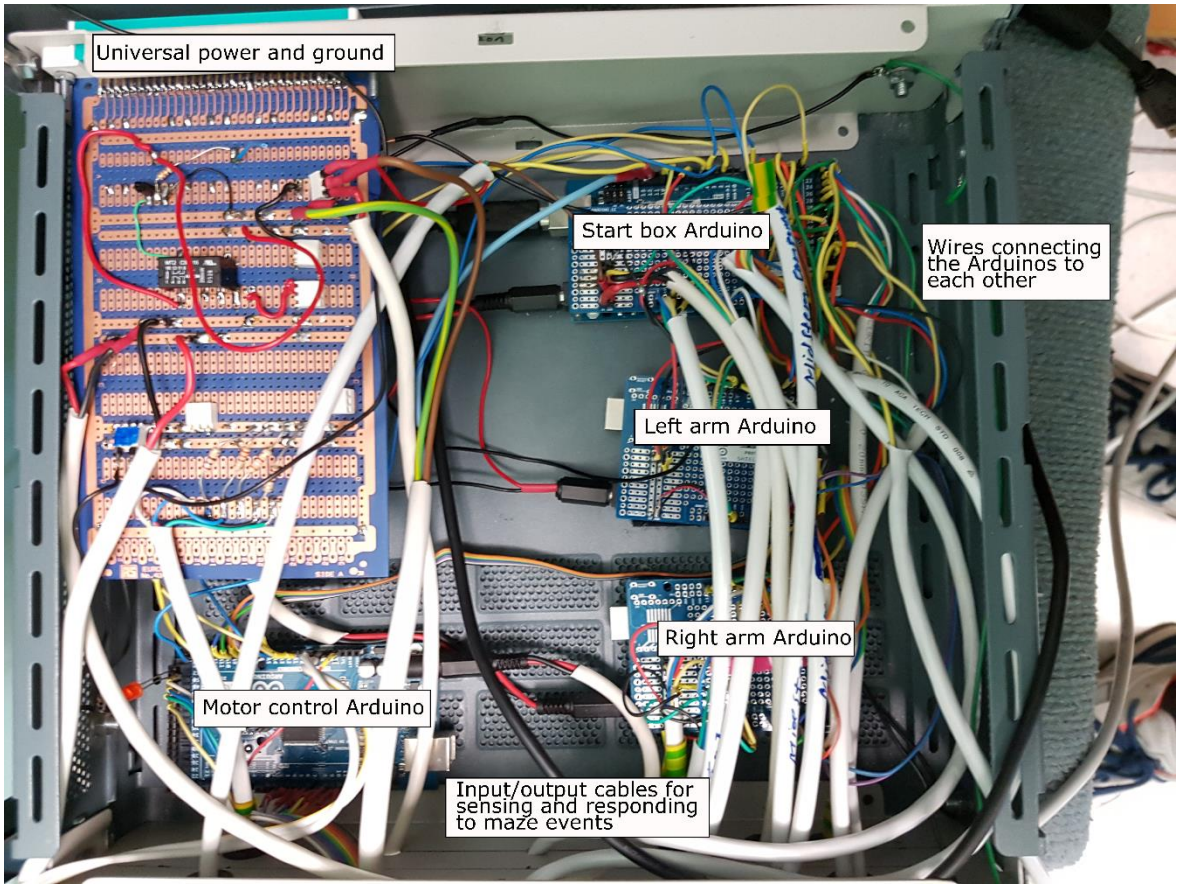

Figure A4. Custom-built network of Arduinos used to control the maze.

7.2.3 *Code to control the maze*

7.2.3.1 Left Arduino

```
// touchscreen-related stuff
#include "SPI.h"
#include "Adafruit_GFX.h"
#include "Adafruit_ILI9341.h"
#define TFT_DC 9
#define TFT_CS 10
// Color definitions
#define BLACK           0x0000
#define BLUE            0x001F
#define RED             0xF800
#define GREEN           0x07E0
#define CYAN            0x07FF
#define MAGENTA         0xF81F
#define YELLOW          0xFFE0
#define WHITE           0xFFFF
Adafruit_ILI9341 tft = Adafruit_ILI9341(TFT_CS, TFT_DC);
// needs to open / close vertex door and detect / report beam breaks
const int infraredSensorPin = 7;
const int tellDacqBeamBreak = 0;
const int openVertexSignalled = 2;
const int openVertexDoor = 5; // A2 at motor ctx
const int closeVertexDoor = A1; // A4 at motor ctx
const int tellStartBoxBeamBreak = 1; // goes to pin 19 at startbox
boolean sensorActive = false;
void openFromMidstem(){
  if(digitalRead(openVertexSignalled)){
    sensorActive = true;
    digitalWrite(openVertexDoor, HIGH);
    delay(10);
    digitalWrite(openVertexDoor, LOW);
  }
}
void reportBeamBreak(){
  if(digitalRead(infraredSensorPin) == LOW && sensorActive == true){
```

```
    sensorActive = false;
    digitalWrite(closeVertexDoor, HIGH);
    digitalWrite(tellDacqBeamBreak, HIGH);
    digitalWrite(tellStartBoxBeamBreak, HIGH);
    delay(10);
    digitalWrite(tellDacqBeamBreak, LOW);
    digitalWrite(closeVertexDoor, LOW);
    digitalWrite(tellStartBoxBeamBreak, LOW); // goes to pin 19 at startbox
    tft.fillScreen(BLACK);
  }
}
void setup(){
  pinMode(infraredSensorPin, INPUT);
  pinMode(tellDacqBeamBreak, OUTPUT);
  pinMode(openVertexSignalled, INPUT);
  pinMode(openVertexDoor, OUTPUT);
  pinMode(closeVertexDoor, OUTPUT);
  pinMode(tellStartBoxBeamBreak, OUTPUT);
  tft.begin();
  tft.fillScreen(BLACK);
}
void loop(){
  openFromMidstem();
  reportBeamBreak();
}
```

7.2.3.2 Right Arduino

```
// touchscreen stuff
#include "SPI.h"
#include "Adafruit_GFX.h"
#include "Adafruit_ILI9341.h"
#define TFT_DC 9
#define TFT_CS 10
// Color definitions
#define BLACK          0x0000
#define BLUE           0x001F
#define RED            0xF800
```

```
#define GREEN          0x07E0
#define CYAN           0x07FF
#define MAGENTA        0xF81F
#define YELLOW         0xFFE0
#define WHITE          0xFFFF
Adafruit_ILI9341 tft = Adafruit_ILI9341(TFT_CS, TFT_DC);
// needs to open / close vertex door and detect / report beam breaks
const int infraredSensorPin = 7;
const int tellDacqBeamBreak = 0;
const int openVertexSignalled = 2;
const int openVertexDoor = 5;
const int closeVertexDoor = A1;
const int tellStartBoxBeamBreak = 1; // goes to pin 17 at startbox
boolean sensorActive = false;

void openFromMidstem(){
  if(digitalRead(openVertexSignalled)){
    sensorActive = true;
    digitalWrite(openVertexDoor, HIGH);
    delay(10);
    digitalWrite(openVertexDoor, LOW);
      // tft.fillScreen(RED);
       // tft.fillRect(20, 175, 200, 50, WHITE);
  }
}
void reportBeamBreak(){
  if(digitalRead(infraredSensorPin) == LOW && sensorActive == true){
    sensorActive = false;
    digitalWrite(closeVertexDoor, HIGH);
    digitalWrite(tellDacqBeamBreak, HIGH);
    digitalWrite(tellStartBoxBeamBreak, HIGH);
    delay(50);
    digitalWrite(tellDacqBeamBreak, LOW);
    digitalWrite(closeVertexDoor, LOW);
    digitalWrite(tellStartBoxBeamBreak, LOW); // goes to pin 17 at startbox
    tft.fillScreen(BLACK);
```

```
  }
}
void setup(){
  pinMode(infraredSensorPin, INPUT);
  pinMode(tellDacqBeamBreak, OUTPUT);
  pinMode(openVertexSignalled, INPUT);
  pinMode(openVertexDoor, OUTPUT);
  pinMode(closeVertexDoor, OUTPUT);
  pinMode(tellStartBoxBeamBreak, OUTPUT);
  tft.begin();
  tft.fillScreen(BLACK);
}
void loop(){
  openFromMidstem();
  reportBeamBreak();
}
```

7.2.3.3 Motor control Arduino

```
int delayTime = 50;
// INPUTS
const int closeMidstemSignal = A0;
const int openMidstemSignal = A1;
const int openLeftVertexSignal = A2;
const int openRightVertexSignal = A6;
const int closeAllDoorsSignal = A11;
const int closeLeftVertexAndLowerLeftBarrierSignal = A3; //*****
const int closeLeftVertexSignal = A4; // *****
const int lowerLowerLeftDoorSignal = A5;
const int closeRightDoor = A7;
const int closeRightVertexSignal = A8;
const int openLowerLeftButtonSignal = 52;
const int closeLowerLeftButtonSignal = 50;
const int openLowerRightButtonSignal = 48;
const int closeLowerRightButtonSignal = 46;
const int LEDpin = 53;
// OUTPUTS
```

```
const int closeMidstem = 4;
const int openMidstem = 11;
const int openLeftVertex = 3;
const int closeLeftVertex = 12;
const int openRightVertex = 9;
const int closeRightVertex = 10;
const int raiseLowerRightBarrier = 6;
const int lowerLowerRightBarrier = 8;
const int raiseLowerLeftBarrier = 7;
const int lowerLowerLeftBarrier = 5;
// open midstem and vertex
void openMidstemAndVertex(){
  if(digitalRead(openMidstemSignal)){
    delay(delayTime);
    for(int z = 0; z <20; z++){
      digitalWrite(openRightVertex, HIGH);
       digitalWrite(openLeftVertex, HIGH);
      digitalWrite(openMidstem, HIGH);
      delay(20);
      digitalWrite(openRightVertex, LOW);
      digitalWrite(openLeftVertex, LOW);
      digitalWrite(openMidstem, LOW);
      delay(20);
    }
  }
}
void openRightVertexDoor(){
  if(digitalRead(openRightVertexSignal)){
    delay(delayTime);
    for(int z = 0; z <20; z++){
      digitalWrite(openRightVertex, HIGH);
      digitalWrite(openMidstem, HIGH);
      delay(20);
      digitalWrite(openRightVertex, LOW);
      digitalWrite(openMidstem, LOW);
      delay(20);
```

```
    }
  }
}
// right vertex closes and lower right barrier lowers
// AND MIDSTEM CLOSES
void closeRightVertexDoor(){
  if(digitalRead(closeRightVertexSignal)){
    for(int f = 0; f < 35; f++){
      digitalWrite(closeRightVertex, HIGH);
      digitalWrite(closeLeftVertex, HIGH);
      digitalWrite(raiseLowerRightBarrier, HIGH);
      digitalWrite(closeMidstem, HIGH);
      delay(20);
      digitalWrite(closeRightVertex, LOW);
      digitalWrite(closeLeftVertex, LOW);
      digitalWrite(raiseLowerRightBarrier, LOW);
      digitalWrite(closeMidstem, LOW);
      delay(20);
    }
  }
}
void openLeftVertexDoor(){
  if(digitalRead(openLeftVertexSignal)){
    delay(delayTime);
    for(int z = 0; z <20; z++){
      digitalWrite(openLeftVertex, HIGH);
      digitalWrite(openMidstem, HIGH);
      delay(20);
      digitalWrite(openLeftVertex, LOW);
      digitalWrite(openMidstem, LOW);
      delay(20);
    }
  }
}
void closeLeftVertexDoor(){
  if(digitalRead(closeLeftVertexSignal)){
```

```
    for(int f = 0; f < 35; f++){
      digitalWrite(closeLeftVertex, HIGH);
      digitalWrite(closeRightVertex, HIGH);
      digitalWrite(lowerLowerLeftBarrier, HIGH);
      digitalWrite(closeMidstem, HIGH);
      delay(20);
      digitalWrite(closeLeftVertex, LOW);
      digitalWrite(closeRightVertex, LOW);
      digitalWrite(lowerLowerLeftBarrier, LOW);
      digitalWrite(closeMidstem, LOW);
      delay(20);
    }
  }
}
// Button signals
// open lower left door (drop barrier) with button press
void dropLeftBarrierButton(){
  if(digitalRead(openLowerLeftButtonSignal)){
    for(int p = 0; p < 25; p++){
      digitalWrite(lowerLowerLeftBarrier, HIGH);
      delay(20);
      digitalWrite(lowerLowerLeftBarrier, LOW);
      delay(20);
    }
  }
}
// close lower left door (raise barrier) with button press
void raiseLeftBarrierButton(){
  if(digitalRead(closeLowerLeftButtonSignal)){
    for(int k = 0; k < 25; k++){
      digitalWrite(raiseLowerLeftBarrier, HIGH);
      delay(20);
      digitalWrite(raiseLowerLeftBarrier, LOW);
      delay(20);
    }
  }
```

```
}
// open lower right door (drop barrier) with button press
void dropRightBarrierButton(){
  if(digitalRead(openLowerRightButtonSignal)){
    for(int e = 0; e < 25; e++){
      digitalWrite(lowerLowerRightBarrier, HIGH);
      delay(20);
      digitalWrite(lowerLowerRightBarrier, LOW);
      delay(20);
    }
  }
}
// closer lower right door (raise barrier) with button press
void raiseRightBarrierButton(){
  if(digitalRead(closeLowerRightButtonSignal)){
    for(int g = 0; g < 25; g++){
      digitalWrite(raiseLowerRightBarrier, HIGH);
      delay(20);
      digitalWrite(raiseLowerRightBarrier, LOW);
      delay(20);
    }
  }
}
// close all doors for 10 seconds, then open them
// this is for the surprise trials in the model-updating experimetn
void surpriseCloseDoors(){
  if(digitalRead(closeAllDoorsSignal)){
        for(int f = 0; f < 35; f++){
      digitalWrite(closeLeftVertex, HIGH);
      digitalWrite(closeRightVertex, HIGH);
      digitalWrite(lowerLowerLeftBarrier, HIGH);
      digitalWrite(closeMidstem, HIGH);
      delay(20);
      digitalWrite(closeLeftVertex, LOW);
      digitalWrite(closeRightVertex, LOW);
      digitalWrite(lowerLowerLeftBarrier, LOW);
```

```
      digitalWrite(closeMidstem, LOW);
      delay(20);
    }
    delay(10000); // delay 10 seconds
     for(int z = 0; z <20; z++){
      digitalWrite(openRightVertex, HIGH);
       digitalWrite(openLeftVertex, HIGH);
      digitalWrite(openMidstem, HIGH);
      delay(20);
      digitalWrite(openRightVertex, LOW);
      digitalWrite(openLeftVertex, LOW);
      digitalWrite(openMidstem, LOW);
      delay(20);
    }
  }
} // end of surprise close and then open doors
void closeTheMidstem(){
  if(digitalRead(closeMidstemSignal)){
    for(int b = 0; b < 30; b++){
      digitalWrite(raiseLowerLeftBarrier, HIGH);
      digitalWrite(lowerLowerRightBarrier, HIGH);
      digitalWrite(closeMidstem, HIGH);
      delay(20);
      digitalWrite(lowerLowerRightBarrier, LOW);
      digitalWrite(raiseLowerLeftBarrier, LOW);
      digitalWrite(closeMidstem, LOW);
      delay(5);
    }
  }
}
void setup(){
 pinMode(closeMidstemSignal,INPUT);
 pinMode(openMidstemSignal,INPUT);
 pinMode(openLeftVertexSignal,INPUT);
 pinMode(closeLeftVertexAndLowerLeftBarrierSignal,INPUT);
 pinMode(lowerLowerLeftDoorSignal,INPUT);
```

```
 pinMode(openRightVertexSignal,INPUT);
 pinMode(closeRightDoor,INPUT);
 pinMode(closeRightVertexSignal,INPUT);
 pinMode(openLowerLeftButtonSignal,INPUT);
 pinMode(closeLowerLeftButtonSignal,INPUT);
 pinMode(openLowerRightButtonSignal,INPUT);
 pinMode(closeLowerRightButtonSignal,INPUT);
 pinMode(closeLeftVertexSignal, INPUT);
 pinMode(closeAllDoorsSignal,INPUT);
 pinMode(closeMidstem, OUTPUT);
 pinMode(openMidstem, OUTPUT);
 pinMode(openLeftVertex, OUTPUT);
 pinMode(closeLeftVertex, OUTPUT);
 pinMode(openRightVertex, OUTPUT);
 pinMode(closeRightVertex, OUTPUT);
 pinMode(raiseLowerRightBarrier, OUTPUT);
 pinMode(lowerLowerRightBarrier, OUTPUT);
 pinMode(raiseLowerLeftBarrier, OUTPUT);
 pinMode(lowerLowerLeftBarrier, OUTPUT);
 pinMode(LEDpin, OUTPUT);
}

void loop() {
  surpriseCloseDoors();
  openMidstemAndVertex();
  openRightVertexDoor();
  openLeftVertexDoor();
 closeRightVertexDoor();
 closeLeftVertexDoor();
 closeTheMidstem();
 dropLeftBarrierButton();
 raiseLeftBarrierButton();
 dropRightBarrierButton();
 raiseRightBarrierButton();
}
```

7.2.3.4 Reward delivery Arduino

```
// motor A
const int enMotorA = 13;
const int motorAForward = 12;
const int motorABackward = 11;
// motor B
const int enMotorB = 8;
const int motorBForward = 9;
const int motorBBackward = 10;
const int rightLarge = A1; // motorB dispenses large reward, pin 48 from startbox
const int leftLarge = A5;  // motorA dispenses large reward, pin 39 from SB
const int rightMed = A0;   // motorB dispenses medium reward, pin 49 from SB
const int leftMed = A3;    // motorA dispenses medium reward, pin 46 from SB
const int rotorGatePin= A4; // rotor gate which delivers varying voltages to the arduino
const int largeReward = 1000;
const int medReward = 250;

const int motorSpeed=200;
// values which will change
int rotorGateState = 0; // current state of rotor gate
int lastrotorGateState = 0; // previous state of rotor gate
int upperBound = 0;
int lowerBound = 0;
int counter= 0;
boolean newState = false;
//////////////////////////////////////////
// code for manual reward delivery
//////////////////////////////////////////
void checkRotorGate(){
  rotorGateState = analogRead(rotorGatePin);
  // compare the rotorGateState to its previous state
  if (rotorGateState != lastrotorGateState) {
  delay(100);
   rotorGateState = analogRead(rotorGatePin);
    // check if the state is within a range of the last state
    if (rotorGateState >= lowerBound && rotorGateState <= upperBound){
      newState = false;
```

```
   }else{
     newState = true;
   }
   if(newState == true){
   digitalWrite(motorAForward, HIGH); // the direction of the motor is determined by which one is high or low
     digitalWrite(motorBForward, HIGH);
     digitalWrite(motorABackward, LOW);
     digitalWrite(motorBBackward, LOW);
     analogWrite(enMotorA, motorSpeed);
     analogWrite(enMotorB, motorSpeed);
     Serial.println(rotorGateState);
      delay(rotorGateState);
     digitalWrite(motorAForward, LOW); // the direction of the motor is determined by which one is high or low
     digitalWrite(motorBForward, LOW);
     analogWrite(enMotorA, 0);
     analogWrite(enMotorB, 0);
      lastrotorGateState = rotorGateState;
         lowerBound = lastrotorGateState-100;
         upperBound = lastrotorGateState+100;
         Serial.println(lowerBound);
         Serial.println(upperBound);
      delay(50);
  }
}
}
////////////////////////////////////
void largeLeftReward(){
  if(digitalRead(leftLarge)){
   digitalWrite(motorBForward, HIGH); // the direction of the motor is determined by which one is high or low
     digitalWrite(motorBBackward, LOW);
     analogWrite(enMotorB, motorSpeed);
      delay(largeReward);
     digitalWrite(motorBForward, LOW); // the direction of the motor is determined by which one is high or low
     analogWrite(enMotorB, 0);
```

```
  }
}
void mediumLeftReward(){
  if(digitalRead(leftMed)){
    digitalWrite(motorBForward, HIGH); // the direction of the motor is determined by which one is high or low
      digitalWrite(motorBBackward, LOW);
      analogWrite(enMotorB, motorSpeed);
        delay(medReward);
      digitalWrite(motorBForward, LOW); // the direction of the motor is determined by which one is high or low
      analogWrite(enMotorB, 0);
  }
}
void largeRightReward(){
  if(digitalRead(rightLarge)){
    digitalWrite(motorAForward, HIGH); // the direction of the motor is determined by which one is high or low
      digitalWrite(motorABackward, LOW);
      analogWrite(enMotorA, motorSpeed);
        delay(largeReward);
      digitalWrite(motorBForward, LOW); // the direction of the motor is determined by which one is high or low
      analogWrite(enMotorA, 0);
  }
}
void mediumRightReward(){
  if(digitalRead(rightMed)){
    digitalWrite(motorAForward, HIGH); // the direction of the motor is determined by which one is high or low
      digitalWrite(motorABackward, LOW);
      analogWrite(enMotorA, motorSpeed);
        delay(medReward);
      digitalWrite(motorAForward, LOW); // the direction of the motor is determined by which one is high or low
      analogWrite(enMotorA, 0);
  }
}
```

```
void setup() {
pinMode(enMotorA, OUTPUT);
pinMode(enMotorB, OUTPUT);
pinMode(motorAForward, OUTPUT);
pinMode(motorABackward, OUTPUT);
pinMode(motorBForward, OUTPUT);
pinMode(motorBBackward, OUTPUT);
pinMode(rotorGatePin, INPUT);
pinMode(rightLarge, INPUT);
pinMode(leftLarge, INPUT);
pinMode(rightMed, INPUT);
pinMode(leftMed, INPUT);
    digitalWrite(motorAForward, LOW);
    digitalWrite(motorABackward, LOW);
    digitalWrite(motorBForward, LOW);
    digitalWrite(motorBBackward, LOW);
    digitalWrite(enMotorA, LOW);
    digitalWrite(enMotorB, LOW);
    delay(1000);
    rotorGateState = analogRead(rotorGatePin);
      lastrotorGateState = rotorGateState;
        lowerBound = lastrotorGateState-100;
        upperBound = lastrotorGateState+100;
          digitalWrite(motorAForward, HIGH); // the direction of the motor is determined by
which //one is high or low
    digitalWrite(motorBForward, HIGH);
    digitalWrite(motorABackward, LOW);
    digitalWrite(motorBBackward, LOW);
    analogWrite(enMotorA, motorSpeed);
    analogWrite(enMotorB, motorSpeed);
    Serial.println(rotorGateState);
     delay(3000);
    digitalWrite(motorAForward, LOW); // the direction of the motor is determined by which
one is high or low
    digitalWrite(motorBForward, LOW);
    analogWrite(enMotorA, 0);
    analogWrite(enMotorB, 0);
```

```
}
void loop() {
//checkRotorGate();
 largeLeftReward(); //debugged and works
 largeRightReward(); // debugged and works
 mediumLeftReward(); // debugged and works
 mediumRightReward(); // debugged and works
}
```

7.2.3.5 Start box Arduino

```
boolean leftSensorActive = true;
boolean rightSensorActive = true;
boolean sensorTripped = false;
boolean screenActive=false;
boolean speakerOn = true;
boolean vertexActive = false;
boolean afterBarrierActive = false;
boolean rightBarrierTrial_indicator = false;
boolean leftBarrierTrial_indicator = false;
int textSize =8;
int cursorX = 50;
int cursorY = 100;
int signalChoice;
int signalForced;


// ---------------------> TRIAL TYPES <-----------------------
int FR = 1; // forced choice to right
int FL = 2; // forced choice to left
int C  = 3; // free choice
int endOfTrials = -70;
// -----------------> ARRAY CONTAINING TRIALS <-----------------
// make array of 64 trials - I used 70 just to make sure there is room
int trialType[70] = { 0,
// config 1
C,C,C,FR,
C,FL,C,C,
C,C,C,FR,
```

```
FL,C,C,C,
C,C,C,FR,
C,C,FL,C,
C,FR,C,C,
C,C,C,FL,

// config 2
C,C,FR,C,
FL,C,C,C,
C,FR,C,C,
C,C,FL,C,
FR,C,C,C,
C,C,C,FL,
FR,C,C,C,
FL,C,C,C,
endOfTrials,
};

int trialNumber;
int trialNumber1;
int trialCounter;
int rightCounter;
float percentRight;
int trialNumber2=0;
int trialCounter2=0;
int rightCounter2=0;
float percentRight2 = 0;
// TFT-related stuff
#include "SPI.h"
#include "Adafruit_GFX.h"
#include "Adafruit_ILI9341.h"
// servo stuff
#include <Servo.h>
Servo right_barrier; // big barrier
const int right_barrierOut = 128;
const int right_barrierIn = 28;
```

```
Servo left_barrier; // little barrier
// this is a continuos servo, so you send it running in a certain direction
// for a certain time; it will not work sending it to a certain position
// 0 = very fast counterclockwise
// 90 = dead stopped
// 180 = very fast clockwise
const int left_barrierOut = 95;
const int left_barrierIn = 90;


#define TFT_DC 9
#define TFT_CS 10
// Color definitions
#define BLACK           0x0000
#define BLUE            0x001F
#define RED             0xF800
#define GREEN           0x07E0
#define CYAN            0x07FF
#define MAGENTA         0xF81F
#define YELLOW          0xFFE0
#define WHITE           0xFFFF
Adafruit_ILI9341 tft = Adafruit_ILI9341(TFT_CS, TFT_DC);
// pin declarations
int LEDpin = 13;
const int closeMidstem = 2;
const int screenPress = 4;
const int screenPower = 7; // power pin for capacitive sensor
const int vertexSensor = 40;
const int rightSensor = 41;
const int leftSensor = 38;
const int lowPower = 0;
const int highPower = 255;
const int callOpenVertexToRight = 16; // pin 2 on others
const int callOpenVertexToLeft = 15; // pin 2 on others
const int callOneLaptoRight = 34; // pin 6 on others
const int callOneLaptoLeft = 36; // pin 6 on others
```

```
const int openMidstemAndVertices = 14; // goes to A1 at motor cortex
const int actLeftScreen = 15; // <---------- might not need this
const int actRightScreen=16; // <------------might not need this
const int openLeftVertexDoor = 19;
const int speaker = 21;
const int OneLapSignalled = 22;
const int rightRewardSensor = 24;
const int leftRewardSensor = 26;
const int closeMidstemButtonPressed = 28;
const int activateMidstem = 30;
const int RIGHTactivateBeamSensor = 17;
const int LEFTactivateBeamSensor = 19;
const int deactivateLeftScreen = 36;
const int tellDacqFreeConfig1Trial = 45;
const int tellDacqFreeConfig2Trial = 44;
const int tellDacqForcedConfig2Trial = A15;
const int tellDacqForcedConfig1Trial = A13;
const int tellDacqReward = A12;
const int tellDacqVertex = 23;
const int tellDacqAfterBarrier = 25;
// REWARD DISPENSING
const int dispenseRightMediumReward = 48;
const int dispenseLeftMediumReward = 49;
const int dispenseLeftLargeReward = 46;
const int dispenseRightLargeReward = 37;
boolean config1 = false;
boolean config2 = false;
boolean configNowSwitched = false;
boolean config1Set = false;
boolean rightBarrierPresent = false;
boolean leftBarrierPresent = false;
// reward variables which change based on configurations
int rightRewardSize;
int leftRewardSize;
// stuff for the melody at the end of the session
#include "pitches.h"
```

```
// notes in the melody:
int melody[] = {
  NOTE_C4, NOTE_G3, NOTE_G3, NOTE_A3, NOTE_G3, 0, NOTE_B3, NOTE_C4
};
// note durations: 4 = quarter note, 8 = eighth note, etc.:
int noteDurations[] = {
  4, 8, 8, 4, 4, 4, 4, 4
};
//////////////////////////////////////////////////
int configSwitch =32;
//////////////////////////////////////////////////
//////// CONFIG DETAILS FOR TODAY
//////////////////////////////////////////////////
//////////////////
//// PHASE 1
//////////////////
int rightRewardSize1 = dispenseRightLargeReward;
//int rightRewardSize1 = dispenseRightMediumReward;
int leftRewardSize1  = dispenseLeftMediumReward;
//int leftRewardSize1  = dispenseLeftLargeReward;
boolean rightBarrier1 = true;
boolean leftBarrier1 = false;
//////////////////////
// PHASE 2 DETAILS
//////////////////////
int rightRewardSize2 = dispenseRightMediumReward;
//int rightRewardSize2 = dispenseRightLargeReward;
int leftRewardSize2  = dispenseLeftLargeReward;
//int leftRewardSize2  = dispenseLeftMediumReward;
boolean rightBarrier2 = false;
boolean leftBarrier2 = true;
//////////////////////////////////////////////////
//////////////////////////////////////////////////
void setConfig1(){
  if(config1Set == false){
    config1Set = true;
```

```
config1=true;
config2=false;
// set the reward sizes
rightRewardSize = rightRewardSize1;
leftRewardSize  = leftRewardSize1;
signalChoice = tellDacqFreeConfig1Trial;
signalForced = tellDacqForcedConfig1Trial;
// set the barriers
if(rightBarrier1 == true){
  right_barrier.attach(12);
  right_barrier.write(right_barrierIn);
  delay(200);
  right_barrier.detach();
  rightBarrierPresent = true;
}
if(leftBarrier1 == true){
  left_barrier.attach(13);
  left_barrier.write(left_barrierIn);
  delay(50);
  left_barrier.detach();
  leftBarrierPresent = true;
}
if(rightBarrier1 == false){
  right_barrier.attach(12);
  right_barrier.write(right_barrierOut);
  delay(200);
  right_barrier.detach();
  rightBarrierPresent = true;
}
if(leftBarrier1 == false){
  left_barrier.attach(13);
  left_barrier.write(left_barrierOut);
  delay(750);
  left_barrier.detach();
  leftBarrierPresent = true;
}
```

```
  }
} // end of setConfig1
void changeConfig(){
  if(trialNumber > configSwitch){ // once we've had 32 trials of a given configuration, change the maze to a new config.
    if(configNowSwitched == false){
      configNowSwitched = true;
    config1 = false;
    config2 = true;
      tft.fillScreen(RED);
    tft.fillRect(30, 10, 40, 300, WHITE);
    tft.fillRect(100, 10, 40, 300, WHITE);
    tft.fillRect(170, 10, 40, 300, WHITE);
      tft.fillScreen(BLACK);
      tft.setTextColor(YELLOW);
      tft.setTextSize(textSize);
      tft.setCursor(cursorX, cursorY);
      tft.println(trialNumber);
// set the reward sizes
    rightRewardSize = rightRewardSize2;
    leftRewardSize  = leftRewardSize2;
        signalChoice = tellDacqFreeConfig2Trial;
        signalForced = tellDacqForcedConfig2Trial;
    // check out the barriers
     // set the barriers
    if(rightBarrier2 == true){
      right_barrier.attach(12);
      right_barrier.write(right_barrierIn);
      delay(200);
      right_barrier.detach();
      rightBarrierPresent = true;
    }
    if(leftBarrier2 == true){
      left_barrier.attach(13);
      left_barrier.write(left_barrierIn);
      delay(50);
      left_barrier.detach();
```

```
      leftBarrierPresent = true;
    }
    if(rightBarrier2 == false){
      right_barrier.attach(12);
      right_barrier.write(right_barrierOut);
      delay(200);
      right_barrier.detach();
      rightBarrierPresent = true;
    }
    if(leftBarrier2 == false){
      left_barrier.attach(13);
      left_barrier.write(left_barrierOut);
      delay(750);
      left_barrier.detach();
      leftBarrierPresent = true;
    }
}
  }
  } // end of changeConfig
void reportVertex(){
if(digitalRead(vertexSensor) == LOW && vertexActive == true){
  vertexActive = false;
  digitalWrite(tellDacqVertex,HIGH);
  delay(50);
  digitalWrite(tellDacqVertex,LOW);
    tft.fillScreen(GREEN);
}
}
void reportAfterBarrier(){
if(digitalRead(rightSensor) == LOW && afterBarrierActive == true){
  afterBarrierActive = false;
  digitalWrite(tellDacqAfterBarrier,HIGH);
  delay(50);
  digitalWrite(tellDacqAfterBarrier,LOW);
    tft.fillScreen(RED);
}
```

```
if(digitalRead(leftSensor) == LOW && afterBarrierActive == true){
  afterBarrierActive = false;
  digitalWrite(tellDacqAfterBarrier,HIGH);
  delay(50);
  digitalWrite(tellDacqAfterBarrier,LOW);
    tft.fillScreen(RED);
}
}
void endTrials(){
  if(trialNumber > 64){
    if(speakerOn == true){
      for(int songLoop = 0; songLoop < 2; songLoop++){
        for (int thisNote = 0; thisNote < 8; thisNote++) {
    // to calculate the note duration, take one second
    // divided by the note type.
    //e.g. quarter note = 1000 / 4, eighth note = 1000/8, etc.
    int noteDuration = 1000 / noteDurations[thisNote];
    tone(speaker, melody[thisNote], noteDuration);
    // to distinguish the notes, set a minimum time between them.
    // the note's duration + 30% seems to work well:
    int pauseBetweenNotes = noteDuration * 1.30;
    delay(pauseBetweenNotes);
    // stop the tone playing:
    noTone(speaker);
  }
    } speakerOn =false;
    }
  }
}
// choice trial set by array index
void choice_trialInitiated(){
   if(digitalRead(screenPress) && trialType[trialNumber] == C){
     if(screenActive == true){
       analogWrite(screenPower, lowPower);
       vertexActive = true;
       screenActive = false;
```

```
      tft.fillScreen(RED);
      tft.setTextColor(WHITE);
      tft.setTextSize(textSize);
      tft.setCursor(cursorX, cursorY);
      tft.println(trialNumber);
      delay(10);
          if(config1==true){
    trialNumber1++;
    }
    if(config2 ==true){
      trialNumber2++;
    }
       digitalWrite(signalChoice, HIGH); // signals the start of a trial of config1
       digitalWrite(openMidstemAndVertices,HIGH); // opens vertices
       digitalWrite(callOpenVertexToRight, HIGH); // activates the infrared sensor
       digitalWrite(callOpenVertexToLeft, HIGH);
       delay(50);
       digitalWrite(openMidstemAndVertices,LOW);
       digitalWrite(callOpenVertexToRight, LOW);
       digitalWrite(callOpenVertexToLeft, LOW);
       digitalWrite(signalChoice, LOW);
       trialCounter++;
       delay(100);
       leftBarrierTrial_indicator=false;
       rightBarrierTrial_indicator=false;
     }
   }
}
// forced choice set by trial index
void forcedRight_trialInitiated(){
   if(digitalRead(screenPress) && trialType[trialNumber] == FR){
     if(screenActive == true){
       analogWrite(screenPower, lowPower);
       vertexActive = true;
       screenActive = false;
      tft.fillScreen(RED);
```

```
      tft.setTextColor(WHITE);
      tft.setTextSize(textSize);
      tft.setCursor(cursorX, cursorY);
      tft.println(trialNumber);
      delay(10);
          if(config1==true){
    trialNumber1++;
    }
    if(config2 ==true){
      trialNumber2++;
    }
       digitalWrite(signalForced, HIGH); // tells dacqusb that a forced choice has started
       digitalWrite(callOpenVertexToRight, HIGH); // activates the infrared sensor
       delay(50);
       digitalWrite(callOpenVertexToRight, LOW);
       digitalWrite(signalForced, LOW);
       trialCounter++;
     }
   }
}
// forced left choice set by trial index
void forcedLeft_trialInitiated(){
   if(digitalRead(screenPress) && trialType[trialNumber] == FL){
     if(screenActive == true){
       analogWrite(screenPower, lowPower);
             vertexActive = true;
       screenActive = false;
      tft.fillScreen(RED);
      tft.setTextColor(WHITE);
      tft.setTextSize(textSize);
      tft.setCursor(cursorX, cursorY);
      tft.println(trialNumber);
          digitalWrite(signalForced, HIGH); // tells dacqusb that a forced choice has started
      delay(10);
          if(config1==true){
    trialNumber1++;
```

```
    }
    if(config2 ==true){
      trialNumber2++;
    }
       digitalWrite(callOpenVertexToLeft, HIGH); // activates the infrared sensor
       delay(50);
       digitalWrite(callOpenVertexToLeft, LOW);
 digitalWrite(signalForced,LOW);
       trialCounter++;
           if(config1==true){
    rightCounter++;
    }
    if(config2 ==true){
      rightCounter2++;
    }
       delay(100);
       leftBarrierTrial_indicator=false;
       rightBarrierTrial_indicator=false;
     }
   }
}
void activateMidstemSensor_right(){
  if(digitalRead(RIGHTactivateBeamSensor)){
    leftSensorActive = true;
    rightSensorActive = false;
        afterBarrierActive= true;
    digitalWrite(rightRewardSize,HIGH);
    delay(50);
    digitalWrite(rightRewardSize,LOW);
    if(config1==true){
    rightCounter++;
    }
    if(config2 ==true){
      rightCounter2++;
    }
    tft.fillScreen(BLACK);
```

```
      tft.setTextColor(YELLOW);
      tft.setTextSize(textSize);
      tft.setCursor(cursorX, cursorY);
      tft.println(trialNumber);
  }
}
void activateMidstemSensor_left(){
  if(digitalRead(LEFTactivateBeamSensor)){
    leftSensorActive = false;
    rightSensorActive = true;
        afterBarrierActive= true;
    digitalWrite(leftRewardSize,HIGH);
    delay(50);
    digitalWrite(leftRewardSize,LOW);
    tft.fillScreen(BLACK);
      tft.setTextColor(YELLOW);
      tft.setTextSize(textSize);
      tft.setCursor(cursorX, cursorY);
      tft.println(trialNumber);
  }
}
void closeMidstemWithSensor(){
  if(digitalRead(leftRewardSensor) == LOW && leftSensorActive == true){
    leftSensorActive = false;
    rightSensorActive = false;
    sensorTripped = true;
     }
     if (digitalRead(rightRewardSensor) == LOW && rightSensorActive == true){
    rightSensorActive = false;
    leftSensorActive = false;
    sensorTripped = true;
     }
     if(sensorTripped ==true){
      sensorTripped = false;
    digitalWrite(tellDacqReward, HIGH);
      delay(50);
```

```
    digitalWrite(tellDacqReward, LOW);
    delay(200);
    digitalWrite(closeMidstem, HIGH);
    delay(50);
    digitalWrite(closeMidstem, LOW);
    screenActive = true;
    analogWrite(screenPower, highPower);
    analogWrite(screenPower, highPower);
          tft.fillScreen(BLACK);
         tft.setTextSize(textSize);
      tft.setCursor(cursorX, cursorY);
      tft.setTextColor(BLUE);
      percentRight = 100*((float)rightCounter/(float)trialNumber1);
      tft.println(percentRight,0);
           tft.setTextSize(textSize);
      tft.setCursor(cursorX, cursorY+100);
      tft.setTextColor(RED);
      percentRight2 = 100*((float)rightCounter2/(float)trialNumber2);
      tft.println(percentRight2,0);
      trialNumber++;
    }
   }
 void setup(){
   pinMode(closeMidstem, OUTPUT);
   pinMode(screenPress, INPUT);
   pinMode(openMidstemAndVertices, OUTPUT);
   pinMode(actLeftScreen, OUTPUT);
   pinMode(actRightScreen, OUTPUT);
   pinMode(openLeftVertexDoor, OUTPUT);
   pinMode(speaker, OUTPUT);
   pinMode(OneLapSignalled, INPUT);
   pinMode(rightRewardSensor, INPUT);
   pinMode(leftRewardSensor, INPUT);
   pinMode(closeMidstemButtonPressed, INPUT);
   pinMode(activateMidstem, INPUT);
   pinMode(RIGHTactivateBeamSensor, INPUT);
```

```
pinMode(LEFTactivateBeamSensor, INPUT);
pinMode(deactivateLeftScreen, OUTPUT);
pinMode(tellDacqForcedConfig1Trial, OUTPUT);
pinMode(tellDacqFreeConfig1Trial, OUTPUT);
pinMode(tellDacqFreeConfig2Trial, OUTPUT);
pinMode(LEDpin, OUTPUT);
pinMode(callOpenVertexToRight, OUTPUT);
pinMode(vertexSensor,INPUT);
pinMode(rightSensor,INPUT);
pinMode(leftSensor,INPUT);
pinMode(tellDacqForcedConfig2Trial, OUTPUT);
pinMode(tellDacqReward, OUTPUT);
pinMode(tellDacqVertex,OUTPUT);
pinMode(tellDacqAfterBarrier,OUTPUT);
digitalWrite(tellDacqFreeConfig1Trial, LOW);
digitalWrite(tellDacqForcedConfig2Trial, LOW);
digitalWrite(tellDacqForcedConfig1Trial, LOW);
digitalWrite(tellDacqFreeConfig2Trial, LOW);
digitalWrite(tellDacqReward, LOW);
digitalWrite(tellDacqVertex,LOW);
digitalWrite(tellDacqAfterBarrier,LOW);
analogWrite(screenPower, lowPower);
pinMode(dispenseRightMediumReward, OUTPUT);
pinMode(dispenseLeftMediumReward, OUTPUT);
pinMode(dispenseRightLargeReward, OUTPUT);
pinMode(dispenseLeftLargeReward, OUTPUT);
digitalWrite(dispenseRightMediumReward, LOW);
digitalWrite(dispenseLeftMediumReward, LOW);
digitalWrite(dispenseRightLargeReward, LOW);
digitalWrite(dispenseLeftLargeReward, LOW);
analogWrite(screenPower, lowPower);
tft.begin();
tft.fillScreen(BLUE);
     tft.setTextColor(YELLOW);
   tft.setTextSize(10);
   tft.setCursor(cursorX-10, cursorY+20);
```

```
    tft.println("GO!");
    tft.fillScreen(RED);
    tft.fillScreen(WHITE);
     tft.fillScreen(BLUE);
     tft.setTextColor(YELLOW);
    tft.setTextSize(10);
    tft.setCursor(cursorX-10, cursorY+20);
    tft.println("GO!");
}
void loop(){
 reportAfterBarrier();
 reportVertex();
 choice_trialInitiated();
 forcedRight_trialInitiated();
 forcedLeft_trialInitiated();
 changeConfig();
 setConfig1();
 closeMidstemWithSensor();
 activateMidstemSensor_right();
 activateMidstemSensor_left();
 endTrials(); }
```

7.3 Custom microdrive

Microdrives are an essential component for in-vivo, single-unit electrophysiology because they allow for implanted electrodes to be moved each day, thereby increasing the number of unique neurons recorded in an experiment. Prior to my PhD, the Bilkey lab had hand-made a microdrive (Bilkey & Muir, 1999). I found this approach very time-consuming, labour-intensive, and prone to significant variance from microdrive to microdrive. Therefore, I decided to design and 3D-print a microdrive. The finished product is presented in Figure A5.

Figure A5. Custom-designed, 3D-printed brain implant. The implant is approximately 1.5cm tall, .5cm wide, and .5cm long and weighs approximately 5 grams.

I opted for a stereolithography approach to 3D printing because that process produces pieces which are biologically inert and to be made at very fine scales (~.5mm tolerances). Developing this implant saved quite a bit of time and money. For instance, using the prior method, each implant cost approximately 5 NZD to produce whereas these new implants cost 3 NZD each. Furthermore, the prior implants required about three days to manufacture whereas these new implants take one day. In addition to saving time and money, this new implant was standardized and more precise, which greatly reduced the variability from implant to implant.

7.4 Appendix references

Bilkey, D. K., & Muir, G. M. (1999). A low cost, high precision subminiature microdrive for extracellular unit recording in behaving animals. Journal of Neuroscience Methods, 92(1–2), 87–90.

Hillman, K. L., & Bilkey, D. K. (2010). Neurons in the rat anterior cingulate cortex dynamically encode cost-benefit in a spatial decision-making task. J Neurosci, 30(22), 7705–7713.

Hillman, K. L., & Bilkey, D. K. (2012). Neural encoding of competitive effort in the anterior cingulate cortex. Nature Neuroscience, 15(9), 1290–1297.